Visual-motor neural mechanisms underlying peri-saccadic perceptual alterations

Dissertation

der Mathematisch-Naturwissenschaftlichen Fakultät

der Eberhard Karls Universität Tübingen

zur Erlangung des Grades eines

Doktors der Naturwissenschaften

(Dr. rer. nat.)

vorgelegt von

Matthias Philipp Baumann

aus Bad Kreuznach

Tübingen

2025

Gedruckt mit Genehmigung der Mathematisch-Naturwissenschaftlichen Fakultät der Eberhard Karls Universität Tübingen.

Tag der mündlichen Qualifikation:	13.08.2025
Dekan:	Prof. Dr. Thilo Stehle
1. Berichterstatter/-in:	Prof. Dr. Ziad Hafed
2. Berichterstatter/-in:	Prof. Dr. Jan Benda
3. Berichterstatter/-in:	Prof. Dr. Markus Lappe

Erklärung

Ich, Matthias Philipp Baumann, erkläre, dass ich die zur Promotion eingereichte Arbeit mit dem Titel *Visual-motor neural mechanisms underlying peri-saccadic perceptual alterations*, selbstständig verfasst, nur die angegebenen Quellen und Hilfsmittel benutzt und wörtlich oder inhaltlich übernommene Stellen als solche gekennzeichnet habe. Ich versichere an Eides statt, dass diese Angaben wahr sind und dass ich nichts verschwiegen habe. Mir ist bekannt, dass die falsche Abgabe einer Versicherung an Eides statt mit Freiheitsstrafe bis zu drei Jahren oder mit Geldstrafe bestraft wird.

Declaration

I, Matthias Philipp Baumann, hereby declare that I have produced the work entitled *Visual-motor neural mechanisms underlying peri-saccadic perceptual alterations*, submitted for the award of a doctorate, on my own (without external help), have used only the sources and aids indicated and have marked passages included from other works, whether verbatim or in content, as such. I swear upon oath that these statements are true and that I have not concealed anything. I am aware that making a false declaration under oath is punishable by a term of imprisonment of up to three years or by a fine.

Tübingen, den ……

Datum Unterschrift

Contents

List of Abbreviations

4AFC	Four-alternative forced-choice
CD	Corollary discharge
FEF	Frontal eye fields
fMRI	Functional magnetic resonance imaging
LFP	Local field potential
LIP	Lateral intraparietal cortex
MD	Mediodorsal thalamus
MST	Medial superior temporal area
MT/V5	Medial temporal area
RF	Receptive field
RGC	Retinal ganglion cell
SC	Superior colliculus
SSVEP	Steady-state visual evoked potentials
STP	Superior temporal polysensory area
V1	Primary visual cortex

Abstract

This thesis explores the visual and motor mechanisms underlying saccadic suppression and perceptual stability, focusing on two interrelated aspects. The first part investigates saccadic suppression, the phenomenon where visual sensitivity is reduced during saccades to prevent motion blur and ensure spatial coherence. Traditionally attributed to motor signals such as corollary discharge, this work demonstrates that visual mechanisms play a more prominent role than previously assumed. The second part revisits motor bursts in the superior colliculus (SC), traditionally regarded as purely motoric, and uncovers their contribution to visual stability through sensory-motor integration.

The first study established the visual origins of saccadic suppression using retinal recordings and human psychophysics. By simulating saccades, suppression was induced without motor signals, driven by stimulus characteristics like spatial frequency and texture. Low spatial frequencies and coarse textures elicited stronger suppression, challenging motor-centric models and highlighting stimulus-stimulus interactions.

The second study examined the influence of luminance contrast polarity on suppression. Psychophysical experiments revealed stronger suppression for dark stimuli on dark backgrounds, even during simulated saccades, further emphasizing the contextual and visually driven nature of suppression.

In the second part, the role of the SC in sensory-motor integration was investigated. The third study demonstrated that SC motor bursts, traditionally viewed as purely motoric, are modulated by the visual properties of saccade targets, such as spatial frequency and contrast. This finding highlights the SC's dual function in encoding visual features and generating predictive signals for eye movements.

The fourth study addressed perisaccadic mislocalization, where visual stimuli are perceived inaccurately during saccades. Human psychophysics revealed that mislocalization depends on visual features and varies across the visual field, with stronger effects in the upper field.

Finally, a novel paradigm confirmed these mislocalization patterns in rhesus macaques, showing parallels with human findings. Mislocalization strength varied with saccade direction and visual field location, supporting the SC's role in visual stability and providing a robust framework for future research.

Together, this work reveals that both saccadic suppression and visual stability rely heavily on visual mechanisms and the SC's sensory-motor integration, offering a refined understanding of how seamless vision is maintained during eye movements.

Zusammenfassung

Diese Dissertation untersucht die Mechanismen der sakkadischen Suppression und der Wahrnehmungsstabilität, mit einem Fokus auf zwei miteinander verbundene Aspekte. Der erste Teil beschäftigt sich mit der sakkadischen Suppression, einem Phänomen, bei dem die visuelle Empfindlichkeit während Sakkaden reduziert wird, um Bewegungsunschärfe zu vermeiden und räumliche Kohärenz zu gewährleisten. Während dies traditionell motorischen Signalen wie dem corollary discharge zugeschrieben wird, zeigt diese Arbeit, dass visuelle Mechanismen eine weitaus wichtigere Rolle spielen als bisher angenommen. Der zweite Teil untersucht die motorischen Bursts im Colliculus superior (SC), die traditionell als rein motorisch angesehen werden, und zeigt deren Beitrag zur visuellen Stabilität durch sensomotorische Integration auf.

Die erste Studie belegte die visuellen Ursprünge der sakkadischen Suppression mithilfe von retinalen Aufzeichnungen und psychophysikalischen Experimenten am Menschen. Durch die Simulation von Sakkaden konnte Suppression ohne motorische Signale ausgelöst werden, wobei sie durch Reizmerkmale wie räumliche Frequenz und Textur bestimmt wurde. Niedrige räumliche Frequenzen und grobe Texturen führten zu stärkerer Suppression, was motorzentrierte Modelle infrage stellt und die Bedeutung von Reiz-Reiz-Interaktionen hervorhebt.

Die zweite Studie untersuchte den Einfluss der Luminanzkontrastpolarität auf die Suppression. Psychophysikalische Experimente zeigten, dass dunkle Reize auf dunklem Hintergrund eine stärkere Suppression hervorrufen, selbst während simulierten Sakkaden, was die kontextuelle und visuell getriebene Natur der Suppression weiter unterstreicht.

Im zweiten Teil wurde die Rolle des SC in der sensomotorischen Integration untersucht. Die dritte Studie zeigte, dass motorische Bursts im SC, die traditionell als rein motorisch angesehen wurden, durch visuelle Eigenschaften der Sakkadenziele, wie räumliche Frequenz und Kontrast, moduliert werden. Diese Erkenntnis verdeutlicht die doppelte Funktion des SC, visuelle Merkmale zu kodieren und prädiktive Signale für Augenbewegungen zu generieren.

Die vierte Studie beschäftigte sich mit perisakkadischer Fehlverortung, bei der visuelle Reize während Sakkaden an falschen Positionen wahrgenommen werden. Psychophysikalische Experimente am Menschen zeigten, dass die Fehlwahrnehmung von visuellen Merkmalen abhängt und systematisch über das Gesichtsfeld variiert, mit stärkeren Effekten im oberen Gesichtsfeld, was SC-Asymmetrien widerspiegelt.

Abschließend bestätigte ein neuartiges Paradigma diese perisakkadische Fehlverortung bei Rhesusaffen und zeigte Parallelen zu den menschlichen Befunden. Die Stärke der Fehlwahrnehmung variierte je nach Sakkadenrichtung und Position im Gesichtsfeld, was die Rolle des SC in der visuellen Stabilität unterstreicht und eine solide Grundlage für weitere Untersuchungen bietet.

Zusammen zeigen diese Studien, dass sowohl die sakkadische Suppression als auch die visuelle Stabilität stark auf visuellen Mechanismen und der sensomotorischen Integration des SC beruhen, und liefern ein verfeinertes Verständnis darüber, wie eine nahtlose visuelle Wahrnehmung während Augenbewegungen gewährleistet wird.

List of Publications and Contributions

Publication 1

Perceptual Saccadic Suppression Starts in the Retina, 2020**,** Nature Communications

Saad Idrees*, Matthias P. Baumann*, Felix Franke, Thomas A. Münch, Ziad M. Hafed

*contributed equally

TAM and ZHM conceptualized the overall study. I together with SI, TAM, and ZMH, designed the study and the experiments. SI performed the ex vivo retina electrophysiology experiments and analyzed its data together with FF and TAM. I performed the human psychophysics experiments and analyzed it together with ZMH. I together with the other authors interpreted the data and wrote the manuscript.

Declaration: This project was started as part of my M.Sc. thesis (January 2019); around this time, we also published the first preprint (doi: https://doi.org/10.1101/562595). The data included in the preprint is shown in the final publication in Figures 1, 6 and 8 and supplementary Figure 2, 3, 8, 9 and 10. Till the paper was finally published in February 2020, we conducted further experiments and changed the manuscript significantly. The data I acquired and analyzed as a PhD-student is presented in the final publication in Figures 2, 5, 7, 9 and 10 and supplementary Figures 4 and 7.

Publication 2

Dependence of perceptual saccadic suppression on peri-saccadic image flow properties and luminance contrast polarity, 2021, Journal of Vision (Special Issue: From Peripheral to Transsaccadic and Foveal Perception)

Matthias P. Baumann, Saad Idrees, Thomas A. Münch, Ziad M. Hafed

I together with SI, TAM and ZMH conceptualized the overall study. I and ZMH designed the study and the experiments. I performed the human psychophysics experiments and analyzed it together with ZMH. I together with the other authors interpreted the data and wrote the manuscript.

Publication 3

Sensory tuning in neuronal movement commands, 2023, Proceedings of the National Academy of Sciences

Matthias P. Baumann*, Amarender R. Bogadhi*, Anna F. Denninger, Ziad M. Hafed

*contributed equally

ARB and ZMH conceptualized the overall study. I together with ARB, AFD and ZMH designed the study and experiments. I and ARB performed the research. ARB did the spike sorting. I and AFD preprocessed the eye data. ARB did some initial data analysis of the spiking data, I finalized and added to the data analysis. AFD analyzed the LFP data. I together with the other authors interpreted the data and wrote the manuscript.

Publication 4

Perisaccadic perceptual mislocalization strength depends on the visual appearance of saccade targets, 2025, Journal of Neurophysiology

Matthias P. Baumann*, Anna F. Denninger*, Ziad M. Hafed

*contributed equally

I together with AFD and ZMH conceptualized the overall study and designed the experiments. I collected and analyzed the human perisaccadic mislocalization data with ZMH; AFD collected and analyzed the human saccadic suppression data with ZMH. I together with the other authors interpreted the data and wrote the manuscript.

Publication 5

Two-dimensional perisaccadic visual mislocalization in rhesus macaque monkeys, 2025, under revision in eNeuro

Matthias P. Baumann, Ziad M. Hafed

I and ZMH conceptualized the overall study and designed the experiments. I trained the three animals and recorded the data. Tong Zhang, Tatiana Malevich and Antimo Buonocore also collected some data once the animals learned the task. I and ZMH analyzed, interpreted the data and wrote the manuscript.

Introduction

When we look out at a bustling street, our visual perception presents a seamless and stable world, richly detailed and steady. It feels as though we see everything at once, effortlessly and continuously. Yet this experience is an illusion, carefully constructed from limited and fragmented sensory input. The brain weaves these fragments into a coherent whole, creating the impression of completeness far beyond the quality of the raw input (Melcher, 2011; Nassi & Callaway, 2009; O'regan, 1992; Podvalny et al., 2017; Wurtz, 2008). This remarkable illusion raises a fundamental question: how does the brain transform noisy, fragmented sensory information into a stable and unified perception of the world? The visual input to the brain is far from perfect: it is disrupted by frequent eye movements (Yarbus, 1967; Zuber et al., 1968), constrained by the limited high-resolution area of the fovea (Rossi & Roorda, 2010), and shaped by the brain's need to balance computational efficiency with perceptual accuracy (Hoffman, 2012). A striking example of this conflict between visual input and perception arises from saccadic eye movements, rapid shifts of gaze that occur several times per second. These movements displace the visual image on the retina, introducing the potential for motion blur and perceptual instability. Yet we remain completely unaware of this disruption. This visual stability across saccades is built up on two components, a suppression of the visual input around the saccade and the ability to integrate and retain visual information across successive saccades (Dodge, 1900; Krekelberg, 2010; Matin, 1974; Melcher, 2011; Wurtz, 2008; Wurtz et al., 2011; Zimmermann & Bremmer, 2016). Understanding visual stability provides profound insights into how the brain integrates sensory input with motor actions. It highlights the predictive nature of perception; the brain anticipates the disruptions caused by its own movements and actively corrects for them. Moreover, deficits in mechanisms like corollary discharge, the internal motor signal predicting the sensory consequences of movements, have been linked to disorders such as schizophrenia (Lencer et al., 2021; Thakkar et al., 2015). In such cases, impaired distinction between self-generated and external inputs can lead to perceptual instability and hallucinations.

Goal of the Thesis

By addressing the challenges of visual stability across saccades, we uncover broader principles of brain function, including predictive coding, sensorimotor integration, and the selective filtering of sensory input. These principles explain not only how the brain resolves conflicts between movement and perception but also provide a framework for understanding stability and coherence across other sensory systems. Ultimately, visual stability exemplifies the brain's remarkable ability to transform fragmented, dynamic input into a unified perception of the world. This thesis explores the interplay between visual and motor mechanisms to deepen our understanding of how we maintain perceptual stability across saccades. Before the discussion of my work, I will introduce our current view on saccadic suppression. After this I will describe the role of the superior colliculus in a broader context of visual stability. The main part is organized in three chapters:

Chapter 1 examines the origins and classical properties of saccadic suppression, emphasizing the critical role of visual mechanisms in shaping this phenomenon. I demonstrate that saccadic suppression begins as early as the retina, highlighting its predominantly visual origin. Furthermore, I show that the suppression's low spatial frequency selectivity can be fully explained by visual processing alone (*Publication 1*). Building on this, I explore how stimulus-stimulus interactions, particularly luminance polarity, affect visual sensitivity during saccades (*Publication 2*). Together, these findings provide strong evidence for the visual basis of saccadic suppression and lay the foundation for an integrative understanding of visual stability, where visual and motor mechanisms closely coordinate to ensure a seamless perceptual experience.

Chapter 2 (*Publication 3*) revisits the superior colliculus (SC), a structure traditionally regarded as a motor center responsible for generating eye movement commands. While it is well-established that motor signals from the SC are relayed as corollary discharge to the cortex, my findings reveal an unexpected layer of sensory tuning within these signals. Notably, I recorded SC saccade-related motor bursts while monkeys generated saccades to different images. I discovered that the motor bursts embed within them a sensory representation of the appearance of the saccade target. This sensory tuning does not influence the motor output of the saccade itself, likely encoded by the population-based place code of the SC (and also downstream in the

brainstem). Instead, we propose that the rate code carrying sensory tuning operates independently of the saccade execution. This sensory component may serve a different, yet critical, purpose: it provides additional sensory or visual information about the saccade target, enriching the predictive signals that inform subsequent processing. By incorporating sensory details beyond the saccade vector, this mechanism enables a more precise prediction of the visual consequences of eye movements. These findings challenge the traditional view of the SC as purely motoric and suggest a broader, more integrative role in visual-motor processing that supports the stabilization of perception during movement.

Chapter 3 explores the consequences of sensory tuning in the SC for visual stability, using saccadic mislocalization as a model system. In the first part of this chapter, I present findings from a human behavioral study (*Publication 4*), demonstrating that the visual appearance of the saccade target significantly influences perisaccadic mislocalization. These results underscore the importance of visual features in shaping how saccades impact spatial perception. Building on these insights, I introduce a flexible behavioral paradigm for non-human primates designed to investigate the neural mechanisms underlying perisaccadic mislocalization (*Publication 5*). This paradigm allows for precise manipulation of visual stimuli and saccadic behavior, making it a highly versatile tool for future electrophysiological studies aimed at uncovering the role of sensory tuning in the SC. In addition, I demonstrate, from a scientific perspective, that monkey perisaccadic mislocalization changes properties with saccade direction, exactly like earlier human studies (Grujic et al., 2018), further motivating the utility of my paradigm. Together, these findings reveal how visual and sensory information contribute to stabilizing perception during saccades, advancing our understanding of the interplay between motor signals and sensory predictions.

Part I: Review of Saccadic Suppression

History of Saccadic Suppression

The historical exploration of visual stability began as early as the 11th century, when the Middle Eastern scholar Ibn al-Haytham (Alhazen) provided one of the first descriptions of visual perception and its stability, laying the groundwork for later scientific inquiries (Smith, 1992). In the 19th century, Hermann von Helmholtz proposed the idea of “Willensanstrengung” (“effort of will”), suggesting that the brain must distinguish between image shifts caused by eye movements and those caused by changes in the external world (Von Helmholtz, 1867). The modern investigation of saccadic suppression began with Erdmann and Dodge (1898). They observed that visual information in the periphery could not be clearly perceived during eye movements, particularly when reading. Dodge (1900) conducted experiments showing that visual stimuli presented during saccades appear blurred or smeared, but they are typically not perceived. He suggested that this suppression arises due to both peripheral mechanisms, such as blur by retinal motion, and central processes, such as neural inhibition. 50 years ago, Matin (1974) summarized in great detail in a review paper on saccadic suppression the understanding of the phenomenon at the time. Already back then it was clear that the causes of saccadic suppression are multifaceted. Prominent theories were masking (visual), and a central inhibition (motor). Today's understanding of the phenomenon is still rooted in these ideas.

Visual Mechanisms

The bulk of visual theories regarding saccadic suppression lies in visual masking, specifically backward masking (metacontrast), where visual stimuli presented shortly after a saccade suppresses earlier stimuli. For instance, light or patterns in the postsaccadic period can mask the smeared image produced during the saccade (Campbell & Wurtz, 1978; Ibbotson & Cloherty, 2009; MacKay, 1970a, 1970b; Matin et al., 1972; Richards, 1968). It was discussed in the 1970s that backward masking masks the image during the movement; I will later argue that the same mechanism of backward masking, but this time with the shift as the backward masker, is masking any stimulus before the movement and might play a role in explaining even presaccadic suppression without actual motor commands. In the 1990s some studies showed that such masking is also modulated by attention implying that masking that is traditionally

viewed as preattentive depends also on top-down mechanisms (Ramachandran & Cobb, 1995; Shelley-Tremblay & Mack, 1999). While initial feedforward processing might be preattentive, it is suggested that attention is necessary for higher-level visual processing contributing to perception during visual masking (Fahrenfort et al., 2007; Poiese et al., 2008).

Today's view of the visual origins of saccadic suppression still lies in visual masking, but now with mechanisms realized already in the retina. Visual masking emerges from the interactions of sequential stimuli and the inherent processing properties of the retinal circuitry. The suppression begins with the photoreceptors, particularly the cone photoreceptors, whose relatively slow response kinetics set the stage for dynamic visual interactions (Heikkinen et al., 2008; Idrees et al., 2022). When two stimuli occur in close temporal proximity, such as during rapid visual transients caused by saccadic eye movements followed by a probe onset, the retinal ganglion cell (RGC) response to the second probe stimulus is suppressed (*Publication 1*).

The suppression observed in RGCs is most prominent within their receptive field (RF) center and arises as a direct consequence of how cones encode and relay visual information (Idrees et al., 2022). During a rapid change, such as a luminance step or texture displacement (caused by eyeball rotation), the initial stimulus creates a large shift in photoreceptor output. If a subsequent stimulus, like a flash, follows this shift, its response is diminished due to the ongoing adaptation of the cone signals (Mazade et al., 2019; Yu et al., 2022) and the nonlinear integration performed by the retinal circuitry (Freeman et al., 2015; Idrees et al., 2022). Importantly, this suppression does not rely on inhibitory signals but is an emergent property of the retinal processing cascade.

In addition to the RF center, suppression also involves interactions across the RF surround. For ON-type RGCs, suppression is further influenced by two distinct components: a global component and a surround component. The global component originates from far beyond the cell’s immediate RF (Idrees et al., 2022) and is mediated by GABAergic inhibition from wide-field amacrine cells (Hoggarth et al., 2015). In contrast, the surround component appears to arise from local feedback mechanisms, such as horizontal cell modulation of cone output (Chapot et al., 2017; Verweij et al., 1996). These components act together to shape the overall suppression dynamics, with their relative contributions differing between ON and OFF RGCs. Notably, these

additional components cause stronger suppression in ON RGCs, and their recovery takes longer compared to OFF RGCs. Overall, the retina serves as a unifying neural substrate for these phenomena, initiating suppression early in the visual processing hierarchy.

Motor Mechanisms

Saccadic suppression begins just before the eye movement, peaks during the saccade, and persists briefly into the postsaccadic period. The temporal dynamics of suppression have been confirmed in experiments measuring thresholds for visual flashes presented at different time points relative to saccades. Studies have shown that the suppression effect starts before the eye physically moves, suggesting it is tied to motor signals (Bremmer et al., 2009; Latour, 1962; Riggs et al., 1974; Volkmann et al., 1968). The idea of central inhibition has been proposed as a key mechanism, involving a neural process that suppresses visual perception during saccades building the foundation of a suppression that is related to internal generated signals. This inhibition might result from corollary discharge (CD), a signal sent alongside motor commands to inform the brain of the eye movement (Berman et al., 2017; Cavanaugh et al., 2016; Wurtz et al., 2011).

Von Holst and Mittelstaedt (1950) and Sperry (1950) introduced the concepts of efference copy and corollary discharge, respectively. While these terms are often used synonymously today, they were originally distinct. Efference copy refers to an exact duplicate of the motor command sent to the muscles, simultaneously relayed to sensory systems to predict the sensory consequences of self-generated movements. This precise mechanism operates near the motor output stage, enabling the brain to distinguish between self-induced and external sensory changes. In contrast, corollary discharge represents a broader motor-related signal that modulates sensory processing across multiple stages of the motor control hierarchy. Unlike efference copy, CD signals do not require a perfect replication of the motor command and can emerge at different levels of the nervous system (Crapse & Sommer, 2008).

Over time the concept of central inhibition shifted towards a more nuanced network approach, integrating mechanisms involving cortical inhibition (e.g., FEF, V4), subcortical pathways (e.g., SC), and their interactions with visual suppression. These processes are still unified by the broader concept of being motor-driven. In the next

section I will elaborate on the neurophysiological work beyond the retina, that builds our current understanding of the phenomenon of saccadic suppression.

Neurophysiology of Saccadic Suppression

Saccadic Suppression in Lateral Geniculate Nucleus

The lateral geniculate nucleus (LGN,) as the first relay in the retino-geniculo-cortical pathway, was initially thought to play little role in saccadic suppression, particularly in primates. Early work by Duffy and Burchfiel (1975) reported no suppression of LGN firing rates during spontaneous saccades in complete darkness, leading to the conclusion that suppression was primarily cortical. However, this view has since been challenged by studies using visual stimulation during saccades, revealing subtle but significant suppression effects.

In the neurophysiology literature, related studies can be grouped into two classes. One class examines saccadic suppression as the modulation of neural activity around saccades without peri-saccadic probes. The other class includes peri-saccadic probes, similar to human psychophysics studies. Across both approaches, saccades induce a biphasic modulation of LGN activity in primates: a weak suppression immediately following saccade onset, followed by a transient enhancement (Reppas et al., 2002; Royal et al., 2006). When peri-saccadic probes are used, the visual response is reduced during the suppression phase and enhanced during the transient enhancement (Reppas et al., 2002). The psychophysical observation that saccadic suppression is selective for low spatial frequencies but does not affect chromatic stimuli (Burr et al., 1994; Ross et al., 2001) is elusive in the neurophysiology literature. While some results indicated that suppression was stronger in magnocellular neurons (Reppas et al., 2002), which are sensitive to low spatial frequencies, compared to parvocellular neurons, other electrophysical studies in primates observe a suppression for both paths (Ramcharan et al., 2001; Royal et al., 2006). Moreover, functional magnetic resonance imaging (fMRI) studies in humans show that saccades suppress visually evoked activity in the LGN only under visual stimulation. Interestingly they did not see a stronger magnocellular suppression by comparing suppression in different stimuli conditions that target magno and parvo independently (Kleiser et al., 2004; Sylvester & Rees, 2006). Thus, the question of whether saccadic suppression is pathway selective or not arises. In a recent study Zhang et al. (2024) systematically

tested this question using steady-state visual evoked potentials (SSVEPs) to isolate visual responses to chromatic (parvocellular) and luminance (magnocellular) stimuli. Their results demonstrated robust saccadic suppression for both pathways, also contradicting earlier claims of magnocellular specificity. Importantly, suppression was implemented as a reduction in response gain, scaling down visual responses without altering contrast sensitivity.

The conflicting results raise an open question: does saccadic suppression selectively target the magnocellular pathway, or does it operate more broadly? Different measurement techniques and species differences contribute to the discrepancies but also differences in experimental conditions including illumination and visual appearances of stimuli play a role. I will discuss this further and how my work fits here into the literature in chapter 1 of the main discussion.

Saccadic Suppression in the Primary Visual Cortex

In the primary visual cortex (V1), saccadic suppression is more robust and spatially refined, reflecting both the downstream effects of LGN suppression and additional cortical mechanisms. Unlike the LGN, suppression in V1 has been more consistently observed across multiple studies, even when retinal motion is eliminated through saccades in the dark and without visual stimulation via probes (Duffy & Burchfiel, 1975). It is suggested that suppression primarily targets input layers of V1, particularly layer 4, which receives thalamic input (Maier et al., 2008). For example, Maier et al. (2008) demonstrated in primates that suppression in local field potentials (LFPs), which reflect synaptic input to a neuronal population, occurs earlier and is stronger than suppression in single-unit spiking activity. In contrast to LFPs, the spiking activity reflects the output of individual neurons. This temporal relationship highlights that saccadic suppression first reduces feedforward input into V1 where LGN signals terminate. Only subsequently does this suppression propagate to the spiking activity, which represents the output signals relayed to downstream cortical areas. In addition, suppression in the BOLD fMRI signal, which integrates activity across broader spatial and temporal scales, aligns more closely with LFP suppression, further emphasizing that saccadic suppression predominantly targets the input stage of V1 processing.

The spatial precision of suppression in V1 is particularly noteworthy. Early work by Duffy and Burchfiel (1975) demonstrated that suppression is directionally specific, with

activity most reduced when saccade direction matched the neurons preferred direction of motion tuning. This finding aligns suppression with the tuning properties of V1 neurons, which are highly sensitive to motion direction. By selectively suppressing neurons that would otherwise respond to the retinal motion caused by saccades, the visual system might minimize the perception of disruptive visual smear.

In addition to suppression, V1 exhibits presaccadic enhancement that prepares the visual system to process relevant information at the saccade target. This enhancement is spatially localized and occurs before saccade onset, aligning with the predictive nature of visual processing. Super et al. (2004) showed that V1 neurons increase their activity approximately 100–200 ms before a saccade, when the saccade target aligns with their receptive fields. This enhancement likely reflects a corollary discharge signal from oculomotor areas, such as the SC or frontal eye fields (FEF), that primes V1 for the anticipated visual input at the postsaccadic fixation.

Following suppression, V1 neurons also exhibit a postsaccadic enhancement (Kagan et al., 2008; Rajkai et al., 2008). This enhancement biases visual processing toward the new fixation location, complementing the preparatory role of presaccadic enhancement. Together, suppression and enhancement in V1 form a dynamic mechanism that might stabilize vision during eye movements while ensuring rapid and efficient processing of the visual scene at the saccade target. Across the V1 studies three response types are mentioned, neurons getting suppressed in their activity (Duffy & Burchfiel, 1975; Kagan et al., 2008; Maier et al., 2008; Stella & Lee, 2000), enhanced neurons (Kagan et al., 2008; Rajkai et al., 2008; Super et al., 2004) and neurons that remain unmodulated during eye movements (Kagan et al., 2008; Maier et al., 2008; Stella & Lee, 2000; Super et al., 2004). How these response classes are positioned through the layers of V1 and how much of these responses can be and are modulated by visual context remains an open question for now.

Another important consideration when interpreting the literature is that suppression can be observed in different ways; there could be a decrease in baseline activity but there is also a modulation of the visual response to stimuli presented around the saccade. In human psychophysics saccadic suppression is only measurable with stimuli presented around saccades, so the physiological data is not always reflecting the circumstances in which psychophysical experiments take place. However, the

neurophysiology could still hint at how peri-saccadic stimuli will be processed. For example, suppression and enhancement in the dark could indicate the level of excitability of cortical circuits (Rajkai et al., 2008). This level of excitability will be reflected in how they respond to peri-saccadic probes. Moreover, as I show next, more recent studies (e.g. in the superior colliculus), have explicitly tried to replicate the approach of the psychophysical studies by presenting peri-saccadic probe stimuli.

Saccadic Suppression in the Superior Colliculus

The superior colliculus (SC) plays a critical role in generating and relaying corollary discharge (CD) signals that are thought to drive saccadic suppression in various visual areas like LGN and V1, via thalamic pathways. I will discuss its connectivity regarding CD signals in a broader framework of visual stability in the second part of the introduction. Despite being one of the sources for the CD, primate colliculus neurons have been demonstrated to show saccadic suppression around microsaccades (Hafed & Krauzlis, 2010) and larger saccades (Berman et al., 2017; Robinson & Wurtz, 1976). The suppression in visual responses in SC neurons has been demonstrated in superficial and intermediate layers. In these layers are neurons that have visual bursts. Interestingly the visual motor neurons in the intermediate layers were spatial frequency selective (Chen & Hafed, 2017) matching the observations human perception (Burr et al., 1994; Ross et al., 2001). The superficial layers, however, do not show such a selectivity in their suppression, and they have generally weaker suppression magnitudes (Chen et al., 2015).

The classic idea for suppression within SC was that saccade commands in visual motor and motor neurons of the intermediate and deeper layer are fed back to superficial purely visual neurons to not only cause suppression in this layer but also to jumpstart a putative feedback pathway for cortical suppression through the pulvinar (Berman & Wurtz, 2008, 2010, 2011; Isa & Hall, 2009; Lee et al., 2007; Phongphanphanee et al., 2011; Wurtz, 2008; Wurtz et al., 2011). While this idea is based on experiments in the mice SC (Isa & Hall, 2009; Lee et al., 2007; Phongphanphanee et al., 2011) primate electrophysiology is pointing into another direction. The different properties in suppression across the layers that Chen and Hafed (2017) describes and overall stronger suppression in visual motor compared to visual neurons prompt towards more

nuanced mechanisms in primates (Chen & Hafed, 2017; Chen et al., 2015; Hafed et al., 2015; Hafed & Krauzlis, 2010).

Saccadic Suppression in Higher Cortical Areas: MST, MT and V4

Saccadic suppression extends across multiple visual areas and is characterized by functionally specific modulations in neural responses. Saccadic suppression in motion-sensitive dorsal stream areas, such as medial superior temporal (MST) and medial temporal (MT/V5) area, reflects functional adaptations to stabilize visual motion perception during eye movements. Thiele et al. (2002) showed that in MST, some neurons are selectively silenced during saccade-induced motion, while others exhibit a reversal of their preferred motion direction, effectively canceling out oppositely directed motion signals. This provides a mechanism for suppressing motion percepts caused by saccades. Berman et al. (2017) added to this picture that presaccadic suppression begins earliest in the superficial layers of the SC, followed by suppression in MT and the pulvinar, suggesting that the SC initiates suppression through corollary discharge signals that propagate to cortical visual areas.

In parallel, Kleiser et al. (2004) demonstrated that saccadic suppression occurs broadly across visual cortical areas, including V1, V2, V3, V4, and MT/V5, using human fMRI data. Importantly, suppression was strongest in motion-sensitive areas such as MT/V5, aligning with their vulnerability to retinal motion and confirming that extraretinal mechanisms play a critical role in saccadic suppression. In area V4 it is thought that saccadic suppression operates through two distinct mechanisms: a multiplicative suppression affecting visual responses broadly during saccades, and an additive suppression reducing peripheral activity post-saccadically, driven by increased alpha oscillations, highlighting a shared neural circuitry between saccadic suppression and attentional processes (Zanos et al., 2016). Moreover, saccade-related modulations in area V4 are not limited to suppression but also include enhancement effects that reflect both attentional and oculomotor influences. While V4 neurons generally exhibit an increase in firing rate when saccades are directed toward their receptive fields, a more reliable signature of saccade preparation is a reduction in response variability, suggesting that suppression and enhancement in V4 are dynamically regulated to optimize visual processing at the target location (Steinmetz & Moore, 2010). Additionally, receptive fields in V4 undergo rapid spatial shifts and shrinkage prior to

saccades, prioritizing processing at the upcoming fixation point rather than applying uniform suppression across the visual field (Tolias et al., 2001). Even when saccade preparation is dissociated from attentional demands, V4 responses remain modulated, showing increases in firing rate, stimulus selectivity, and response reliability (Steinmetz & Moore, 2014). These findings highlight the complex interplay between suppression and enhancement in V4, indicating that saccadic suppression is not merely a reduction in activity but a reorganization of visual processing that facilitates perceptual stability and efficient target selection.

Saccadic Suppression in Higher Cortical Areas: FEF and LIP

Higher-order oculomotor and attentional areas, such as the frontal eye fields (FEF) and the lateral intraparietal area (LIP), integrate suppression with spatial target selection. In the FEF, presaccadic suppression of visual responses occurs specifically in visual neurons, while visuomotor neurons were largely unaffected (Krock & Moore, 2016). This suppression begins approximately 80 ms before saccade onset and occurs independently of motor-related activity, suggesting a preparatory mechanism that stabilizes visual inputs prior to eye movements. Importantly, suppression in the FEF equally affected both luminance contrast and color stimuli, indicating a general reduction of visual sensitivity that is not pathway-specific (Krock & Moore, 2016). LIP has location-specific suppression of distractor responses; this suppression sharpens the priority map by reducing neural responses to irrelevant distractors while enhancing target-related signals. Additionally, reward expectation in the LIP modulated suppression, improving target-distractor discriminability and facilitating efficient saccadic target selection (Falkner et al., 2010).

Ibbotson and Krekelberg (2011) provide a unifying framework for these observations, describing a characteristic biphasic modulation of neural responses across visual and oculomotor areas. Suppression occurs during and just before saccades to minimize retinal motion artifacts, followed by a postsaccadic enhancement that reallocates resources to process the new fixation point efficiently. This pattern, observed in LGN, V1, MT, MST, FEF, and LIP, reflects the integration of corollary discharge signals with local computations that stabilize and optimize visual perception.

Together, these findings illustrate that saccadic suppression is a hierarchical and functionally specific process. Early areas like V1 primarily suppress feedforward input,

whereas higher cortical areas such as MT, MST, FEF, and LIP integrate suppression with target prioritization and predictive mechanisms. In humans, suppression is widespread but enhanced in motion-sensitive areas (Kleiser et al., 2004), aligning with the functional demands of stabilizing motion perception during eye movements.

Part II: The Role of the Superior Colliculus in Visual Stability

The superior colliculus (SC) is a midbrain structure involved in sensorimotor integration, guiding orienting behaviors such as saccadic eye movements toward stimuli of interest.

Anatomy of the Superior Colliculus

Anatomically, the SC is a layered structure divided into two major regions: the superficial layers (I-III) and the deep layers (IV-VII). The superficial layers, primarily sensory, receive direct inputs from the retina and indirect projections from the visual cortex. These layers contain a precise retinotopic map of the contralateral visual field, with a magnified representation of the central visual field (Chen et al., 2019). Neurons in these layers respond strongly to visual stimuli and are organized to detect changes in the environment with high spatial precision (Cynader & Berman, 1972; Goldberg & Wurtz, 1972; Hafed et al., 2023). In contrast, the deep layers integrate multisensory inputs, visual, auditory, and somatosensory making the SC an essential hub for orienting movements. Neurons in the deep layers have larger receptive fields and are responsible for coordinating motor outputs such as saccadic eye movements, head turns, and even full-body orienting responses (May, 2006; Werner et al., 1997). The sensory and motor maps in these deep layers are spatially aligned, ensuring a seamless translation of sensory signals into motor commands.

The connectivity of the superior colliculus further illustrates its role in sensory-motor integration. Inputs to the superficial layers originate from the retina, primary visual cortex, and other visual centers, while the deep layers receive inputs from cortical regions, brainstem nuclei, and the spinal cord. Outputs from the superficial layers project to visual centers such as the LGN and pulvinar, whereas the deep layers send motor signals to brainstem nuclei and spinal cord regions that control movements. This

extensive network enables the SC to act as a bridge between sensory perception and motor execution, particularly for orienting behaviors.

The SC is an evolutionarily conserved structure that shares its origins with the optic tectum in non-mammalian vertebrates, such as fish and amphibians. In these species, the tectum serves as the primary visual processing center, directly integrating retinal inputs to guide reflexive orienting behaviors. Similarly, in mammals with less-developed cortical visual systems, such as rodents, the SC retains a dominant role in visual processing, functioning analogously to V1. This is reflected not only in its extensive retinal input but also in its central role in detecting and processing visual stimuli. In primates the main visual input comes through V1. It is even a current question whether the retino-collicular pathway is functional at all in primates. For example muscimol inactivating LGN or V1 results in a substantial loss of visual responses in the intermediate layers of the SC (Katz et al., 2024; Malevich et al., 2024). However, Schiller and colleagues demonstrated more than 50 years ago that the most superficial SC layers remain unaffected by V1 loss (Schiller et al., 1974).

Functions of the Superior Colliculus

Functionally, the SC plays a pivotal role in visual processing, motor control, and multisensory integration. Its superficial layers detect visual stimuli and process retinotopically organized signals, while the deep layers integrate sensory inputs across modalities. Cynader and Berman (1972) demonstrated that neurons in the superficial layers of the SC respond strongly to light onset and moving stimuli, exhibiting center-surround receptive fields that enhance spatial contrast sensitivity. The deep layers, on the other hand, respond to a combination of visual, auditory, and somatosensory inputs, allowing the SC to coordinate precise orienting movements toward salient stimuli. Electrical stimulation of the deep SC reliably evokes saccadic eye movements, with the direction and amplitude of these movements corresponding to the stimulation site within the SC (place code) (Robinson, 1972; Schiller & Stryker, 1972; Stryker & Schiller, 1975; Wurtz & Albano, 1980). This observation underscores the SC's role as a sensorimotor interface, where visual signals are converted into spatially aligned motor commands. The dominant view of the colliculus is as a motor structure (Gandhi & Katnani, 2011). Besides the place code that encodes the saccade vector, there is

also a rate code, in which the peri-saccadic firing rate levels of SC neurons are thought to encode saccade kinematics, like the eye velocity (Smalianchuk et al., 2018).

Lesion studies provide further evidence of the SC's critical role in saccadic control and visual behavior. Schiller et al. (1987) demonstrated that unilateral lesions of the SC in rhesus monkeys eliminate express saccades, short-latency saccadic eye movements, contralateral to the lesion. These express saccades, which typically occur with latencies under 100 milliseconds, are thought to be reflexive visual responses facilitated by the SC's direct retinotectal pathway. In contrast, lesions to the frontal eye fields (FEF) have minimal long-term effects on saccadic latencies, suggesting that the SC is the dominant structure for rapid, reflexive saccade generation, while the FEF may contribute more to voluntary control. The distinction between SC and FEF lesions highlights the SC's specialization in fast, stimulus-driven behaviors, a function critical for survival.

The SC's contributions are also evident in studies involving cortical lesions. Visual responses in higher cortical areas, such as the superior temporal polysensory area (STP), persist after striate cortex ablation due to input from the SC via the pulvinar (Bruce et al., 1986). This finding show that the SC supports visual functions even in the absence of cortical pathways. Such tectofugal projections of the SC might help to compensate for cortical damage, allowing some level of visually guided behavior to remain intact like in cortically blind patients that exhibit blindsight.

Visual Perspective on the Superior Colliculus

The SC exhibits sophisticated visual feature processing, making it a critical structure for rapid and efficient visual perception. SC neurons are highly sensitive to features such as motion, spatial frequency, and contrast, with a preference for low spatial frequencies and dark contrasts over bright ones, which optimizes detection under natural conditions (Bogadhi & Hafed, 2023; Chen & Hafed, 2018; Hafed et al., 2022; Malevich et al., 2022). A striking characteristic of the SC is its upper visual field bias, where neurons show faster response latencies and smaller receptive fields for stimuli in the upper visual field. This likely reflects evolutionary demands to monitor distant or elevated objects, such as predators or threats (Hafed, 2024; Hafed & Chen, 2016; Soares et al., 2017).

In primates, the SC also demonstrates an enlarged representation of the foveal region, aligning with the need for precise visual processing in regions of high acuity. SC neurons play a key role in foveal vision through their involvement in generating microsaccades, which enhance visual detail and maintain active fixation. Additionally, the SC is specialized for rapid threat detection, responding quickly to looming stimuli and biologically relevant shapes, such as predators (Maior et al., 2012; Soares et al., 2017) and faces (Bogadhi et al., 2021; Hafed et al., 2023; Nguyen et al., 2014; Nguyen et al., 2016; Quaia & Krauzlis, 2024; Yu et al., 2024). These visual properties underscore the SC's role as a structure finely tuned for both active perception and reflexive visual behaviors, ensuring survival and effective interaction with the environment.

Role of the Superior Colliculus for Attention

Beyond its role in visual and motor control, recent research has revealed the SC as a pivotal structure in attention and decision-making (Basso & May, 2017; Bogadhi et al., 2021; Crapse et al., 2018; Krauzlis et al., 2013). SC neurons encode target priority, enabling the selection of relevant stimuli from complex environments (Carello & Krauzlis, 2004; Kim & Basso, 2008). This function demonstrates the SC's involvement in spatial attention, expanding its contributions beyond orienting movements. Advances in circuit-based approaches, such as transgenic mouse models, further reveal the SC's microcircuits as critical for decision-making under uncertainty, providing a neural substrate for complex behaviors (Basso & May, 2017; Wang et al., 2020). A recent study demonstrated that the SC encodes abstract visual categories with remarkable speed and robustness, often surpassing LIP in strength and latency of responses. In a delayed match-to-category task, SC neurons rapidly encoded learned visual categories, with activity emerging earlier than in LIP. Furthermore, SC inactivation caused significant categorization deficits, greater than those observed with LIP inactivation. These results challenge traditional cortical-dominant views of abstract cognitive tasks, positioning the SC as an essential hub for sensory-to-cognitive transformations (Peysakhovich et al., 2024). Complementing these findings, Stine et al. (2023) explored the dynamic interplay between SC and LIP in perceptual decision-making. While LIP activity aligns with drift-diffusion models, accumulating evidence to guide decisions, SC neurons exhibit burst-like activity that signals decision thresholds, marking transitions from deliberation to action. SC inactivation prolonged decision-

making, underscoring its role in decision termination. Together, these studies suggest a hierarchical relationship: LIP integrates sensory evidence, and the SC initiates fast, decisive actions once thresholds are met.

Predictive Remapping and Spatial Stability

Early work by Stevens et al. (1976) highlighted perceptual shifts associated with eye movement plans. Using paralytic agents (curare) to suppress eye movements in awake humans, they observed that attempted eye movements caused the visual world to perceptually “jump” in the intended movement direction. This phenomenon suggested the presence of an internal signal, a corollary discharge, informing the brain about motor intentions, even without physical movement. Sommer and Wurtz (2006) demonstrated predictive remapping in FEF, where neurons shift receptive fields to postsaccadic locations before saccades begin. This process anticipates visual input at the new line of sight, relying on corollary discharge signals from the SC via the mediodorsal thalamus (MD). Disrupting the SC-MD-FEF pathway impairs remapping precision, as evidenced by studies showing deficits in saccadic endpoint perception and sequential saccade coordination following MD inactivation (Sommer & Wurtz, 2002, 2004, 2006, 2008).

Zirnsak et al. (2014) expanded this understanding, revealing that remapping involves not just one-to-one receptive field shifts but also distributed shifts around saccade targets. This activity forms a focus of convergence at the saccade endpoint, reflecting population-level neuronal reorganization. Such distributed remapping aligns with the selection and processing of saccade goals.

The SC itself exhibits predictive remapping properties. Also SC neurons respond to stimuli expected to enter their receptive fields after a saccades (Walker et al., 1995). In recent work Zhang et al. (2025) describe a prediction error, a stronger visual response of foveal neurons when the saccade target and therefore the content of the receptive field when landing is changed intersaccadic. This anticipatory activity integrates sensory inputs with motor commands, maintaining spatial coherence during eye movements.

Perisaccadic Mislocalization

Such predictive remapping is closely related to perisaccadic mislocalization, where visual stimuli are perceived as shifted toward saccade targets, when they are presented post- or intersaccadic. It is suggested that this phenomenon reflects the distributed receptive field shifts observed during remapping. Compression of visual space around the saccade target may be an emergent property of this process (Ross et al., 1997; Zirnsak et al., 2014).

Such mislocalization errors, akin to visual illusions, arise when the visual system temporarily distorts spatial relationships during saccades. Extraretinal signals, such as CD, enable the system to predict and adjust for retinal shifts caused by eye movements. These transient distortions are not failures but artifacts of the system's ability to compensate for saccadic disruptions, dynamically constructing perception around action. Perisaccadic mislocalization comprises two primary components: a uniform shift and a compression of visual space toward the saccade target. These components appear to be governed by distinct mechanisms, as the strength of compression correlates with saccadic peak velocity (Ostendorf et al., 2007). This indicates that the processes underlying spatial distortions during saccades are more complex than initially assumed. Additionally, post-saccadic processes play a crucial role in mitigating these distortions. Mislocalization may reflect the visual system's attempt to align pre- and post-saccadic visual inputs, thereby ensuring spatial stability (Hamker et al., 2008). Errors in mislocalization are also influenced by visual field position, as the magnitude and direction of errors vary depending on where a stimulus appears. These spatial distortions are further modulated by the availability of visual references, highlighting the role of contextual information in perisaccadic perception (Kaiser & Lappe, 2004; Zimmermann et al., 2014). Saccadic adaptation introduces a dynamic aspect to mislocalization, as it shifts the focus of compression toward newly learned saccade targets. This adaptability underscores the plasticity of the visual system in maintaining spatial accuracy despite changes in saccadic behavior (Awater et al., 2005). More recent work stresses out dependencies of mislocalization to the saccade direction, upward saccades for example cause bigger mislocalization errors than downward saccades (Grujic et al., 2018). This supports the involvement of the SC, as mentioned in contrast to other retinotopic areas the SC has a magnification of

the upper visual field, that could cause more variability in the remapping of RFs in this hemifield.

Despite its utility, a critical debate persists: Is remapping directly responsible for visual stability, or does it primarily prepare the visual system for post-saccadic processing? While mislocalization might reflect the preparatory role of remapping, its occurrence also offers a glimpse into the mechanisms underlying spatial coherence across saccades.

Current Theories of Visual Stability

Theories of visual stability explore how we perceive a continuous and stable world despite the disruptions caused by frequent saccadic eye movements. One of the earliest explanations is the corollary discharge theory (Crapse & Sommer, 2008; Sommer & Wurtz, 2008; Sperry, 1950), which proposes that the brain sends an internal copy of the motor command for an eye movement to visual areas. This signal informs the brain about the impending movement, allowing it to attribute the resulting motion of the retinal image to eye movement rather than changes in the external world. Building on this idea, retinotopic remapping (Duhamel et al., 1992; Melcher & Colby, 2008; Sommer & Wurtz, 2006) extends the corollary discharge concept by demonstrating that receptive fields in higher visual areas, such as LIP and FEF, shift predictively to align with the new gaze location even before the saccade occurs. This remapping mechanism allows the brain to prepare for the incoming visual input at the new fixation point, effectively updating retinotopic maps without requiring the active fusion of pre- and post-saccadic information.

In contrast to remapping, transsaccadic memory (Deubel et al., 2002; Gottlieb et al., 1998; Henderson, 1997; Hollingworth et al., 2008; Irwin, 1991; Melcher, 2005; Rolfs et al., 2011; Tas et al., 2012; Zimmermann & Lappe, 2016) emphasizes the integration of visual information across saccades. Here, the visual system retains the pre-saccadic input in short-term memory and actively combines it with post-saccadic input to construct a coherent and stable visual representation. This process ensures that specific features, such as object identity, shape, and position, are seamlessly fused across eye movements, highlighting the role of predictive memory systems in stabilizing perception. The no-fusion hypothesis (Deubel & Schneider, 1996; Watson & Krekelberg, 2011) challenges this view by proposing that visual stability arises not

from integration but from post-saccadic dominance, where the brain resets its visual representation after each saccade. According to this perspective, pre-saccadic information is largely discarded, and the post-saccadic input becomes the primary source of visual perception, eliminating the need for transsaccadic integration.

Finally, the spatiotopic representation theory (Burr & Morrone, 2011; Cavanagh et al., 2010) suggests that the brain maintains a stable, world-centered map of space that is independent of the shifting retinotopic coordinates caused by saccades. Neurons in areas like the parietal cortex encode visual information in a way that aligns with spatial positions relative to the environment rather than the retina, providing a consistent spatial framework for perception. Together, these theories corollary discharge, retinotopic remapping, transsaccadic memory, no-fusion, and spatiotopic representation reflect a progression of ideas that explore how the brain predicts, updates, and organizes visual information to ensure perceptual stability across eye movements.

Main Discussion

Chapter 1.1 Perceptual Saccadic Suppression Starts in the Retina

To study visual stability, we first explored saccadic suppression, a phenomenon where visual sensitivity is reduced around saccadic eye movements. Despite decades of research, the origins of saccadic suppression remain unresolved, with two primary hypotheses prevailing. One attributes suppression to visual-only mechanisms, particularly visual masking effects. The other emphasizes motor-related mechanisms, such as corollary discharge, a motor command copy informing visual areas of impending eye movements.

Methods and Key Observations (Publication 1)

Retinal Recordings

We began our investigation by analyzing retinal responses to saccade-like rapid image shifts using ex vivo multi-electrode array recordings in mouse and pig retinae. Saad Idrees conducted these experiments in Thomas Münch's lab. The stimuli consisted of rapid image displacements simulating saccadic visual flow, followed by brief flash presentations to measure retinal ganglion cell (RGC) responses. Figure 3 illustrates that coarse textures produced significantly stronger suppression of RGC responses compared to fine textures, indicating an image dependency in the suppression mechanism.

We saw a conserved suppression mechanism across mouse and pig retinae, despite differences in oculomotor behavior and eye size. These findings, detailed in Figure 3e, suggest that fundamental visual processes underlying saccadic suppression are shared across mammalian species, providing a basis for broader comparative studies.

Human Psychophysics

To test whether this image dependency translated to perceptual suppression, I conducted human psychophysics experiments in Ziad Hafed's lab. Subjects made saccades across coarse and fine textured backgrounds, during which brief low-contrast flashes were presented. In a four-alternative forced-choice (4AFC) task, participants identified flash locations. As shown in Figure 1, human perception mirrored

the retinal findings: stronger suppression occurred over coarse textures, confirming that perceptual saccadic suppression also exhibits image dependency.

To further isolate visual contributions from motor influences, we designed a simulated saccade paradigm. Here, subjects maintained fixation while textured backgrounds underwent saccade-like displacements. Perceptual suppression was again observed, including the same texture dependency, as illustrated in Figure 6. Suppression in this simulated condition lasted longer than during real saccades, suggesting that motor-related mechanisms may serve to shorten, rather than initiate, visually-driven suppression. Additionally, suppression occurred even before texture displacements began, likely due to backward masking effects.

One striking observation was the temporal mismatch between retinal and perceptual suppression. Retinal suppression persisted beyond the perceptual window, as shown in Figures 3 and 4, highlighting the potential role of cortical areas in refining suppression duration. This temporal discrepancy supports the hypothesis that motor signals act primarily to modulate suppression duration, optimizing visual performance during natural saccades.

Building on Burr et al.'s (1994) work, we then explored whether saccadic suppression selectively targets low spatial frequencies. Using gratings of varying spatial frequencies superimposed on coarse and fine textures, we confirmed that suppression was stronger for low spatial frequencies during real saccades (Figure 8b). Remarkably, this selective suppression persisted in the simulated saccade condition, further supporting the dominance of visual mechanisms (Figure 8d). However, altering the background textures abolished selective suppression, implicating stimulus-stimulus interactions rather than pathway-specific suppression (Figure 8e and f).

Discussion (Publication 1)

Our findings challenge the long-standing notion that motor-related signals, such as corollary discharge, are essential for initiating saccadic suppression. By demonstrating that perceptual suppression, including its selective nature for low spatial frequencies, can arise purely from visual mechanisms, we provide compelling evidence for the primacy of visual processes in this phenomenon. The texture-dependence of suppression and its replication in simulated saccade conditions, as well as the

presence of similar texture-dependence in the retina, highlight the importance of stimulus-stimulus interactions over pathway-specific suppression.

While the time course of suppression starting before the actual movement (Latour, 1962) is often used as an argument for an involvement of extraretinal signals, we observed perceptual suppression, with texture displacements also before the actual onset of the shift. This is likely due to backward masking, where the subsequent texture shift masks the flash stimulus presented shortly beforehand. Importantly, a perceptual suppression occurring before the onset of the movement can therefore be fully explained by visual mechanisms alone. Therefore, perceptual suppression before saccade onset does not necessarily require a motor signal. Moreover, we observed that suppression persisted longer during simulated saccades compared to real ones. This temporal discrepancy suggests that motor-related mechanisms may play a modulatory role by truncating visually-driven suppression, thereby optimizing visual performance in natural viewing conditions.

Our findings also revisit the influential study by Burr et al. (1994), which proposed that saccadic suppression selectively targets the magnocellular visual pathway. Their conclusion was based on observing suppression of only low but not high spatial frequencies. While we replicated their results of stronger suppression for low spatial frequencies under real saccade conditions, our simulated saccade experiments demonstrated that this selective suppression could be abolished by manipulating background textures. This allowed us to then abolish selective suppression with real saccades as well. Thus, the observed selectivity may arise from contextual visual interactions rather than intrinsic pathway-specific suppression. In 2024, we discussed this work in an editorial focus on recent findings by Zhang et al. (2024). Their results also support a non-selective mechanism in the early visual pathways, aligning with our conclusion that selective suppression is influenced more by contextual visual interactions than by pathway-specific suppression (Hafed et al., 2024). In a review article in 2021 we additionally extended this perspective by showing parallels between human psychophysics and the suppression patterns observed in different layers of the superior colliculus (SC) (Hafed et al., 2021). The intermediate SC layers exhibit selective suppression for low spatial frequencies, mirroring behavioral observations, while superficial layers show non-selective suppression akin to the behavior we observed with altered background textures. This could reflect different amounts of

surround integration implemented by the different SC layers, which is supported by intra-collicular circuit investigations (Phongphanphanee et al., 2014).

Critics of our approach argue that simulated and real saccades differ in their perceptual impact, as texture displacements are visually perceived during simulated saccades but not during real ones (Binda & Morrone, 2022). While I acknowledge these differences, it is important to note that retinal input during both conditions remains comparable. Thus, our findings underscore the value of comparing detection thresholds and suppression dynamics across conditions to better understand the visual mechanisms underpinning saccadic suppression.

In conclusion, our work highlights the critical role of visual mechanisms in saccadic suppression, emphasizing the influence of stimulus-stimulus interactions and challenging traditional motor-based explanations. These insights refine our understanding of visual stability and open new avenues for exploring context-dependent visual processing in naturalistic settings.

Chapter 1.2 Dependence of Perceptual Saccadic Suppression on Peri-Saccadic Image Flow Properties and Luminance Contrast Polarity

Experimental Setup (Publication 2)

Building on our prior retinal findings, which demonstrated that saccadic suppression originates as a visual phenomenon within the retina, we conducted a series of psychophysics experiments to explore perceptual dependencies of saccadic suppression in human observers. Subjects performed saccades across various backgrounds, including uniform fields, luminance stripes, and luminance edges (Figure 1a). Peri-saccadic contrast thresholds were measured using brief flashes, systematically varying luminance contrast polarity. To isolate visual contributions, additional experiments utilized simulated saccades, where backgrounds moved across the retina during fixation (Figure 2). These methods allowed us to disentangle visual from motor-related mechanisms.

Key Observations (Publication 2)

Saccades across uniform gray backgrounds induced minimal suppression. However, saccades over luminance-defined features, such as stripes or edges, significantly elevated perceptual thresholds, indicating stronger suppression (Figure 4c). This effect depended heavily on the interaction between the stimulus and the background. Suppression was strongest when stimuli appeared on darker backgrounds, with dark stimuli experiencing more suppression than bright ones. Conversely, on bright backgrounds, both positive and negative polarity flashes were suppressed equally strongly (Figure 6).

Simulated saccades replicated these stimulus-background interactions. Notably, stimulus polarity significantly influenced suppression strength; flashes with negative polarity on dark backgrounds experienced greater suppression than positive polarity flashes under the same conditions (Figures 8b-c).

Discussion (Publication 2)

Our results further support the hypothesis that saccadic suppression is fundamentally visual, driven by interactions between stimulus properties and background context. Consistent with previous studies, suppression strength varied depending on the nature of the visual flow during saccades (*Publication 1*; Zimmermann, 2020). For instance, the presence of luminance edges enhanced suppression compared to uniform backgrounds. This highlights the critical role of visual context, as suppression was most pronounced in conditions with greater luminance contrast transitions.

The dependency on stimulus polarity adds another layer of complexity. We observed that negative polarity flashes on dark backgrounds consistently produced stronger suppression than positive polarity flashes. This result is intriguing, as one might have expected weaker suppression for dark flashes based on our previous work in the retina, where OFF RGCs exhibit weaker suppression (Idrees et al., 2022).

Importantly, our simulated saccade experiments demonstrated that these effects persist in the absence of motor commands, providing compelling evidence for the dominance of visual mechanisms. By replicating suppression patterns observed during real saccades, we confirmed that suppression originates from visual-visual

interactions, rather than relying solely on extraretinal signals such as corollary discharge.

The temporal dynamics of suppression offer new insights into how the visual system maintains stability. The prolonged suppression observed during simulated saccades suggests that motor signals primarily serve to refine the timing of suppression, ensuring rapid recovery of visual sensitivity post-saccadic.

Chapter Summary

My work on saccadic suppression supports an interplay between visual and motor mechanisms: while the initial suppression, its image dependencies and stimulus interaction appear to be visual, motor mechanisms shape the time course and our perception during saccades. Visual mechanisms limit visual input for later stages in the brain. Motor mechanisms do not necessarily contribute to the suppression of stimuli presented during the saccade; their role seems more nuanced in the context of maintaining overall visual stability, through spatial selective visual processing around the time of an eye-movement.

Therefore, my subsequent work shifted attention more toward these motor-related processes. Specifically, I sought to understand how motor signals from the superior colliculus contribute to visual stability; not necessarily as the primary source of suppression, as traditionally believed, but potentially as modulatory components. This perspective led me to investigate the long-held view of motor bursts in the intermediate and deep layers of the SC as saccade controllers. Historically characterized as purely motor commands for saccade execution, I questioned whether these bursts might play a broader role in integrating sensory information and supporting visual stability.

Chapter 2 Sensory Tuning in Neuronal Movement Commands

Before delving into sensory tuning within the neuronal movement commands of the SC, it is essential to mention two pivotal publications from us that paved the way for this study.

First, Malevich et al. (2022) investigated the visual responses of SC neurons in two macaque monkeys to discs of varying contrast, including both positive and negative luminance polarity. The study revealed that SC neurons exhibit diverse sensitivities to dark and bright stimuli. Interestingly, most neurons displayed faster response latencies to dark stimuli, regardless of their overall sensitivity preference. Even neurons with stronger responses to bright stimuli demonstrated smaller latencies for dark stimuli. This dissociation between response latency and sensitivity indicates that the SC supports temporal prioritization in visual processing, likely aiding rapid detection of critical environmental features. This is consistent with even earlier work from the lab with spatial frequencies (Chen & Hafed, 2018).

Second, Zhang et al. (2022) challenged the classical view that the strength of SC motor bursts directly encodes eye velocity during saccades. By recording motor bursts from saccade-related neurons, the study found asymmetric motor burst strengths for saccades directed to the upper versus lower visual fields, yet the kinematics of these movements remained consistent. Furthermore, a comparison of visually guided and memory-guided saccades revealed that SC neurons could exhibit significantly different motor burst strengths despite matched saccade metrics across tasks. These findings suggest that SC motor burst strength reflects more complex, task-dependent neural processes rather than directly encoding movement dynamics.

With the finding in mind that the motor burst is drastically altered by the presence of a visual saccade target, we aimed to further narrow down what is encoded in the rate code of saccade-related SC neurons.

Experimental Setup (Publication 3)

We let two rhesus macaques (*Macaca mulatta*) perform visually guided and delayed saccades toward a range of saccade targets, including gratings, discs, and real-life

object images. Neural activity was recorded from the intermediate and deep SC layers using electrode arrays, focusing on movement-related response fields.

In the delayed visually guided saccade paradigm, saccade targets were gratings with different spatial frequencies, contrasts, and orientations. In another set of experiments, natural object images and their scrambled counterparts were used to test high-level sensory tuning. In a further set we tested visually guided saccades without delay period to discs varying in contrast and polarity. By vector-matching saccades across different conditions within each image manipulation, we ensured that any observed differences in motor bursts were attributable to visual properties of the targets rather than saccade kinematics.

Key Observations (Publication 3)

Sensory tuning in SC motor bursts was evident across all tested conditions, with motor bursts modulating according to the visual features of saccade targets (Figure 2a and 4b). In Figure 1f we see an example neuron's activity; gratings with lower spatial frequencies elicited stronger motor bursts compared to higher spatial frequencies, demonstrating a clear feature dependency. At the population level, motor bursts consistently exhibited stronger feature discrimination than visual bursts, particularly during the perisaccadic period, underscoring the SC’s robust sensory function (Figure 3). Real-life object images further emphasized the ecological relevance of this tuning, as they elicited stronger motor bursts than their scrambled versions, reflecting the SC’s sensitivity to behaviorally meaningful stimuli (Figure 4b). Notably, SC motor bursts transformed peripheral visual target representations by amplifying weaker visual signals, such as mid-spatial frequencies and lower contrasts, in contrast to their initial visual responses (Figure 3d, e and f). In Figure 2b-f we controlled for saccade kinematics, which remain unchanged despite the differences in motor burst strengths, supporting that the rate code of these bursts encodes visual properties of the saccade target.

Discussion (Publication 3)

Our findings challenge the classical view of SC motor bursts as purely motor signals, revealing their robust sensory tuning. This dual role supports a more nuanced understanding of the SC’s function in bridging sensory and motor domains. The sensory information embedded in motor bursts provides an internal estimate of

saccade target appearance, likely aiding visual stability during the rapid retinal shifts caused by saccades.

Importantly, sensory tuning in SC motor bursts persisted across all tested image manipulations, from simple features like contrast to complex real-life objects. This suggests that SC motor commands are intrinsically sensory-modulated, with their strength reflecting the visual salience and coherence of targets. Furthermore, the transformation of visual signals within motor bursts, particularly the amplified representation of weaker stimuli.

The ecological relevance of these findings is underscored by the SC's preferential tuning to coherent, naturalistic stimuli: the tuning is strongest for real-life objects. This highlights the SC's role in prioritizing salient environmental features, a critical function for adaptive behavior in dynamic settings.

Finally, the observed dissociation between SC motor burst modulation and saccade kinematics strengthens the argument that sensory signals dominate SC activity during saccades. This aligns with predictive coding models, where the brain anticipates sensory disruptions and adjusts processing accordingly. In 2011, Melcher predicted that visual brain structures involved in remapping and encoding object features, such as the FEF and LIP, should also be capable of remapping these features, not just the spatial pointer (Melcher, 2011). By providing a sensory preview of saccade targets, SC motor bursts likely facilitate transsaccadic integration and visual stability, ensuring seamless perception across eye movements.

Chapter 3.1 Perisaccadic Perceptual Mislocalization Strength Depends on the Visual Appearance of Saccade Targets

Perisaccadic perceptual mislocalization, where briefly presented visual stimuli are perceived at erroneous locations during eye movements, offers key insights into how the brain integrates sensory and motor information to maintain perceptual stability. This phenomenon is closely tied to the process of remapping, where neural mechanisms align visual and motor reference frames during saccades to stabilize our visual experience despite rapid retinal shifts. Traditionally, remapping has been considered primarily a motor-driven process, relying on corollary discharge signals from motor regions such as the superior colliculus. However, the previous chapter presented evidence suggesting that these signals may also integrate sensory information about saccade targets, challenging traditional views and reshaping our understanding of their role in perceptual stability.

The finding that SC motor bursts encode sensory information about saccade targets during movements fundamentally challenged the classical view of these signals as purely motoric. This led us to ask: if SC motor bursts integrate sensory and motor information, how does this integration influence perisaccadic remapping and the resulting perceptual mislocalization?

Experimental Setup Human Psychophysics (Publication 4)

To explore these questions, we investigated how the visual appearance of saccade targets influences perisaccadic mislocalization. Eight human participants performed a visual localization task, fixating a spot before making a saccade toward a Gabor grating of either low (0.5 cycles/deg) or high (5 cycles/deg) spatial frequency. During saccades, a brief, high-contrast probe was flashed at various temporal intervals relative to saccade onset, and participants used a mouse cursor to report its perceived location (Figure 1). Eye movements were recorded with a video-based eye tracker at 1 kHz, and the experiment was conducted in a dark room with stimuli presented on a calibrated CRT display. Key analyses included Euclidean distance measures between actual and reported probe locations to quantify mislocalization and statistical tests to determine the effects of target spatial frequency and flash timing. Additional control experiments verified that probe visibility was unaffected by target appearance.

Key Observations (Publication 4)

We demonstrate that perisaccadic mislocalization is more pronounced when saccades are directed toward low spatial frequency targets compared to high-frequency ones, particularly during the saccadic and early post-saccadic periods (Figures 2–4). Additionally, mislocalization showed a clear dependence on the visual field, with stronger effects observed for probes presented in the upper visual field, aligning with known asymmetries in the superior colliculus (Figure 5).

There was a strong correlation between secondary eye movements during the response phase and the reported probe locations, indicating that spatial encoding was consistent across response modalities (Figure 6). Furthermore, my colleague Anna Denninger conducted experiments confirming that probe visibility remained consistent regardless of the target's spatial frequency, ruling out visibility differences as a confound (Figures 7–8). These findings suggest that the visual appearance of saccade targets significantly influences perisaccadic mislocalization.

Discussion (Publication 4)

Our results demonstrate that the appearance of the saccade influences the mislocalization. This aligns with our evidence showing that SC motor bursts vary depending on target appearance, even when saccade vectors remain identical. This visual feature encoding in SC motor bursts may enhance predictive processes essential for trans-saccadic perception.

The stronger mislocalization observed for low spatial frequency targets suggests that corollary discharge signals are not solely spatial but are modulated by the sensory features of saccade targets. This aligns with findings by Lappe et al. (2000) and Ross et al. (1997), who described the interaction between visual context and mislocalization patterns. Our results further extend this work by showing how specific target features can alter the internal mapping of visual space, supporting models that integrate sensory magnification and predictive coding in the SC.

Stronger mislocalization for upper visual field probes highlights the influence of SC asymmetries. The SC’s greater magnification of the upper visual field likely amplifies these perceptual effects. These SC-driven asymmetries differ from the cortical biases seen in non-saccadic tasks, where lower visual field advantages dominate,

underscoring the SC's unique role in perisaccadic processing and its interaction with cortical spatial mechanisms.

Our findings also support models of perisaccadic mislocalization, such as the compression effect, which attributes probe position convergence to retinotopic shifts on distorted visual maps. The SC's topographic distortions, coupled with visual feature tuning, may enrich these models by introducing feature-specific dynamics alongside spatial factors (Ross et al., 1997; VanRullen, 2004).

Control experiments confirmed that differences in mislocalization were not due to variations in probe visibility. High-contrast probes were equally detectable across spatial frequency conditions, eliminating simple visual-visual interactions as a confound. Instead, these results point to a complex interplay between visual and motor signals, mediated by SC pathways and its downstream targets, such as the pulvinar and medial-dorsal thalamus. These structures, involved in relaying CD, likely integrate spatial and feature-specific information for cortical processing.

Chapter 3.2 Two-Dimensional Perisaccadic Visual Mislocalization in Rhesus Macaque Monkeys

Experimental Setup Monkey Behavior (Publication 5)

This study explored perisaccadic visual mislocalization in rhesus macaques using a novel two-dimensional paradigm. Data were collected from three adult male monkeys trained to perform a saccade sequence. Each trial began with fixation on an eccentric target, followed by a visually-guided saccade toward a central Gabor grating. Once the saccade onset was detected, a brief (12 ms) visual probe flash was presented at one of three positions relative to the saccade target. After a delay, the monkeys made a memory-guided saccade to the perceived flash location (Figure 1). Eye movements were recorded with high precision using the scleral search coil technique. This design enabled comparisons of reported flash positions across different saccade directions and flash timings to evaluate mislocalization patterns (Figure 3).

Key Observations (Publication 5)

We found strong perisaccadic mislocalization in all three monkeys, consistent with human results. Backward mislocalization toward the saccade target was most

pronounced for probe flashes presented shortly after saccade onset (30 ms). To observe mislocalization only towards the saccade target was expected, given our postsaccadic presentations. It is reported that mislocalization away from the saccade target takes place only when the probe flashes were presented presaccadically, and in complete darkness (Honda, 1991). Additionally, our effect varied systematically with saccade direction. Mislocalization was stronger for upward saccades than for downward ones, as shown in Figures 5A–C and 6. Horizontal saccades also exhibited stronger mislocalization for flashes in the upper visual field compared to the lower field, same as the human results in *Publication 4*. These results are detailed in Figures 9A–E, which illustrate mislocalization strength and recovery over time.

Discussion (Publication 5)

This study successfully demonstrated that rhesus macaques exhibit two-dimensional perisaccadic visual mislocalization, similar to humans. The results confirm that mislocalization strength depends on both saccade direction and visual field location. Stronger mislocalization for upward saccades, as reported here, aligns with prior human studies and reflects differences in visual processing between the upper and lower visual fields (Grujic et al., 2018). This finding suggests that neural circuits in the superior colliculus and other sensory-motor integration areas may underlie these effects. Importantly, the paradigm was robust across different saccade directions, paving the way for future neurophysiological investigations to explore the underlying mechanisms.

While subtle effects of saccade target appearance on mislocalization were noted, they were less consistent than the directional influences. The small but consistent visual dependency that we saw across the majority of participants in the human study (*Publication 4*), may have been hidden in the variability of the monkeys' reports. However, we cannot exclude the possibility that monkeys do not show this dependency. We systematically analyzed baseline trials to verify that memory-guided errors were minor compared to perisaccadic mislocalization, reinforcing the reliability of the paradigm. Overall, this work establishes a critical methodological framework for translating human perceptual findings to animal models, contributing to the understanding of sensory-motor integration during eye movements.

Beyond mislocalization, these results support a broader role for SC-driven corollary discharge in trans-saccadic feature integration, ensuring seamless visual continuity across eye movements. Future work could explore how SC projections modulate cortical visual responses during saccades and further investigate the feature tuning properties of relay areas like the pulvinar and medial-dorsal thalamus to clarify their contributions to saccade-related visual processing. In all, this study established a methodological advance that will allow future neurophysiological discoveries about perisaccadic perception.

References

Awater, H., Burr, D., Lappe, M., Morrone, M. C., & Goldberg, M. E. (2005). Effect of saccadic adaptation on localization of visual targets. *Journal of neurophysiology*, *93*(6), 3605-3614.

Basso, M. A., & May, P. J. (2017). Circuits for action and cognition: a view from the superior colliculus. *Annual review of vision science*, *3*(1), 197-226.

Berman, R. A., Cavanaugh, J., McAlonan, K., & Wurtz, R. H. (2017). A circuit for saccadic suppression in the primate brain. *Journal of neurophysiology*, *117*(4), 1720-1735.

Berman, R. A., & Wurtz, R. H. (2008). Exploring the pulvinar path to visual cortex. *Progress in brain research*, *171*, 467-473.

Berman, R. A., & Wurtz, R. H. (2010). Functional identification of a pulvinar path from superior colliculus to cortical area MT. *Journal of Neuroscience*, *30*(18), 6342-6354.

Berman, R. A., & Wurtz, R. H. (2011). Signals conveyed in the pulvinar pathway from superior colliculus to cortical area MT. *Journal of Neuroscience*, *31*(2), 373-384.

Binda, P., & Morrone, M. C. (2022). Vision: Optimizing each glimpse. *Current Biology*, *32*(12), R567-R569.

Bogadhi, A. R., & Hafed, Z. M. (2023). Express detection of visual objects by primate superior colliculus neurons. *Scientific Reports*, *13*(1), 21730.

Bogadhi, A. R., Katz, L. N., Bollimunta, A., Leopold, D. A., & Krauzlis, R. J. (2021). Midbrain activity shapes high-level visual properties in the primate temporal cortex. *Neuron*, *109*(4), 690-699. e695.

Bremmer, F., Kubischik, M., Hoffmann, K.-P., & Krekelberg, B. (2009). Neural Dynamics of Saccadic Suppression. *The Journal of Neuroscience*, *29*(40), 12374-12383. https://doi.org/10.1523/jneurosci.2908-09.2009

Bruce, C. J., Desimone, R., & Gross, C. G. (1986). Both striate cortex and superior colliculus contribute to visual properties of neurons in superior temporal polysensory area of macaque monkey. *Journal of neurophysiology*, *55*(5), 1057-1075.

Burr, D. C., & Morrone, M. C. (2011). Spatiotopic coding and remapping in humans. *Philosophical Transactions of the Royal Society B: Biological Sciences*, *366*(1564), 504-515.

Burr, D. C., Morrone, M. C., & Ross, J. (1994). Selective suppression of the magnocellular visual pathway during saccadic eye movements. *Nature*, *371*(6497), 511-513.

Campbell, F. W., & Wurtz, R. H. (1978). Saccadic omission: why we do not see a grey-out during a saccadic eye movement. *Vision research*, *18*(10), 1297-1303.

Carello, C. D., & Krauzlis, R. J. (2004). Manipulating intent: evidence for a causal role of the superior colliculus in target selection. *Neuron*, *43*(4), 575-583.

Cavanagh, P., Hunt, A. R., Afraz, A., & Rolfs, M. (2010). Visual stability based on remapping of attention pointers. *Trends in cognitive sciences*, *14*(4), 147-153.

Cavanaugh, J., Berman, R. A., Joiner, W. M., & Wurtz, R. H. (2016). Saccadic corollary discharge underlies stable visual perception. *Journal of Neuroscience*, *36*(1), 31-42.

Chapot, C. A., Behrens, C., Rogerson, L. E., Baden, T., Pop, S., Berens, P., Euler, T., & Schubert, T. (2017). Local signals in mouse horizontal cell dendrites. *Current Biology*, *27*(23), 3603-3615. e3605.

Chen, C.-Y., & Hafed, Z. M. (2017). A neural locus for spatial-frequency specific saccadic suppression in visual-motor neurons of the primate superior colliculus. *Journal of neurophysiology*, *117*(4), 1657-1673.

Chen, C.-Y., & Hafed, Z. M. (2018). Orientation and contrast tuning properties and temporal flicker fusion characteristics of primate superior colliculus neurons. *Frontiers in neural circuits*, *12*, 58.

Chen, C.-Y., Hoffmann, K.-P., Distler, C., & Hafed, Z. M. (2019). The foveal visual representation of the primate superior colliculus. *Current Biology*, *29*(13), 2109-2119. e2107.

Chen, C.-Y., Ignashchenkova, A., Thier, P., & Hafed, Z. M. (2015). Neuronal response gain enhancement prior to microsaccades. *Current Biology*, *25*(16), 2065-2074.
Crapse, T. B., Lau, H., & Basso, M. A. (2018). A role for the superior colliculus in decision criteria. *Neuron*, *97*(1), 181-194. e186.
Crapse, T. B., & Sommer, M. A. (2008). Corollary discharge circuits in the primate brain. *Current opinion in neurobiology*, *18*(6), 552-557.
Cynader, M., & Berman, N. (1972). Receptive-field organization of monkey superior colliculus. *Journal of neurophysiology*, *35*(2), 187-201.
Deubel, H., & Schneider, W. X. (1996). Saccade target selection and object recognition: Evidence for a common attentional mechanism. *Vision research*, *36*(12), 1827-1837.
Deubel, H., Schneider, W. X., & Bridgeman, B. (2002). Transsaccadic memory of position and form. *Progress in brain research*, *140*, 165-180.
Dodge, R. (1900). Visual perception during eye movement. *Psychological review*, *7*(5), 454.
Duffy, F. H., & Burchfiel, J. L. (1975). Eye movement-related inhibition of primate visual neurons. *Brain Research*, *89*(1), 121-132.
Duhamel, J.-R., Colby, C. L., & Goldberg, M. E. (1992). The updating of the representation of visual space in parietal cortex by intended eye movements. *Science*, *255*(5040), 90-92.
Erdmann, B., & Dodge, R. (1898). *Psychologische Untersuchungen über das Lesen auf experimenteller Grundlage*. Niemeyer.
Fahrenfort, J. J., Scholte, H. S., & Lamme, V. A. (2007). Masking disrupts reentrant processing in human visual cortex. *Journal of cognitive neuroscience*, *19*(9), 1488-1497.
Falkner, A. L., Krishna, B. S., & Goldberg, M. E. (2010). Surround suppression sharpens the priority map in the lateral intraparietal area. *Journal of Neuroscience*, *30*(38), 12787-12797.
Freeman, J., Field, G. D., Li, P. H., Greschner, M., Gunning, D. E., Mathieson, K., Sher, A., Litke, A. M., Paninski, L., & Simoncelli, E. P. (2015). Mapping nonlinear receptive field structure in primate retina at single cone resolution. *ELife*, *4*, e05241.
Gandhi, N. J., & Katnani, H. A. (2011). Motor functions of the superior colliculus. *Annual review of neuroscience*, *34*(1), 205-231.
Goldberg, M. E., & Wurtz, R. H. (1972). Activity of superior colliculus in behaving monkey. I. Visual receptive fields of single neurons. *Journal of neurophysiology*, *35*(4), 542-559.
Gottlieb, J. P., Kusunoki, M., & Goldberg, M. E. (1998). The representation of visual salience in monkey parietal cortex. *Nature*, *391*(6666), 481-484.
Grujic, N., Brehm, N., Gloge, C., Zhuo, W., & Hafed, Z. M. (2018). Perisaccadic perceptual mislocalization is different for upward saccades. *Journal of neurophysiology*, *120*(6), 3198-3216.
Hafed, Z. M. (2024). Superior colliculus peri-saccadic field potentials are dominated by a visual sensory preference for the upper visual field. *bioRxiv*, 2024.2010. 2030.621170.
Hafed, Z. M., & Chen, C.-Y. (2016). Sharper, stronger, faster upper visual field representation in primate superior colliculus. *Current Biology*, *26*(13), 1647-1658.
Hafed, Z. M., Chen, C.-Y., & Khademi, F. (2022). Superior colliculus visual neural sensitivity at the lower limit of natural self-induced image displacements. *bioRxiv*, 2022.2006. 2026.497631.
Hafed, Z. M., Chen, C.-Y., & Tian, X. (2015). Vision, perception, and attention through the lens of microsaccades: mechanisms and implications. *Frontiers in systems neuroscience*, *9*, 167.
Hafed, Z. M., Chen, C.-Y., Tian, X., Baumann, M. P., & Zhang, T. (2021). Active vision at the foveal scale in the primate superior colliculus. *Journal of neurophysiology*, *125*(4), 1121-1138.
Hafed, Z. M., Hoffmann, K.-P., Chen, C.-Y., & Bogadhi, A. R. (2023). Visual functions of the primate superior colliculus. *Annual review of vision science*, *9*(1), 361-383.

Hafed, Z. M., Idrees, S., & Baumann, M. P. (2024). Not so early! Revisiting the question of visual pathway selectivity of saccadic suppression. In (Vol. 132, pp. 570-572): American Physiological Society Rockville, MD.
Hafed, Z. M., & Krauzlis, R. J. (2010). Microsaccadic suppression of visual bursts in the primate superior colliculus. *Journal of Neuroscience*, *30*(28), 9542-9547.
Hamker, F. H., Zirnsak, M., & Lappe, M. (2008). About the influence of post-saccadic mechanisms for visual stability on peri-saccadic compression of object location. *Journal of vision*, *8*(14), 1-1.
Heikkinen, H., Nymark, S., & Koskelainen, A. (2008). Mouse cone photoresponses obtained with electroretinogram from the isolated retina. *Vision research*, *48*(2), 264-272.
Henderson, J. M. (1997). Transsaccadic memory and integration during real-world object perception. *Psychological Science*, *8*(1), 51-55.
Hoffman, D. D. (2012). The construction of visual reality. *Hallucinations: Research and practice*, 7-15.
Hoggarth, A., McLaughlin, A. J., Ronellenfitch, K., Trenholm, S., Vasandani, R., Sethuramanujam, S., Schwab, D., Briggman, K. L., & Awatramani, G. B. (2015). Specific wiring of distinct amacrine cells in the directionally selective retinal circuit permits independent coding of direction and size. *Neuron*, *86*(1), 276-291.
Hollingworth, A., Richard, A. M., & Luck, S. J. (2008). Understanding the function of visual short-term memory: transsaccadic memory, object correspondence, and gaze correction. *Journal of Experimental Psychology: General*, *137*(1), 163.
Honda, H. (1991). The time courses of visual mislocalization and of extraretinal eye position signals at the time of vertical saccades. *Vision research*, *31*(11), 1915-1921.
Ibbotson, M., & Krekelberg, B. (2011). Visual perception and saccadic eye movements. *Current opinion in neurobiology*, *21*(4), 553-558.
Ibbotson, M. R., & Cloherty, S. L. (2009). Visual perception: saccadic omission—suppression or temporal masking? *Current Biology*, *19*(12), R493-R496.
Idrees, S., Baumann, M.-P., Korympidou, M. M., Schubert, T., Kling, A., Franke, K., Hafed, Z. M., Franke, F., & Münch, T. A. (2022). Suppression without inhibition: how retinal computation contributes to saccadic suppression. *Communications Biology*, *5*(1), 692.
Irwin, D. E. (1991). Information integration across saccadic eye movements. *Cognitive psychology*, *23*(3), 420-456.
Isa, T., & Hall, W. C. (2009). Exploring the superior colliculus in vitro. *Journal of neurophysiology*, *102*(5), 2581-2593.
Kagan, I., Gur, M., & Snodderly, D. M. (2008). Saccades and drifts differentially modulate neuronal activity in V1: effects of retinal image motion, position, and extraretinal influences. *Journal of vision*, *8*(14), 19-19.
Kaiser, M., & Lappe, M. (2004). Perisaccadic mislocalization orthogonal to saccade direction. *Neuron*, *41*(2), 293-300.
Katz, L. N., Yu, G., & Krauzlis, R. J. (2024). Visual activity in primate superior colliculus depends on visual cortex. *Journal of vision*, *24*(10), 744-744.
Kim, B., & Basso, M. A. (2008). Saccade target selection in the superior colliculus: a signal detection theory approach. *Journal of Neuroscience*, *28*(12), 2991-3007.
Kleiser, R., Seitz, R. J., & Krekelberg, B. (2004). Neural correlates of saccadic suppression in humans. *Current Biology*, *14*(5), 386-390.
Krauzlis, R. J., Lovejoy, L. P., & Zénon, A. (2013). Superior colliculus and visual spatial attention. *Annual review of neuroscience*, *36*(1), 165-182.
Krekelberg, B. (2010). Saccadic suppression. *Current Biology*, *20*(5), R228-R229.
Krock, R. M., & Moore, T. (2016). Visual sensitivity of frontal eye field neurons during the preparation of saccadic eye movements. *Journal of neurophysiology*, *116*(6), 2882-2891.
Latour, P. (1962). Visual threshold during eye movements. *Vision research*, *2*(3), 261-262.

Lee, P. H., Sooksawate, T., Yanagawa, Y., Isa, K., Isa, T., & Hall, W. C. (2007). Identity of a pathway for saccadic suppression. *Proceedings of the National Academy of Sciences*, *104*(16), 6824-6827.

Lencer, R., Meyhöfer, I., Triebsch, J., Rolfes, K., Lappe, M., & Watson, T. (2021). Saccadic suppression in schizophrenia. *Scientific Reports*, *11*(1), 13133.

MacKay, D. (1970a). Elevation of visual threshold by displacement of retinal image. *Nature*, *225*(5227), 90-92.

MacKay, D. (1970b). Interocular transfer of suppressive effects of retinal image displacement. *Nature*, *225*(5235), 872-873.

Maier, A., Wilke, M., Aura, C., Zhu, C., Ye, F. Q., & Leopold, D. A. (2008). Divergence of fMRI and neural signals in V1 during perceptual suppression in the awake monkey. *Nature neuroscience*, *11*(10), 1193-1200.

Maior, R. S., Hori, E., Uribe, C. E., Saletti, P. G., Ono, T., Nishijo, H., & Tomaz, C. (2012). A role for the superior colliculus in the modulation of threat responsiveness in primates: toward the ontogenesis of the social brain. *Reviews in the Neurosciences*, *23*(5-6), 697-706.

Malevich, T., Yu, Y., Baumann, M. P., Zhang, T., & Hafed, Z. M. (2024). Sound activates a dormant visual-motor pathway bypassing primary visual cortex. *Journal of vision*, *24*(10), 532-532.

Malevich, T., Zhang, T., Baumann, M. P., Bogadhi, A. R., & Hafed, Z. M. (2022). Faster detection of “darks” than “brights” by monkey superior colliculus neurons. *Journal of Neuroscience*, *42*(50), 9356-9371.

Matin, E. (1974). Saccadic suppression: a review and an analysis. *Psychological bulletin*, *81*(12), 899.

Matin, E., Clymer, A. B., & Matin, L. (1972). Metacontrast and saccadic suppression. *Science*, *178*(4057), 179-182.

May, P. J. (2006). The mammalian superior colliculus: laminar structure and connections. *Progress in brain research*, *151*, 321-378.

Mazade, R. E., Flood, M. D., & Eggers, E. D. (2019). Dopamine D1 receptor activation reduces local inner retinal inhibition to light-adapted levels. *Journal of neurophysiology*, *121*(4), 1232-1243.

Melcher, D. (2005). Spatiotopic transfer of visual-form adaptation across saccadic eye movements. *Current Biology*, *15*(19), 1745-1748.

Melcher, D. (2011). Visual stability. In (Vol. 366, pp. 468-475): The Royal Society.

Melcher, D., & Colby, C. L. (2008). Trans-saccadic perception. *Trends in cognitive sciences*, *12*(12), 466-473.

Nassi, J. J., & Callaway, E. M. (2009). Parallel processing strategies of the primate visual system. *Nature reviews neuroscience*, *10*(5), 360-372.

Nguyen, M. N., Matsumoto, J., Hori, E., Maior, R. S., Tomaz, C., Tran, A. H., Ono, T., & Nishijo, H. (2014). Neuronal responses to face-like and facial stimuli in the monkey superior colliculus. *Frontiers in Behavioral Neuroscience*, *8*, 85.

Nguyen, M. N., Nishimaru, H., Matsumoto, J., Van Le, Q., Hori, E., Maior, R. S., Tomaz, C., Ono, T., & Nishijo, H. (2016). Population coding of facial information in the monkey superior colliculus and pulvinar. *Frontiers in neuroscience*, *10*, 583.

O'regan, J. K. (1992). Solving the" real" mysteries of visual perception: the world as an outside memory. *Canadian Journal of Psychology/Revue canadienne de psychologie*, *46*(3), 461.

Ostendorf, F., Fischer, C., Finke, C., & Ploner, C. J. (2007). Perisaccadic compression correlates with saccadic peak velocity: differential association of eye movement dynamics with perceptual mislocalization patterns. *Journal of Neuroscience*, *27*(28), 7559-7563.

Peysakhovich, B., Zhu, O., Tetrick, S. M., Shirhatti, V., Silva, A. A., Li, S., Ibos, G., Rosen, M. C., Johnston, W. J., & Freedman, D. J. (2024). Primate superior colliculus is causally engaged in abstract higher-order cognition. *Nature neuroscience*, 1-10.

Phongphanphanee, P., Marino, R. A., Kaneda, K., Yanagawa, Y., Munoz, D. P., & Isa, T. (2014). Distinct local circuit properties of the superficial and intermediate layers of the rodent superior colliculus. *European Journal of Neuroscience*, *40*(2), 2329-2343.
Phongphanphanee, P., Mizuno, F., Lee, P. H., Yanagawa, Y., Isa, T., & Hall, W. C. (2011). A circuit model for saccadic suppression in the superior colliculus. *Journal of Neuroscience*, *31*(6), 1949-1954.
Podvalny, E., Yeagle, E., Mégevand, P., Sarid, N., Harel, M., Chechik, G., Mehta, A. D., & Malach, R. (2017). Invariant temporal dynamics underlie perceptual stability in human visual cortex. *Current Biology*, *27*(2), 155-165.
Poiese, P., Spalek, T. M., & Di Lollo, V. (2008). Attentional involvement in subitizing: Questioning the preattentive hypothesis. *Visual Cognition*, *16*(4), 474-485.
Quaia, C., & Krauzlis, R. J. (2024). Object recognition in primates: what can early visual areas contribute? *Frontiers in Behavioral Neuroscience*, *18*, 1425496.
Rajkai, C., Lakatos, P., Chen, C.-M., Pincze, Z., Karmos, G., & Schroeder, C. E. (2008). Transient cortical excitation at the onset of visual fixation. *Cerebral cortex*, *18*(1), 200-209.
Ramachandran, V. S., & Cobb, S. (1995). Visual attention modulates metacontrast masking. *Nature*, *373*(6509), 66-68.
Ramcharan, E., Gnadt, J., & Sherman, S. (2001). The effects of saccadic eye movements on the activity of geniculate relay neurons in the monkey. *Visual neuroscience*, *18*(2), 253-258.
Reppas, J. B., Usrey, W. M., & Reid, R. C. (2002). Saccadic eye movements modulate visual responses in the lateral geniculate nucleus. *Neuron*, *35*(5), 961-974.
Richards, W. (1968). Visual suppression during passive eye movement. *JOSA*, *58*(8), 1159-1160.
Riggs, L., Merton, P., & Morton, H. (1974). Suppression of visual phosphenes during saccadic eye movements. *Vision research*, *14*(10), 997-1011.
Robinson, D. A. (1972). Eye movements evoked by collicular stimulation in the alert monkey. *Vision research*, *12*(11), 1795-1808.
Robinson, D. L., & Wurtz, R. H. (1976). Use of an extraretinal signal by monkey superior colliculus neurons to distinguish real from self-induced stimulus movement. *Journal of neurophysiology*, *39*(4), 852-870.
Rolfs, M., Jonikaitis, D., Deubel, H., & Cavanagh, P. (2011). Predictive remapping of attention across eye movements. *Nature neuroscience*, *14*(2), 252-256.
Ross, J., Morrone, M. C., & Burr, D. C. (1997). Compression of visual space before saccades. *Nature*, *386*(6625), 598-601.
Ross, J., Morrone, M. C., Goldberg, M. E., & Burr, D. C. (2001). Changes in visual perception at the time of saccades. *Trends in neurosciences*, *24*(2), 113-121.
Rossi, E. A., & Roorda, A. (2010). The relationship between visual resolution and cone spacing in the human fovea. *Nature neuroscience*, *13*(2), 156-157.
Royal, D. W., Sary, G., Schall, J., & Casagrande, V. (2006). Correlates of motor planning and postsaccadic fixation in the macaque monkey lateral geniculate nucleus. *Experimental brain research*, *168*, 62-75.
Schiller, P. H., Sandell, J. H., & Maunsell, J. H. (1987). The effect of frontal eye field and superior colliculus lesions on saccadic latencies in the rhesus monkey. *Journal of neurophysiology*, *57*(4), 1033-1049.
Schiller, P. H., & Stryker, M. (1972). Single-unit recording and stimulation in superior colliculus of the alert rhesus monkey. *Journal of neurophysiology*, *35*(6), 915-924.
Schiller, P. H., Stryker, M., Cynader, M., & Berman, N. (1974). Response characteristics of single cells in the monkey superior colliculus following ablation or cooling of visual cortex. *Journal of neurophysiology*, *37*(1), 181-194.
Shelley-Tremblay, J., & Mack, A. (1999). Metacontrast masking and attention. *Psychological Science*, *10*(6), 508-515.
Smalianchuk, I., Jagadisan, U. K., & Gandhi, N. J. (2018). Instantaneous midbrain control of saccade velocity. *Journal of Neuroscience*, *38*(47), 10156-10167.

Smith, A. M. (1992). Al Sabra. The Optics of Ibn al-Haytham. Books I, II, II: On Direct Vision. With Translation, Introduction, Commentary, Glossaries. London: The Warburg Institute, 1989. Pp. 735 (in two vols.). ISBN 0-85481-072-2. *The British Journal for the History of Science*, *25*(3), 358-359.
Soares, S. C., Maior, R. S., Isbell, L. A., Tomaz, C., & Nishijo, H. (2017). Fast detector/first responder: interactions between the superior colliculus-pulvinar pathway and stimuli relevant to primates. *Frontiers in neuroscience*, *11*, 67.
Sommer, M. A., & Wurtz, R. H. (2002). A pathway in primate brain for internal monitoring of movements. *Science*, *296*(5572), 1480-1482.
Sommer, M. A., & Wurtz, R. H. (2004). What the brain stem tells the frontal cortex. I. Oculomotor signals sent from superior colliculus to frontal eye field via mediodorsal thalamus. *Journal of neurophysiology*, *91*(3), 1381-1402.
Sommer, M. A., & Wurtz, R. H. (2006). Influence of the thalamus on spatial visual processing in frontal cortex. *Nature*, *444*(7117), 374-377.
Sommer, M. A., & Wurtz, R. H. (2008). Brain circuits for the internal monitoring of movements. *Annu. Rev. Neurosci.*, *31*(1), 317-338.
Sperry, R. W. (1950). Neural basis of the spontaneous optokinetic response produced by visual inversion. *Journal of comparative and physiological psychology*, *43*(6), 482.
Steinmetz, N. A., & Moore, T. (2010). Changes in the response rate and response variability of area V4 neurons during the preparation of saccadic eye movements. *Journal of neurophysiology*, *103*(3), 1171-1178.
Steinmetz, N. A., & Moore, T. (2014). Eye movement preparation modulates neuronal responses in area V4 when dissociated from attentional demands. *Neuron*, *83*(2), 496-506.
Stella, X. Y., & Lee, T. S. (2000). What do V1 neurons tell us about saccadic suppression? *Neurocomputing*, *32*, 271-277.
Stevens, J. K., Emerson, R. C., Gerstein, G. L., Kallos, T., Neufeld, G. R., Nichols, C. W., & Rosenquist, A. C. (1976). Paralysis of the awake human: visual perceptions. *Vision research*, *16*(1), 93-IN99.
Stine, G. M., Trautmann, E. M., Jeurissen, D., & Shadlen, M. N. (2023). A neural mechanism for terminating decisions. *Neuron*, *111*(16), 2601-2613. e2605.
Stryker, M. P., & Schiller, P. H. (1975). Eye and head movements evoked by electrical stimulation of monkey superior colliculus. *Experimental brain research*, *23*, 103-112.
Super, H., van der Togt, C., Spekreijse, H., & Lamme, V. A. (2004). Correspondence of presaccadic activity in the monkey primary visual cortex with saccadic eye movements. *Proceedings of the National Academy of Sciences*, *101*(9), 3230-3235.
Sylvester, R., & Rees, G. (2006). Extraretinal saccadic signals in human LGN and early retinotopic cortex. *Neuroimage*, *30*(1), 214-219.
Tas, A. C., Moore, C. M., & Hollingworth, A. (2012). An object-mediated updating account of insensitivity to transsaccadic change. *Journal of vision*, *12*(11), 18-18.
Thakkar, K. N., Schall, J. D., Heckers, S., & Park, S. (2015). Disrupted saccadic corollary discharge in schizophrenia. *Journal of Neuroscience*, *35*(27), 9935-9945.
Thiele, A., Henning, P., Kubischik, M., & Hoffmann, K.-P. (2002). Neural mechanisms of saccadic suppression. *Science*, *295*(5564), 2460-2462.
Tolias, A. S., Moore, T., Smirnakis, S. M., Tehovnik, E. J., Siapas, A. G., & Schiller, P. H. (2001). Eye movements modulate visual receptive fields of V4 neurons. *Neuron*, *29*(3), 757-767.
VanRullen, R. (2004). A simple translation in cortical log-coordinates may account for the pattern of saccadic localization errors. *Biological cybernetics*, *91*(3), 131-137.
Verweij, J., Kamermans, M., & Spekreijse, H. (1996). Horizontal cells feed back to cones by shifting the cone calcium-current activation range. *Vision research*, *36*(24), 3943-3953.
Volkmann, F. C., Schick, A. M., & Riggs, L. A. (1968). Time course of visual inhibition during voluntary saccades. *JOSA*, *58*(4), 562-569.
Von Helmholtz, H. (1867). *Handbuch der physiologischen Optik* (Vol. 9). Voss.

Von Holst, E., & Mittelstaedt, H. (1950). Das reafferenzprinzip: Wechselwirkungen zwischen zentralnervensystem und peripherie. *Naturwissenschaften*, *37*(20), 464-476.
Walker, M. F., Fitzgibbon, E. J., & Goldberg, M. E. (1995). Neurons in the monkey superior colliculus predict the visual result of impending saccadic eye movements. *Journal of neurophysiology*, *73*(5), 1988-2003.
Wang, L., McAlonan, K., Goldstein, S., Gerfen, C. R., & Krauzlis, R. J. (2020). A causal role for mouse superior colliculus in visual perceptual decision-making. *Journal of Neuroscience*, *40*(19), 3768-3782.
Watson, T., & Krekelberg, B. (2011). An equivalent noise investigation of saccadic suppression. *Journal of Neuroscience*, *31*(17), 6535-6541.
Werner, W., Dannenberg, S., & Hoffmann, K.-P. (1997). Arm-movement-related neurons in the primate superior colliculus and underlying reticular formation: comparison of neuronal activity with EMGs of muscles of the shoulder, arm and trunk during reaching. *Experimental brain research*, *115*, 191-205.
Wurtz, R. H. (2008). Neuronal mechanisms of visual stability. *Vision research*, *48*(20), 2070-2089.
Wurtz, R. H., & Albano, J. E. (1980). Visual-motor function of the primate superior colliculus. *Annual review of neuroscience*, *3*(1), 189-226.
Wurtz, R. H., Joiner, W. M., & Berman, R. A. (2011). Neuronal mechanisms for visual stability: progress and problems. *Philosophical Transactions of the Royal Society B: Biological Sciences*, *366*(1564), 492-503.
Yarbus, A. L. (1967). Eye movements during perception of complex objects. *Eye movements and vision*, 171-211.
Yu, G., Katz, L. N., Quaia, C., Messinger, A., & Krauzlis, R. J. (2024). Short-latency preference for faces in primate superior colliculus depends on visual cortex. *Neuron*, *112*(16), 2814-2822. e2814.
Yu, Z., Turner, M. H., Baudin, J., & Rieke, F. (2022). Adaptation in cone photoreceptors contributes to an unexpected insensitivity of primate On parasol retinal ganglion cells to spatial structure in natural images. *ELife*, *11*, e70611.
Zanos, T. P., Mineault, P. J., Guitton, D., & Pack, C. C. (2016). Mechanisms of saccadic suppression in primate cortical area V4. *Journal of Neuroscience*, *36*(35), 9227-9239.
Zhang, T., Bogadhi, A., & Hafed, Z. M. (2025). Signaling of trans-saccadic prediction error by foveal neurons of the monkey superior colliculus. *bioRxiv*.
Zhang, Y., Valsecchi, M., Gegenfurtner, K. R., & Chen, J. (2024). The execution of saccadic eye movements suppresses visual processing of both color and luminance in the early visual cortex of humans. *Journal of neurophysiology*, *131*(6), 1156-1167.
Zimmermann, E., & Bremmer, F. (2016). Visual neuroscience: The puzzle of perceptual stability. *Current Biology*, *26*(5), R199-R201.
Zimmermann, E., & Lappe, M. (2016). Visual space constructed by saccade motor maps. *Frontiers in Human Neuroscience*, *10*, 225.
Zimmermann, E., Morrone, M. C., & Burr, D. C. (2014). The visual component to saccadic compression. *Journal of vision*, *14*(12), 13-13.
Zirnsak, M., Steinmetz, N. A., Noudoost, B., Xu, K. Z., & Moore, T. (2014). Visual space is compressed in prefrontal cortex before eye movements. *Nature*, *507*(7493), 504-507.
Zuber, B., Semmlow, J., & Stark, L. (1968). Frequency characteristics of the saccadic eye movement. *Biophysical journal*, *8*(11), 1288-1298.

Acknowledgements

Whatever I have accomplished in this dissertation, I could not have done it alone. Many individuals have supported, guided, and inspired me throughout this journey, and I am deeply grateful for their contributions.

First and foremost, my deepest gratitude goes to my supervisor, Ziad, the greatest supervisor I could have asked for. Your passion for science is truly contagious, and I have learned so much from you, not only about research but also about navigating the world of academia. But beyond that, you also showed me a new world. Thanks to you, I had the opportunity to travel to countless conferences across the globe, broadening my academic and personal horizons in ways I could have never imagined.

Your dedication to your students goes far beyond the lab. I will always remember when I was preparing for a job talk while I was six time zones away. You sacrificed several nights, staying up for Zoom calls to help me prepare. That level of commitment and mentorship is rare, and I am incredibly grateful for it. Thank you for putting so much energy, effort, and trust in me, and for your outstanding leadership. I am truly thankful and proud to have been part of the Hafed Lab.

I also want to thank all members of the Hafed Lab, past and present, an amazing group of people who have made this journey so special. A special thanks to Antimo and Amar for teaching me their craft and for their patience in answering my endless stream of questions. Tanya, thank you for our great discussions and for always providing the most honest opinions. Tong, I truly appreciate your willingness to help out whenever needed. Yue, you never ceased to surprise me in the best ways. Anna and Julia, I am grateful for the fantastic collaborations we shared.

I want to thank Saad and Thomas for demonstrating what true collaboration is; an exchange of ideas, refining perspectives, and building something meaningful together. I also appreciate Giulia and Ari for their contributions and for being part of a collaborative environment that has shaped my scientific journey.

A big thank you to the Thier Lab for sharing their space with me and for being so welcoming. Special thanks to Akshay, Uwe and Peter Dicke, whose support and insights were invaluable.

Beyond academia, I am deeply grateful to my parents, Sabine and Wolfgang, my brother, Momo, and my uncle, Jürgen, for their unconditional love and support. Your presence has given me the security to pursue my own path without fear. To my friends and housemates, thank you for always supporting me and keeping me grounded through this process.

Finally, I want to acknowledge the monkeys who participated in this research. Their role has been fundamental in advancing our understanding of the brain, and I recognize the responsibility that comes with conducting animal research. I acknowledge their contribution with the utmost respect and gratitude.

To all those who have supported me in ways big and small, thank you! This work would not have been possible without you!

Appendix A: Publication 1

Perceptual saccadic suppression starts in the retina

Idrees, S., Baumann, M. P., Franke, F., Münch, T. A., & Hafed, Z. M.

Nature Communications, (2020) 11:1977

doi: 10.1038/s41467-020-15890-w.

nature COMMUNICATIONS

ARTICLE

https://doi.org/10.1038/s41467-020-15890-w OPEN

Perceptual saccadic suppression starts in the retina

Saad Idrees[1,5], Matthias P. Baumann[1,2,5], Felix Franke[3], Thomas A. Münch[1,4]✉ & Ziad M. Hafed[1,2]✉

Visual sensitivity, probed through perceptual detectability of very brief visual stimuli, is strongly impaired around the time of rapid eye movements. This robust perceptual phenomenon, called saccadic suppression, is frequently attributed to active suppressive signals that are directly derived from eye movement commands. Here we show instead that visual-only mechanisms, activated by saccade-induced image shifts, can account for all perceptual properties of saccadic suppression that we have investigated. Such mechanisms start at, but are not necessarily exclusive to, the very first stage of visual processing in the brain, the retina. Critically, neural suppression originating in the retina outlasts perceptual suppression around the time of saccades, suggesting that extra-retinal movement-related signals, rather than causing suppression, may instead act to shorten it. Our results demonstrate a far-reaching contribution of visual processing mechanisms to perceptual saccadic suppression, starting in the retina, without the need to invoke explicit motor-based suppression commands.

[1] Werner Reichardt Centre for Integrative Neuroscience, Tübingen University, 72076 Tübingen, Germany. [2] Hertie Institute for Clinical Brain Research, Tübingen University, 72076 Tübingen, Germany. [3] Bio Engineering Laboratory, ETH Zürich, 4058 Basel, Switzerland. [4] Institute for Ophthalmic Research, Tübingen University, 72076 Tübingen, Germany. [5] These authors contributed equally: Saad Idrees, Matthias P. Baumann. ✉email: thomas.muench@uni-tuebingen.de; ziad.m.hafed@cin.uni-tuebingen.de

Saccadic eye movements are a prominent feature of visual behavior; they allow successive sampling of information from the environment. However, from the perspective of visual information flow into the brain, these rapid eye movements constitute highly disruptive events, introducing spurious motions that should normally go perceptually unnoticed, or canceled. The question of how and why such perceptual cancelation takes place has intrigued philosophers and scientists for many decades[1–4]. Indeed, sensitivity to brief peri-saccadic visual probes is strongly impaired, in a phenomenon known as saccadic suppression that has repeatedly been demonstrated in a multitude of experiments[5–14].

Despite the robustness of saccadic suppression as a perceptual phenomenon, the mechanisms behind it remain highly controversial. On the one hand, perceptual suppression may arise through internal knowledge of planned eye movements and their associated motor commands[5,12,15–18]. According to this popular view, eye movement commands are a necessary prerequisite for saccadic suppression: a movement-related signal[16,17], such as corollary discharge from (pre-)motor areas, may act as a suppressive command for visual neurons to cause perceptual suppression, and maybe even in a pathway-selective manner[10].

On the other hand, perceptual saccadic suppression could also arise as a result of the visual consequences of retinal image shifts[2,19–30]. After all, the early visual system, including the retina, is a highly sensitive light sensing device, and can capture visual transients associated with saccade-induced retinal image shifts. Such early processing of visual transients could modulate the retinal output, jumpstarting an image processing cascade to mediate perceptual suppression.

In this study, rather than arguing either strictly for or against one of these seemingly contrasting hypotheses, we asked to what extent they might interact with and support each other to ultimately serve perception. We were specifically motivated by the fact that the very first visual processing stage in the brain, the retina, is not only sensitive to visual transients (such as saccade-induced image shifts), but it also possesses rich image processing circuitry that could regularize the visual disruptions[31–35] caused by saccades. We therefore asked: how much of the characteristics of perceptual saccadic suppression can be explained by visual-only mechanisms? And, to the extent that there are visual-only mechanisms, would the first neural locus for them indeed be the very first stage of visual processing in the brain, the retina?

We used a multi-disciplinary approach in which we experimentally mimicked the visual consequences of saccades and recorded neural activity from ex vivo retinae of different animal models. We also measured human perceptual reports using both real saccades and saccade-like image displacements to simulate the saccadic visual flow. We found a surprisingly far-reaching contribution of visual processing mechanisms to perceptual saccadic suppression, starting in the retina, without the need to invoke explicit motor-based suppression commands. Intriguingly, the role of motor-based commands seems to be the opposite of what has been proposed before. Rather than sending an explicit suppressive command to reduce visual system sensitivity, motor-based commands instead seem to minimize the duration of visually derived saccadic suppression.

Results

Perceptual saccadic suppression depends on image content. We first asked human subjects to generate saccades across textured backgrounds, akin to how saccades may be made in real life. Subjects viewed coarse or fine textures (Fig. 1a, Methods and Supplementary Fig. 1). Starting from one of four locations on the display, subjects made 4.8 deg saccades towards display center (Fig. 1a, left). We varied saccade onset and endpoint locations, as well as texture images, across trials to avoid subjects remembering specific texture patterns. At a random time, a luminance pedestal (probe flash) was added to the texture background, for one display frame (~12 ms), at one of four locations relative to saccade endpoint (7 deg eccentricity; Fig. 1a, right). Subjects localized the probe flash (4-alternative-forced-choice paradigm), and we analyzed how well they did so. We ensured that the retinal region of flash location was stimulated with the background texture (rather than the edge of the monitor or the black surround of the dark laboratory) throughout any given trial, and that the probe flash was larger than the image blobs in the coarse texture, such that average luminance variation within each flash was matched across trials and textures. Coarse and fine textures had blobs that approximated the sizes of retinal ganglion cell (RGC) or retinal bipolar cell receptive fields, respectively, at the retinal flash locations[36] (Methods).

For both coarse and fine textures, subjects were strongly impaired in their ability to localize peri-saccadic flashes, thus experiencing strong perceptual saccadic suppression (Fig. 1b, c). Importantly, the suppression clearly depended on background visual images: it started earlier and recovered later with saccades across coarse rather than fine textures (Fig. 1d; the highlighted time intervals show significant differences between coarse and fine textures with $p < 0.001$, cluster-based random permutation test[37,38]). Moreover, the peak amount of suppression was stronger with the coarse textures (Fig. 1d). However, for both types of textures, performance reached a floor effect, masking an even larger difference (addressed below and in Fig. 2). This dependence of perceptual saccadic suppression on background texture was robust across individual subjects (Supplementary Fig. 2a; also see Supplementary Fig. 4 for further individual subject effects).

To rule out the possibility that flashes might simply be easier to see over the fine texture, we performed a control experiment in which we collected full psychometric curves of perceptual performance during fixation. Without any saccades, probe flash visibility was identical over coarse and fine textures (Supplementary Fig. 3a, b). Therefore, the image dependence demonstrated in Fig. 1 was related to saccadic suppression itself and not to the baseline visibility of brief flashes over the different textures. Similarly, analyzing eye movement properties showed that the results of Fig. 1 were also not due to different saccade kinematics for the different textures (Supplementary Fig. 3c, d).

We next employed a more sensitive procedure to evaluate perceptual thresholds. We repeated the same experiment of Fig. 1 on five subjects (three being the same as in the earlier experiment). This time, however, we collected full psychometric curves (Methods; similar to Supplementary Fig. 3a, b). As collecting full psychometric curves for each texture and each time point relative to saccade onset would be a very data-intensive endeavor, we expedited data collection by implementing a real-time saccade detection algorithm, described by Chen and Hafed[39]. This allowed us to present the probe flash at only four defined times after online saccade detection, strategically chosen to evaluate peak suppression (shortly after saccade onset), as well as the recovery time course after a saccade. We used an adaptive QUEST[40] procedure to estimate perceptual threshold per condition and flash time (Methods), with perceptual threshold (for the purposes of QUEST) being defined as the flash contrast value resulting in 62.5% correct performance. Besides the QUEST procedure, we also collected more trials showing different flash contrast levels relative to the estimated threshold, in order to obtain full psychometric curves. The results are shown in Fig. 2, and they match those of Fig. 1: relative to the baseline psychometric curves of flash visibility long after saccades (dashed

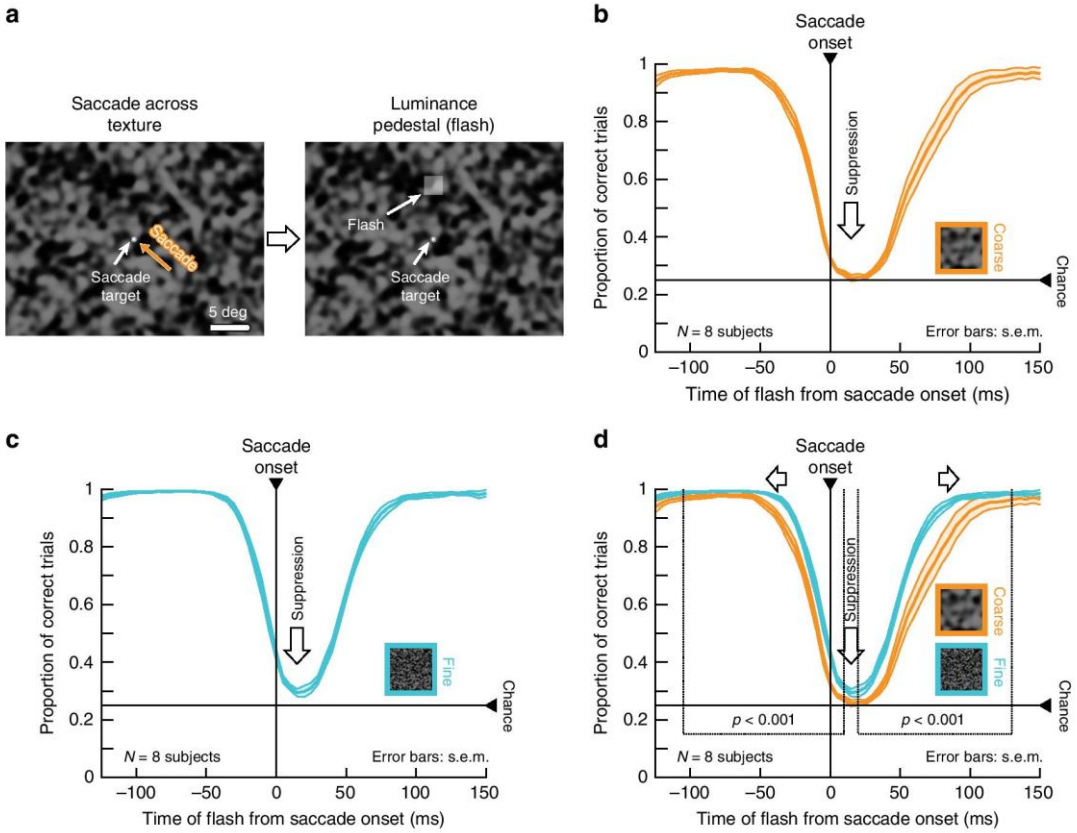

Fig. 1 Image dependence of perceptual saccadic suppression. a Human subjects generated saccades across a texture (here: coarse) from one of four diagonal locations towards display center (here: from the lower right). A luminance pedestal was flashed peri-saccadically at one of four locations around display center (right, left, up, or down; here: up). The insets in **c**, **d** show fine textures for comparison; also see Supplementary Fig. 1 and Methods. **b**, **c** Subjects failed to localize peri-saccadic flashes with both coarse (**b**) and fine (**c**) textures (perceptual reports were binned as a function of flash time from saccade onset using 50-ms bins moving in steps of 5 ms). **d** Perceptual suppression started earlier and lasted longer with a coarse background (also see Fig. 2). The highlighted times denote significantly different ($p < 0.001$, two-tailed random permutation test) time clusters between coarse and fine conditions (Methods). Curves show averages ± s.e.m. of individual subjects' suppression curves ($N = 8$). Supplementary Figs. 2, 3 show individual subject results, as well as controls for flash visibility (in the absence of saccades) and saccade motor variability.

curves), peri-saccadic psychometric curves were clearly shifted towards higher thresholds (Fig. 2a–d), consistent with Fig. 1. Critically, the more sensitive approach of full psychometric curves revealed that perceptual saccadic suppression was much stronger for coarse than fine textures at peak suppression; that is, perceptual thresholds (defined as luminance increments required for a specific correct performance level; Methods) near peak suppression were higher for coarse than fine textures (Fig. 2e). Supplementary Fig. 4 shows the individual subject psychometric curves.

To summarize, perceptual saccadic suppression is associated with a visual component directly influencing its strength and time course: saccades across coarse textures are associated with both stronger and longer-lasting perceptual suppression than saccades across fine textures, even when eye movement kinematics (and thus underlying motor commands) are controlled for.

Perceptual saccadic suppression originates in the retina. To test if this visual component of perceptual saccadic suppression originates in the retina, we isolated mouse and pig retinae and performed multi-electrode array recordings (Methods). We continuously exposed each retina to coarse and fine textures, matched to ganglion and bipolar cell receptive field sizes in the recorded species (Supplementary Fig. 1). We rapidly translated the textures to simulate saccade-like image displacements (Fig. 3a). Such displacements can robustly activate RGCs, as is evident from the example mouse RGC shown in Fig. 3b. In fact, most recorded RGCs (mouse: 83% of 1,423 cells, pig: 73% of 394 cells) responded to texture displacements, indicating that saccade-induced visual transients during active gaze behavior constitute strong signals to the retina. Next, at different times relative to texture displacements, we introduced a luminance pedestal (probe flash) to the entire texture for 16 or 33 ms, similar in principle to the perceptual experiments of Figs. 1 and 2. Such flashes, when presented in isolation (that is, temporally removed from texture displacements), elicited responses in a sizable fraction of RGCs (baseline response; mouse: 688 of 1423 RGCs; pig: 228 of 394 RGCs). This allowed us to evaluate the consequences of texture displacements on flash responses in these cells—conceptually similar to the experiments in Figs. 1 and 2 (in which we evaluated the consequences of saccades on flash perception). The same example RGC of Fig. 3b showed much suppressed neural responses to the flash when it was presented immediately after texture displacements compared to baseline (Fig. 3c, d). This suppression of flash-induced responses (Fig. 3d) looks remarkably similar to suppression of visual responses in, say, macaque superior colliculus for stimuli presented after real saccades[13,14,41]. Thus, neuronally, there does exist "saccadic suppression" of visual sensitivity at the very first stage of visual processing, the retina,

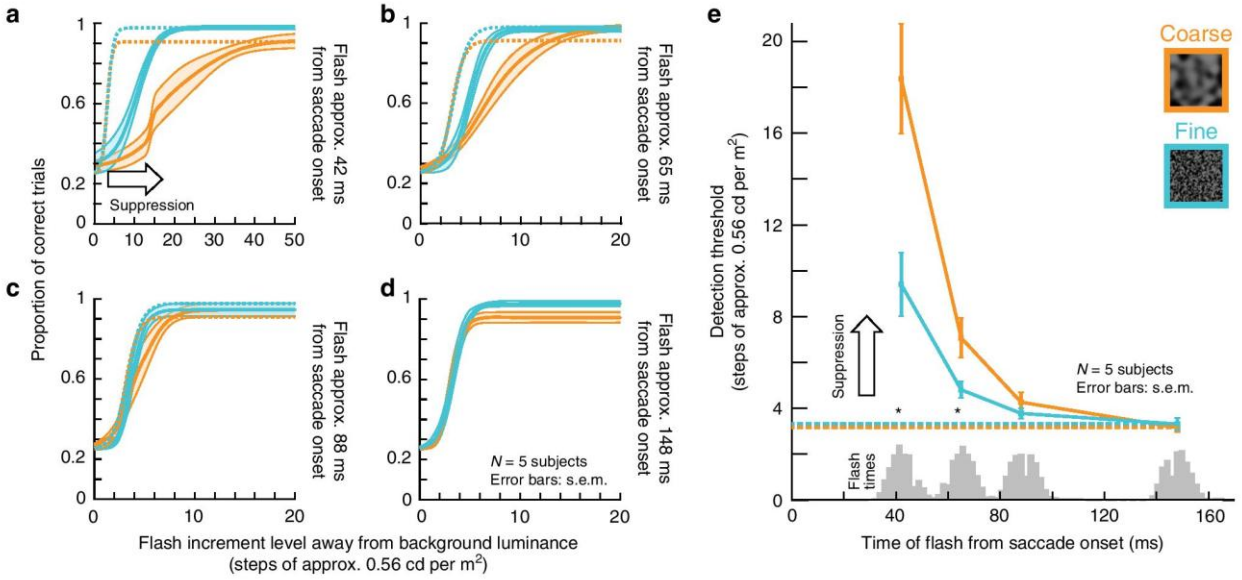

Fig. 2 Image-dependent elevation of perceptual thresholds across saccades. a–d Full psychometric curves of flash visibility with the paradigm like in Fig. 1. Solid curves: mean ± s.e.m of the individual psychometric curves of $N = 5$ subjects (individual results in Supplementary Fig. 4). Dashed curves: psychometric curves near recovery from suppression long after saccades (same data as in **d**). Orange and light-blue: data for coarse and fine textures, respectively. **a** For flashes approximately 42 ms from saccade onset, strong perceptual saccadic suppression occurred (compare solid with dashed curves), and coarse textures yielded stronger perceptual saccadic suppression than fine textures. **b** At approximately 65 ms after saccade onset, substantial recovery was visible (note the different *x*-axis scale from **a**), still with stronger suppression for coarse than fine textures. **c**, **d** Recovery of visibility continued at later times after saccade onset (88 ms, **c**, and 168 ms, **d**), consistent with Fig. 1. **e** Perceptual detection thresholds (i.e., flash luminance levels needed to achieve a certain correct performance rate; Methods) from **a–d** as a function of flash times from saccade onset. Since flash times were determined using online saccade detection, there was some variability of actual displayed flash times; the gray histograms on the *x*-axis show the actual distributions of flash times for each group of data from **a–d**. Asterisks denote significant ($p < 0.05$) differences between coarse and fine textures (two-tailed two-sample *t*-test). Exact *p*-values at each flash time: 42 ms ($p = 0.012$) and 65 ms ($p = 0.044$). The dashed horizontal lines show the detection thresholds at the longest flash times (**d**); note that these thresholds are also similar to those in the control experiments for visibility (Supplementary Fig. 3a, b).

and it looks qualitatively indistinguishable from saccadic suppression at downstream neural sites[13,14,41] and, indeed, perception (Figs. 1 and 2).

Importantly, retinal "saccadic suppression" strongly depended on background texture (Fig. 3e), exactly like in perception (Figs. 1 and 2). Specifically, we quantified retinal "saccadic suppression" by calculating a neuronal modulation index, defined as $(r_d - r_b)/(r_d + r_b)$. r_d is the response strength to the probe flash presented with a delay d relative to the texture displacement onset, and r_b is the baseline response strength (Methods). The great majority of RGCs were strongly suppressed during and after texture displacements (indicated by negative modulation indices), with gradual recovery afterwards (Fig. 3e; Supplementary Fig. 5 shows the underlying population data), and suppression was more pronounced for coarse than fine textures (Fig. 3e and Supplementary Fig. 5). These results are consistent with the dependence of human perceptual saccadic suppression on background texture statistics (Figs. 1 and 2), suggesting that this dependence starts already in the retina.

We also found that retinal "saccadic suppression" was a robust phenomenon across many different RGCs with diverse properties (Supplementary Fig. 6). Further, it occurred both in mouse (Fig. 3e, left) and pig (Fig. 3e, right) retinae, two mammalian species with different native oculomotor behavior, different lifestyles, and different eye sizes. Thus, our results so far suggest that perceptual saccadic suppression (Figs. 1 and 2), including its dependence on background texture statistics, most likely originates in the retina (Fig. 3), being the outcome of very general retinal-circuit mechanisms that are conserved across species.

Stimulus–stimulus interactions underlie retinal suppression. To understand the underlying mechanisms for "saccadic suppression" in the retina in more detail, we explored its properties using different analyses and additional stimulus manipulations. First, we wondered about neural activity saturation, given that saccade-like texture displacements before flash onset could activate RGCs (e.g., Fig. 3b). Specifically, if RGC activity is elevated by the texture displacement, then any subsequent flash-induced response could have caused the cell to reach activity saturation. However, this was not sufficient to explain our results. For example, we observed that suppression often also occurred in RGCs that did not respond strongly to the texture displacements in the first place (Fig. 4a).

Second, we investigated whether retinal "saccadic suppression" critically depended on particular saccade-like speed profiles. In the original experiments (Fig. 3), we simulated saccade-induced image translation speeds to the best of our abilities (given display refresh rates; Methods). However, if we replaced the original translation over 100 ms with a sudden texture jump in one display update (an infinite-speed texture jump), then the same suppression took place, with similar dependence on texture statistics (Fig. 4b). Similarly, in yet another manipulation, we presented the probe flash before the texture displacement; the second response (now to the texture displacement) was suppressed (Fig. 4c). This suggests that retinal "saccadic suppression" can be explained by general stimulus–stimulus interaction effects. As a result, it is a phenomenon that is unlikely to critically depend (qualitatively) on the specific oculomotor repertoire of either mice, pigs, or humans.

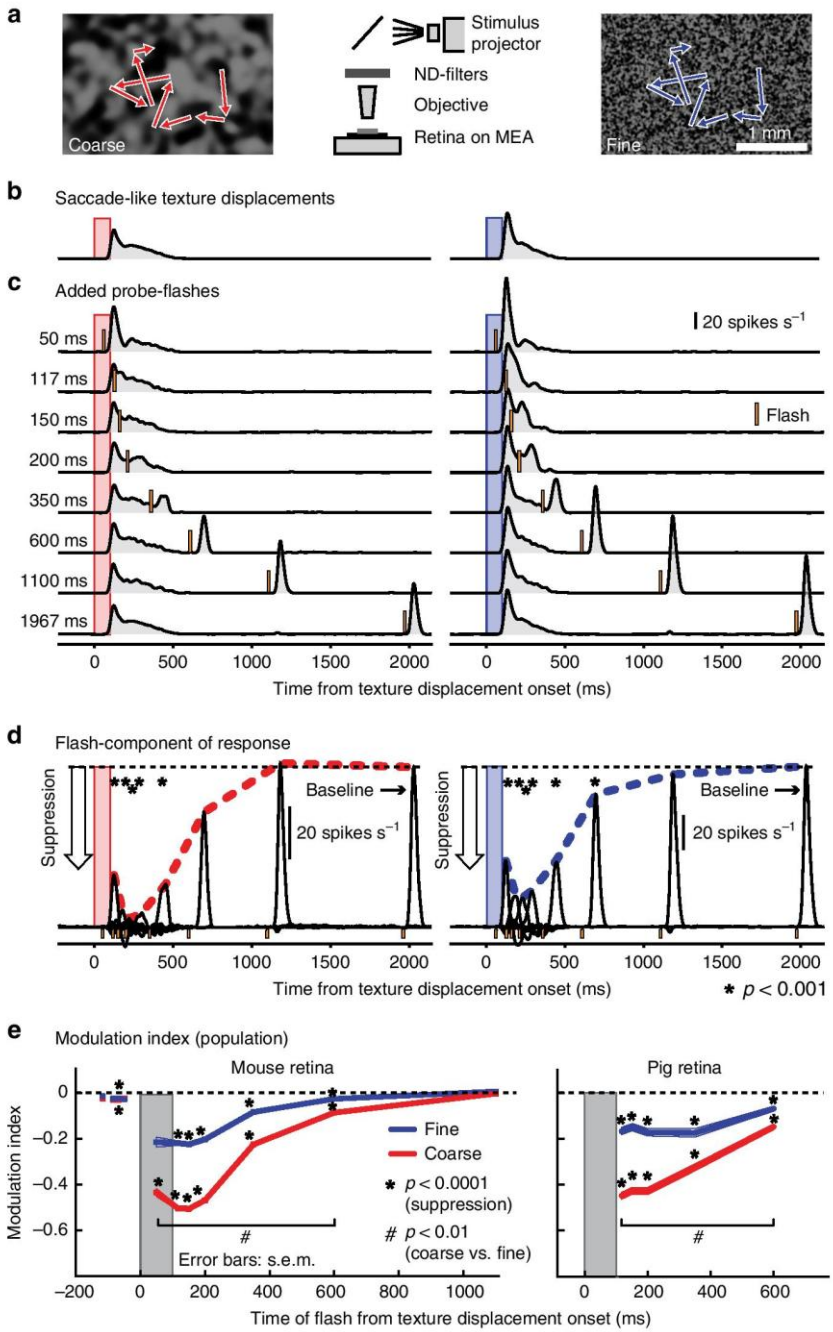

Fig. 3 "Saccadic suppression" in retina. a We recorded RGC activity from ex vivo retinae placed on multi-electrode arrays (MEA). A coarse (left) or fine (right) texture was repeatedly translated in a saccade-like manner (red or blue scan paths), and we presented brief visual flashes at different times relative to "saccades" (similar to Fig. 1). **b**, **c** Average activity of an example RGC to 39 texture displacements alone (**b**) or followed by probe flashes at different time delays (**c**). Red and blue bars show the timings of the texture displacements; orange bars indicate probe flashes. Flash-induced responses were strongly suppressed immediately following saccade-like texture displacements. **d** Isolated flash responses of the same RGC obtained by subtracting responses in **b** from those in **c**. Dashed colored lines highlight the time courses of retinal "saccadic suppression" relative to baseline flash-induced responses. Asterisks indicate flash-induced responses that are significantly suppressed from baseline ($p < 0.001$, one-tailed sign test; Methods). **e** Population modulation index (mean ± s.e.m.) across individual RGCs highlighting retinal "saccadic suppression" (Methods; negative values indicate suppressed flash-induced neural responses). Both mouse and pig retinae showed strong suppression during and after texture displacements, which also depended on texture statistics (similar to perception; Figs. 1 and 2). Asterisks indicate statistically significant suppression ($p < 0.0001$, two-tailed Wilcoxon signed-rank test; Methods). Hash symbols indicate significant differences in suppression between coarse and fine textures ($p < 0.01$, two-tailed Wilcoxon signed-rank test; Methods). Exact p-values are indicated in Supplementary Fig. 5. The numbers of recorded cells at each flash time in **e** were: mouse RGCs: $N = 179$ (-177 ms, -84 ms, -50 ms), 161 (-67 ms), 136 (50 ms), 527 (117 ms), 520 (150 ms), 502 (200 ms, 600 ms), 688 (350 ms), 345 (1100 ms); pig RGCs: $N = 228$ for each time point. Supplementary Figs. 5 and 6 show the population data underlying panel **e**.

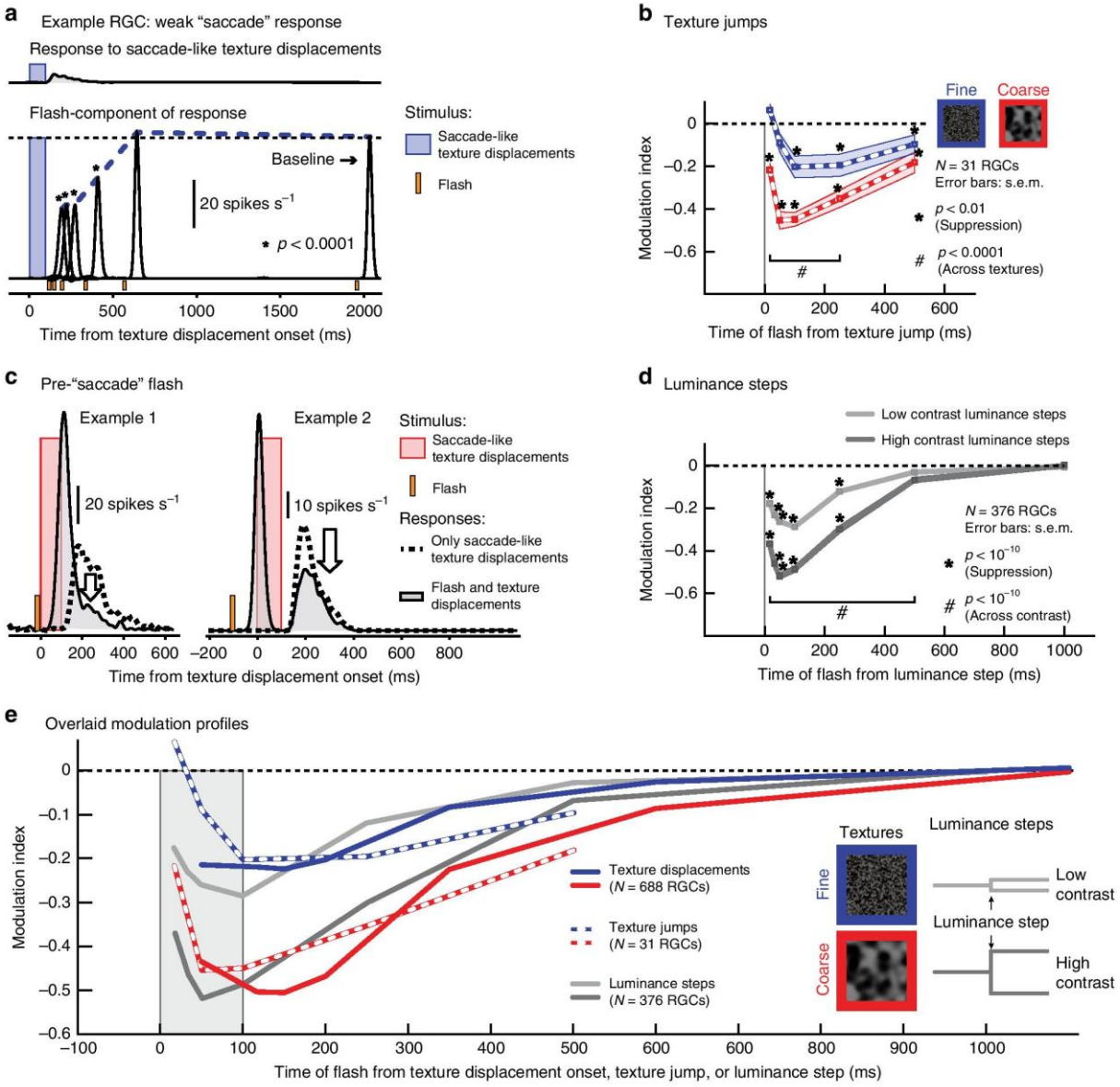

Fig. 4 Stimulus-stimulus interactions in retinal "saccadic suppression". **a** Example RGC responding only weakly to texture displacements (top), but nevertheless exhibiting strong suppression of flash-induced responses (bottom; curves plotted at the same scale). Asterisks indicate significantly suppressed flash-induced responses ($p < 0.0001$, one-tailed sign test, $N = 39$ independent observations; Methods). Exact p-values at each flash time: 117 ms ($p = 10^{-5}$), 150 ms (10^{-5}), 200 ms (10^{-6}), 350 ms (10^{-5}), and 600 ms (0.26). **b** Population modulation index (mean ± s.e.m., $N = 31$ RGCs) when the textures jumped from their start to end positions instantaneously. Strong suppression (*$p < 0.01$, two-tailed Wilcoxon signed-rank test) and significant differences between coarse (red) and fine (blue) textures (#$p < 0.0001$, two-tailed Wilcoxon signed-rank test) still occurred. Exact p-values at each flash time (coarse, fine, across): 17 ms ($p = 10^{-6}$, $p = 0.027$, $p = 10^{-6}$), 50 ms (10^{-6}, 0.021, 10^{-6}), 100 ms (10^{-5}, 0.001, 10^{-6}), 250 ms (10^{-6}, 0.001, 10^{-4}), and 500 ms (0.002, 0.04, 0.06). **c** Two example RGCs showing that a flash before saccade-like texture displacements suppressed the response to the displacements, suggesting that stimulus-stimulus interactions drive retinal "saccadic suppression". **d** Population modulation index (mean ± s.e.m., $N = 376$ RGCs) for a paradigm similar to **b**, but with textures replaced by spatially uniform backgrounds of different intensity (i.e., instantaneous luminance steps). Suppression of flash-induced responses was preserved (*$p < 10^{-10}$, two-tailed Wilcoxon signed-rank test), and differences between low-contrast (light gray) and high-contrast (dark gray) luminance steps (#$p < 10^{-10}$, two-tailed Wilcoxon signed-rank test) resembled the differences between fine and coarse texture jumps in **b**. Exact p-values at each flash time (high contrast, low contrast, across contrasts): 17 ms ($p = 10^{-48}$, $p = 10^{-32}$, $p = 10^{-43}$), 33 ms (10^{-55}, 10^{-41}, 10^{-48}), 50 ms (10^{-60}, 10^{-46}, 10^{-51}), 100 ms (10^{-57}, 10^{-50}, 10^{-42}), 250 ms (10^{-39}, 10^{-33}, 10^{-26}), 500 ms (10^{-8}, 0.02, 10^{-8}) and 1000 ms (0.9, 0.7, 0.8). **e** Overlaid modulation profiles from texture displacements (Fig. 3e), texture jumps (**b**), and contrast steps (**d**). Coarse texture displacements, coarse texture jumps, and high-contrast luminance steps had similar effects; and so did fine texture displacements, fine texture jumps, and low-contrast luminance steps.

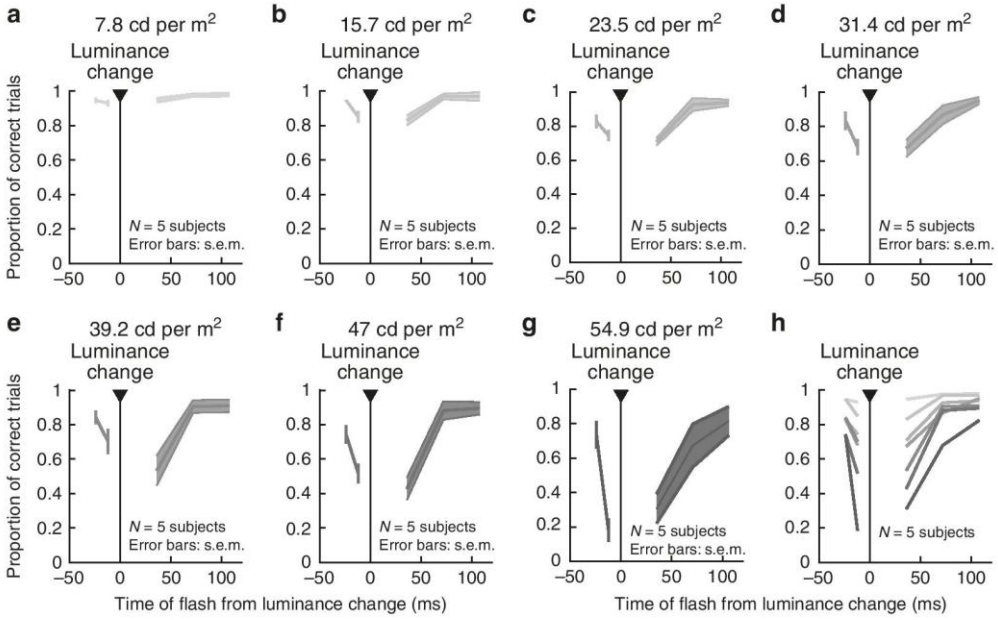

Fig. 5 Stimulus-stimulus interactions in perceptual suppression without saccades (similar experiment to the retinal paradigm of Fig. 4d). Subjects fixated and detected brief probe flashes as in the experiments of Figs. 1 and 2; here, the flashes happened around the time of a luminance step (i.e., a sudden change in background luminance) instead of a saccade. The title above each panel indicates the absolute value of the luminance change that took place. **a**–**g** Proportion of correct responses as a function of flash time from the time of background luminance step. There was progressively stronger perceptual suppression with increasing contrast of the luminance step, consistent with the retinal results of Fig. 4d. **h** Summary of panels **a**–**g**. Darker colors denote larger absolute values of background luminance changes. Since coarse textures (Figs. 1–4) presumably cause larger contrast variations over retinal receptive fields, this suggests that the image dependence of perceptual saccadic suppression (Figs. 1 and 2) is mediated by stimulus-stimulus interaction effects originating in the retina (Fig. 4d).

The most compelling evidence for stimulus–stimulus interactions underlying retinal "saccadic suppression" came from experiments replacing the texture displacements with structure-free luminance steps (Fig. 4d). Specifically, instead of a background texture that we displaced, we exposed the retina to a uniform gray background and introduced a sudden luminance increase or decrease as the visual transient. This luminance step was either of high (±0.20 to ±0.40 Michelson contrast) or low contrast (±0.03 to ±0.15 Michelson contrast, Methods). The probe flash then followed the luminance step as in the original experiments. Flash responses were indeed suppressed after luminance steps, and this suppression was stronger after high- than after low-contrast visual transients. Interestingly, suppression after high- and low-contrast luminance steps resembled suppression after coarse and fine texture displacements, respectively (e.g., Fig. 3), both in terms of time course and strength (Fig. 4e). Presumably, moving the larger blobs of a coarse texture across the retina would result in high-contrast changes within individual relevant retinal receptive fields (e.g., from a bright blob in a receptive field before texture displacement to a dark blob thereafter), while the smaller blobs in the fine texture would be spatially averaged within receptive fields, resulting in low-contrast changes.

When we next performed human psychophysical experiments mimicking the luminance step retinal experiments, we found remarkably congruent results (Fig. 5). Specifically, subjects maintained saccade-free fixation, and we changed the luminance of the homogenous background (Methods). At random times relative to the change, we presented brief probe flashes like in Fig. 1. All subjects experienced clear perceptual suppression around the luminance steps. Importantly, perceptual suppression depended on the contrast of the luminance change: with a small change in background luminance, suppression was minimal; with a large change, suppression was strong and long lasting (Fig. 5). As we discuss below, we also observed perceptual suppression even for flashes before the background luminance changes; this matters for interpretations of pre-movement perceptual saccadic suppression (e.g., see Fig. 6 below).

Therefore, the most likely mechanism for retinal "saccadic suppression" is that it emerges as a result of retinal-circuit image processing that is initiated by visual transients; whether they be through texture displacements, infinite-speed texture jumps, or luminance steps (Fig. 4e). It is intriguing that such stimulus–stimulus retinal effects may be inherited deep into the brain's visual processing hierarchy, including cortical (frontal eye field) and subcortical (superior colliculus) areas[42] that are implicated in saccadic suppression[14,41,43,44].

Motor-related signals shorten visually derived suppression. In retina, we not only observed similarities to perceptual saccadic suppression (the presence of retinal suppression, and its dependence on texture statistics or luminance step contrast). We additionally noticed that retinal "saccadic suppression" was particularly long lasting (e.g., Fig. 3e). To explore the potential perceptual implications of this observation, we next asked our subjects to maintain fixation while we introduced saccade-like texture displacements in a manner similar to the retinal experiments of Fig. 3 (Fig. 6a); brief flashes occurred around the time of these "simulated saccades" like in Fig. 1. This time, due to the absence of real saccades (trials with microsaccades were excluded), non-visual (motor-related) components could not influence flash-induced neural responses and perception. Still, given the retinal results (Figs. 3 and 4), we had three hypotheses that we validated: (1) strong perceptual suppression still occurred regardless of texture details (Fig. 6b, c);

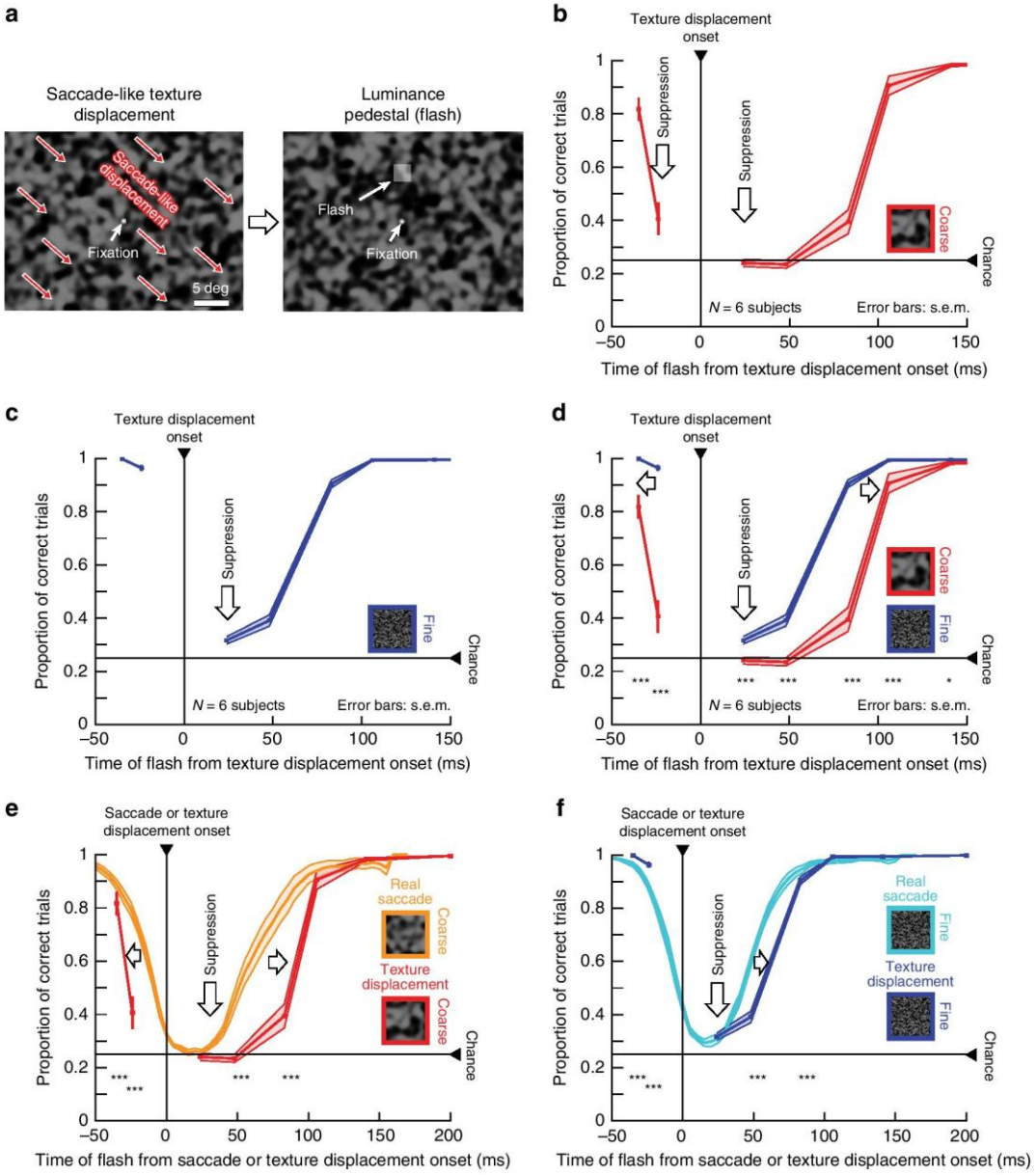

Fig. 6 Image dependence of perceptual suppression without saccades. a Rapid texture displacements simulating saccade-like image displacements, similar to the retina experiments (Fig. 3). We used the same flashes and simulated saccade directions as in Fig. 1. The example shows a coarse texture (fine textures shown in insets in **c**, **d**, and **f**). **b**, **c** Pre-, peri-, and post-displacement perceptual suppression (mean ± s.e.m. over $N = 6$ individual subjects) occurred for both coarse (**b**) and fine (**c**) textures. **d** As with real saccades (Fig. 1), suppression started earlier and lasted longer with coarse textures (also compare to similar retinal effects in Fig. 3e). Notably, pre-displacement suppression depended on texture statistics, just like with real saccades (Fig. 1). **e**, **f** Simulated saccades were associated with significantly longer suppression than real saccades for both fine and coarse textures. For coarse textures (**e**, which were most effective in causing suppression overall), flashes presented before the "saccade" event were suppressed earlier in the simulated saccade condition than in the real saccade condition (also see Fig. 7); thus, prolonged suppression with texture displacements was not restricted to post-displacement flashes only. Asterisks denote significant differences between coarse and fine textures (**d**) or between real and simulated saccades (**e**, **f**) at each indicated time point (χ^2 tests with Bonferroni corrections; $^*p < 0.005$ in **d** and $p < 0.007$ in **e**, **f**; $^{***}p < 0.0001$ in **d** and $p < 0.00014$ in **e**, **f**). Supplementary Fig. 2 shows individual subject results.

(2) suppression strength and duration depended on texture statistics (Fig. 6d); and (3) suppression outlasted suppression with real saccades (Fig. 6e, f). This last point, in particular, suggests that motor-related saccadic signals may act to shorten the perceptual interruption resulting from visually induced saccadic suppression, while maintaining the putatively retinally determined (Figs. 3 and 4) dependence on image statistics. Note also that the first and third points above are consistent with earlier observations by Diamond et al.[16].

In humans, we observed perceptual suppression also prior to saccade-like texture displacements[19,26] (Fig. 6). This was again consistently dependent on texture statistics (Fig. 6b–d; also see Fig. 7 below for additional evidence). Further, like the suppression after saccade onset, this pre-saccadic perceptual suppression

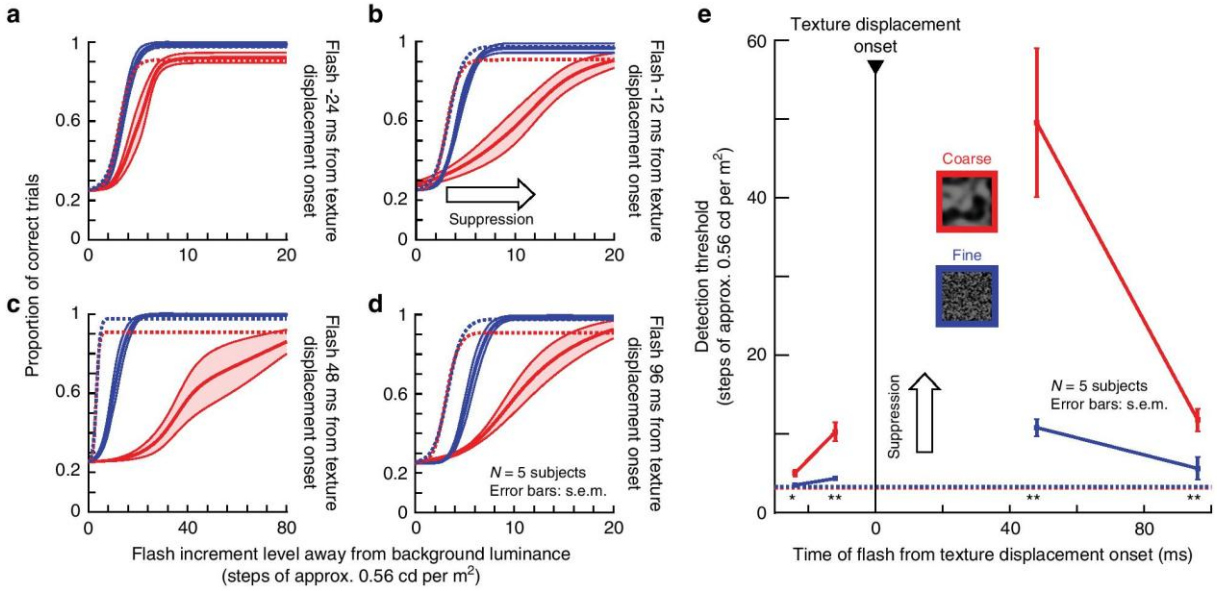

Fig. 7 Image-dependent elevation of perceptual thresholds without saccades. Full psychometric curves of flash visibility around the time of simulated saccades (similar to Fig. 2, paradigm similar to Fig. 6). **a–d** Solid curves: mean ± s.e.m of individual psychometric curves of $N = 5$ subjects (individual subject results: Supplementary Fig. 7). Dashed curves: baseline data from the same subjects without simulated saccades and long after any real saccades (same data as in Fig. 2d; also similar to Supplementary Fig. 3a, b with additional subjects). Red and blue: data for coarse and fine textures, respectively. **a** Flash 24 ms before texture displacement onset: coarse texture (red) requires higher flash contrasts (that is, reduced sensitivity) relative to baseline. This effect was much weaker with fine textures (blue). **b** Flash 12 ms before displacement onset: both coarse and fine textures were associated with significant perceptual suppression relative to baseline, consistent with Fig. 6. Suppression was stronger for coarse than fine textures. **c** Perceptual suppression was the strongest (note the different *x*-axis scale from the other panels) immediately after texture displacement onset. **d** 96 ms after texture displacement onset, there was still significant perceptual suppression, again significantly stronger for coarse than fine textures. This result is consistent with Fig. 6 and highlights the longer-lasting suppression around simulated saccades compared to real saccades (Figs. 1 and 2). **e** Detection thresholds from **a–d** as a function of flash time from texture displacement onset. Pre- and post-displacement perceptual suppression occurred and was stronger with coarse textures. Asterisks: significant differences between coarse and fine textures (two-tailed two-sample *t*-test; $*p < 0.05$; $**p < 0.01$). Horizontal dashed lines: baseline detection thresholds from Fig. 2d, e. All other conventions are similar to Figs. 1, 2, 6.

was shorter during real saccades than during simulated saccades (due to later onset of suppression, Fig. 6e). Even in our retinal data, we found very slight "pre-saccadic" suppression. However, for retinal responses, the effect size before texture displacements was much smaller than after texture displacements: the strongest "pre-saccadic" retinal effect occurred at −67 ms with a median population modulation index of −0.024 ($p = 6 \times 10^{-8}$, Wilcoxon signed-rank test) compared to −0.55 ($p = 3 \times 10^{-82}$) for "post-saccadic" suppression at 150 ms delay (Fig. 3e and Supplementary Fig. 5b). It is therefore likely that this particular phenomenon, perceptual pre-saccadic suppression (Fig. 6b–f), arises from visual (not movement-command-related) processing further downstream of the retina, perhaps through backwards masking[28,45]. This also holds true for our experiments with background luminance steps (Fig. 5), and it can also explain why peak suppression time in our retinal experiments (Figs. 3 and 4) appeared slightly different from peak suppression time with real saccades (Figs. 1 and 2).

Next, we determined explicit perceptual thresholds for the texture displacement paradigm introduced in Fig. 6, using the QUEST and full psychometric curve procedures described for Fig. 2. We again picked four specific time points relative to texture displacement onset, chosen strategically to highlight perceptual threshold elevations at maximal suppression, to characterize differences in recovery time between coarse and fine textures, and to fill the gap before texture displacement onset. The net conclusion (Fig. 7) was the same as that in Fig. 6. There was robust elevation of perceptual thresholds before, during, and after texture displacements. Most importantly, the elevation was much stronger and longer-lasting (both before and after texture displacements) for coarse than for fine textures. The effect was also robust across individual subjects (Supplementary Fig. 7).

Therefore, our long-lasting RGC suppression effects (Figs. 3 and 4) were not an idiosyncrasy of our ex vivo electrophysiological procedures, but they were reflected in the longer duration of perceptual suppression after simulated saccades. Importantly, they were indicative of a potential shortening of visually derived suppression in association with real saccades.

Visually derived suppression underlies even more phenomena. Our results so far suggest that visual contributions can go a long way in explaining perceptual properties of saccadic suppression (e.g., the presence of suppression, and the dependencies on image content), without the need for invoking mechanisms related to motor commands. We wondered whether visual contributions can also explain classic suppression phenomena in experiments when uniform, rather than textured, backgrounds are used. One such robust phenomenon has been the selective suppression of low spatial frequencies. In a classic study[10], subjects viewed briefly flashed Gabor gratings over a uniform background. Around the time of saccades, visibility of low spatial frequency gratings was suppressed more strongly than of high-frequency gratings. This was interpreted as a motor-related influence on magnocellular pathways[16,17]. Still, convincing neural mechanisms for this phenomenon remain elusive[14,21,29,30,46–50]. Can the strong prominence of visual contributions to saccadic suppression revealed by our results also be extended to account for this

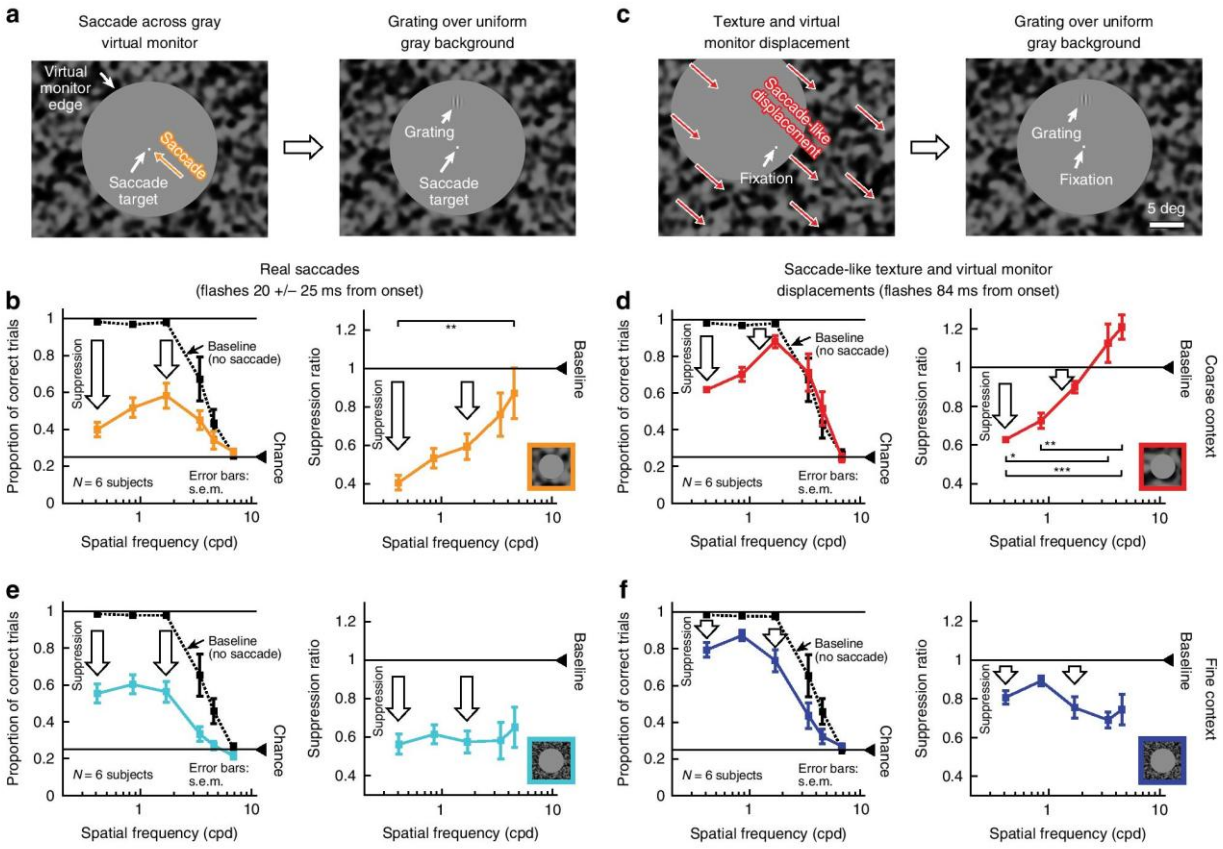

Fig. 8 Selective peri-saccadic suppression of low spatial frequencies[10] is a visual phenomenon. a Left: subjects made saccades towards display center. Right: gratings were flashed peri-saccadically over a uniform gray background (circular "virtual monitor" surrounded by a coarse texture; saccade directions and flash locations: similar to Figs. and 6). **b** Left: proportion of correct grating localizations with different spatial frequencies during fixation ("Baseline"; dashed curve) and for peri-saccadically flashed gratings (solid curve). Low spatial frequencies were associated with the strongest suppression relative to baseline. Right: ratio of peri-saccadic to baseline performance (highest spatial frequency not shown because it was at chance performance even in baseline). Suppression depended on grating spatial frequency ($\chi^2 = 13.46$, $p = 0.0092$, df = 4, Kruskal–Wallis test; $^{**}p < 0.01$ for post-hoc pairwise comparisons between the lowest and highest spatial frequencies). **c** Left: simulated saccade-induced image displacements by translating the virtual monitor and surrounding texture from one corner towards display center. Right: gratings appeared as in **a**. **d** The same selective suppression of low spatial frequencies occurred as with real saccades (**b**). "Baseline" in this context means both no saccades and no virtual monitor and texture displacements. Suppression depended on spatial frequency ($\chi^2 = 25.33$, $p < 0.0001$, df = 4, Kruskal–Wallis test; $^{*}p < 0.05$, $^{**}p < 0.01$, $^{***}p < 0.001$ for post-hoc pairwise comparisons between individual spatial frequencies). **e**, **f** With a fine surround texture, both real (**e**) and simulated (**f**) saccades were associated with suppression for all spatial frequencies; suppression selectivity[10] was eliminated ($\chi^2 = 0.8$, $p = 0.938$, df = 4 for **e** and $\chi^2 = 7.74$, $p = 0.102$, df = 4 for **f**, Kruskal–Wallis test). Error bars: s.e.m. across individual subjects' curves. Supplementary Figs. 8–10: full time courses and controls with black surrounds around the virtual monitor. Note that in **d**, **f**, we exploited the longer time course of visual suppression (Fig. 6 and Supplementary Figs. 8 and 9) to probe perception at a later time than in **b**, **e**. This also explains why suppression appeared quantitatively weaker in **d**, **f** than in **b**, **e**.

classic phenomenon? In other words, is peri-saccadic selective suppression of low spatial frequencies[10] fundamentally a visual, rather than motor, phenomenon?

We considered this phenomenon from the perspective of visual input during such experiments: saccades across a uniform background invariably involve moving the image of the video monitor (or other form of display) in visual coordinates. Therefore, the image of any edge discontinuity associated with the display monitor (or with the surrounding cardboard paper around it[10]) will invariably move across the retina. This allows us to ask if one can replicate selective suppression of low spatial frequencies[10] without any saccades at all, solely based on the visual flow during such experiments.

We first replicated the classic phenomenon itself (Methods). Subjects localized briefly flashed vertical Gabor gratings with different spatial frequencies; the flashes occurred peri-saccadically as in Fig. 1a. Here, however, the screen was homogeneous, like in the classic experiment, with the exception of a surround region showing a stationary texture (the coarse texture used in our earlier experiments, Fig. 8a). We call the large homogeneous region (diameter: 20 deg) the "virtual monitor". The outcome confirmed the classic findings: Fig. 8b (left) shows localization performance for flashed gratings around saccade onset, compared to flashes without saccades (and without any other display transients), and Fig. 8b (right) plots the ratio of those percepts. Perception of low spatial frequency gratings was selectively suppressed (relevant statistics are shown in Fig. 8; full time courses of these effects are shown in Supplementary Figs. 8 and 9). These results are consistent with the classic phenomenon[10].

The presence of the textured surround allowed us to next isolate the effects of visual flow. In separate trials, subjects fixated, and we presented saccade-like image motion. For example, in order to simulate a real saccade from the lower right corner to display center (Fig. 8a), the virtual monitor moved together with

its textured surround from the top left corner towards display center (Fig. 8c). We then briefly presented the same Gabor gratings as in Fig. 8a, b. Relative to fixation position, this experiment was comparable to the situation with real saccades: there was a uniform background against which a brief Gabor grating was flashed. And, indeed, we observed the same selective suppression of low spatial frequencies despite the absence of saccades (Fig. 8d). Moreover, again consistent with our results from Figs. 1–7, the suppression lasted longer than with real saccades (robust selective suppression in Fig. 8d occurred even 84 ms after simulated saccades; Supplementary Figs. 8 and 9). Similar results were obtained with a uniform black surround around the virtual monitor, as might be the case in typical laboratory settings (Supplementary Fig. 10). Therefore, visual mechanisms account even for the results of Burr et al.[10] and similar experiments[14] using uniform backgrounds, without the need to invoke non-visual (motor-related) mechanisms.

Motivated by the differences between coarse and fine textures in Figs. 1–7, we next replaced the coarse texture around the virtual monitor (Fig. 8c) with a fine texture, and we repeated the experiments with simulated saccades (Fig. 8f). Surprisingly, we observed uniform suppression for all spatial frequencies (Fig. 8f). In other words, the specific suppression of low spatial frequencies (Fig. 8c, with saccade-like visual flow, but without eye movements) depended on the visual context containing a coarse texture in the visual surround. This led to a very strong prediction: if saccadic suppression properties do indeed rely on visual processing, then suppression during real saccades should depend mainly on visual context; one should be able to easily violate the classic phenomenon (namely, the specific suppression of low spatial frequencies[10]). This is exactly what we found (Fig. 8e): for real saccades across the virtual monitor, and with the surrounding visual context being a fine rather than coarse texture, we observed perceptual suppression for all gratings, abolishing suppression selectivity for low spatial frequencies. In all cases, the effects were not explained by motor variability across surround texture conditions (Supplementary Fig. 3e, f).

We further confirmed all these observations by collecting full psychometric curves (Methods), similar to Figs. 2 and 7 above: Fig. 9 shows results for real saccades, and Fig. 10 for simulated saccades. In both cases, with a coarse surround texture, perceptual threshold was elevated more strongly for low spatial frequency Gabor patches. With a fine surround texture, perceptual threshold was elevated non-specifically for all probe Gabor patches.

In summary, perceptual saccadic suppression occurred in all of our experiments, either with or without real saccades, simply as a function of visual flow (Figs. 1, 2, 6–10). Simple visual transients, without the need for saccade-like stimulus kinematics, were sufficient to elicit suppression in both retina and perception (Figs. 4 and 5). Such suppression quantitatively depended on scene statistics, both for full-field textures (Figs. 1, 2, 6, 7) in a manner predicted by retinal processing (Figs. 3–5), and for textures limited to the surround (Figs. 8–10). Even the suppression selectivity of low spatial frequency Gabor probes[10] was determined by visual context (Figs. 8–10).

Discussion

We found that visual image processing accounts for a large component of classic perceptual demonstrations of saccadic suppression, and that such image processing occurs as early as in the very first stage of visual processing, the retina. In fact, we found remarkable congruence between the image dependence of three seemingly disparate phenomena: perceptual suppression with real saccades (Figs. 1 and 2), perceptual suppression with simulated saccades (Figs. 6 and 7), and neural suppression in RGCs, which carry the retinal output (Figs. 3 and 4). In all cases, modifying the background texture statistics resulted in highly predictable changes in suppression profiles. This was further corroborated in both the retina (Fig. 4d) and perception (Fig. 5) when we replaced texture displacements with simple background luminance steps.

Key to all our observations is the single insight that, from the perspective of visual image processing, a saccade itself generates a potent visual stimulus. For example, our RGCs often responded vigorously to saccade-like image displacements (Fig. 3b). Therefore, when probing peri-saccadic perceptual sensitivity using brief flashes, as in classic studies of perceptual saccadic suppression, the visual system is not only responding to the externally provided flashes, but it is also responding to the self-induced visual flows caused by eyeball rotations. These saccade-induced retinal image shifts trigger visual mechanisms that can suppress the retinal response to subsequent stimulation. Such suppression is not exclusive to saccades. It instead occurs for any scenario that involves sequential visual stimulation, including visual masking[2,27,28,45] and double-flash[42] paradigms. It is, therefore, not surprising that the outcome is also comparable: the response to a second stimulus is suppressed by the presence of a first stimulus, be it a mask, a flash, or transients caused by saccades. Indeed, our own results demonstrate that simpler sequential visual stimulation with luminance steps plus probe flashes shows qualitatively similar perceptual (Fig. 5) and retinal (Fig. 4d) suppression profiles to those seen with simulated saccades. Therefore, classic saccadic suppression paradigms, employing brief peri-saccadic visual probes, are essentially stimulus–stimulus paradigms from the perspective of visual flow on the retina.

Additional support for the above sentiment emerges from the time courses of stimulus–stimulus neural adaptation effects in areas like the frontal eye field and superior colliculus[42]. These time courses are particularly intriguing because they agree with our observations that retinal (Figs. 3 and 4) and perceptual (Figs. 6 and 7) suppression with simulated saccades had longer suppression time courses than observed with real saccades (Figs. 1 and 2). Indeed, the time courses of the neural adaptation effects in the frontal eye field and superior colliculus[42], and related brain areas, are similar to our observed perceptual time courses without real saccades. Given that both the frontal eye field and superior colliculus have previously been implicated in saccadic suppression[14,41,43,44], it is thus conceivable that suppression in these areas is inherited, at least partially, from the retina.

Looking forward, it is imperative to investigate the neural mechanisms behind visual masking in much more detail. In our perceptual experiments with simulated saccades (Figs. 6 and 7), we saw clear suppression even with probe flashes before texture displacement. That is, perceptual localization of the probes was masked, backwards in time, by the subsequent texture displacement. In the past, pre-saccadic suppression with real saccades (e.g., Fig. 1) was sometimes taken as evidence that perceptual saccadic suppression is fundamentally driven by motor-related signals like corollary discharge. However, our results (Figs. 6 and 7) show that a visual transient is sufficient. Even simple background luminance steps were associated with pre-step perceptual suppression (Fig. 5). These effects have been described as backwards visual masking[45], but what are the underlying neural mechanisms? Such backwards masking was not present in our retinal results, certainly not as clearly as in perception, so it must emerge through visual mechanisms in other brain structures.

One possibility could be related to the fact that priors strongly influence the perceptual interpretation of sensory evidence. In the case of global retinal image motion, which is caused by eye movements in most real-world scenarios, priors could influence the percept of a flash occurring before a saccade or texture

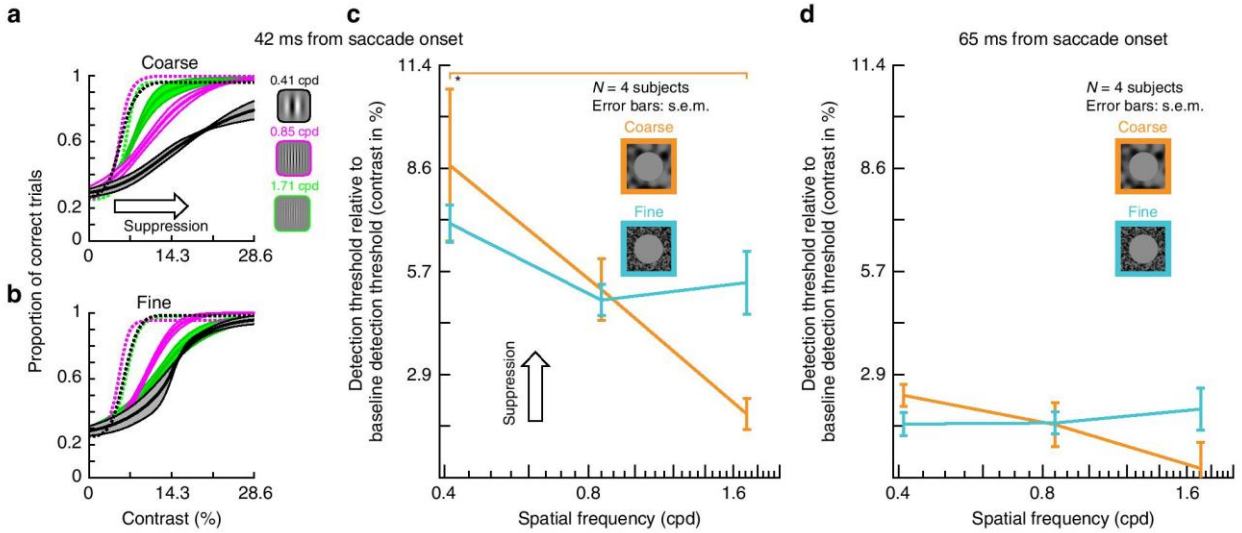

Fig. 9 Selective and unselective saccadic suppression measured using full psychometric curves. a We repeated the real saccade experiments of Fig. 8, and obtained full psychometric curves by using different Gabor grating contrasts (Methods). Different colors indicate different spatial frequencies of the flashed gratings. When the gratings were flashed ~42 ms after saccade onset (Methods) and there was a coarse surround texture, perceptual suppression clearly depended on spatial frequency: detection thresholds were highest for the lowest spatial frequency, and they progressively decreased with increasing spatial frequency. Each curve shows mean ± s.e.m. of four subjects' psychometric curves. Dashed psychometric curves show perceptual detectability without saccadic suppression (obtained similarly to Fig. 8). **b** When the surround context was fine, rather than coarse, perceptual suppression was not selective for low spatial frequencies (consistent with Fig. 8). **c** Detection thresholds from **a**, **b** as a function of grating spatial frequency for flashes ~42 ms after saccade onset. With a coarse surround, detection thresholds were highest for low spatial frequencies and progressively decreased with increasing spatial frequency (1-way ANOVA, $p = 0.0168$, $F = 6.6608$; $p = 0.0133$ for post-hoc comparison between lowest and highest spatial frequency, indicated by *). With a fine surround, detection thresholds did not depend on spatial frequency. **d** Same as in **c** but now for grating flashes occurring ~65 ms after saccade onset. For both surround textures, detection thresholds decreased, indicating perceptual recovery. There was still a trend for dependence of perception on spatial frequency in the coarse condition, consistent with **c**.

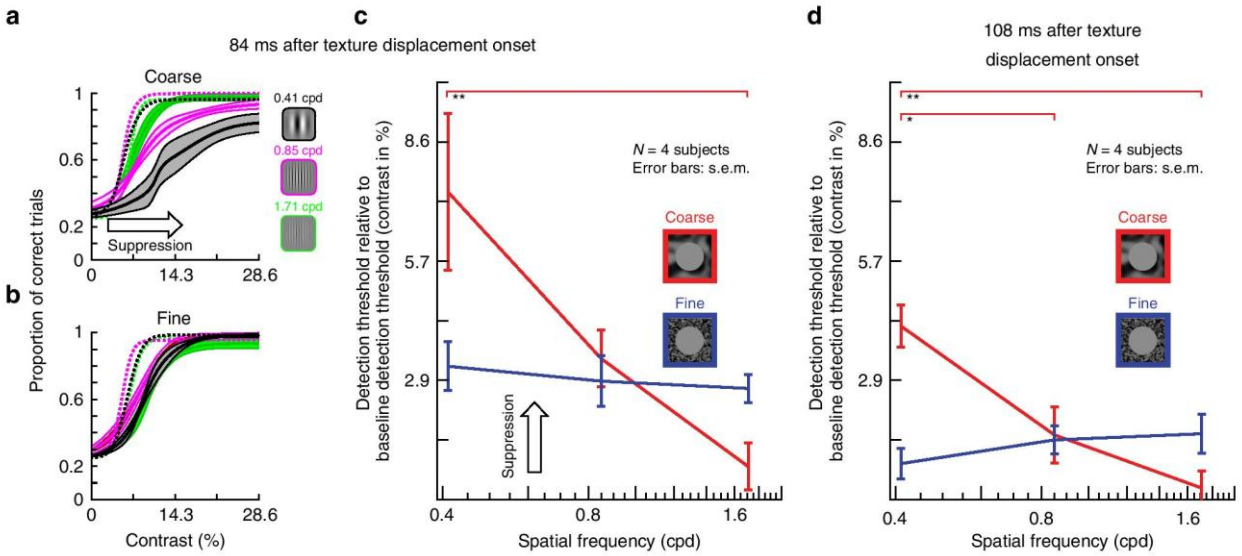

Fig. 10 Selective and unselective saccadic suppression without any saccades. This figure is identical to Fig. 9, except that real saccades were replaced (in the same subjects) with simulated saccades (exactly as in Fig. 8). All of the same conclusions were reached. There was selective suppression for low spatial frequencies when the texture surround was coarse (**a**); suppression was unselective for grating spatial frequency with a fine surround (**b**); and there was gradual recovery with time (**c**, **d**). In fact, perceptual suppression was clearer and longer lasting in this condition than with real saccades (also consistent with Figs. 1, 6, 8). All other conventions are as in Fig. 9. In **c**, the coarse texture surround showed a significant main effect of spatial frequency (1-way ANOVA, $p = 0.0113$, $F = 7.6878$; $p = 0.0092$ for post-hoc comparison between lowest and highest spatial frequency, indicated by **). In **d**, the coarse surround also showed a significant main effect of spatial frequency (1-way ANOVA, $p = 0.0019$, $F = 13.5276$; $p = 0.0017$ for post-hoc comparison between lowest and highest spatial frequency, and $p = 0.0186$ for post-hoc comparison between lowest and intermediate spatial frequency).

displacement. Specifically, such priors may cause perception to "omit" the pre-saccadic flash even though it evokes a strong retinal transient. This would happen exactly because of the pairing of the flash with a very likely occurrence of a saccade, interpreted as such due to the global image motion, even if its neural transient in the retina is weakened by the prior flash. This would result in a kind of credit assignment problem due to a strong prior association of global image motion with saccades.

More generally, our results suggest that visual flow is important in perceptual saccadic suppression, even in paradigms that have often been taken as indication for motor-related top-down suppression (Figs. 8–10). It would be interesting in the future to further test the generalizability of this notion. We were indeed greatly surprised when we found that selective suppression of low spatial frequencies[10] can be violated in two important ways. First, the suppression selectivity can be abolished with a simple change of visual context. Second, the same selective suppression of low spatial frequencies can be obtained without saccades. Thus, with or without saccades, either selective or nonselective suppression could occur as a function of visual flow. In hindsight, this might shed light on a surprising recent finding in superior colliculus[14]. There, using essentially the same paradigms, only one type of superior colliculus visually responsive neurons (so-called visual-motor neurons) exhibited selective suppression of low spatial frequency sensitivity. The other type of visually responsive neurons (visual-only neurons) showed mild but, critically, non-selective suppression[14]. These two types of neurons occupy different superior colliculus laminae and have different patterns of lateral interactions from across this structure's visual field representation[51]. It is now conceivable, considering our current results (Figs. 8–10), that both patterns of suppression (selective or not) may be embedded simultaneously in these different neuronal populations with specific circuitry and tuning for visual peripheral contexts.

Finally, motor-related mechanisms still likely play an important role in perceptual saccadic suppression. Such mechanisms appear to shorten suppression originating from visual processing (Fig. 6), and might therefore minimize the duration of saccade-induced disruptions. Indeed, a variety of cortical areas exhibit post-saccadic excitability enhancement[52–54]. It would be interesting to further investigate how such enhancement may contribute to the shortened time courses of perceptual saccadic suppression that we observed (e.g., Fig. 6e, f). Furthermore, besides just suppression, saccades are also associated with "omission", the lack of awareness of intra-saccadic background image motion[22,55]. It would, therefore, also be interesting to study the neural mechanisms through which strong saccade-induced neural transients in the retina (Fig. 3b) are perceptually "omitted" to give the illusion of continuous perception across saccades. More intriguingly, saccades also cause spatial updating of visual reference frames (compensating the image shifts that they cause). Information contained in the motor command itself is likely critical for adjusting spatial receptive fields across saccades, as observed in some brain areas[56,57]. Our findings leave open the possibility, however, that trans-saccadic image flow might play a role in this phenomenon as well.

Methods

Ethics approvals. We performed electrophysiological experiments on ex vivo mouse and pig retinae as well as non-invasive perceptual experiments on human subjects.

Animal use was in accordance with German and European regulations, and animal experiments were approved by the Regierungspräsidium Tübingen.

Human subjects provided written, informed consent, and they were paid 8–15 Euros per session of 45–90 min each. Depending on the experiment, each subject was measured for 2–10 sessions (detailed trial and session numbers are provided below). Human experiments were approved by ethics committees at the Medical Faculty of Tübingen University, and they were in accordance with the Declaration of Helsinki.

Retina electrophysiology laboratory setup. We used retinae extracted from *PV-Cre x Thy-S-Y* mice (*B6;129P2-Pvalb$^{tm1(cre)Arbr}$/J × C57BL/6-tg (ThystopYFPJS)*), which are functionally wild type[58–60]. Twenty-three retinae from seven male and fifteen female mice (3–12-months-old) were used. We also replicated experiments on pig retinae obtained from domestic female pigs after they had been sacrificed during independent studies at the Department of Experimental Surgery in our Medical Faculty. We used nine pig retinae.

We housed mice on a 12/12 h light/dark cycle in ambient temperature, ranging between 20–22 °C, and humidity levels of ~40%. Mice were dark adapted for 4–16 h before experiments. We then sacrificed them under dim red light, removed the eyes, and placed eyecups in Ringer solution (in mM: 110 NaCl, 2.5 KCl, 1 $CaCl_2$, 1.6 $MgCl_2$, 10 D-glucose, and 22 $NaHCO_3$) bubbled with 5% CO_2 and 95% O_2. We removed the retina from the pigment epithelium and sclera while in Ringer solution.

Pigs were anesthetized using atropine, azaperone, benzodiazepine (midazolam), and ketamine, and then sacrificed with embutramide (T61). Before embutramide administration, heparin was injected. The pigs were dark adapted for 15–20 min before sacrifice. Immediately after sacrifice, the eyes were enucleated under dim red light, and the cornea, lens, and vitreous were removed. Eyecups were kept in CO_2-independent culture medium (Gibco) and protected from light. We transported eyecups to our laboratory and cut pieces from mid-peripheral or peripheral retinae. Only those retinae that were healthy and showed ganglion cell responses to light stimuli were used in our experiments.

We recorded retinal ganglion cell (RGC) activity using either low- or high-density multi-electrode arrays (MEAs). The low-density setup consisted of a perforated 60-electrode MEA (60pMEA200/30ir-Ti-gt, Multichannel Systems, Reutlingen, Germany) having a square grid arrangement and 200 µm inter-electrode distance. We mounted an isolated retina on a nitrocellulose filter (Millipore) with a central 2 × 2 mm hole. The mounted retina was placed with the RGC-side down into the recording chamber, and good electrode contact was achieved by negative pressure through the MEA perforation. We superfused the tissue with Ringer solution at 30–34 °C during recordings, and we recorded extracellular activity at 25 kHz using a USB-MEA-system (USB-MEA 1060, Multichannel Systems) or a memory-card based system (MEA1060, Multichannel Systems). Data were acquired using MC Rack version 4.6.2 (Multichannel Systems). More details are provided in Reinhard et al.[61].

The high-density MEA setup consisted of either a HiDens CMOS MEA[62] (developed by the lab of Andreas Hierlemann, Basel, Switzerland) or a MaxOne system[63] (Maxwell Biosystems, Basel, Switzerland). The HiDens CMOS MEA featured 11,011 metal electrodes with inter-electrode (center-to-center) spacing of 18 µm placed in a honeycomb pattern over an area of 2 × 1.75 mm. Any combination of 126 electrodes could be selected for simultaneous recording. The MaxOne MEA featured 26,400 metal electrodes with center-to-center spacing of 17.5 µm over an area of 3.85 × 2.1 mm. In this system, up to 1024 electrodes could be selected for simultaneous recordings. For each experiment, a piece of isolated retina covering almost the entire electrode array was cut and placed RGC-side down in the recording chamber. We achieved good electrode contact by applying pressure on the photoreceptor side of the retina by carefully lowering a transparent permeable membrane (Corning Transwell polyester membrane, 10 µm thick, 0.4 µm pore diameter) with the aid of a micromanipulator. The membrane was drilled with 200 µm holes, with center-center distance of 400 µm, to improve access of the Ringer solution to the retina. We recorded extracellular activity at 20 kHz using FPGA signal processing hardware. In the case of the HiDens CMOS MEA, data were acquired using custom data acquisition software, called MEA 1k Scope (developed by the lab of Andreas Hierlemann, Basel, Switzerland). In the case of the MaxOne MEA, data were acquired using MaxLab software provided by Maxwell Biosystems, Basel, Switzerland.

In total, we performed 36 recordings, 24 from mouse and 12 from pig retina. Fifteen of the 36 recordings were done using low-density MEAs. Once a basic experimental protocol was established, we shifted to HiDens CMOS MEA providing much higher throughput. Twelve experiments were done using this setup. We upgraded to the MaxOne MEA for even higher throughput and did our final nine recordings using this setup.

We presented light stimuli to the retinal piece that was placed on the MEA using a DLP projector running at 60 Hz (Acer K11 for low-density MEA experiments and Lightcrafter 4500 for high-density MEA experiments). In all, 60 Hz is above the flicker fusion frequency of both mouse and pig retinae; therefore, the framerate of these projectors was adequate for our purposes. The Acer K11 projector had a resolution of 800 × 600 pixels covering 3 × 2.25 mm on the retinal surface. Lightcrafter 4500 had a resolution of 1280 × 800 pixels, extending 3.072 × 1.92 mm on the retinal surface. We focused images onto the photoreceptors using a condenser (low-density MEA recordings, illumination from below) or a 5x objective (high-density MEAs, illumination from above). In each case, the light path contained a shutter and two motorized filter wheels with a set of neutral density (ND) filters (Thorlabs NE10B-A to NE50B-A), having optical densities from 1 (ND1) to 5 (ND5). Light intensity was adjusted to be in the mesopic range.

We measured the spectral intensity profile (in μW cm^{-2} nm^{-1}) of our light stimuli with a calibrated USB2000 + spectrophotometer (Ocean Optics) and converted the physical intensity into a biological equivalent of photoisomerizations per rod photoreceptor per second (R* rod^{-1} s^{-1}), as described before[60]. Light intensities of the projector output covered a range of 3 log units (i.e., 1,000-fold difference between black and white pixels, over an 8-bit range). We linearized the projector output, and we used only grayscale images of limited contrast, spanning at most the range from 0 to 120 in the 8-bit range of the projector (see stimulus description below for details). Absolute light intensities were set to the mesopic level, where a stimulus intensity of "30" in our 8-bit DLP projector scale (0-255) corresponded to 225 to 425 R* rod^{-1} s^{-1}, depending on the experimental rig used for the experiment (i.e., different DLP projectors and MEAs). We pooled all data from the different rigs because separate individual analyses from the individual setups revealed no effects of recording conditions in the different setups.

Human psychophysics laboratory setup. We used a similar laboratory setup to our recent experiments[38,64,65]. Briefly, subjects sat in a dark room 57 cm in front of a CRT monitor (85 Hz refresh rate; 41 pixels per deg resolution) spanning 34.1 × 25.6 deg (horizontal x vertical). Head fixation was achieved with a custom head, forehead, and chin rest[64], and we tracked eye movements (of the left eye) at 1 kHz using a video-based eye tracker (EyeLink 1000, SR Research Ltd, Canada). Gray and texture backgrounds (e.g., Figs. 1, 6, 8–10) were always presented at an average luminance of 22.15 cd m^{-2}, and the monitor was linearized (8-bit resolution) such that equal luminance increments and decrements were possible around this average for textures and gratings. For the experiments in which we used luminance steps of the background as the visual transients replacing saccade-induced transients (Fig. 5), details of the luminances used are presented below with the experimental procedures.

Human Experiment 1 (Fig. 1) was performed by eight subjects (two female) who were 21–25-year-old. All subjects were naive to the purposes of the experiment, except for subject MB (an author). For Human Experiment 2, the "simulated saccade" version of Human Experiment 1 (Fig. 6), six of the same subjects participated. A control experiment for testing visibility of flashes without saccades and without saccade-like texture displacements (Supplementary Fig. 3a, b) was performed by six of the same subjects plus one non-naive subject, Z.H. (another author).

In the variants of Human Experiments 1 and 2 in which we collected full psychometric curves and perceptual thresholds (e.g., Figs. 2 and 7 and Supplementary Figs. 4 and 7), five subjects (24–29-year-old; one female) participated. Three of these subjects were the same as those who performed Human Experiments 1 and 2 above, confirming that both variants of the experiments (either with a fixed flash contrast or with full threshold calculations) allowed similar conclusions.

In the control experiment (Fig. 5) mimicking the retinal results of Fig. 4d, we collected data from five subjects (25–29-year-old; two female). Two of these subjects were the same as those who performed all experiments.

Human Experiment 3 tested suppression selectivity for low spatial frequencies (Fig. 8). Six subjects (three females, 23–25-year-old) participated, and only subject MB was non-naive. Three subjects had also participated in Human Experiments 1 and 2 and most of their control versions above. A control version of Human Experiment 3 was also performed with black surrounds (Supplementary Fig. 10). This control experiment was performed by the same subjects that participated in Human Experiment 3.

We also ran a variant of Human Experiment 3 describing full psychometric curves of perceptual detectability (Figs. 9 and 10). For each of the real (Fig. 9) or simulated (Fig. 10) variants, we ran four subjects (24–29-year-old; one female; three being the same as those who performed the experiments of Fig. 8).

Across all experiments, we ensured that the same subjects performed real and "simulated" saccade versions of a given paradigm so that we could make meaningful comparisons between these two eye movement conditions.

Coarse and fine textures. We created coarse and fine textures (Supplementary Fig. 1a) by convolving a random binary (i.e., white or black) pixel image with a two-dimensional Gaussian blurring filter[66] with the kernel

$$G(x, y) = e^{\frac{-(x^2+y^2)}{2\sigma^2}} \quad (1)$$

The parameter σ of the kernel influenced the amount of blurring. This resulted in textures having effectively low-pass spectral content (Supplementary Fig. 1b) with a cutoff frequency (f_c) depending on σ. As we describe below, we picked cutoff frequencies for coarse and fine textures that resulted in dark and bright image blobs approximating the receptive field sizes of RGCs (for coarse textures) and retinal bipolar cells (for fine textures). In other words, for a given species, coarse textures matched the resolution of RGCs, and fine textures matched the resolution of one processing stage earlier, the retinal bipolar cells.

For the ex vivo experiments with mouse and pig retinae, we assumed receptive field diameters for RGCs of at least 150 μm (Supplementary Fig. 1c; the parameter σ of the Gaussian blurring filter would be half that value), and diameters for bipolar cells of 25 μm (see Zhang et al.[67]). For human psychophysics experiments, we estimated, from the literature[36], the sizes of human parasol RGC receptive fields at eccentricities >6 deg from the fovea (our flash eccentricities were 7 deg) to be around 200 μm. This translated into a cutoff frequency of ~0.68 cycles per deg (cpd) (Supplementary Fig. 1b). Bipolar cell receptive field sizes at this eccentricity were estimated to be 10 μm (corresponding to a cutoff frequency of ~13.7 cpd), based on sizes of human midget RGC receptive fields in the fovea[36]. When calculating the textures, the actual value of the parameter σ (in pixel-dimensions) always incorporated the specific experimental magnification factor between the stimulation screen and the retinal projection of the image. Calculating power spectra for coarse and fine textures confirmed that cutoff frequencies for a given species were consistent with our aimed designs described above (Supplementary Fig. 1b).

For both retinal and perceptual experiments, we normalized pixel intensities in the textures to have uniform variations in luminance around a given mean. In the retinal experiments, we used pixel intensities (from our 8-bit resolution scale) ranging from 0 to 60 around a mean of 30, or ranging from 30 to 90 around a mean of 60 (see Retina electrophysiology experimental procedures below for when each paradigm was used). For the human experiments, textures had a mean luminance of 22.15 cd m^{-2} with undulations in luminance in the texture within the range of 7.5–35.5 cd m^{-2}.

As each texture, particularly when coarse, could have patterns of dark and bright blobs that human subjects can remember or interpret as potential shapes/objects/figures, we varied the displayed texture images from trial to trial. This was also necessary to avoid afterimages. We generated sets of 20 coarse and 20 fine textures, which we randomly interleaved across trials. Moreover, the textures themselves were designed to be larger than the viewable display area, allowing us to jitter the displayed sub-rectangle of each texture (within the viewable area of the display) from trial to trial (we jittered the displayed sub-rectangle within a range of 0.6 × 0.6 deg in steps of 0.024 deg). This way, even fine patterns at foveal fixation locations could not be memorized by the subjects across trials.

Retina electrophysiology experimental procedures. To simulate saccades in our ex vivo retina electrophysiology experiments, we displaced the texture across the retina in 6 display frames (100 ms at 60 Hz refresh rate). For easier readability, we sometimes refer to these saccade-like texture displacements as "saccades". The textures were displaced in each frame by a constant distance along a linear trajectory. While each "saccade" lasted 100 ms, displacement direction was varied randomly for each "saccade" (uniformly distributed across all possible directions), and "saccade" amplitude could range from 310 to 930 μm (corresponding to a velocity range of 3100–9300 μm s^{-1} on the retinal surface). In visual degrees, this corresponds to a velocity range of 100–300 deg s^{-1} and displacement range of 10–30 deg in mice, well in the range of observed mouse saccade amplitudes[68]. In fact, similar to primates, mice also have oculomotor behavior, even under cortical control[69]. For example, they make, on average, 7.5 saccade-like rapid eye movements per minute when their head is fixed[68] (humans make several saccades per second). We used the same retinal displacement range of 310 to 930 μm for pig retinae. To the best of our knowledge, pig oculomotor behavior has not been documented in the literature. However, with their larger eyeball sizes, our translations of the retinal image would correspond to slower saccades (e.g., small saccades in humans and monkeys), which are also associated with saccadic suppression. Moreover, we showed (Fig. 4) that retinal "saccadic suppression" is not critically dependent on the details of movement kinematics.

Each "trial" consisted of 39 successive sequences that each combined a "saccade" with a probe flash, as follows: there was first a "pre-saccade" fixation of 2 s, then a 100 ms "saccade", followed by "post-saccade" fixation. The background texture was switched on at the beginning of each trial and was translated across the retina during each "saccade". At a certain time from "saccade" onset (delay d, range: −177 to 2100 ms), we presented a probe flash. In most cases, the probe flash had a duration of 1 frame (~16 ms). We used 2 frames (~33 ms) in a subset of experiments (mouse: 161 of 688 cells analyzed for "saccadic suppression"; pig: 112 of 228 cells). Results were pooled across these paradigms as they were indistinguishable. For sequences containing no probe flash, the next "saccade" happened 4 s after the previous one. The probe flash was a full-screen positive ("bright") or negative ("dark") stimulus transient. In different experiments, only a subset of possible delays was used within a given set of trials, depending on total recording time for a given retina (see below).

Bright or dark probe flashes could happen in two different ways across our experiments. The results were indistinguishable between the two ways, so we pooled results across them. Briefly, in one manipulation, the probe flash was a homogeneous bright (pixel intensity of 60 in our 8-bit projectors) or dark (pixel intensity of 0) full-screen rectangle replacing the background texture (in these experiments, the textures themselves had intensities ranging from 0 to 60 pixel intensity; see Coarse and fine textures above). This way, the flash contrast from the underlying background luminance was variable (e.g., a bright flash on a bright portion of a texture had lower contrast from the underlying texture than the same flash over a dark portion of the texture). In the second manipulation, the bright and dark flashes were simply luminance increments or decrements (by pixel values of 30 on our 8-bit projectors) over the existing textures (like in our human perceptual experiments). This way, local contrast relationships in the background textures were maintained. In these experiments, the textures themselves had a range of 30–90 pixel intensities and a mean pixel value of 60 (on our 8-bit projectors). Three-hundred thirty-two of 688 cells that we analyzed for "saccadic suppression"

experienced such probe flashes, whereas the rest (356 cells) experienced the homogenous probe flash. For pig retina recordings, we always used the homogenous framework. However, in the subset of pig experiments where the 2-frame probe flash was employed (112 of 228 RGCs), we used a high-contrast probe flash such that a bright flash would be achieved by first going completely dark in the first frame followed by the bright flash in the next frame and vice versa for a dark flash. Again, all data were pooled across these different paradigms because their outcomes were indistinguishable.

The number of trials required during a physiology experiment depended on the number of conditions that we ran on a specific day. For example, testing 7 different flash delays required 15 trials (7 with bright probe flashes, 7 with dark probe flashes, and 1 without probes). In a given experiment, we always interleaved all conditions; that is, in any one of the 15 necessary trials, each of the 39 "saccades" could be followed by a bright or a dark probe at any of the 7 delays, or no probe at all. Moreover, we repeated the total number of conditions (e.g., the interleaved 15 trials) four times per session, and we averaged responses across repetitions. Since one trial typically lasted for 2 min, the example of 15 trials repeated 4 times lasted for ~2 h. This was usually combined with additional conditions (e.g., other background textures), such that typical recordings lasted 10–12 h. If the combination of conditions would have required even longer recordings in a given session, we typically reduced the number of conditions (e.g., we presented flashes at fewer delays).

We sometimes replaced the 100 ms "saccade" with an instantaneous texture jump, to test the sensitivity of retinal "saccadic suppression" (Fig. 3) to the kinematic properties of saccade-like texture displacements (Fig. 4b). Here, the texture simply jumped, in one display frame, from the pre- to the post-displacement position. All other procedures were like described above. Thirty-one RGCs were recorded with this paradigm.

In the control experiments of Fig. 4d, we used no textures at all. The screen was always a homogenous gray field, and the visual event of a "saccade" was replaced by an instantaneous step to a different gray value. The gray backgrounds had intensities between 30 and 90 (on our 8-bit projector). This instantaneous change in intensity caused either a positive contrast step (+0.03 to +0.50 Michelson contrast) or a negative contrast step (–0.03 to –0.50 Michelson contrast). A "trial" consisted of either 57 or 157 successive sequences that each combined a contrast step with a probe flash, as follows: there was first a "pre-step" fixation of 2 s (analogous to "pre-saccade" fixation in texture displacements), then an instantaneous switch to "post-step" fixation. At a certain time from the contrast step (delay: 17, 33, 50, 100, 250, 500, 1000, or 2000 ms), we presented a 2-frame (~33 ms) probe flash. For sequences containing no probe flash, the next contrast step happened 4 s after the previous one. The probe flash was either a uniform negative step of –0.33 Michelson contrast ("dark") or a uniform positive step of +0.33 Michelson contrast ("bright").

Finally, we used other stimuli unrelated to the main experiments to help us characterize RGC types and other receptive field properties (e.g., response polarity, latency, transiency, and spatial receptive fields). These stimuli had the same mean intensities and intensity ranges as the textures used in each experiment. Below, we describe these stimuli for the condition in which the texture intensities ranged from 0 to 60 pixel intensity (represented as grayscale RGB values in the units of our 8-bit projects). In experiments in which the textures ranged in intensity from 30 to 90, all intensities reported below were shifted upward by 30. (1) Full-field contrast steps. ON steps: stepping from 0 to 30 (+1 Michelson contrast) and from 30 to 60 (+0.33) for 2 s. OFF steps: stepping from 60 to 30 (–0.33) and from 30 to 0 (–1) for 2 s. (2) Full-field Gaussian flicker, 1 min. Screen brightness was updated every frame and was drawn from a Gaussian distribution with mean 30 and standard deviation 9. This stimulus was used to calculate the linear receptive field filters of ganglion cells through reverse correlation (spike-triggered averaging of the stimulus history). (3) Binary checkerboard flicker, 10–15 min. The screen was divided into a checkerboard pattern; each checker either covered an area of 55 × 55 μm, 60 × 60 μm, or 65 × 65 μm depending on the recording rig. The intensity of each checker was updated independently from the other checkers and randomly switched between 10 and 50 or 0 and 120. This stimulus also allowed us to calculate the linear filters of cells' receptive fields.

Human psychophysics experimental procedures. In Human Experiment 1, we presented a coarse or fine background texture (Fig. 1) for 800–1700 ms in every trial. Over the texture, a white fixation marker (square of 7.3 × 7.3 arcmin) surrounded by a uniform gray circle of 30 min arc radius was presented at one screen location in order to guide gaze fixation onto the marker. The fixation marker was always at 4.8 deg eccentricity from display center, but its specific location was varied from trial to trial (up-right, up-left, down-right, or down-left relative to display center; 45 deg direction from horizontal). After the end of the initial interval, the fixation marker jumped to display center, instructing subjects to generate a saccade.

At a random time from the saccade instruction (47, 94, 153, 200, 247, or 507 ms), a luminance pedestal (probe flash) was applied for one display frame (~12 ms) at one of four locations relative to display center (7 deg above, below, to the right of, or to the left of center). Note that because the display was rasterized (that is, drawn by the computer graphics board from the top left corner in rows of pixels), the actual exact flash time and duration depended on the location of the flash on the display (but in a manner like other psychophysical experiments studying the same phenomenon, and also in a manner that is unlikely to affect our results). The luminance pedestal consisted of a square of 147.8 × 147.8 min arc in which we added or subtracted a value of 4.8 cd m^{-2} to the texture pattern. Therefore, local contrast within the luminance pedestal was the same as that without the pedestal. Since all of our analyses revealed identical results whether the pedestal was a luminance increment or decrement, we combined these conditions in all analyses. At the end of the trial, subjects had to report their perceived flash location by pressing one of four buttons, corresponding to the four possible flash locations, on a hand-held response box.

As saccadic reaction times were 156.9 ± 3.3 ms s.e.m. across subjects, our choice of flash times above meant that we could analyze trials in which flashes appeared before or after saccade onset, allowing us to obtain full time courses (e.g., Fig. 1). Also, because of the display geometry, the retinal region that experienced a flash before, during, or after a saccade was always a region that was visually stimulated by the texture before flash onset (rather than by the monitor edge or the black surround of the laboratory). Therefore, we maintained pre- and post-flash visual stimulation by texture background, as in the retinal experiments. We also ensured that flash locations were not coincident with saccade goal locations both retinotopically and also in display coordinates. We confirmed in separate analyses that similar effects of suppression (e.g., Fig. 1) occurred for each flash location separately.

We collected 576 trials per session in this experiment. Six subjects participated in six sessions each, and the remaining two participated in three or four sessions.

Human Experiment 2 (Fig. 6) was identical, except that the initial fixation marker was presented at display center and remained there for the entire duration of a trial. Instead of instructing a saccade 800–1700 ms after fixation marker onset, we translated the entire background texture (switched on at trial onset) rapidly to simulate a saccade-like image displacement. Texture displacement consisted of a 6-frame translation at a speed of 176 deg s^{-1}. Note that, because of our display refresh rate and geometry, this meant a slightly larger displacement (of 12.4 deg) when compared to the saccade sizes in Human Experiment 1. However, we chose this translation because it resulted in a sufficiently fast average speed of the displacement (average speed in the real saccades of Human Experiment 1 was 160 deg s^{-1}). This choice is not problematic because our retinal experiments revealed that visual mechanisms related to saccadic suppression were not sensitive to parameters of individual motion patterns (Fig. 4b).

In this experiment, the texture displacement happened in a diagonal direction to simulate the directions of saccadic displacements of Human Experiment 1 (and also to dissociate the direction of motion flow from the locations of the flashes, again as in Human Experiment 1). For example, the texture could move globally down-right, as might be expected (in terms of image motion) if subjects made upward-leftward saccades in Human Experiment 1. Also, flash times were chosen relative to the onset of texture displacement from among the following values: –35, –24, 24, 47, 84, 108, 141, 200, 259, 494 ms.

All subjects participated in ten sessions each in this experiment.

We also performed a control experiment, in which there was neither a real saccade (Human Experiment 1) nor a texture displacement (Human Experiment 2), but otherwise identical to these two experiments. Subjects simply fixated display center, and we presented (after 1200 to 2400 ms from trial onset) a luminance pedestal exactly as in Human Experiments 1 and 2. To obtain full psychometric curves, we varied the luminance increment from among six values (Supplementary Fig. 3a, b). Subjects performed two sessions each of this experiment (600 trials per session).

To explore perceptual thresholds in a more quantitative manner for Human Experiments 1 and 2, we also performed additional real or simulated saccade experiments collecting full psychometric curves (Figs. 2 and 7; and Supplementary Figs. 4 and 7). The logic of both additional experiments (real or simulated) was the same as that of Human Experiments 1 and 2, except that we varied the luminance of the probe flash from trial to trial (like in the above control experiment of flash visibility; Supplementary Fig. 3a, b). As this endeavor (allowing us to measure full psychometric curves) was very data intensive, we reduced the time samples relative to saccade onset or texture displacement onset at which we probed perceptual performance. For the experiment with real saccades, we used an automatic procedure to detect saccade onset in real-time based on eye velocity, as described by Chen and Hafed[39]. We then presented the probe flash at 42, 65, 88, or 148 ms after saccade detection. These times were chosen because they covered intervals of maximum perceptual saccadic suppression as well as recovery, allowing us to get a time course of perceptual threshold elevation associated with saccadic suppression. In subsequent data analyses, we confirmed that these flash times were as planned (within the expected variability due to the asynchronous nature of saccade times relative to display update times; Fig. 2). For the experiment with simulated saccades, we presented the probe flash at –24, –12, 48, or 96 ms relative to the onset time of the texture displacement. In this case, we introduced a new negative time sample to the set (–12 ms) because the original Human Experiment 2 did not probe this particular time (e.g., Fig. 6). It was therefore important to clarify that the time course of perceptual suppression for simulated saccades was continuous and well-behaved, exactly like that for real saccades.

In order to also estimate perceptual thresholds online in these additional experiments, and therefore optimize the numbers of trials needed, we applied an adaptive QUEST procedure[40] on each randomly interleaved condition. Specifically,

the first 40 trials of each randomly interleaved condition (e.g., flash time −24 ms and coarse texture, or flash −12 ms time and fine texture, and so on) were part of the QUEST procedure. The remaining trials in the session interleaved four additional flash luminances per condition, which were chosen to lie around the threshold luminance of each condition as detected by the QUEST procedure. These additional flashes had luminances that were ±1 or ±2 times a pre-defined luminance increment for a given condition, depending on the detected threshold and earlier pilot data. Specifically, if the detected threshold (according to QUEST) was very low (e.g., no suppression effect), the pre-defined luminance increment was 1 step of luminance (dictated by the luminance resolution of our display; Supplementary Fig. 3a). That is, the four additional flashes were at ±1 and ±2 display-determined luminance steps from the detected threshold. If the detected threshold (according to QUEST) was high (e.g., strong suppression), we made the pre-defined luminance increment 2 or 5 display-determined luminance steps (that is, ±2 and ±4 display-determined luminance steps or ±5 and ±10 display-determined luminance steps, respectively). This allowed fitting the psychometric curves during subsequent data analyses, including measurements from the full dynamic range of perceptual performance. The reasoning behind this approach is as follows: depending on the amount of perceptual saccadic suppression to be expected per condition (e.g., peak suppression during saccades or texture displacements, or very weak suppression during recovery), it is expected that the psychometric curves would be shifted by different amounts from baseline depending on the particular condition (e.g., flash time or coarse versus fine texture). Finally, also note that we only used bright flashes in these particular experiments instead of both bright and dark flashes. In total, we collected 240 trials per condition per subject.

In yet another control experiment for Human Experiments 1 and 2, we mimicked the retinal results of Fig. 4d. Subjects fixated a central fixation spot over a gray background. The background had one of eight luminances (22.4, 30.24, 38.08, 45.92, 53.76, 61.6, 69.44, 77.28 cd m^{-2}). After a random initial fixation duration (similar to Human Experiment 2), the luminance of the background was changed suddenly (in one display frame update) to one of the remaining seven luminances. This meant that across trials, we had seven total levels of contrast change in the background as our visual transient. At one of five different possible times relative to the time of background luminance change (−24, −12, 36, 72, or 108 ms), a luminance pedestal was flashed briefly, exactly like in Human Experiments 1 and 2. We ensured that the contrast of the flash (relative to the currently displayed background luminance) was always the same across all trials. We also ensured that baseline visibility of the pedestal in the absence of the contrast change was at ceiling performance (see the longest sampled time value in Fig. 5, demonstrating near perfect detection performance for all background luminance steps). Subjects maintained fixation throughout all trials and simply reported the locations of the brief flashes. Subjects performed one session, each, of this experiment, with 1120 trials per session.

In Human Experiment 3 (Fig. 8), the flashes of Human Experiments 1 and 2 were replaced by vertical Gabor gratings having one of five different spatial frequencies (0.41, 0.85, 1.71, 3.42, 4.56, or 6.8 cpd). The contrast of the grating (defined as the difference between maximum and minimum luminance in the grating divided by the sum of the same luminances) was 14.3%. Spatial phase was randomized from trial to trial, and the σ parameter of the Gaussian envelope was 0.49 deg. Also, a virtual monitor of 20 deg diameter was present at display center at the time of Gabor grating flashes. The virtual monitor had a uniform gray luminance equal to the average of the textures used in Human Experiments 1 and 2. Surrounding the virtual monitor, a coarse or fine texture could be visible.

In one block of trials, subjects generated saccades towards display center using the same procedures as in Human Experiment 1. Grating flash times were similar to Human Experiment 1, and the subjects performed 6 sessions each (576 trials per session).

In another block of trials, subjects maintained fixation at display center. In one third of the trials, the virtual monitor and surrounding texture did not move. These trials provided us with "baseline" visual performance (i.e., without saccades or virtual monitor displacements). It was necessary to have these trials because perceptual visibility of different spatial frequencies is not equal due to the well-known human contrast sensitivity function[70]. Therefore, we needed to establish "baseline" grating visibility first and then compare the effects of saccades or saccade-like virtual monitor displacements on such visibility. In the remaining two thirds of the trials, the virtual monitor and surrounding texture initially appeared displaced from display center at a location near one corner of the display and along one of the diagonal directions. After 800–1700 ms, the virtual monitor and surrounding texture were translated rapidly towards display center to simulate visual flow associated with the diagonal saccades of the real-saccade version of the paradigm (the translation parameters were similar to Human Experiment 2). Grating flashes happened 84 ms or 108 ms after virtual monitor and texture displacement. Note that we reduced the number of flash times here because of the larger number of conditions (five different spatial frequencies of the Gabor gratings) that needed to be collected. However, our data were consistent with all other experiments in terms of recovery time courses of suppression (e.g., Figs. 1, 6, 8 and Supplementary Figs. 8–10).

As the initial displaced position of the virtual monitor (and texture) provided a cue to subjects that grating onset was expected soon, and because such a cue was not present in the one third of trials without image motion, we equalized subject expectations across these conditions by dimming the fixation point to black from the time of image motion onset until 200 ms after flash onset (equal timing was ensured in the one third of trials without image motions, such that the same expectation of grating onset was established by fixation marker dimming). The fixation marker then disappeared, and subjects had to report flash location.

Subjects performed six sessions each of this condition, with 576 trials per session (two subjects performed seven and five sessions each instead of six).

We also repeated the same experiment but with a black surround around the virtual monitor instead of a coarse or fine texture. Note that a black surround is theoretically equivalent to an infinitely coarse surround. We therefore expected results conceptually similar to those with a coarse surround. Also, in this control experiment, we randomly interleaved all trial types together in the same session (fixation with virtual monitor displacement, real saccade, and fixation with neither virtual monitor displacement nor saccade). This allowed us to further confirm that our results from Human Experiment 3 were not influenced by the separate blocking of real saccade trials and virtual monitor displacement trials.

We also repeated Human Experiment 3 to collect full psychometric curves, like we did for Human Experiments 1 and 2 above. In these additional experiments, because of the data-intensive nature of full psychometric curves, we concentrated on the three lowest spatial frequencies of the Gabor gratings. This was sufficient to observe selectivity or lack of selectivity of perceptual suppression as a function of spatial frequency (e.g., Fig. 8). More importantly, these three lowest spatial frequencies were associated with ceiling baseline visibility (Fig. 8), thus simplifying interpretations of any suppression that we would observe. The experiments were the same as Human Experiment 3, except that the contrast of the flashed Gabor grating was varied from trial to trial. We used a similar adaptive procedure to that used in Figs. 2 and 7 to select contrast from trial to trial, in order to optimize finding perceptual thresholds and fitting of psychometric curves (see procedures above). We also used the same online saccade detection algorithm as in the experiments of Fig. 2 to decide on the time of Gabor grating flash onset (see procedures above). For both real and simulated saccade variants of these experiments, we used two times relative to the "saccade" event, one within a period associated with strong perceptual suppression and one at a late time point associated with perceptual recovery (see Figs. 9 and 10).

Retina electrophysiology data analysis and statistics. Low-density MEA recordings were high-pass filtered at a 500 Hz cutoff frequency using a tenth-order Butterworth filter. We extracted spike waveforms and times using thresholding, and we semi-manually sorted spikes using custom software. For high-density MEA recordings, we performed spike sorting by an offline automatic algorithm[71] and assessed the sorted units using UnitBrowser[72]. We judged the quality of all units using inter-spike intervals and spike shape variation. Low-quality units, such as ones with high inter-spike intervals, missing spikes, or contamination, were discarded. All firing rate analyses were based on spike times of individual units.

We first characterized the properties of RGCs. We calculated linear filters in response to full-field Gaussian flicker and binary checkerboard flicker by summing the 500-ms stimulus history before each spike. The linear filters allowed determining cell polarity. Specifically, the amplitude of the first peak of the filter was determined. If the peak was positively deflected, the cell was categorized as an ON cell; if negatively deflected, the cell was an OFF cell. ON cells were later always analyzed with respect to their responses to bright probe flashes in the main experiment, and OFF cells were analyzed with dark probe flashes. We determined the spatial receptive fields of RGCs by calculating the linear filters for each region (checker) defined by the binary checkerboard flickering stimulus. The modulation strength of each linear filter, measured as the s.d. along the 500 ms temporal kernel, is an estimate for how strongly that region drives ganglion cell responses. We fitted the resulting 2D-map of s.d. values with a two-dimensional Gaussian and took the 2-σ ellipse (long axis) as the receptive field diameter. For all other figures and analyses, we converted spike times to estimates of firing rate by convolving these times with a Gaussian of $\sigma = 10$ ms standard deviation and amplitude 0.25 $\sigma^{-1}e^{1/2}$.

For each RGC, we used responses to full-field contrast steps to calculate an ON-OFF index, a transiency index, and a response latency index. These indices were used to characterize the properties of RGCs (Supplementary Fig. 6) that we included in our analyses. The ON-OFF index was calculated by dividing the difference between ON and OFF step peak response by their sum. The resulting index values ranged between −1 (OFF) and +1 (ON) and were then scaled to span between 0 (OFF) and +1 (ON). The transiency index was defined as the ratio of the response area within the first 400 ms and the total response area spanning 2000 ms. The resulting index had a value of 1 for pure transient cells. Response latency was calculated as the time from stimulus onset to 90% of peak response. This value was normalized to the maximum response latency in our dataset to create the response latency index.

To quantify retinal "saccadic suppression", we first determined a "baseline response", defined as the response to a probe flash ~2 s after texture displacement onset (delay between 1967 and 2100 ms, depending on the specific flash times used in a specific experiment). This baseline response was compared to responses of the same cell to the same flash when it occurred at an earlier time (i.e., closer in time to the "saccade"). Usually, the saccade-like texture displacements themselves caused significant neural responses even without flashes ("saccade-response", e.g., Fig. 3b), and the responses to the flashes were superimposed on these "saccade-responses"

(Fig. 3c). We therefore first isolated the component of the responses caused by the flashes by subtracting the "saccade-responses" from the composite responses.

To get a robust estimate of the response to "saccades" alone (i.e., without any flashes), we averaged spike rate from before "saccade" onset up until the next "saccade" onset for conditions in which no flash was presented, or until just before the flash onset for conditions in which a "post-saccade" flash was presented. This was done for each of the 39 successive "saccades" in a given trial.

We then computed a neural modulation index, ranging from −1 to +1. A value of −1 represents complete suppression of flash-induced responses, whereas +1 indicates "complete enhancement" of flash-induced responses (that is, there was only a response to a flash after saccades, but not to a flash in isolation). A modulation index of 0 meant no change in flash-induced response relative to the "baseline" response. The modulation index of an RGC for a given flash delay d after "saccade" onset was calculated as $(r_d - r_b)/(r_d + r_b)$ where r_d is the peak firing rate for the flash-component of the response (see above for how we isolated this from the composite "saccade" +flash response) and r_b is the peak firing rate for the baseline flash response (i.e., the same flash but occurring ~2 s away from any "saccade"; see above). In all cases, peak firing rate was estimated after averaging responses from all repetitions of a given condition (delay d or baseline) for a given RGC. For ON cells, the modulation index was based only on responses to bright flashes, and for OFF cells, it was based on responses to dark flashes. For some analyses, we also calculated modulation indices of RGCs for each of the 39 individual "saccades" using the same procedure.

In some cells and trials, individual "saccades" from the sequence of 39 were discarded. This happened when the baseline response peak was <60% of the median baseline response peak across the 39 "saccades" of a given trial. We did this to ensure that our modulation indices were not marred by a numerator and denominator approaching zero (e.g., if both flash and baseline responses were weak). We did, however, re-include sequences in which the peak response to the flash after the "saccade" was above the median baseline response peak (across the 39 "saccades"). This was done in order to re-include sequences (if discarded by the first step) for which the baseline flash response was weak but a flash after "saccades" nonetheless gave a robust response. For example, this could happen if a cell did not respond to a flash in isolation but the "saccade" enhanced the response to a flash following it. Our main results (e.g., Fig. 3) were highly robust to such scenarios.

Finally, to perform statistics, we applied tests at either the individual cell level or at the level of the population. At the individual cell level, we determined whether a given RGC's modulation index for a probe flash presented at a given delay was significantly different from 0 (i.e., "Is the response of this cell modulated by the "saccade"?"). For this, we performed a one-tailed sign test of the null hypothesis that the 39 individual modulation indices came from a distribution with zero median against the alternative hypothesis that the median was below (for negative modulation index) or above (for positive modulation index) zero. The modulation index was considered significant (i.e., the flash response was modulated by the "saccade") at $p < 0.05$ if the test had a power $(1 - \beta)$ of at least 0.8. At the population level, we determined whether the retinal output as a whole was modulated by "saccades". For this, we performed a two-tailed Wilcoxon signed-rank test of the null hypothesis that the median of the distribution of modulation indices did not differ from 0. Lastly, we tested whether the modulation index of the population was significantly different across textures. For this, we performed a two-tailed Wilcoxon signed rank test of the null hypothesis that the median of the distribution of modulation indices did not differ across textures. Since our modulation index was based on responses to the brief probe flashes, it could only be computed for cells that did respond to these flash stimuli (mouse: $N = 688$ of 1423 recorded cells; pig: $N = 228$ of 394). Only these cells, showing a measurable baseline flash response, were included in our analyses for retinal "saccadic suppression" (Fig. 3e and Supplementary Fig. 5).

To quantify retinal "saccadic suppression" in our control experiments with structure-free uniform backgrounds and luminance steps in place of textures and texture displacements (Fig. 4d), we used the same analyses and statistical procedures to those described above for the texture displacement paradigm. The only difference was that instead of 39 successive "saccades" in a trial, we now had either 57 or 157 successive full-field luminance steps (depending on experiment setting). Twenty-two of 57 or 66 of 157 steps had a Michelson contrast in the range of ±0.03 to ±0.15 and these steps were used to quantify suppression for low-contrast luminance steps. Twenty-four of 57 or 58 of 157 steps had a Michelson contrast in the range of ±0.20 to ±0.40 and were used to quantify suppression for high-contrast luminance steps. From the perspective of visual transients across the retina, low-contrast luminance steps are equivalent to fine texture displacements over receptive fields, and high-contrast luminance steps are equivalent to coarse texture displacements. This is simply because of the spatial relationship between receptive field sizes and texture spatial scales: a fine texture presents both dark and bright blobs within individual receptive fields both before and after the texture displacement (resulting in a low-contrast change in luminance over the receptive fields); on the other hand, a coarse texture has dark or bright blobs that are of similar size to the receptive fields (resulting in the potential for a very large contrast change in luminance over the receptive fields after the texture displacement). As shown in Fig. 4d, low and high-contrast luminance steps resulted in the modulation of ganglion cell responses to the probe flashes that was reminiscent of the modulation observed after displacement of fine and coarse textures, respectively (also validated perceptually in Fig. 5). Similar to the texture displacement paradigm, the modulation index was based on responses to brief probe flashes, and it could therefore only be computed for cells that did respond to these flash stimuli ($N = 376$ of 650 recorded RGCs in mouse). The modulation index for ON RGCs was calculated from responses to bright probe flashes, and that for OFF RGCs was calculated from responses to dark flashes.

Human psychophysics data analysis and statistics. We analyzed eye movements in all trials. We detected saccades using established methods[39,73], and we manually inspected all trials to correct for mis-detections. In experiments requiring a saccade (e.g., Fig. 1), we excluded from analysis any trials with premature (before saccade instruction) or late (>500 ms reaction time) saccades. We also rejected all trials in which saccades landed >0.5 deg from the saccade target. In experiments requiring fixation, we excluded from analysis any trials in which a saccade or microsaccade happened anywhere in the interval from 200 ms before to 50 ms after any flash or grating onset.

For experiments with saccades (e.g., Fig. 1), we obtained time courses of perception by calculating, for each trial, the time of flash or grating onset from saccade onset. We then binned these times into 50 ms bins that were moved in 5 ms bin-steps relative to saccade onset. Within each bin, we calculated the proportion of correct trials, and we obtained full time courses of this perceptual measure. We obtained time course curves for each subject individually, and we then averaged the curves for the individual subjects in summary figures. All of our analyses were robust at the individual subject level as well (e.g., Supplementary Fig. 2).

For experiments with simulated saccades (i.e., saccade-like texture displacements), or background luminance steps (Fig. 5), there were discrete flash or grating times relative to "simulated saccade" onset, so no temporal binning was needed. At each flash or grating time, we simply calculated the proportion of correct trials.

When we fitted performance to psychometric curves (e.g., Supplementary Fig. 3a, b), we used the psignifit 4 toolbox[74], and we used an underlying beta-binomial model. In all psychometric curve fits, we also included lapse parameters among the fitted parameters, in order to account for potential small deviations from either perfect ceiling performance or perfect floor (chance) performance at the extremes of the psychometric curves.

We also used the same toolbox to analyze the variants of Human Experiments 1 and 2 in which we collected full psychometric curves (Figs. 2 and 7). For these experiments, we defined the threshold of an individual subject as the flash luminance level that resulted in correct perceptual performance at a value of 62.5% of the total dynamic range of the subject's psychometric curve (that is, 62.5% of the dynamic range of the fitted psychometric curve after the inclusion of lapse rates). We then plotted the value of such threshold as a function of flash time relative to real or simulated saccade time.

For some analyses of Human Experiment 3 and its control version, we calculated a "suppression ratio" as a visualization aid (e.g., Fig. 8). This was obtained as follows. For a given spatial frequency grating, we calculated the fraction of correct trials within a given time window (from either simulated or real saccade onset) divided by the fraction of correct trials for the same spatial frequency when there was neither a saccade nor a virtual monitor and texture displacement (i.e., baseline perception of a given spatial frequency). This ratio therefore revealed the effect of suppression independently from the underlying visibility of any given spatial frequency[14]. However, note that we also report raw proportions of correct trials in all conditions.

All error bars that we show denote s.e.m. across individual subjects, except where we report individual subject analyses and control analyses. For individual subject performance, error bars denote s.e.m. across trials; for control analyses, error bars denote 95% confidence intervals (e.g., Supplementary Fig. 3a, b) or s.d. (e.g., Supplementary Fig. 3d, f). All error bar definitions are specified in the corresponding figures and/or legends.

To statistically validate if the time courses for perceptual localization performance for saccades across the different background textures (coarse versus fine) differed significantly from each other (e.g., Fig. 1), we used a random permutation test with correction for time clusters of adjoining significant p-values[37,38]. First, for each time bin, we calculated a test statistic comparing performance for coarse versus fine background textures. This test statistic was the difference between the proportion of correct responses for the different textures. Then, we performed a random permutation with 1000 repetitions for each time bin; that is, we collected all trials of both conditions, within a given time bin, into a single large set, and we randomly assigned measurements as coming from either coarse or fine textures, while at the same time maintaining the relative numbers of observations per time bin for each texture condition. From this resampled data, we calculated the test statistic again, and we repeated this procedure 1000 times. Second, we checked, for each time bin, whether our original test statistic was bigger than 95% of the resampled test statistics (i.e., significant), and we counted the number of adjoining time bins that were significant at this level (i.e. clusters of time bins in which there was a difference between coarse and fine textures). We then repeated this for all 1000 resampled test statistics. The p-value for our original clusters was then calculated as the number of resampled clusters that were bigger or the same size as the original clusters, divided by the total number of repetitions

(1000). This procedure was described in detail elsewhere[38]. We followed a conservative approach, paying no attention to which bins in the resampled data formed a cluster of time bins. As discussed elsewhere[38], our statistical analysis constituted a highly conservative approach to establishing significance of differences between time courses for coarse and fine textures. In Human Experiment 3, we used the same approach to compare time courses of suppression ratio for coarse and fine surround contexts with real saccades.

For Human Experiment 2, we had discrete flash times relative to texture displacement onset. Here, the comparison between coarse and fine textures was tested with a Bonferroni-corrected χ^2 test at corresponding flash times. To compare between real and simulated saccades in Human Experiments 1 and 2, we also ran a Bonferroni-corrected χ^2 test. We only considered time bins in the real saccade data that corresponded to the discrete flash times in the simulated saccade data. A Bonferroni correction was necessary because we tested the same data sets on multiple time bins with the same hypothesis (that there is a difference in time courses).

In Human Experiment 3, we also compared suppression ratios for real and simulated saccades for a given texture surround. We again used a Bonferroni-corrected χ^2 test. This was justified because within a given surround, baseline data were the same for real and simulated saccades. Therefore, the relationship between the proportion of correct localizations and suppression ratio was identical. In contrast, testing suppression ratios between fine and coarse surrounds in the same experiment with a χ^2 test was not applicable because baseline values differed. Therefore, we used instead a random permutation test with 5000 repetitions. To compare the different spatial frequency Gabor gratings in one bin or time stamp, we used the Kruskal–Wallis test.

For the psychometric versions of Human Experiment 3 (Figs. 9 and 10), we used similar analyses on perceptual thresholds to those used in the psychometric versions of Human Experiments 1 and 2 (Figs. 2 and 7).

All analyses were done in MATLAB (The MathWorks Inc).

Reporting summary. Further information on research design is available in the Nature Research Reporting Summary linked to this article.

Data availability

All data presented in this paper are stored and archived on secure institute computers and are available upon reasonable request.

Received: 5 April 2019; Accepted: 30 March 2020;
Published online: 24 April 2020

References

1. O'Regan, J. K. & Noë, A. A sensorimotor account of vision and visual consciousness. *Behav. Brain Sci.* **24**, 939–973 (2001).
2. Wurtz, R. H. Neuronal mechanisms of visual stability. *Vis. Res.* **48**, 2070–89 (2008).
3. Wurtz, R. H., Joiner, W. M. & Berman, R. A. Neuronal mechanisms for visual stability: progress and problems. *Philos. Trans. R. Soc. B Biol. Sci.* **366**, 492–503 (2011).
4. Thiele, A., Henning, P., Kubischik, M. & Hoffmann, K. P. Neural mechanisms of saccadic suppression. *Science (80-.)* **295**, 2460–2462 (2002).
5. Zuber, B. L. & Stark, L. Saccadic suppression: Elevation of visual threshold associated with saccadic eye movements. *Exp. Neurol.* **16**, 65–79 (1966).
6. Beeler, G. W. Visual threshold changes resulting from spontaneous saccadic eye movements. *Vis. Res.* **7**, 769–775 (1967).
7. Matin, E. Saccadic suppression: a review and an analysis. *Psychol. Bull.* **81**, 899–917 (1974).
8. Riggs, L. A. & Manning, K. A. Saccadic suppression under conditions of whiteout. *Invest. Ophthalmol. Vis. Sci.* **23**, 138–143 (1982).
9. Volkmann, F. C. Human visual suppression. *Vis. Res.* **26**, 1401–1416 (1986).
10. Burr, D. C., Morrone, M. C. & Ross, J. Selective suppression of the magnocellular visual pathway during saccadic eye movements. *Nature* **371**, 511–513 (1994).
11. Ross, J., Burr, D. C. & Morrone, M. C. Suppression of the magnocellular pathway during saccades. *Behav. Brain Res.* **80**, 1–8 (1996).
12. Bremmer, F., Kubischik, M., Hoffmann, K. -P. & Krekelberg, B. Neural dynamics of saccadic suppression. *J. Neurosci.* **29**, 12374–12383 (2009).
13. Hafed, Z. M. & Krauzlis, R. J. Microsaccadic suppression of visual bursts in the primate superior colliculus. *J. Neurosci.* **30**, 9542–9547 (2010).
14. Chen, C. -Y. & Hafed, Z. M. A neural locus for spatial-frequency specific saccadic suppression in visual-motor neurons of the primate superior colliculus. *J. Neurophysiol.* **117**, 1657–1673 (2017).
15. Duffy, F. H. & Lombroso, C. T. Electrophysiological evidence for visual suppression prior to the onset of a voluntary saccadic eye movement. *Nature* **218**, 1074–1075 (1968).
16. Diamond, M. R., Ross, J. & Morrone, M. C. Extraretinal control of saccadic suppression. *J. Neurosci.* **20**, 3449–3455 (2000).
17. Ross, J., Morrone, M. C., Goldberg, M. E. & Burr, D. C. Changes in visual perception at the time of saccades. *Trends Neurosci.* **24**, 113–121 (2001).
18. Gremmler, S. & Lappe, M. Saccadic suppression during voluntary versus reactive saccades. *J. Vis.* **17**, 1–10 (2017).
19. Mackay, D. M. Elevation of visual threshold by displacement of retinal image. *Nature* **225**, 90–92 (1970).
20. García-Pérez, M. A. & Peli, E. Visual contrast processing is largely unaltered during saccades. *Front. Psychol.* **2**, 1–15 (2011).
21. Ilg, U. J. & Hoffmann, K. P. Motion perception during saccades. *Vis. Res.* **33**, 211–220 (1993).
22. Campbell, F. W. & Wurtz, R. H. Saccadic omission: why we do not see a grey-out during a saccadic eye movement. *Vis. Res.* **18**, 1297–1303 (1978).
23. Mitrani, L., Mateeff, S. & Yakimoff, N. Is saccadic suppression really saccadic? *Vis. Res.* **11**, 1157–1161 (1971).
24. Matin, E., Clymer, A. B. & Matin, L. Metacontrast and saccadic suppression. *Science* **178**, 179–182 (1972).
25. Mitrani, L., Yakimoff, N. & Mateeff, S. Saccadic suppression in the presence of structured background. *Vis. Res.* **13**, 517–521 (1973).
26. Mateeff, S., Yakimoff, N. & Mitrani, L. Some characteristics of the visual masking by moving contours. *Vis. Res.* **16**, 489–492 (1976).
27. Brooks, B. A., Impelman, D. M. K. & Lum, J. T. Backward and forward masking associated with saccadic eye movement. *Percept. Psychophys.* **30**, 62–70 (1981).
28. Macknik, S. L. & Livingstone, M. S. Neuronal correlates of visibility and invisibility in the primate visual system. *Nat. Neurosci.* **1**, 144–149 (1998).
29. Castet, E., Jeanjean, S. & Masson, G. S. 'Saccadic suppression'–no need for an active extra-retinal mechanism. *Trends Neurosci.* **24**, 316–317 (2001).
30. Castet, E. Perception of intra-saccadic motion. In *Dynamics of Visual Motion Processing* 141–160 (Springer US, 2010). https://doi.org/10.1007/978-1-4419-0781-3
31. Krueger, J. & Fischer, B. Strong periphery effect in cat retinal ganglion cells. Excitatory responses in ON- and OFF-center neurones to single grid displacements. *Exp. Brain Res.* **18**, 316–318 (1973).
32. Noda, H. & Adey, W. R. Retinal ganglion cells of the cat transfer information on saccadic eye movement and quick target motion. *Brain Res.* **70**, 340–345 (1974).
33. Enroth-Cugell, C. & Jakiela, H. G. Suppression of cat retinal ganglion cell responses by moving patterns. *J. Physiol.* **302**, 49–72 (1980).
34. Roska, B. & Werblin, F. Rapid global shifts in natural scenes block spiking in specific ganglion cell types. *Nat. Neurosci.* **6**, 600–608 (2003).
35. Passaglia, C. L., Freeman, D. K. & Troy, J. B. Effects of remote stimulation on the modulated activity of cat retinal ganglion cells. *J. Neurosci.* **29**, 2467–2476 (2009).
36. Dacey, D. M. & Petersen, M. R. Dendritic field size and morphology of midget and parasol ganglion cells of the human retina. *Proc. Natl Acad. Sci.* **89**, 9666–9670 (1992).
37. Maris, E. & Oostenveld, R. Nonparametric statistical testing of EEG- and MEG-data. *J. Neurosci. Methods* **164**, 177–190 (2007).
38. Bellet, J., Chen, C. -Y. & Hafed, Z. M. Sequential hemifield gating of α- and β-behavioral performance oscillations after microsaccades. *J. Neurophysiol.* **118**, 2789–2805 (2017).
39. Chen, C. -Y. & Hafed, Z. M. Postmicrosaccadic enhancement of slow eye movements. *J. Neurosci.* **33**, 5375–5386 (2013).
40. Watson, A. B. & Pelli, D. G. Quest: a Bayesian adaptive psychometric method. *Percept. Psychophys.* **33**, 113–120 (1983).
41. Robinson, D. L. & Wurtz, R. H. Use of an extraretinal signal by monkey superior colliculus neurons to distinguish real from self-induced stimulus movement. *J. Neurophysiol.* **39**, 852–870 (1976).
42. Mayo, J. P. & Sommer, M. A. Neuronal adaptation caused by sequential visual stimulation in the frontal eye field. *J. Neurophysiol.* **100**, 1923–1935 (2008).
43. Krock, R. M. & Moore, T. Visual sensitivity of frontal eye field neurons during the preparation of saccadic eye movements. *J. Neurophysiol.* **116**, 2882–2891 (2016).
44. Chen, C. -Y., Ignashchenkova, A., Thier, P. & Hafed, Z. M. Neuronal response gain enhancement prior to microsaccades. *Curr. Biol.* **25**, 2065–2074 (2015).
45. Breitmeyer, B. G. Visual masking: past accomplishments, present status, future developments. *Adv. Cogn. Psychol.* **3**, 9–20 (2007).
46. Castet, E. & Masson, G. S. Motion perception during saccadic eye movements. *Nat. Neurosci.* **3**, 177–83 (2000).
47. Ramcharan, E. J., Gnadt, J. W. & Sherman, S. M. The effects of saccadic eye movements on the activity of geniculate relay neurons in the monkey. *Vis. Neurosci.* **18**, 253–258 (2001).

48. Reppas, J. B., Usrey, W. M. & Reid, R. C. Saccadic eye movements modulate visual responses in the lateral geniculate nucleus. *Neuron* **35**, 961–974 (2002).
49. Kleiser, R., Seitz, R. J. & Krekelberg, B. Neural correlates of saccadic suppression in humans. *Curr. Biol.* **14**, 386–390 (2004).
50. Royal, D. W., Sáry, G., Schall, J. D. & Casagrande, V. A. Correlates of motor planning and postsaccadic fixation in the macaque monkey lateral geniculate nucleus. *Exp. Brain Res.* **168**, 62–75 (2006).
51. Phongphanphanee, P. et al. Distinct local circuit properties of the superficial and intermediate layers of the rodent superior colliculus. *Eur. J. Neurosci.* **40**, 2329–2343 (2014).
52. Rajkai, C. et al. Transient cortical excitation at the onset of visual fixation. *Cereb. Cortex* **18**, 200–209 (2008).
53. Ibbotson, M. R., Crowder, N. A., Cloherty, S. L., Price, N. S. C. & Mustari, M. J. Saccadic modulation of neural responses: possible roles in saccadic suppression, enhancement, and time compression. *J. Neurosci.* **28**, 10952–60 (2008).
54. Cloherty, S. L., Mustari, M. J., Rosa, M. G. P. & Ibbotson, M. R. Effects of saccades on visual processing in primate MSTd. *Vis. Res.* **50**, 2683–2691 (2010).
55. Ibbotson, M. R. & Cloherty, S. L. Visual perception: saccadic omission–suppression or temporal masking? *Curr. Biol.* **19**, R493–6 (2009).
56. Duhamel, J. R., Colby, C. L. & Goldberg, M. E. The updating of the representation of visual space in parietal cortex by intended eye movements. *Science* **255**, 90–2 (1992).
57. Sommer, M. A. & Wurtz, R. H. Influence of the thalamus on spatial visual processing in frontal cortex. *Nature* **444**, 374–377 (2006).
58. Münch, T. A. et al. Approach sensitivity in the retina processed by a multifunctional neural circuit. *Nat. Neurosci.* **12**, 1308–1316 (2009).
59. Farrow, K. et al. Ambient illumination toggles a neuronal circuit switch in the retina and visual perception at cone threshold. *Neuron* **78**, 325–338 (2013).
60. Tikidji-Hamburyan, A. et al. Retinal output changes qualitatively with every change in ambient illuminance. *Nat. Neurosci.* **18**, 66–74 (2015).
61. Reinhard, K. et al. Step-by-step instructions for retina recordings with perforated multi electrode arrays. *PLoS ONE* **9**, e106148 (2014).
62. Frey, U., Egert, U., Heer, F., Hafizovic, S. & Hierlemann, A. Microelectronic system for high-resolution mapping of extracellular electric fields applied to brain slices. *Biosens. Bioelectron.* **24**, 2191–2198 (2009).
63. Müller, J. et al. High-resolution CMOS MEA platform to study neurons at subcellular, cellular, and network levels. *Lab Chip* **15**, 2767–2780 (2015).
64. Hafed, Z. M. Alteration of visual perception prior to microsaccades. *Neuron* **77**, 775–786 (2013).
65. Grujic, N., Brehm, N., Gloge, C., Zhuo, W. & Hafed, Z. M. Perisaccadic perceptual mislocalization is different for upward saccades. *J. Neurophysiol.* **120**, 3198–3216 (2018).
66. Schwartz, G. W. et al. The spatial structure of a nonlinear receptive field. *Nat. Neurosci.* **15**, 1572–80 (2012).
67. Zhang, Y., Kim, I. -J., Sanes, J. R. & Meister, M. The most numerous ganglion cell type of the mouse retina is a selective feature detector. *Proc. Natl Acad. Sci.* **109**, E2391–E2398 (2012).
68. Sakatani, T. & Isa, T. Quantitative analysis of spontaneous saccade-like rapid eye movements in C57BL/6 mice. *Neurosci. Res.* **58**, 324–331 (2007).
69. Itokazu, T. et al. Streamlined sensory motor communication through cortical reciprocal connectivity in a visually guided eye movement task. *Nat. Commun.* **9**, 338 (2018).
70. Peli, E., Arend, L. E., Young, G. M. & Goldstein, R. B. Contrast sensitivity to patch stimuli: effects of spatial bandwidth and temporal presentation. *Spat. Vis.* **7**, 1–14 (1993).
71. Diggelmann, R., Fiscella, M., Hierlemann, A. & Franke, F. Automatic spike sorting for high-density microelectrode arrays. *J. Neurophysiol.* **120**, 3155–3171 (2018).
72. Idrees, S., Franke, F., Diggelmann, R., Hierlemann, A. & Münch, T. A. UnitBrowser-a tool to evaluate and post-process units sorted by automatic spike sorting algorithms (Abstract). *Front. Neurosci.* **10**, https://doi.org/10.3389/conf.fnins.2016.93.00054 (2016).
73. Bellet, M. E., Bellet, J., Nienborg, H., Hafed, Z. M. & Berens, P. Human-level saccade detection performance using deep neural networks. *J. Neurophysiol.* **121**, 646–661 (2019).
74. Schütt, H. H., Harmeling, S., Macke, J. H. & Wichmann, F. A. Painfree and accurate Bayesian estimation of psychometric functions for (potentially) overdispersed data. *Vis. Res.* **122**, 105–123 (2016).

Acknowledgements

Andreas Hierlemann provided the HiDens CMOS MEA system and helped establish our high-density MEA recordings. Roland Diggelmann helped in setting up the pipeline (including providing code) for automatic spike sorting of high-density MEA recordings. Our work was supported by funds of the Deutsche Forschungsgemeinschaft (DFG) to the Werner Reichardt Center for Integrative Neuroscience (EXC 307) and to T.A.M. (MU3792/3-1). T.A.M. received support from the Tistou and Charlotte Kerstan Foundation. T.A.M. and Z.M.H. were also supported by an intra-mural funding program (Projekt 2013-05) of the Werner Reichardt Center for Integrative Neuroscience. F.F. was supported by a Swiss National Science Foundation Ambizione grant (PZ00P3_167989), and M.P.B. and Z.M.H. were further funded by the SFB 1233 on "Robust Vision" (DFG) - project number 276693517.

Author contributions

S.I., M.B., T.A.M., Z.M.H. designed the overall study; S.I., M.B., T.A.M., Z.M.H. designed experiments; S.I. performed ex vivo retina experiments; M.B., Z.M.H. performed human psychophysics experiments; S.I., M.B., F.F., T.A.M., Z.M.H. analyzed data; S.I., M.B., F.F., T.A.M., Z.M.H. wrote manuscript.

Competing interests

The authors declare no competing interests.

Additional information

Supplementary information is available for this paper at https://doi.org/10.1038/s41467-020-15890-w.

Correspondence and requests for materials should be addressed to T.A.M. or Z.M.H.

Peer review information *Nature Communications* thanks Frank Bremmer and other, anonymous, reviewer(s) for their contributions to the peer review of this work. Peer review reports are available.

Reprints and permission information is available at http://www.nature.com/reprints

Publisher's note Springer Nature remains neutral with regard to jurisdictional claims in published maps and institutional affiliations.

Perceptual saccadic suppression starts in the retina

Saad Idrees†, Matthias P. Baumann†, Felix Franke,
Thomas A. Münch*, and Ziad M. Hafed*

Supplementary information

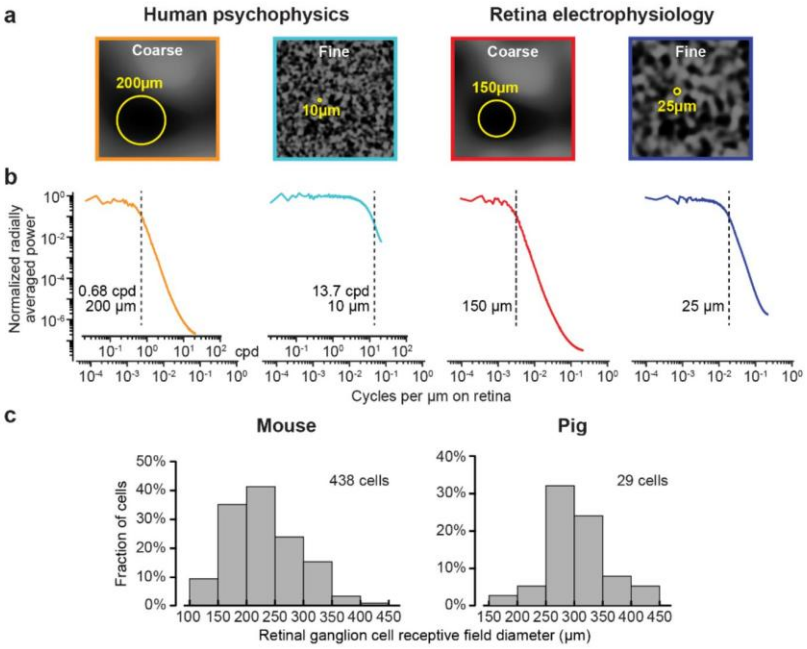

Supplementary Figure 1 Textured backgrounds tailored to receptive field sizes of retinal ganglion cells (coarse) or bipolar cells (fine) in the different species that we studied. (a) We created textures by convolving random binary pixel images with a Gaussian blurring filter. We varied the σ parameter of the Gaussian blurring filter (Methods) to define a so-called spatial scale for the resulting texture (indicated as yellow circles in the examples shown). For each species, we picked the spatial scale to result in dark or bright image blobs that approximated the sizes of either retinal ganglion cell (coarse) or bipolar cell (fine) receptive fields, and we then set σ to half the spatial scale value (Methods). **(b)** Radially-averaged power spectra for textures like in **a**, normalized to the maximum average power. Low-pass characteristics in all spatial scales were clear, as expected: less than 5% of the total average power was above the spatial frequency corresponding to the specific spatial scale of a given texture (vertical dashed lines). The inset x-axes in the first two spectra (used for human perceptual experiments) show units of cycles per degree (cpd) in addition to cycles per μm on the retina. **(c)** Histograms showing the distributions of receptive field diameters (Methods) in mouse (left) and pig (right) for a subset of retinal ganglion cells that we recorded. Since the distributions were generally similar, we used the same spatial scale parameter for the retinal recordings in both species. Human spatial scale parameters were estimated based on human receptive field diameters from the literature (Methods).

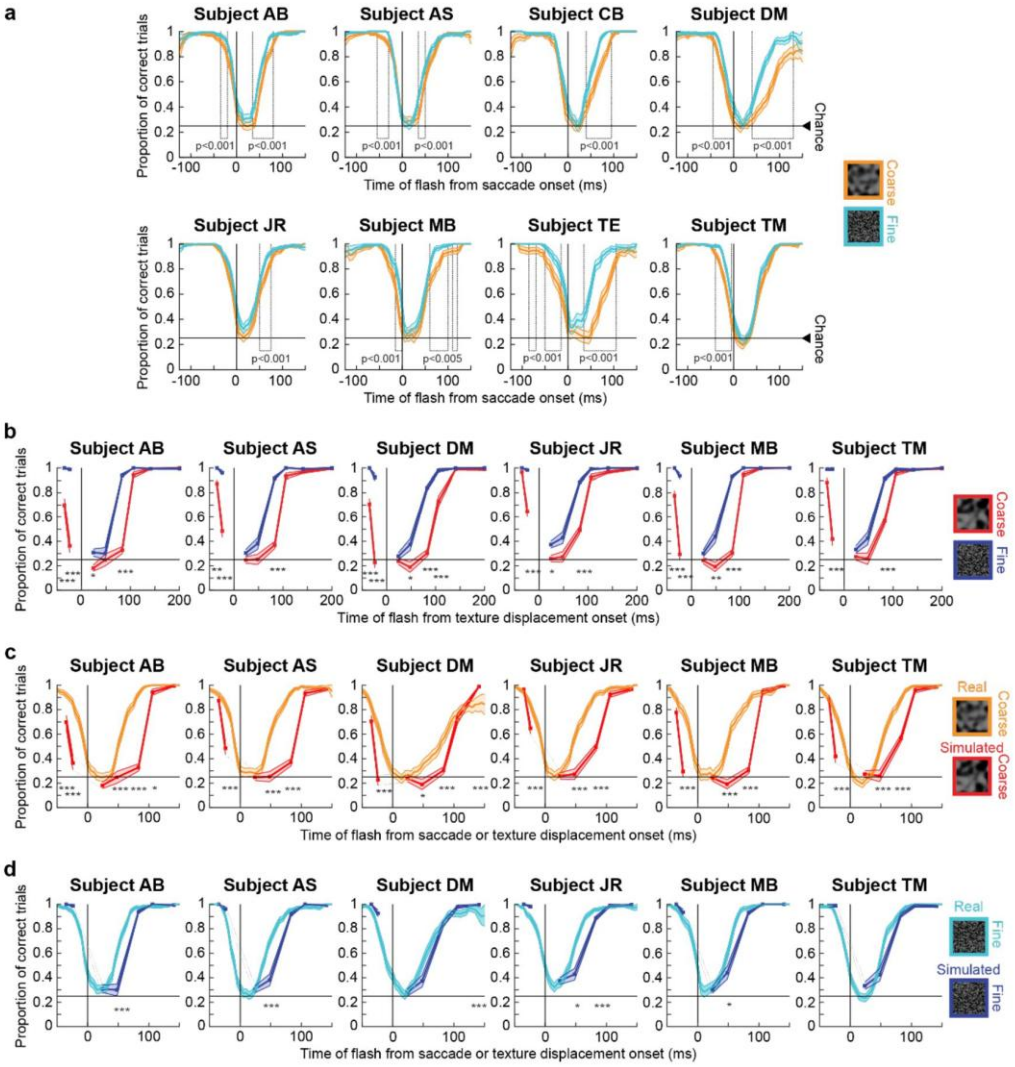

Supplementary Figure 2 Individual subject results from the perceptual experiments of Figs. 1, 6. (a) Identical analyses to Fig. 1d, shown separately for each individual subject. Error bars: s.e.m. across trials. All subjects experienced strong perceptual saccadic suppression, going from near-perfect localization performance to near-chance performance at peak suppression. Moreover, using strict statistical criteria (two-tailed random permutation test; indicated in the figure and described in detail in Methods), all subjects had significant time clusters during which perception was different between saccadic suppression for saccades generated across coarse or fine textures. Also see Fig. 2 and Supplementary Fig. 4. **(b)** Same analyses as in Fig. 6d, but now showing individual subject results when saccades were replaced by saccade-like texture displacements during fixation. All subjects showed longer suppression after coarse texture displacements than after fine texture displacements; all subjects also showed earlier and stronger "pre-saccadic" suppression for coarse textures. Note that this "pre-saccadic" effect is purely visual, since the subjects never made saccades in this condition. Also, note that all subjects who participated in this experiment had also participated in the version with real saccades in **a**. Therefore, whether with or without saccades, perceptual suppression depended on image

statistics. Also see Fig. 7 and Supplementary Fig. 7. **(c, d)** Comparisons of perceptual suppression between real and simulated saccades across coarse **(c)** and fine **(d)** textures, as in Fig. 6e, f but now separating data from individual subjects. Note how even pre-saccadic suppression was prolonged in simulated relative to real saccades (i.e. started earlier in simulated saccades) in the coarse texture condition, which was most effective in causing suppression overall. Error bars: s.e.m. across trials. Asterisks in **b** denote a significant difference between coarse and fine conditions at the indicated flash time (χ^2 tests with Bonferroni corrections; $*$ $p<0.005$, $**$ $p<0.001$, $***$ $p<0.0001$). Asterisks in **c**, **d** denote significant differences (χ^2 tests with Bonferroni corrections; $*$ $p<0.007$, $**$ $p<0.0014$, $***$ $p<0.00014$) between real and simulated saccades, comparing perception of a flash at the indicated time delay after simulated saccades to the corresponding time bin (+/- 25 ms) from the real saccade condition.

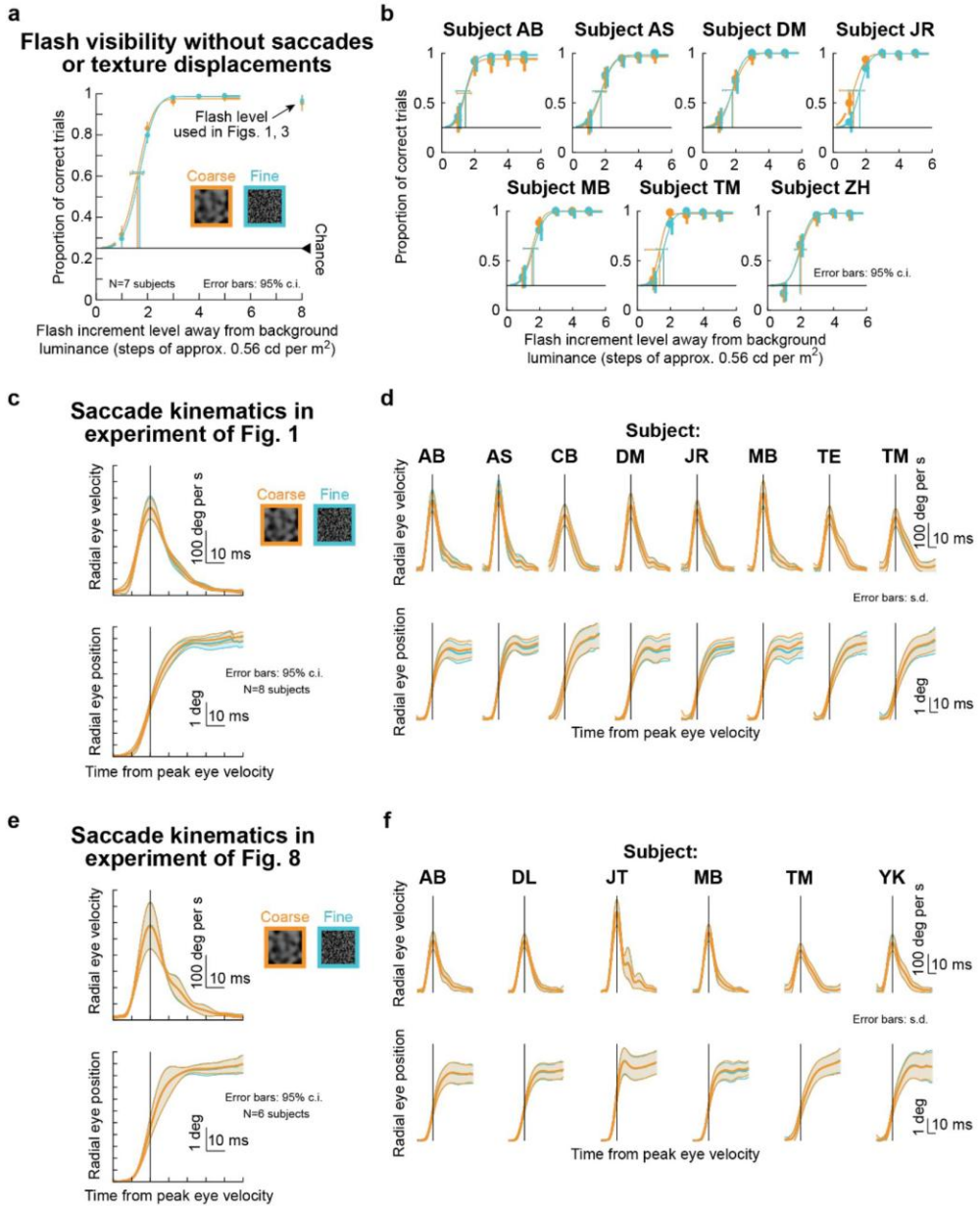

Supplementary Figure 3 Controls for flash visibility and motor variability in our perceptual experiments of Figs. 1, 6, 8. (a) For the same textures as in Figs. 1, 6, we asked subjects to maintain fixation. At a random time, a luminance pedestal appeared as in the main experiments (Figs. 1, 6), but this time, we varied its contrast across trials (Methods). We ensured that no microsaccades occurred near the flash onset time (Methods). Psychometric curves of localization performance (mean across subjects with 95% c.i.; N = 7 subjects) indicate that, at the flash contrast used in Figs. 1, 6 (highlighted by the black arrow), subjects could easily detect flashes during simple fixation. Importantly, flash visibility was identical for coarse or fine textures at all contrasts. Therefore, flash visibility alone (or lack thereof) did not explain the main experiments' results (Figs. 1, 6). The strong perceptual suppression observed in Figs. 1, 6 was instead likely a function of interaction between visual transients associated

with saccades or texture displacements and the flashes. Also see Figs. 2, 7. **(b)** This idea is further supported by the fact that all individual subjects showed consistent results. All of these subjects had also participated in the experiments of Figs. 1, 6 (with the exception of subject ZH who only performed the control experiment). Psychometric curves were fit using the *psignifit 4 toolbox*[1], and error bars denote 95% confidence intervals centered on the flash levels resulting in threshold perceptual performance (Methods). **(c)** We also checked for potential effects of motor variability on perceptual performance, in order to rule out the possibility that differences in performance between textures (Fig. 1) were due to differences in eye movement kinematics. For the experiments of Fig. 1, we plotted average radial eye velocity (top) and average radial eye position (bottom) across subjects (N = 8 subjects; error bars denote 95% confidence intervals across the individual subjects' curves). There was no effect of background texture on movement kinematics. **(d)** This was also true for each subject individually (mean +/- s.d. across trials). Saccade kinematics were not different when saccades were made across coarse or fine textures. **(e, f)** Same kinematic analyses, but now for the saccades of the experiment of Fig. 8. **(e)** Radial eye velocity and position averaged across subjects (N = 6 subjects; error bars denote 95% confidence intervals across the individual subjects' curves). **(f)** Saccade kinematics for each subject (mean +/- s.d. across trials). Scale bars are defined in their respective panels.

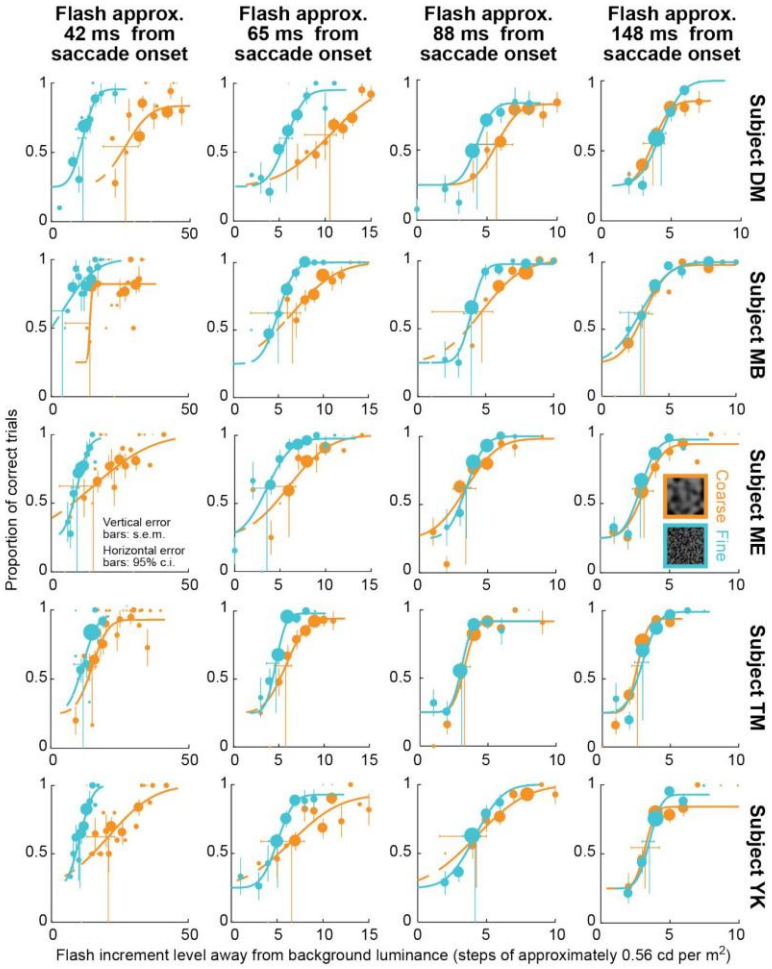

Supplementary Figure 4 Individual subject results from the perceptual experiment of Fig. 2. Each row shows psychometric curves like those shown in Fig. 2a-d, but for a single individual subject. Different rows show results from different subjects. The same conventions as in Fig. 2a-d apply. Here, we also scaled the size of each data point shown by the number of repetitions collected during the experiment. Note that we only show vertical error bars for data points with >10 repetitions, for clarity. Vertical error bars denote s.e.m. across repetitions of a given condition; horizontal error bars indicate 95% confidence intervals for the detection threshold of a given psychometric curve (i.e. the flash contrast resulting in threshold perceptual performance; Methods). Note that the x-axis ranges for the different columns (i.e. different flash times from saccade onset) are different from each other because of the varying amounts of perceptual saccadic suppression that occurred (Figs. 1-2). As can be seen, all subjects showed strong perceptual suppression near the time of saccade onset, with recovery occurring later in time, consistent with Fig. 1. Moreover, all subjects showed stronger perceptual suppression with coarse textures when compared to fine textures, again consistent with Fig. 1.

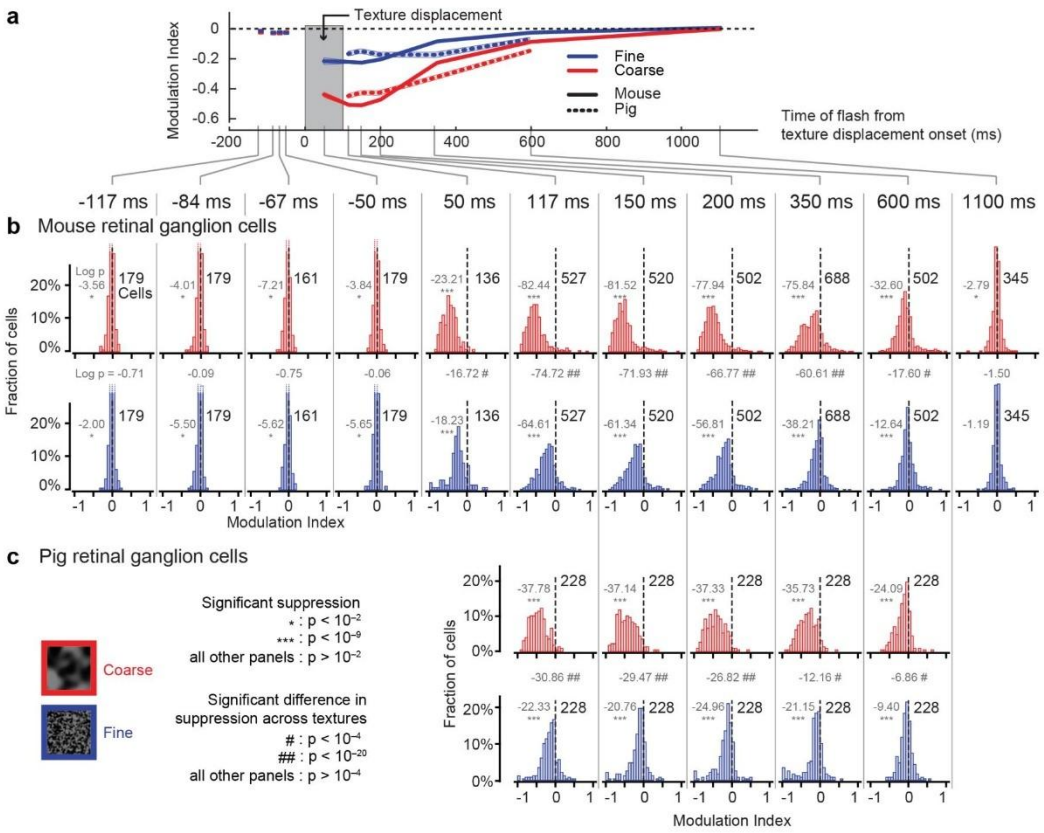

Supplementary Figure 5 Population data detailing the properties of retinal "saccadic suppression". (a) Replication of Fig. 3e, showing the time courses of retinal "saccadic suppression" in mouse and pig retinae. **(b, c)** Histograms of modulation indices for mouse **(b)** and pig **(c)** RGCs at different flash times relative to texture displacement onset. Red and blue denote coarse and fine textures, respectively. Black numbers in each panel indicate the numbers of RGCs analyzed for each condition; gray numbers next to asterisks in each panel show the logarithm (base 10) of the exact p-value (two-tailed Wilcoxon signed-rank test to determine if the population median was shifted away from 0). Gray numbers next to hashes between coarse (red) and fine (blue) panels show the logarithm (base 10) of the exact p-value comparing suppression indices across the two textures (two-tailed Wilcoxon signed-rank test).

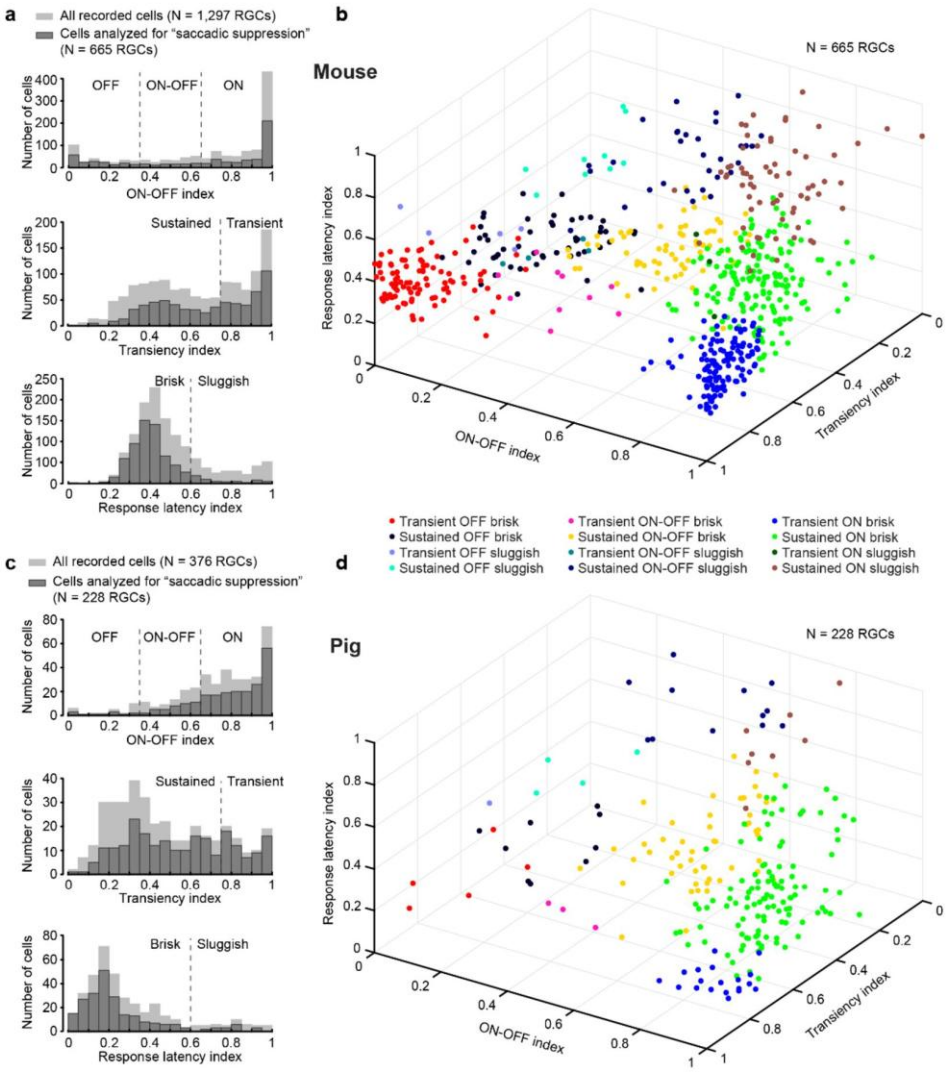

Supplementary Figure 6 Diverse properties of RGCs included in our analysis. We quantified the response properties of all recorded mouse **(a, b)** and pig **(c, d)** RGCs with respect to three neuronal response metrics (see Methods): ON-OFF index, transiency index, and response latency index. Each histogram **(a**, **c)** was divided into 2 or 3 groups: RGCs could be OFF, ON-OFF, or ON (top histograms); transient or sustained (middle histograms); and brisk (short response latency) or sluggish (long response latency) (bottom histograms). Combined, this resulted in 12 response categories to which each recorded RGC belonged. The cells that could be analyzed for "saccadic suppression" and for which the response properties could be computed (dark gray histograms) spanned the entire range of response indices exhibited by all recorded cells for which these response properties were analyzed (light gray histograms). The three-dimensional scatter plots **(b**, **d)** show the projection of the RGC subsets considered in our analysis for "saccadic suppression" onto the 3 neuronal response indices. The 12 response categories, formed by the combination of histograms in **(a**, **c)**, can be seen in different colors.

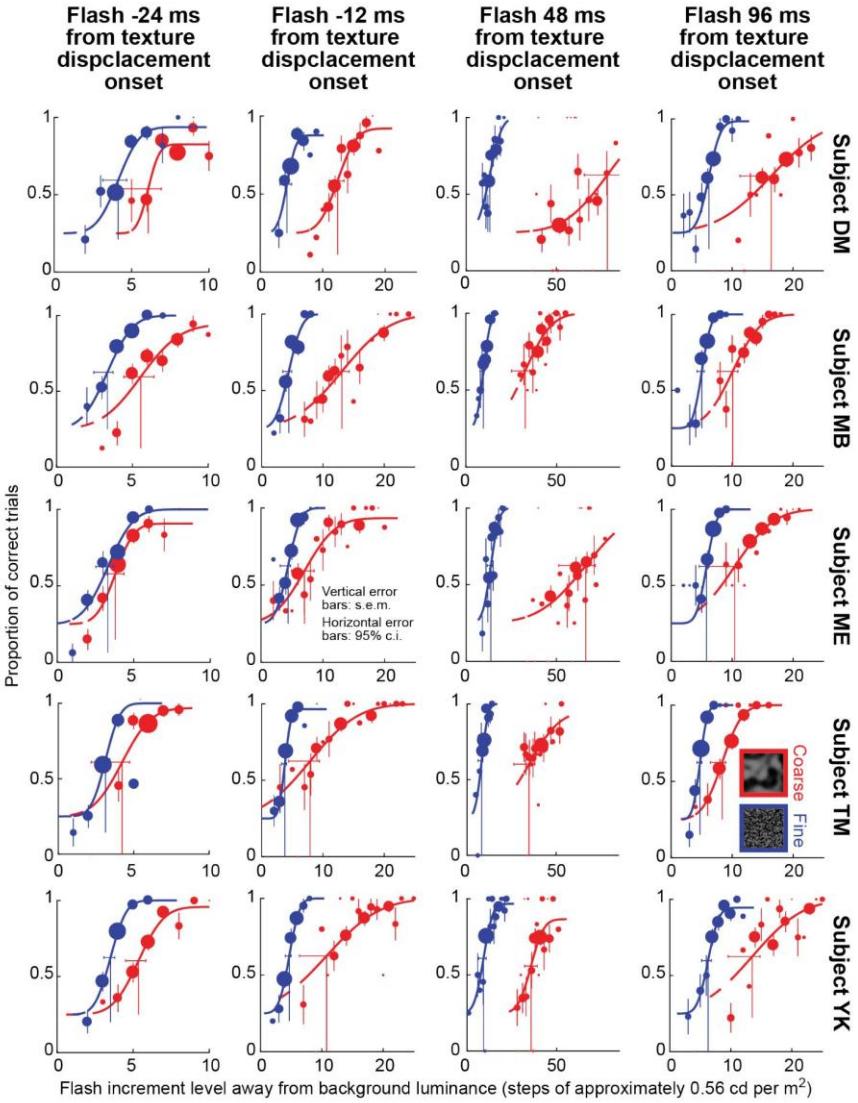

Supplementary Figure 7 Individual subject results from the perceptual experiment of Fig. 7. Same as Supplementary Fig. 4, but now for the experiment of Fig. 7. All subjects showed similar results: there was strong perceptual suppression before and after texture displacements in the absence of saccades, and the suppression effect was stronger when the displaced texture was coarse rather than fine. Note that in this experiment, we added an additional time sample prior to texture displacement onset, in comparison to Fig. 6, in order to demonstrate the robustness of this pre-displacement effect, and also to demonstrate the continuity of perceptual suppression in a time-locked fashion to texture displacement onset (Fig. 6).

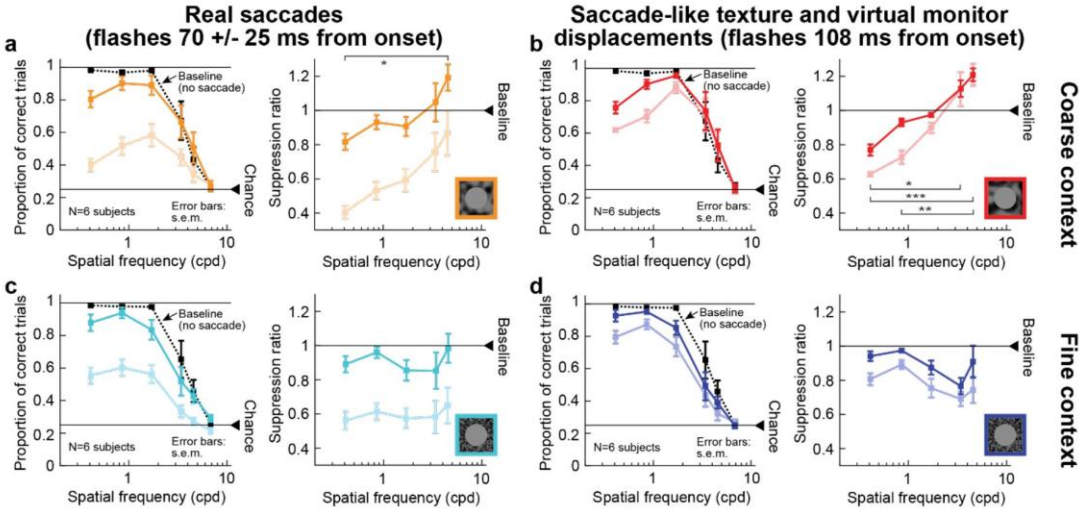

Supplementary Figure 8 Recovery, with time, of perceptual suppression with real and simulated saccades in the experiment of Fig. 8. (a) Same analysis as in Fig. 8b, but at a later time point of grating flash onsets relative to saccade onset. Faint curves show the data from Fig. 8b for comparison. At around 70 ms after saccade onset, perceptual recovery from saccadic suppression emerged, but the selectivity of suppression across different spatial frequencies was still present (there was a main effect of spatial frequency on suppression ratio; χ^2=11.4, p=0.022, df=4, Kruskal-Wallis test; $*$ p<0.05, post-hoc pairwise test between the lowest and highest spatial frequencies). All other conventions are as in Fig. 8b). **(b)** Same analysis as in Fig. 8d, but at a later time point of flash onset after virtual monitor and texture displacement. The same observations as in **a** were made: perceptual recovery occurred at the later time point, but selectivity of suppression was still obvious (χ^2=25.26, p=0.00004, df=4, Kruskal-Wallis test; $*$ p<0.05, $**$ p<0.01, $***$ p<0.001 for post-hoc pairwise tests between different indicated pairs of spatial frequencies). The faint curves show the data from Fig. 8d for comparison. Note how this condition of displacements of the virtual monitor and texture surround resulted in longer lasting suppression than with real saccades (also see Supplementary Fig. 9). **(c, d)** Same analyses as in **a** and **b**, but with a fine texture surrounding the virtual monitor (Fig. 8e, f). Error bars in all panels denote s.e.m. All other conventions are as in Fig. 8.

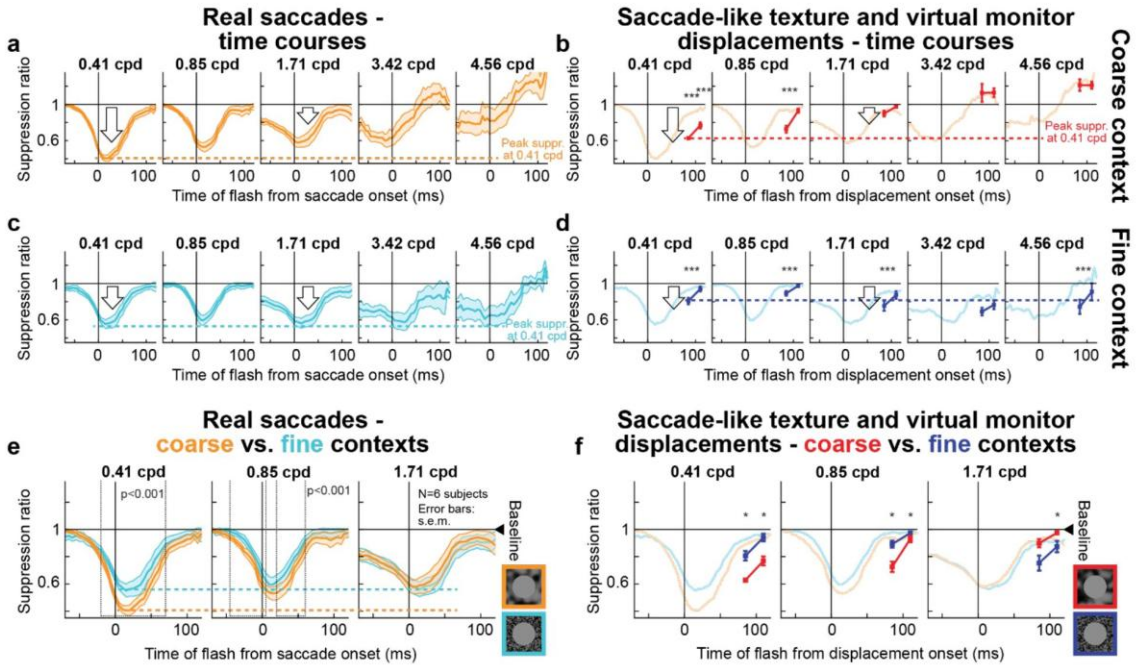

Supplementary Fig. 9 Time courses of perceptual suppression with real and simulated saccades, as well as coarse and fine textures, in the experiment of Fig. 8. (a) Time courses of suppression from Fig. 8a, b with a coarse surround around the virtual monitor. We used similar binning procedures to Fig. 1. Peak suppression was strongest when 0.41 cpd gratings were flashed and progressively weakened for higher spatial frequency gratings (horizontal colored dashed line across panels). **(b)** With simulated saccade-like virtual monitor and texture displacements, we sampled two grating flash times relative to displacement onset. Recovery at the later time point for each grating spatial frequency was evident. Moreover, selectivity of suppression as a function of grating spatial frequency was evident (horizontal colored dashed line across panels demonstrating the peak suppression for the lowest spatial frequency). The faint curves show time courses from **a** for comparison. Note how simulated saccades caused longer-lasting suppression than real saccades, exactly as in the experiment of Fig. 6. **(c, d)** Similar analyses for fine texture surrounds around the virtual monitor. In this case, suppression was the same across all spatial frequencies (horizontal colored dashed lines across panels). In **b**, **d**, asterisks denote significant differences in perceptual suppression between the simulated condition and a corresponding time bin in the real condition (*** $p<0.0001$, χ^2 tests with Bonferroni corrections). **(e)** For real saccades, and for low spatial frequencies of gratings (i.e. when both coarse and fine surround contexts were associated with strong saccadic suppression), the coarse surround was associated with longer lasting suppression than the fine surround ($p<0.001$, two-tailed random permutation test). This is consistent with the results of Fig. 1 when saccades were generated across full-screen textures. **(f)** This texture-dependence was also true with simulated saccades (* $p<0.05$, two-tailed random permutation test comparing coarse and fine textures at a given grating flash time). In all panels: N = 6 subjects; and error bars denote s.e.m. All other conventions are as in Figs. 1, 6, 8.

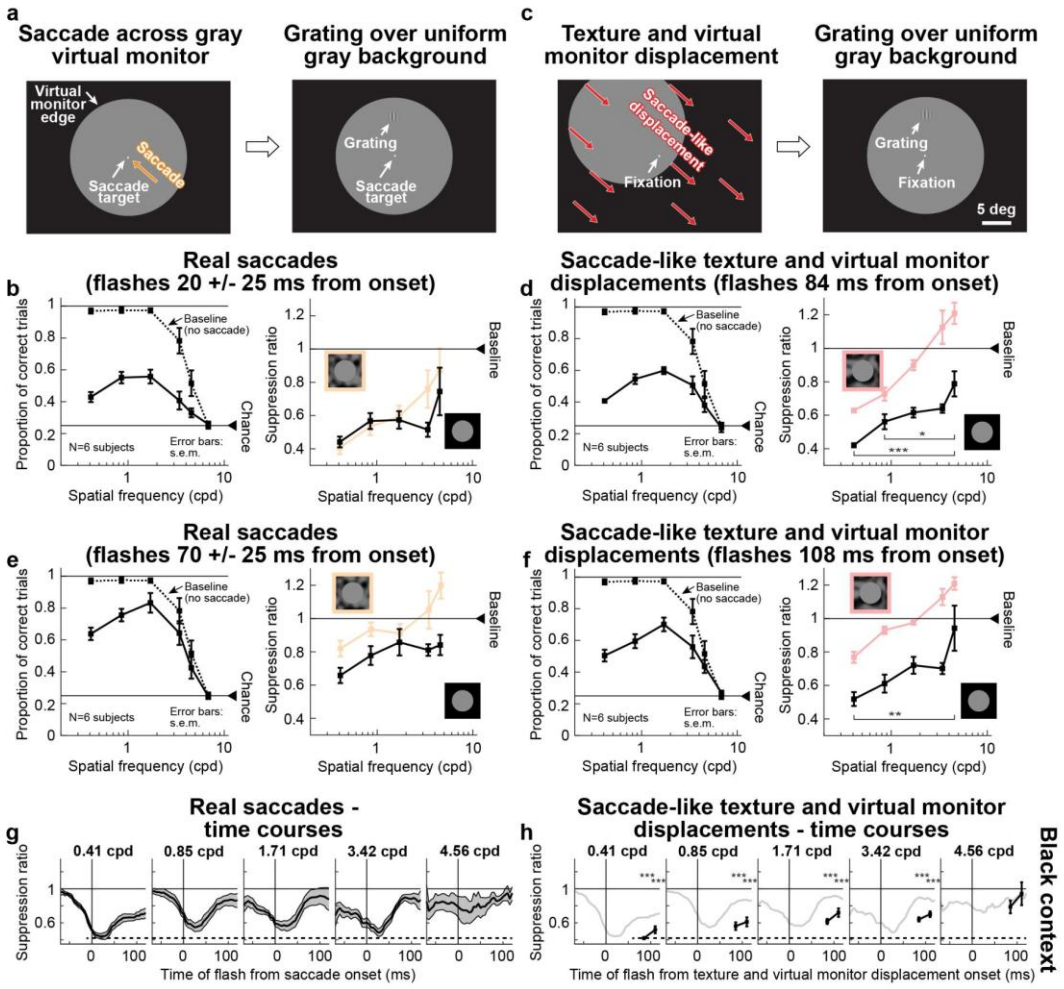

Supplementary Fig. 10 Replicating the results of Fig. 8 but with black surrounds around a uniform gray display. (a) We repeated the same experiment as in Fig. 8a but this time using a black surround around the virtual monitor, as we might normally do in experiments on saccadic suppression[2,3]. Note that a black (or white) surround is theoretically equivalent to an infinitely coarse surround; hence, we expected observations more similar to Fig. 8a-d (i.e. selectivity of suppression for low spatial frequencies) than Fig. 8e, f. **(b)** Similar suppression selectivity for low spatial frequencies occurred with real saccades as in Fig. 8b (faint curves replicate that data for comparison). **(c)** Same experiment as in Fig. 8c, but with a black surround. **(d)** Selectivity of suppression for low spatial frequencies was even more evident with simulated saccades (effect of spatial frequency on suppression ratio during simulated saccades: χ^2=18.84, p=0.0008, df=4, Kruskal-Wallis test; $*$ p<0.05, $***$ p<0.001 for post-hoc pairwise tests between the highest spatial frequency and either the lowest or second lowest spatial frequency). Faint curves show results from Fig. 8d for comparison. **(e, f)** Similar analyses at a later time point, identical to Supplementary Fig. 8. There was recovery for both real (**e**) and simulated (**f**) saccades (effect of spatial frequency on suppression ratio during simulated saccades: χ^2=15.12, p=0.0045, df=4, Kruskal-Wallis test; $**$ p<0.01 for post-hoc pairwise comparisons between individual spatial frequencies). Faint colored curves show data from Supplementary Fig. 8a, b at

the same time points for easier comparison. Note that with black surrounds, suppression strength was larger overall than with either coarse or fine texture surrounds (as if the black surround was indeed an extension of the coarseness of the texture). **(g, h)** Full time courses of suppression as in Supplementary Fig. 9. All error bars denote s.e.m., and all conventions are similar to Fig. 8 and Supplementary Figs. 8, 9. In **h** asterisks denote significant differences in perceptual suppression between the simulated condition and a corresponding time bin in the real condition, both with a black background (∗∗∗ $p<0.001$, two-tailed random permutation test).

1 Schutt, H. H., Harmeling, S., Macke, J. H. & Wichmann, F. A. Painfree and accurate Bayesian estimation of psychometric functions for (potentially) overdispersed data. *Vision Res* **122**, 105-123 (2016).

2 Hafed, Z. M. & Krauzlis, R. J. Microsaccadic suppression of visual bursts in the primate superior colliculus. *J Neurosci* **30**, 9542-9547 (2010).

3 Chen, C. Y. & Hafed, Z. M. A neural locus for spatial-frequency specific saccadic suppression in visual-motor neurons of the primate superior colliculus. *J Neurophysiol* **117**, 1657-1673 (2017).

Appendix B: Publication 2

Dependence of perceptual saccadic suppression on peri-saccadic image flow properties and luminance contrast polarity

Baumann, M. P., Idrees, S., Münch, T. A., & Hafed, Z. M.

Journal of Vision (Special Issue:
From Peripheral to Transsaccadic and Foveal Perception), (2021) 21(5): 15, 1-22

doi: 10.1167/jov.21.5.15.

Dependence of perceptual saccadic suppression on peri-saccadic image flow properties and luminance contrast polarity

Matthias P. Baumann
Werner Reichardt Centre for Integrative Neuroscience, Tübingen University, Tübingen, Germany
Hertie Institute for Clinical Brain Research, Tübingen University, Tübingen, Germany

Saad Idrees
Werner Reichardt Centre for Integrative Neuroscience, Tübingen University, Tübingen, Germany

Thomas A. Münch
Werner Reichardt Centre for Integrative Neuroscience, Tübingen University, Tübingen, Germany

Ziad M. Hafed
Werner Reichardt Centre for Integrative Neuroscience, Tübingen University, Tübingen, Germany
Hertie Institute for Clinical Brain Research, Tübingen University, Tübingen, Germany

Across saccades, perceptual detectability of brief visual stimuli is strongly diminished. We recently observed that this perceptual suppression phenomenon is jumpstarted in the retina, suggesting that the phenomenon might be significantly more visual in nature than normally acknowledged. Here, we explicitly compared saccadic suppression strength when saccades were made across a uniform image of constant luminance versus when saccades were made across image patches of different luminance, width, and trans-saccadic luminance polarity. We measured perceptual contrast thresholds of human subjects for brief peri-saccadic flashes of positive (luminance increments) or negative (luminance decrements) polarity. Thresholds were >6–7 times higher when saccades translated a luminance stripe or edge across the retina than when saccades were made over a completely uniform image patch. Critically, both background luminance and flash luminance polarity strongly modulated peri-saccadic contrast thresholds. In addition, all of these very same visual dependencies also occurred in the absence of any saccades, but with qualitatively similar rapid translations of image patches across the retina. This similarity of visual dependencies with and without saccades supports the notion that perceptual saccadic suppression may be fundamentally a visual phenomenon, which strongly motivates neurophysiological and theoretical investigations on the role of saccadic eye movement commands in modulating its properties.

Introduction

Due to their ballistic nature, visual input across saccades invariably includes periods of large image uncertainty. Perceptual cancelation during such periods takes place, resulting in a seamless subjective visual experience despite the occurrence of saccades as often as several times in just one second (Melcher, 2011; Wurtz, 2008; Wurtz, Joiner, & Berman, 2011; Zimmermann & Bremmer, 2016). In the laboratory, the properties of peri-saccadic vision have been studied by presenting very brief and fleeting "probe" stimuli around the time of saccadic eye movements. Such stimuli act as impulses that essentially capture the instantaneous and momentary state of the visual system (Matin, 1974; Ross, Morrone, Goldberg, & Burr, 2001).

When presenting very brief peri-saccadic visual stimuli, a prominent observation is a massive, but transient, suppression of visual sensitivity. In this striking phenomenon, a visual probe goes completely unnoticed if presented within approximately

Citation: Baumann, M. P., Idrees, S., Münch, T. A., & Hafed, Z. M. (2021). Dependence of perceptual saccadic suppression on peri-saccadic image flow properties and luminance contrast polarity. *Journal of Vision*, *21*(5):15, 1–22, https://doi.org/10.1167/jov.21.5.15.

https://doi.org/10.1167/jov.21.5.15 Received November 27, 2020; published May 17, 2021 ISSN 1534-7362

± 50 ms from saccade onset, even if it would be detected effortlessly when presented under fixation (Beeler, 1967; Brooks & Fuchs, 1975; Idrees, Baumann, Franke, Munch, & Hafed, 2020; Latour, 1962). This phenomenon was labeled saccadic suppression (Zuber & Stark, 1966), and it has attracted investigation by vision scientists for many decades (Binda & Morrone, 2018; Castet, Jeanjean, & Masson, 2001; Castet & Masson, 2000; Matin, 1974; Schweitzer & Rolfs, 2020; Wurtz, 2008). Saccadic suppression is robust, and it occurs for both reflexive and deliberate saccades (Gremmler & Lappe, 2017). It also occurs for saccades of all sizes, including microsaccades (Beeler, 1967; Chen & Hafed, 2017; Hafed & Krauzlis, 2010; Hass & Horwitz, 2011; Scholes, McGraw, & Roach, 2018; Zuber & Stark, 1966), and it even acts to shape the long-term dynamics of visual sensitivity well after the eye movements (J. Bellet, Chen, & Hafed, 2017; Benedetto & Morrone, 2017). Most interestingly, neural responses to visual probes in a variety of brain areas are also suppressed if the probes occur peri-saccadically (Berman, Cavanaugh, McAlonan, & Wurtz, 2017; Bremmer, Kubischik, Hoffmann, & Krekelberg, 2009; Chen & Hafed, 2017; Chen, Ignashchenkova, Thier, & Hafed, 2015; Hafed & Krauzlis, 2010; Idrees, Baumann, Franke, et al., 2020; Idrees, Baumann, Korympidou, et al., 2020; Kagan, Gur, & Snodderly, 2008; Reppas, Usrey, & Reid, 2002; Robinson & Wurtz, 1976).

For perhaps as long as saccadic suppression has been investigated, there have been debates on its origins. On the one hand, according to the "active hypothesis," it has been suggested that suppression relies on knowledge of saccade generation commands to actively suppress visual sensitivity, through efference copies or corollary discharge from (pre-) motor areas (Beeler, 1967; Diamond, Ross, & Morrone, 2000; Duffy & Lombroso, 1968; Zuber & Stark, 1966). Perceptually, a showpiece for this hypothesis was the observation that saccadic suppression can be selective (Burr, Morrone, & Ross, 1994): brief flashes of low spatial frequency patterns are suppressed much more than brief flashes of high spatial frequency patterns (Burr et al., 1994). This observation was interpreted as evidence for an active movement-related signal specifically targeting the magnocellular visual pathway, which is sensitive to low spatial frequencies (DeYoe & Van Essen, 1988; Merigan & Maunsell, 1993). On the other hand, according to the "visual hypothesis," it is the visual consequences of saccades that jumpstart suppression. This is supported by the observation that brief probe flashes near the onset of global image translations (similar to those caused by saccades) are also perceptually suppressed (Adey & Noda, 1973; Brooks & Fuchs, 1975; Brooks, Impelman, & Lum, 1981; Castet et al., 2001; Diamond et al., 2000; Idrees, Baumann, Franke, et al., 2020; Mackay, 1970; Mitrani, Mateeff, & Yakimoff, 1971; Mitrani, Radil-Weiss, Yakimoff, Mateeff, & Bozkov, 1975; Mitrani, Yakimoff, & Mateeff, 1973; Noda & Adey, 1974; Yakimoff, Mitrani, & Mateeff, 1974). Moreover, such suppression still takes place when the flashes are presented before the image translations, likely through backward masking effects (Brooks et al., 1981; Idrees, Baumann, Franke, et al., 2020; Macknik & Livingstone, 1998). Recently, we also found that even selective suppression of low spatial frequency patterns may be entirely visual in origin: both selective and unselective suppression can happen with or without saccades, simply as a function of visual context (Idrees, Baumann, Franke, et al., 2020). A key observation was that saccade-like image translations activate, rather than suppress, the retinal image processing cascade and result in afferent activity bursts in retinal ganglion cells; responses to subsequent flashes are, in turn, suppressed through visually-triggered retinal-circuit (and downstream) mechanisms (Idrees, Baumann, Franke, et al., 2020; Idrees, Baumann, Korympidou, et al., 2020). Thus, from a visual perspective, perceptual saccadic suppression involves visual-visual interactions between two kinds of signals: (1) the visual consequences of saccadic eyeball rotations; and (2) the visual consequences of flash onsets (Idrees, Baumann, Franke, et al., 2020).

Here, we explored these visual-visual interactions in more detail at the perceptual level. We varied the image conditions across which gaze translated during saccades, and we also tested image translations in the absence of saccades. We additionally explored influences of flash polarity (luminance increments or decrements relative to the background), motivated by quantitative differences between ON and OFF retinal pathways in saccadic suppression (Idrees, Baumann, Korympidou, et al., 2020). We found that saccadic suppression exhibits a large diversity of visual dependencies, which also emerge with image translations in the absence of saccades. Our results motivate revisiting both the movement-related and visual components of saccadic suppression and investigating how saccade movement commands may interact with visual-visual interactions in shaping trans-saccadic visual perception.

Methods

Subjects and ethical approvals

We collected data from six human subjects (three females) who provided informed consent. Two subjects were authors (MPB and SI); the others were naïve to the purposes of the experiments. The subjects (aged 22–32 years) were compensated 10 euros per 1-hour session. Each subject's data were collected across 10 sessions. The experiments were approved by ethics

committees at the Medical Faculty of Tübingen University, and they were in accordance with the Declaration of Helsinki.

Laboratory setup

The setup was similar to that described in recent studies (Bogadhi, Buonocore, & Hafed, 2020; Idrees, Baumann, Franke, et al., 2020). Subjects sat 57 cm from a CRT display (41 pixels/degrees; 85 Hz) spanning approximately 34 degrees horizontally and 26 degrees vertically. We stabilized subjects' heads using a custom-built device (Hafed, 2013). In addition, we tracked movements of the left eye using a desktop-mounted video-based eye tracker (Eyelink 1000, SR Research Ltd, Canada). Before running the experiments, we linearized the display (8-bit resolution), such that we had equal steps of luminance increments or decrements (relative to the background luminance) for the different experimental variants (Idrees, Baumann, Franke, et al., 2020). All experiments were controlled using the Psychophysics Toolbox (Brainard, 1997; Kleiner, Brainard, & Pelli, 2007; Pelli, 1997), with Eyelink extensions (Cornelissen, Peters, & Palmer, 2002).

Experimental procedures

Our general approach was to present a brief probe flash (one display frame; approximately 12 ms) at a specific time relative to a visual transient. In some conditions, such a visual transient was caused by a real saccade shifting the retinal image globally. In other conditions, it was caused by either a luminance step in the display during fixation or by a transient translation of the display image (to simulate a saccade-like image displacement). The probe was presented at one of multiple possible display locations, which were fixed in position for all experiments. Subjects had to identify, on every trial, at which of the locations the probe flash appeared. Therefore, the experiment utilized a multiple-alternative forced-choice design. If subjects' perception was suppressed, then their proportion of correct responses was expected to significantly decrease relative to normal performance.

To obtain a sensitive measure of perceptual sensitivity across the different conditions, we varied the flash contrast (luminance amplitude, either as an increment or decrement from background luminance) across all trials, and we collected full psychometric curves of perceptual detectability. This allowed us to calculate perceptual thresholds (Idrees, Baumann, Franke, et al., 2020).

Across 10 sessions per subject, we tested five different visual transient conditions, along with two different background luminance conditions at the time of perceptual discrimination (i.e., at the time of probe flash occurrence). We describe these conditions in detail next. Each condition was tested separately in two sessions per subject.

(1) Real saccades across a uniform background: Subjects started by fixating a white fixation spot that appeared at 11.2 degrees to the right or left of, and 3.8 degrees above or below, display center (Figure 1A, top). The spot was a square of 7.3 by 7.3 min arc size and 142.8 cd/m^2 luminance (Idrees, Baumann, Franke, et al., 2020). After a random delay of 800–1700 ms, the fixation spot jumped to display center, instructing a saccade towards the new spot location (Figure 1A, top). We then initiated an automatic program to detect saccade onset. This program was described previously (Chen & Hafed, 2013). Briefly, the program collected a recent history of eye position samples and used those to obtain a running estimate of eye speed. If such speed exceeded a threshold, a saccade was detected. Upon saccade detection, we presented a single-frame probe flash as the perceptual discrimination stimulus (Figure 1A', top). The probe flash occurred after one of four possible time points after online saccade detection: 24, 35, 47, or 59 ms. These time points were guided by our experience in a similar context (Idrees, Baumann, Franke, et al., 2020), and they allowed us to obtain a time course of recovery in perceptual sensitivity after the saccades.

In all experimental conditions in which we used online saccade detection, we re-detected saccades offline, which allowed refining saccade onset time (Chen & Hafed, 2013); see the data analysis section below for further details. Across all conditions with saccades being detected online, we confirmed that the four probe flash times designated above were occurring at 39.53 ± 0.81, 51.38 ± 0.85, 63.05 ± 0.97, or 74.83 ± 0.85 ms (mean value ± *SEM* across all trials from all subjects) after saccade onset (Figures 1B–D shows the distributions of flash times in this and the two other saccade conditions described below). This was similar to the approach that we recently used (Idrees, Baumann, Franke, et al., 2020). Moreover, we confirmed that the flash times after saccade onset were similar across all conditions employing real saccades (see the raw distributions in Figures 1B–D; there was a maximum of 0.8 ms difference in each same-colored distributions' mean times across the three shown experimental conditions; compare vertical solid and dashed or dotted lines across conditions). This way, we could safely conclude that differences in the strength of perceptual saccadic suppression across the different conditions (see Results) could not be attributed to systematic differences in the flash times after saccades.

It should also be noted that with online saccade detection, we did not present flashes pre-saccadically. This was a conscious choice given the large numbers of trials needed in all of our experiments to collect

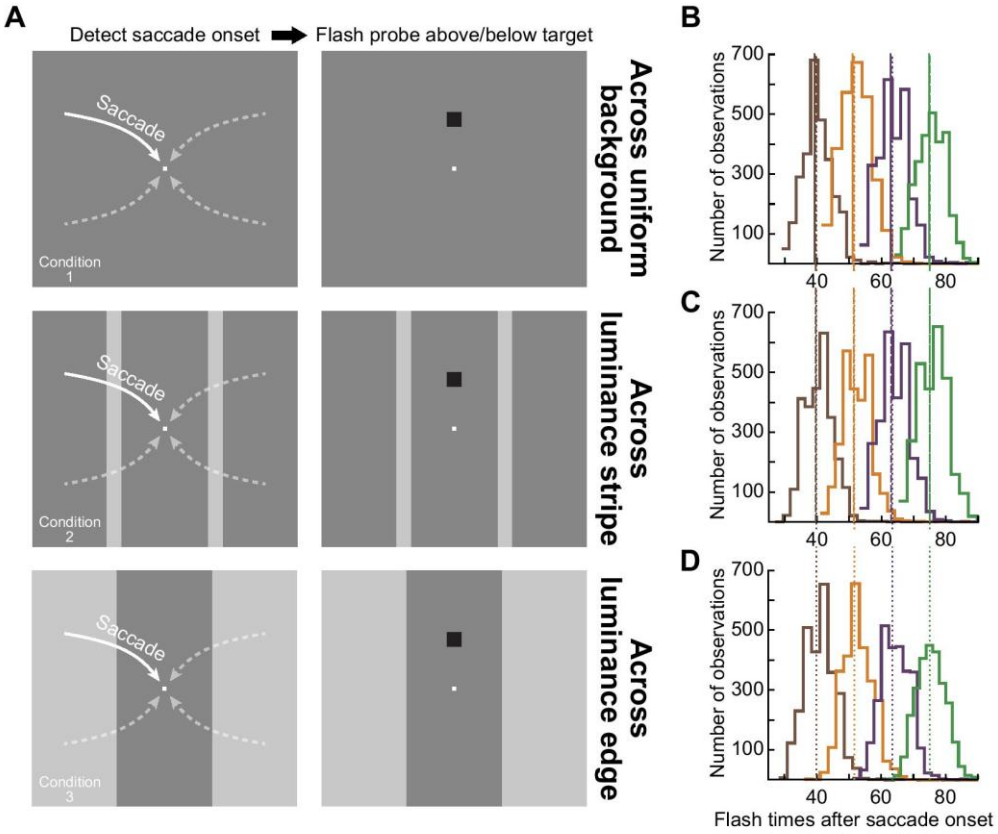

Figure 1. The different saccade conditions tested in our study. (A) Subjects made approximately 11.8 degrees saccades towards display center from one of four possible locations. The saccades (schematized as curved arrows) were predominantly horizontal (see text), and we detected their onset online using a velocity criterion. Upon saccade detection, we presented a brief luminance flash at 7 degrees either above or below the saccade target (right column of images). The flash was presented at one of four different delays from online saccade detection (see B–D). In condition 1 (top row), the saccades were made over a uniform background. In condition 2 (middle row), gaze crossed a vertical luminance stripe. And, in condition 3 (bottom row), the saccades brought gaze across a vertical luminance edge. We varied background luminance or the combination of pre- and post-saccadic background luminances across trials, and the probe flashes could also be of either positive (luminance increments relative to the background) or negative (luminance decrements) polarity. (B) After detecting saccades offline, we plotted the distributions of flash times collected during the experiments in condition 1 across all subjects. Our experimental manipulation succeeded in probing multiple times of perceptual sensitivity after saccade onset. The jitter in the individual distributions was due to variability in online saccade detection, as well as display update timing variability (due to the asynchrony between saccades and display refresh clocks). The solid vertical lines show the means of each distribution. (C, D) Similar distributions of flash times for conditions 2 and 3, suggesting that differences in perceptual thresholds across conditions (see Results) were not attributable to different flash times relative to saccade onset. The vertical lines (dashed in C and dotted in D) show the average flash times for each colored distribution in the respective panel, and they are extended upward towards the distributions in B to facilitate comparison of mean flash times. The mean times (of each colored distribution) were very similar across conditions (with a maximal observed difference of 0.8 ms).

full psychometric curves at each flash time and for each background luminance and for each of either saccade or fixation conditions. This is a strategy that we had also used in our recent experiments (Idrees, Baumann, Franke, et al., 2020). However, in other conditions described below (conditions 4 and 5), we did present flashes before visual transients, confirming that "pre-saccadic" suppression does occur, and that it is consistent with all of our previously described results motivating the current study (J. Bellet et al., 2017; Chen & Hafed, 2017; Hafed & Krauzlis, 2010; Idrees, Baumann, Franke, et al., 2020).

The probe flash presented after saccade detection was a square of 2.4 degrees by 2.4 degrees dimensions (Idrees, Baumann, Franke, et al., 2020). Its luminance consisted of either a decrement (shown in the examples of Figure 1A) or increment relative to the background luminance, allowing us to explore the impact of

stimulus polarity on peri-saccadic perceptual sensitivity. The background luminance itself was either bright (77.3 cd/m^2) or dark (22.4 cd/m^2).

Across trials, the probe flash could appear 7 degrees above or below the saccade target location. The subjects' task was to indicate, by pressing one of two buttons on a response box, whether the flash appeared above or below screen center. Note that with our display geometry, the retinotopic position at which the probe flash could appear was visually stimulated before the saccade by the display itself (i.e., a uniform luminance) rather than the (very) dark surround of the laboratory. Thus, across the saccade, the possible retinotopic location of the flash was swept across a uniform luminance rather than across the outer edge of the display.

We collected psychometric curves of flash perception as follows. Across trials, and for a given condition (for example: the combination of dark background; negative contrast flash; flash time 24 ms after saccade detection), we used an adaptive approach to select flash luminance levels resulting in threshold performance (Idrees, Baumann, Franke, et al., 2020). Briefly, in the first session of this condition, we used a QUEST procedure (Watson & Pelli, 1983) for each flash polarity, each background luminance, and each post-saccadic flash time aiming to achieve a percent correct of 75% over 60 trials. Then, after the threshold contrast was found for each QUEST procedure, in the second session, we introduced, for each condition, six additional contrast levels around the detected perceptual threshold obtained with the adaptive procedure. This gave more samples for the psychometric curve of each subject (Idrees, Baumann, Franke, et al., 2020).

Note that in this and all other conditions and analyses throughout this study, we refer to "threshold" as the absolute value of the probe contrast that was used (whether the probe was a luminance increment or decrement). However, we always also explicitly specify whether the probe was of positive (luminance increment) or negative (luminance decrement) polarity. This way, it is simpler to quantitatively compare saccade-related threshold elevations for both types of probe flashes.

We collected 1920 trials per subject in this condition.

(2) Real saccades across a vertical visual stripe: This condition was identical to condition 1 except that each saccade crossed a vertical luminance stripe of width 2.4 degrees. The stripe was centered horizontally on the midway point between initial and final fixation spot locations, and it spanned the full vertical extent of the display (Figure 1A, middle). Therefore, on every trial, the display was configured to have two vertical luminance stripes at 5.7 degrees either to the right or left of display center. The left stripe was crossed by rightward saccades starting from the left side of the display, and the right stripe was crossed by leftward saccades. Across trials, we varied the luminance of either the background or the stripes. Specifically, the stripes had the dark luminance when the rest of the display had the bright luminance, and vice versa (same luminance values as in condition 1). This way, the eye could start and land on either a dark or bright luminance region (like in condition 1), but the difference is that the gaze would have had to cross a luminance stripe of the other luminosity during the saccade. Like in condition 1, the retinal positions of the probe flash locations were visually stimulated by the display before the saccade (rather than by the much darker laboratory surround).

We collected 1920 trials per subject from this condition.

(3) Real saccades across a vertical luminance edge: In this condition, the display was split (along the horizontal dimension) into three areas (one central and two flanks; Figure 1A, bottom): the central region had either a bright or dark luminance, and the flanks were the opposite. The vertical edge between the central region and either of the two flanking regions was at 5.7 degrees horizontally from display center, which is halfway between the initial and final fixation spot's horizontal locations. As a result, there was a vertical edge across which the same saccades as in conditions 1 and 2 were made. The bright and dark luminances on either side of the vertical edge were the same as those of the bright and dark background luminances in conditions 1 and 2, and they were varied across trials (some trials had the central area being bright, and others had the flanking areas being bright, independently of whether the saccade was rightward or leftward). Thus, in this condition, the saccade landed on either a bright or a dark luminance level (like in conditions 1 and 2); however, the initial luminance level at saccade onset was always different from the final luminance level (Figure 1A, bottom). Moreover, the eye crossed only a single vertical luminance edge during the saccade, as opposed to two edges in condition 2. Finally, the probe flashes (whether luminance increments or luminance decrements) were always presented relative to the luminance level at the end of the saccade. That is, the probe flashes appeared on either bright or dark backgrounds (like in conditions 1 and 2).

We collected 1920 trials per subject from this condition.

(4) Simulated saccades across a vertical luminance edge: Subjects maintained fixation at display center, and a visual transient like that in condition 3 was introduced. That is, the display had a central region that was either bright or dark and two flanking regions around it with the opposite brightness from the central region (Figure 2A). Thus, there was a vertical edge, which was then translated horizontally to simulate a saccade across this edge. To achieve the translation, we moved the whole displayed texture (i.e., both the central

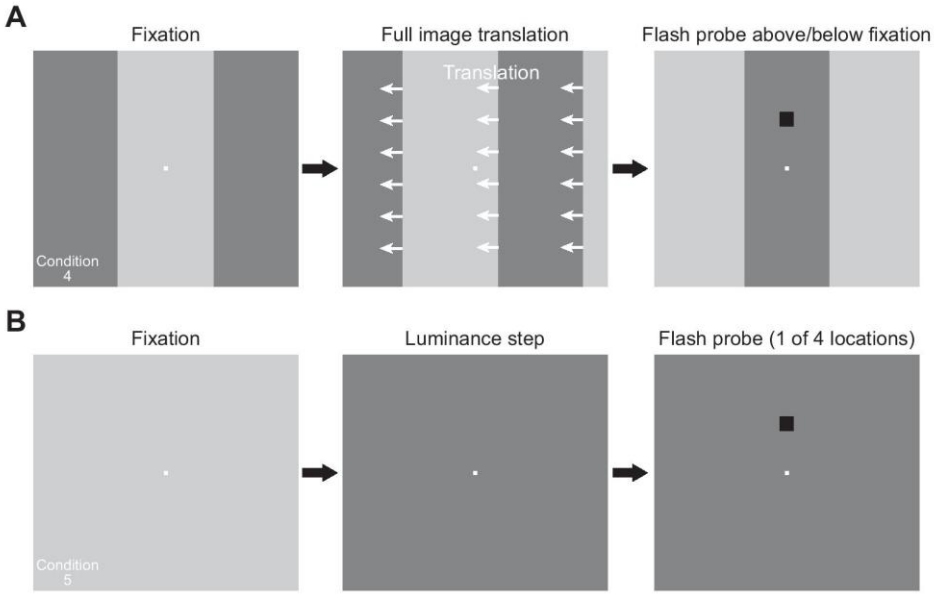

Figure 2. The visual-only conditions tested in our study. (A) In condition 4, subjects fixated the center of the display, and the background was identical to that of condition 3 in Figure 1. After initial fixation was established, the whole background translated horizontally to shift one of the two vertical edges across gaze position. After the translation, gaze was now aimed at a different background luminance. This condition mimicked the real saccade version in condition 3. Note that during translation, we treated the texture as being horizontally periodic (in the shown example, this meant that a bright background was revealed on the right edge of the display monitor during leftward translation). At different times relative to translation onset, we presented a flash either above or below fixation, similar to Figure 1A. In this case, the flashes could be presented either before or after translation onset (Methods). When presented after translation onset, the timing was such that they were presented over the new background luminance after translation end (that is, the edge had crossed display center even for the earliest flash time after translation onset). (B) In condition 5, the subjects fixated the center of a uniform display, and we changed the luminance of the background (from dark to bright or vice versa). Relative to this transient, a probe flash could happen at similar times to those used in A. Note that in this condition only, we had four possible probe flash locations, because this experiment was a replication of our earlier version of it in (Idrees, Baumann, Franke, et al., 2020; Idrees, Baumann, Korympidou, et al., 2020).

and flanking regions) horizontally at high speed. The resulting "simulated" saccade had parameters similar to those used in our recent work (Idrees, Baumann, Franke, et al., 2020). Briefly, we translated the texture (and, therefore, the vertical edge) by 1.9 degrees every display frame (of approximately 12 ms) for six display frames, corresponding to an overall translation of 11.4 degrees in 72 ms. This resulted in a high-speed translation of the vertical edge across the fovea during maintained fixation. The translation matched, in amplitude and duration, the amplitudes and durations of the real saccades that the subjects made in conditions 1–3 above. Specifically, in these conditions, the average saccade amplitude and duration were 11.37 ± 0.14 degrees and 74.89 ± 2.05 ms, respectively, across all trials from all subjects (mean value ± *SEM*).

The sequence of events in a given trial was as follows. An initial fixation spot appeared at the center of the display. The two vertical edges were at 5.7 degrees to the left and right of the fixation spot location (Figure 2A). After a random time of 800–1700 ms, the high-speed translation was started. For a leftward translation, the right vertical edge shifted to become now located at the initial location of the left vertical edge after the entire sequence had ended, and vice versa for a rightward texture shift. To handle display monitor edge effects, we treated the initial displayed pattern (i.e., the whole of the combination of central region and two flanks) as a horizontally periodic pattern. As a result, when a leftward shift happened, the rightward flank translated to become the central region, and a new rightward flank that was the same luminance as the original central region appeared. The corresponding scenario played out for a rightward shift. A probe flash appeared similar to the other conditions described above.

Across trials, we picked two times of probe flashes after the onset of the simulated saccades (47 and 59 ms) and also two times before the onset of the simulated saccades (24 and 35 ms before simulated saccade onset). The use of probe flashes before simulated saccade onset allowed us to demonstrate existence of pretransient suppression, which provides a logical link

to our other work (Idrees, Baumann, Franke, et al., 2020), and which also demonstrates that our lack of pre-saccadic flash times in conditions 1 to 3 above does not necessarily mean that there was no pre-saccadic suppression in these conditions. All other parameters of the experiment were similar to conditions 1 to 3.

We collected 1920 trials per subject from this condition.

(5) Fixation with a luminance change: Subjects maintained fixation at the center of a uniform display, and the visual transient now consisted of a change in background luminance from dark to bright, or vice versa (Figure 2B). Probe flashes could appear either before (24 or 35 ms) or after (35, 71, or 106 ms) the luminance change, like in condition 4. Note that in this condition only, we used a four-alternative forced choice paradigm as opposed to the two-alternative forced choice paradigm in all other conditions. So, instead of just presenting a probe flash 7 degrees above or below the fixation (or saccade) target location, the probe flash could now appear at 7 degrees in any of the four cardinal directions around the fixation spot (right, left, up, or down; Figure 2B). The reason for this is that fixation was always at the center of the display and that the display itself was uniform (allowing us to probe horizontal flash locations without worrying about "pre-saccadic" retinal image regions of horizontal flash locations being visually stimulated by the dark laboratory surround instead of the actual display, or by another luminance on the display like in condition 4). This condition also involved collecting new data from a similar condition (with four alternatives) that we had recently run (Idrees, Baumann, Franke, et al., 2020; Idrees, Baumann, Korympidou, et al., 2020). All other parameters and procedures were the same as in all other conditions.

We collected 2400 trials per subject from this condition.

Data analysis

We detected saccades and microsaccades using our laboratory's established methods (M. E. Bellet, Bellet, Nienborg, Hafed, & Berens, 2019; Chen & Hafed, 2013; Hafed, 2013). For all trials with fixation (conditions 4 and 5), we ensured that there were no microsaccades from –200 to +50 ms relative to probe flash onset. This allowed us to avoid potential changes in visual sensitivity around the time of microsaccades (Chen & Hafed, 2017; Chen et al., 2015; Hafed, Chen, & Tian, 2015). Similarly, for trials with real saccades, we excluded trials with saccades before instruction (i.e., before fixation spot jump) and also trials with saccadic reaction times >500 ms from saccade target onset, and we confirmed that the flash times relative to saccade onset (after post-hoc offline saccade detection) indeed clustered into four different time points, as designed in the task (see above and Figures 1B–D).

We analyzed the proportion of correct trials as a function of probe flash Weber contrast (i.e., absolute value of luminance difference of flash from background luminance, divided by the background luminance). We used Weber contrast, as opposed to Michelson contrast, because our probe flashes were relatively small relative to the uniform background across which they were presented; therefore, the average luminance with the flash was similar to the background luminance, making Weber contrast a more suitable metric. We calculated the proportion of correct trials for each flash luminance used, and independently for whether the probe flash consisted of a luminance increment or a luminance decrement relative to background luminance. We also did this for each flash time used.

For real saccades, we classified all flash times into four "clusters" of flash times centered around the mean values measured after offline saccade detection (in other words, each individually colored distribution of trials in Figures 1B–D contributed to one flash time "cluster" in the analyses). The results with real saccades were not altered when we first combined all flash times in a given condition, regardless of the online-designated delays in Figures 1B–D, and re-binned the trials as a function of time from saccade onset; our choice to use the colored clusters in Figures 1B–D for the temporal binning was only done for simplicity.

Across contrasts (for either increments or decrements), we obtained a psychometric curve fit of perceptual performance using the psignifit 4 toolbox (Schutt, Harmeling, Macke, & Wichmann, 2016). Briefly, we used a beta-binomial model for the psychometric curve. We defined the perceptual threshold as the absolute Weber contrast value resulting in a correct performance level that was at either 75% of the total dynamic range of the fitted psychometric curve (for conditions 1–4 with two-alternative forced choices) or 62.5% of the total dynamic range of the psychometric curve (for condition 5 with four-alternative forced choices). If there was perceptual suppression of sensitivity, then the threshold contrast was elevated. Thus, plots of threshold contrast indicate maximal suppression when the perceptual thresholds are high.

For each background luminance (dark or bright), and for each flash time, we calculated a psychometric curve for either flashes consisting of luminance increments or luminance decrements (i.e., flash stimulus polarity). We used the longer flash times after visual transient onset (either caused by real saccades or visual display updates during fixation) to confirm that there was perceptual recovery with time. Therefore, elevations of threshold contrast above the threshold values at such longer post-transient times were evidence for perceptual suppression.

To summarize results, we first estimated perceptual thresholds for each individual subject, and we then averaged the thresholds across subjects, with indications of inter-subject variance in all figures. To perform statistics, we used repeated-measures two-way ANOVA tests comparing the influences of flash time and condition on perceptual thresholds. We also sometimes performed individual t-tests comparing pairs of conditions at one given flash time; typically, this was the shortest flash time after saccade onset (or after texture translation or contrast change in conditions 4 and 5) since this time was the time associated with maximal perceptual suppression. This flash time was therefore of most interest when comparing suppression strength across the different conditions.

It should also be noted that in conditions 4 and 5, when we had "pre-transient" flashes, the flash appeared on a background that was different from the background for flash onsets occurring after the visual transient. Therefore, in all figures, we always pooled data points based on the background luminance on which a flash actually appeared. For example, pre-transient flashes in condition 4 with, say, a translation from bright to dark background were plotted as flashes over a bright background, whereas post-transient flashes were plotted as flashes over a dark background. This way, we always compared perception with a similar relationship between flash luminance and background luminance at the time of the flash. In statistical analyses of condition 5, we also pooled together, within each subject, the longest two flash times after background luminance change. This was because these two times showed the same effects anyway.

Results

We assessed the visual contributions to perceptual saccadic suppression by measuring perceptual sensitivity for brief flashes presented around the time of saccades across a variety of image types. We also compared such sensitivity to situations in which there were no saccades, but in which comparable visual transients occurred on the retina. In all cases, we compared perceptual sensitivity to a baseline case in which saccades were made across a uniform background. The results that we present below confirm and extend our recent observations that perceptual saccadic suppression may fundamentally be a visual phenomenon (Idrees, Baumann, Franke, et al., 2020; Idrees, Baumann, Korympidou, et al., 2020), and they are also in line with other psychophysical evidence in the literature.

Saccades across a local luminance feature are associated with much stronger perceptual suppression than saccades across a uniform background

We collected perceptual threshold measurements across saccades. In one condition (condition 1), subjects made predominantly horizontal oblique saccades across a uniform background. In another condition, the saccades were made across a 2.4 degrees wide luminance stripe relative to background luminance, but the luminances at both saccade start and saccade end were the same (condition 2). Figure 3 shows example psychometric curves of perceptual detectability obtained from an example subject in the two conditions and at flash times of approximately 40 ms (Figure 3A) and 63 ms (Figure 3B) after saccade onset. In this figure, we show results only from the dark background condition (Methods), and also when the luminance of the probe flash was a decrement relative to background luminance (i.e., negative stimulus polarity). Note that in this and all other figures, we depict the absolute value of Weber contrast, to aid comparison of effects between positive-contrast and negative-contrast probe flashes. Flashes immediately after saccade detection (Figure 3A) were associated with elevated perceptual thresholds in both conditions: this is evidenced by rightward shifts of the psychometric curves for the early time compared to the late one (compare the correspondingly colored curves in Figure 3A and Figure 3B). However, the effect was much stronger for condition 2, in which saccades crossed over a bright luminance stripe of 2.4 degrees width. Specifically, at 40 ms (Figure 3A), the absolute value of perceptual threshold was at >0.8 Weber contrast in condition 2 and at only <0.15 Weber contrast in condition 1. Similarly, at the later time point, even after partial perceptual recovery (Figure 3B), the absolute value of threshold in condition 2 was still at a level of almost 0.3 Weber contrast, but it was already at a level <0.09 in condition 1. Thus, perceptual saccadic suppression is much stronger when saccades are made across a luminance stripe than across a uniform background.

Across subjects, we made very similar observations. For example, the blue curve in Figure 4A shows the average psychometric curve obtained across all subjects (the average of all subjects' individual psychometric curves) in condition 2 for the first flash time (40 ms after saccade onset). This curve was shifted much more strongly to the right than the black curve in the same panel. The black curve summarizes the results across subjects with only a uniform background (condition 1). Similarly, Figure 4B shows recovery results at the 63 ms time point in the same format, again consistent with Figure 3. To summarize the effect size and time course to recovery across the two

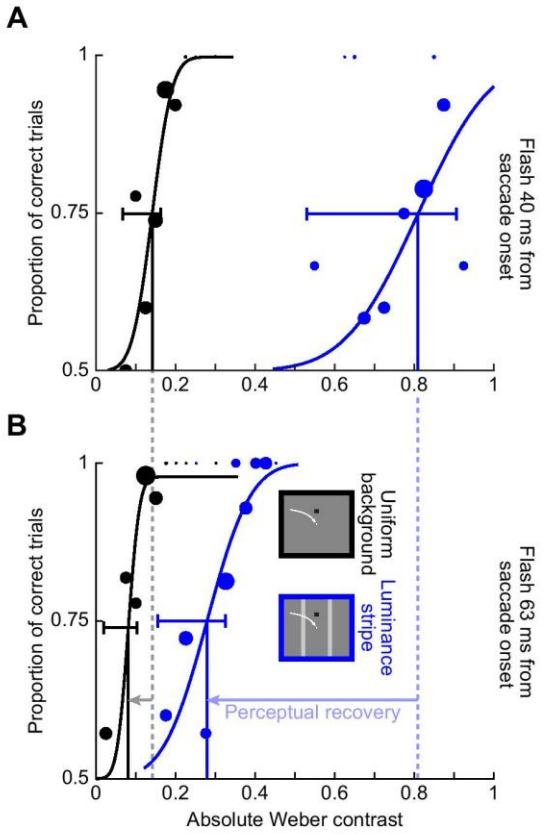

Figure 3. Much stronger saccadic suppression across a luminance stripe than across a uniform background. Example psychometric curves of perceptual detectability from one sample subject, for dark probe flashes over a dark background. Circles show individual data points, with the size of the circle scaled based on the numbers of observations collected. The blue curves show psychometric curves when the saccade crossed a luminance stripe (condition 2), whereas the black curves show the results obtained when the saccade was made across a uniform background (condition 1); see the schematic legend in B. Vertical lines indicate the perceptual threshold values in each condition, and horizontal error bars show 95% confidence intervals for each psychometric curve (obtained using the psignifit 4 toolbox; Methods). (A) Data for probe flashes presented immediately after online saccade detection (40 ms after actual saccade onset; first time cluster in Figures 1B–D). There was a much larger rightward shift in the psychometric curve in the case of condition 2 when compared to condition 1. (B) Data for a later flash time (63 ms after saccade onset; third time cluster in Figures 1B–D). Both curves recovered at this time point (i.e., shifted leftward relative to A; horizontal leftward arrows), but the blue curve still showed much more suppression (i.e., rightward shift) compared to the black curve.

conditions, we then estimated the perceptual threshold for a given condition as the absolute value of Weber contrast in each psychometric curve resulting in a correct performance level of 75% of the dynamic range (Methods, compare the vertical lines in Figure 3) (Idrees, Baumann, Franke, et al., 2020). Figure 4C plots the absolute threshold contrasts at all probe flash times (Figure 1B, C): in blue for condition 2 and in black for condition 1. Error bars denote *SEM* across subjects (Methods). There was much stronger suppression (larger increase in the perceptual threshold contrast) for saccades across the luminance stripe (blue) when compared to saccades across the uniform background (black), and this also persisted as a function of time. Statistically, a repeated-measures two-way ANOVA revealed a significant effect of both factors of flash time ($F(3,3) = 61.4$, $p < 0.01$) and condition ($F(1,5) = 96$, $p < 0.001$). Moreover, there was also a significant interaction between the two factors ($F(3,3) = 31.1$, $p < 0.01$). Post hoc, we compared the thresholds of condition 1 (mean ± *SEM*: 0.13 ± 0.02 Weber contrast) and condition 2 (0.95 ± 0.1 Weber contrast) at 40 ms (the time of maximal suppression in our experiments). There was a significant difference around the time of maximal suppression ($t(5) = 7.9$, $p < 0.001$).

Different pre- and post-saccadic visual stimulation is also associated with strong perceptual saccadic suppression

We next asked whether the final luminance on which the probe flashes appeared peri-saccadically needed to be the same as the "pre-saccadic" luminance at the line of sight for us to obtain the above results. To test this, we replaced the stripe used in condition 2 with a luminance edge (condition 3; Methods; red curves in Figure 4). That is, this time, the subjects initially fixated a bright background, and they then made saccades across a vertical edge, such that the probe flashes (and saccade landing positions) were now over a dark background. The same strong difference in saccadic suppression relative to the uniform dark background was observed (Figure 4, now compare red to black curves). For example, at the first flash time after saccade onset (Figures 4A, C), the average perceptual threshold in both conditions 2 and 3 was >0.75 Weber contrast, whereas it was only 0.13 Weber contrast when saccades were made across a uniform background (Figure 4C). Moreover, statistically, there was still a significant effect of time ($F(3,3) = 13.6$, $p < 0.05$) and condition ($F(1,5) = 41.5$, $p < 0.01$), when now comparing condition 3 to condition 1 (repeated-measures two-way ANOVA). There was also a significant interaction effect ($F(3,3) = 9.9$, $p < 0.05$). Moreover, a paired post hoc

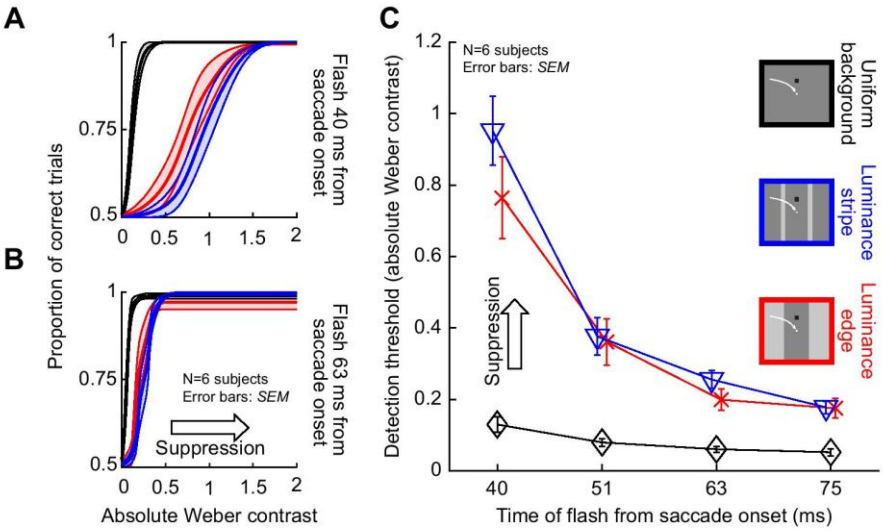

Figure 4. Systematically stronger saccadic suppression across a luminance stripe or luminance edge than across a uniform background. (A) Average psychometric curves of perceptual detectability from all subjects when the probe flashes occurred 40 ms after saccade onset (first time cluster in Figures 1B–D). Black: psychometric curve for condition 1, when saccades were made across a uniform background. Blue: psychometric curve when saccades crossed a luminance stripe (condition 2). Red: psychometric curve for condition 3, when saccades crossed a luminance edge. In all cases, error bands denote *SEM* across subjects. Perceptual thresholds were elevated much more for conditions 2 and 3 than for condition 1. (B) Same as in A but for a later time point (63 ms). There was perceptual recovery, but saccadic suppression was still stronger in conditions 2 and 3 than in condition 1; the subjects always had higher thresholds than in condition 1 (also see C). (C) Perceptual thresholds (average across subjects) for each flash time after saccade onset. Higher values mean stronger saccadic suppression. Error bars denote *SEM* across subjects. Note that the time values on the x-axis are the average flash times obtained after offline saccade detection (Methods and Figures 1B–D). Also note that for each average flash time, we slightly jittered the x-axis position of each data point to not mask individual data points and their error bars (also true in subsequent figures below). There was much stronger saccadic suppression in conditions 2 and 3 than in condition 1.

t-test highlighted a difference at 40 ms ($t(5) = 6.72$, $p = 0.001$; condition 1: 0.13 ± 0.02 *SEM* Weber contrast, and condition 3: 0.76 ± 0.11 *SEM* Weber contrast). In fact, when we compared threshold contrasts across subjects in both conditions 2 and 3 together (colored curves in Figure 4C), we found that suppression was equally strong for both conditions. A repeated-measures two-way ANOVA with the factors time and condition (2 versus 3) revealed no significant interaction between the factors ($F(3,3) = 2.4$, $p = 0.24$) and no significant effect of the condition ($F(1,5) = 1.3$, $p = 0.3$). However, expectedly, the effect of flash time was significant ($F(3,3) = 51.5$, $p < 0.01$).

Therefore, saccadic suppression is also enhanced when gaze crosses a luminance edge rather than a luminance stripe, replicating results from an earlier study (Maij, Matziridi, Smeets, & Brenner, 2012). The difference here is that in our current experiments, we assessed thresholds explicitly, by collecting full psychometric curves. We also varied stimulus polarities of the flashes, and even replaced saccades with image translations, as we describe in more detail shortly.

It is important to note that saccadic suppression still occurred over a uniform background (condition 1), albeit in a weak fashion. To confirm this, we statistically assessed perceptual detectability in condition 1 with a dark background, and we found that there was elevation of contrast immediately after saccade detection when compared to the latest two flash times after saccade onset in Figure 4C (black): a repeated-measures one-way ANOVA with flash time as factor was significant ($F(3,3) = 22.5$, $p = 0.015$), and a post hoc test revealed significant differences for the perceptual thresholds at 40 and 63 ms ($p = 0.035$), 40 and 75 ms ($p = 0.009$), and 51 and 75 ms ($p = 0.002$). Similar results also occurred for a bright background (we address the influence of background luminance more explicitly shortly). This extends the results of (Maij et al., 2012) in an important way. In that study, it could appear that there was no saccadic suppression at all with a uniform background. However, we think that measuring contrast thresholds in our experiments was a more sensitive measure of perceptual sensitivity. The approach of Maij et al could result in floor or

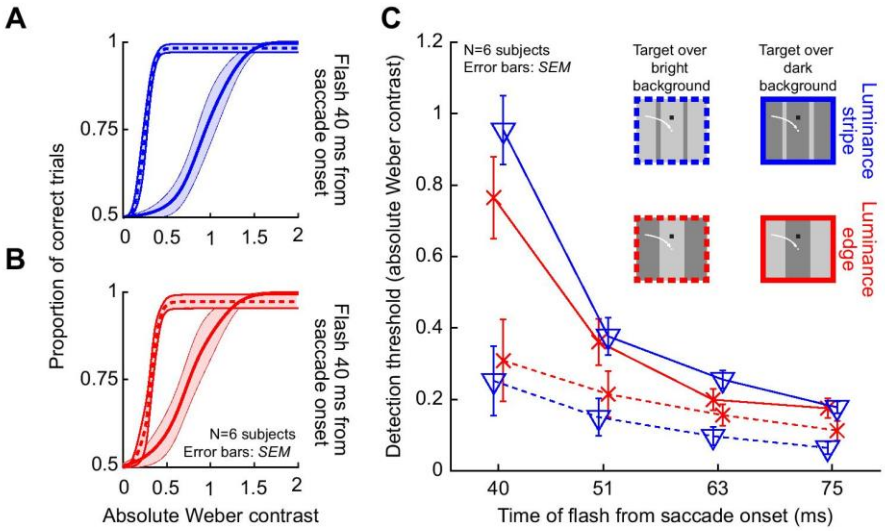

Figure 5. Stronger saccadic suppression over dark backgrounds, whether with luminance edges or luminance stripes. (A) Average psychometric curves of perceptual detectability from all subjects in condition 2, and for probes occurring 40 ms after saccade onset (i.e., the first time cluster in Figures 1B–D). Solid indicates flashes over a dark background (i.e., saccades starting and ending on a dark patch, but crossing a bright stripe), and dashed indicates flashes over a bright background (i.e., saccades starting and ending on a bright patch, but crossing a dark stripe). In both cases, the probe flashes had negative luminance polarity (i.e., they were luminance decrements relative to the background). Saccadic suppression was stronger with dark backgrounds than with bright backgrounds. Error bands denote *SEM* across subjects. (B) Similar results were obtained in condition 3. Flashes over a dark background (when saccades were made from a bright to a dark patch) were associated with stronger suppression than flashes over a bright background (when saccades were made from a dark to a bright patch). (C) Perceptual thresholds (averaged across subjects) for each flash time after saccade onset. Higher values mean stronger saccadic suppression, and error bars denote *SEM* across the subjects. In both conditions 2 and 3, flashes over a dark background (solid) were associated with much stronger saccadic suppression than flashes over a bright background (dashed). All other conventions are similar to Figure 4.

ceiling effects, potentially masking a mild amount of suppression (which we observed).

A visual dependence of saccadic suppression also emerges when considering the luminance of the background across which saccades are made

The above results indicate that the visual conditions across which saccades are made do matter for perceptual saccadic suppression, as we also recently argued (Idrees, Baumann, Franke, et al., 2020). To further demonstrate that perceptual saccadic suppression does indeed have a strong visual component, we next checked whether the luminance of the background mattered for the strength of suppression (Brooks, Impelman, & Lum, 1980). In our experiments, saccades could be made in condition 1 across either a bright or a dark background (Methods). Similarly, in conditions 2 and 3, the final landing position of the saccades, and therefore the final possible probe flash locations, could be either on a bright background or a dark background. In the description of results so far we have focused only on the dark background condition. We now describe the threshold contrasts that were obtained when the probe flashes appeared on a bright background instead.

Figures 5A, B show average psychometric curves across subjects for the first flash time after saccade detection (approximately 40 ms from saccade onset). Here, we directly compare trials having a dark background at flash occurrence (solid lines, replicated from Figure 4A) with trials having a bright background at flash occurrence (dashed lines). In Figure 5A, the data for condition 2 are shown, and in Figure 5B, the data for condition 3 are shown. In both cases, saccadic suppression was much stronger over a dark landing position than over a bright landing position. This effect can be better seen through plots of the time course of saccadic suppression in the two conditions (Figure 5C). Statistically comparing bright versus dark backgrounds, as well as time, in repeated-measures two-way ANOVA tests confirmed that there was a strong effect of background luminance (and time) on saccadic suppression. For both conditions, a repeated-measures two-way ANOVA revealed significant interactions (condition 2: $F(3,3) = 73.9$, $p < 0.01$; condition 3:

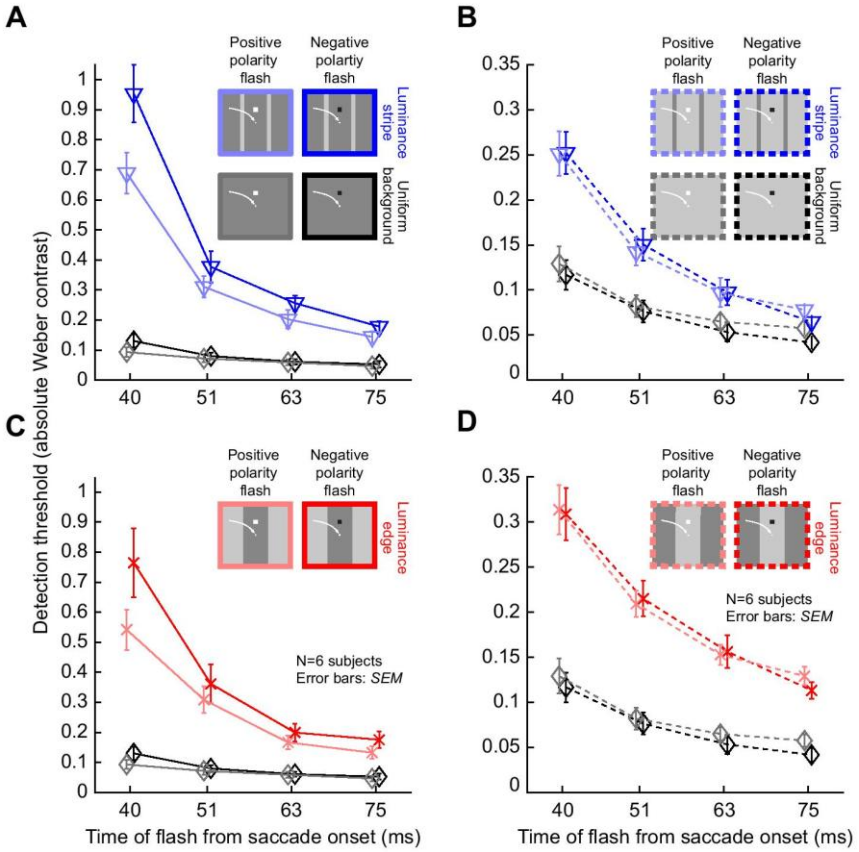

Figure 6. Stronger saccadic suppression for negative polarity flashes over dark backgrounds when compared to positive polarity flashes. Perceptual thresholds across subjects as a function of flash time after saccade onset (error bars denote *SEM* across subjects). (A) Data from condition 2 (blue) and condition 1 (black) with flashes appearing over a dark background. The saturated colors show results with negative polarity flashes, and the unsaturated colors show results with positive polarity flashes. Consistent with earlier figures, perceptual saccadic suppression was much stronger (higher absolute values of perceptual thresholds) in condition 2 than in condition 1 (compare colored to black curves). Within each condition, saccadic suppression was stronger with negative polarity flashes than positive polarity flashes, especially near the time of peak saccadic suppression (40 ms). (B) With bright backgrounds, the effects of flash polarity were absent (but suppression was still stronger than in condition 1). Note that the y-axis is different from A, because suppression was weaker for flashes over bright backgrounds (see Figure 5). (C, D) Similar results from condition 3, with saccades crossing a luminance edge. The black curves in this case are the same as in A, B. All other conventions are similar to Figures 4, 5.

$F(3,3) = 12.5$, $p < 0.05$) between the factors, as well as significant main effects for time (condition 2: $F(3,3) = 41.5$, $p < 0.01$; condition 3: $F(3,3) = 10.8$, $p < 0.05$) and background luminance (condition 2: $F(1,5) = 86.7$, $p < 0.001$; condition 3: $F(1,5) = 16.4$, $p < 0.01$). Note that for simplicity, we still only considered flashes consisting of luminance decrements relative to the background (i.e., of negative stimulus polarity), exactly like in all analyses above. We will explicitly describe the impact of flash luminance polarity relative to the background in a subsequent analysis. In any case, threshold elevations were much stronger with dark backgrounds than with bright backgrounds.

Incidentally, for saccades across a uniform background (condition 1), a repeated-measures two-way ANOVA with the factors time and background luminance showed no interaction between the factors ($F(3,3) = 0.1$, $p = 0.95$). As expected, since suppression still took place in this condition, the main effects of time and background were still significant (time: $F(3,3) = 19.5$, $p < 0.05$; background luminance: $F(1,5) = 9.1$, $p < 0.05$; also see Figure 6).

Therefore, the results of Figure 5 further illustrate the strong visual dependencies of perceptual saccadic suppression. When (negative polarity) probe flashes were presented over dark backgrounds, perceptual thresholds were elevated much more around the time of saccades than when the same negative polarity flashes (of the same contrast) were presented over bright backgrounds. Earlier work related to condition

3 did not analyze the effects of background luminance (Maij et al., 2012) (but see Brooks et al., 1980, which characterized the influence of background luminance for a subset of the conditions that we tested), and our recent experiments only used textured backgrounds (Idrees, Baumann, Franke, et al., 2020).

Flash luminance polarity interacts with background luminance to modulate the strength of saccadic suppression

We observed above that saccades across luminance-defined features are associated with strong perceptual suppression (Figures 3, 4), and that background luminance interacts with the presented brief flashes to modulate the strength of suppression (Figure 5). However, in all of our analyses so far, we only considered negative polarity probe flashes. To check whether probe flash polarity constitutes an additional visual dependence of perceptual saccadic suppression, we then turned our attention to analyzing trials with positive polarity probe flashes.

In Figure 6, we plotted the threshold contrasts across subjects for positive and negative polarity flashes in conditions 1, 2, and 3. In Figures 6A, C, we show the results with flashes presented over a dark background, and in Figures 6B, D, we show the results with flashes presented over a bright background. The top row of the figure (Figures 6A, B) shows results from condition 2 (blue), whereas the bottom row (Figures 6C, D) shows results from condition 3 (red). For each condition, the different shades of color denote whether the flash had negative polarity (saturated colors; these are data replicated from the previous figures) or positive polarity (unsaturated colors) relative to the background. Note that both rows also show the results from condition 1 with a uniform background for reference (black and gray curves). Also note that the y-axes in Figures 6A, C are different from those in Figures 6B, D because of the differential impact of background luminance that we described in Figure 5. As can be seen from Figures 6A, C, negative polarity probe flashes over dark backgrounds had stronger saccadic suppression (higher detection thresholds) than positive polarity probe flashes over the same background, especially at the time of peak saccadic suppression (40 ms). For example, immediately after saccade onset in conditions 2 and 3, perceptual thresholds were at 0.95 and 0.76 Weber contrast across subjects for negative polarity flashes, respectively (Figures 6A, C, colored curves). For positive polarity flashes, the thresholds were elevated to only 0.69 and 0.54, respectively. Statistically, this difference between positive and negative polarity flashes was significant at 40 ms in both condition 2 ($t(5) = 6.69$, $p = 0.001$; positive polarity mean and *SEM*: 0.95 ± 0.1 Weber contrast; negative polarity: 0.69 ± 0.07 Weber contrast) and condition 3 (paired *t*-test: $t(5) = 3.31$, $p = 0.02$; positive polarity mean and *SEM*: 0.76 ± 0.11 Weber contrast; negative polarity: 0.54 ± 0.07 Weber contrast). Interestingly, over a bright background (Figures 6B, D), both conditions 2 and 3 did not show any difference in the strength of saccadic suppression between positive and negative polarity flashes (Figures 6B, D, colored curves). Therefore, there was an interaction between flash polarity and background luminance in modulating the strength of perceptual saccadic suppression, which was also evident statistically. For example, at peak suppression, a repeated-measures two-way ANOVA with the factors background luminance and flash polarity revealed a significant interaction effect (condition 2: $F(1,5) = 40.1$, $p < 0.01$ and condition 3: $F(1,5) = 13.8$, $p < 0.05$).

It is also interesting that for condition 1, similar effects still existed for flash luminance polarity (Figure 6, black and gray curves) despite the very weak perceptual saccadic suppression that occurred: it was still the case that negative polarity flashes over a dark background (mean threshold 0.13 ± 0.02 *SEM* Weber contrast) tended to cause stronger saccadic suppression than positive polarity flashes (mean threshold: 0.09 ± 0.01 *SEM*) over the same background ($t(5) = 3.6$, $p = 0.016$ Weber contrast). Thus, our analyses of probe flash stimulus polarity in all saccade conditions (1, 2, and 3) provide further evidence that perceptual saccadic suppression has strong visual dependencies.

Perceptual suppression occurs equally well, and with the same visual dependencies, for image sweeps that conceptually mimic saccade-induced image shifts

The above evidence is indicative of strong and rich visual-visual interactions in saccadic suppression between the saccade-related retinal image shifts and the probe flashes themselves, as we have recently suggested (Idrees, Baumann, Franke, et al., 2020; Idrees, Baumann, Korympidou, et al., 2020). If that is indeed the case, then the same visual dependencies as those demonstrated in Figures 3–6 should also happen in the complete absence of saccades, but in the presence of saccade-like image shifts and probe flashes. We therefore repeated the above experiments but with so-called "simulated saccades." We asked subjects to fixate, and we swept a vertical luminance-defined edge across the retina to simulate a saccade-like image displacement (Figure 2A). This condition was therefore conceptually similar to condition 3 (Methods). The probe flashes happened identically to how they happened in the real saccade version of the experiment. We also additionally tested pre-shift probe flashes, to check for perceptual

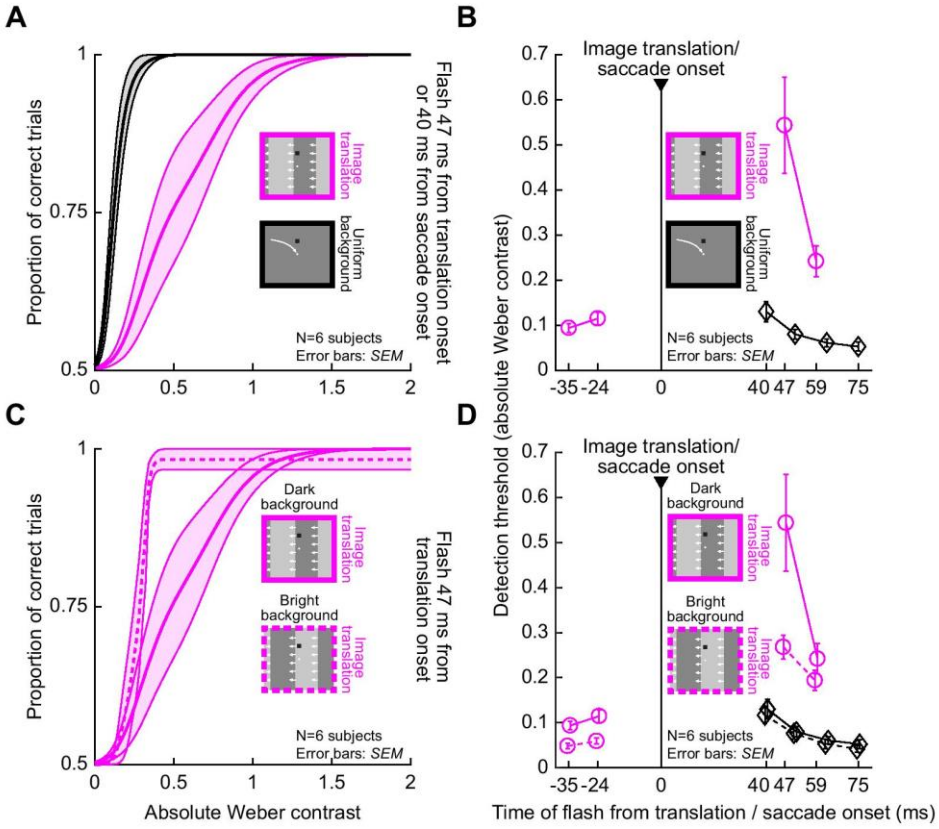

Figure 7. Highly similar visual dependencies of perceptual suppression in the absence of saccades. (A) Psychometric curve of perceptual detectability from condition 4, in which a saccade-like displacement of a vertical luminance edge took place (conceptually similar to condition 3 with real saccades). For reference, the black curve shows the psychometric curve from condition 1 (real saccades over a uniform background) at 40 ms. The saccade-like image displacement caused large suppression (a larger rightward shift of the curve), similar to the large suppression seen with real saccades (e.g., Figure 4). Error bands denote *SEM* across subjects. (B) Time course of perceptual suppression in condition 4. For reference, the time course of saccadic suppression over a uniform background (condition 1) is also shown in black. (C) There was also stronger suppression with (negative polarity) flashes over a dark background than with the same flashes over a bright background, exactly like with real saccades (e.g., Figure 5). The average psychometric curve was shifted more to the right with a dark background (solid). (D) The dependence of perceptual suppression on background luminance was also clear in the whole time course, and this dependence was similar to that seen with real saccades in a similar visual condition of crossing an edge (e.g., Figure 5). For reference, the black curves show the results obtained with real saccades across a uniform dark (solid) or bright (dashed) background (same as in Figure 6).

suppression before "simulated saccade" onset (Idrees, Baumann, Franke, et al., 2020).

We replicated all of the above observations that were made with real saccades. First, we confirmed that immediately after saccade-like image translation, strong perceptual suppression occurred, which was much stronger than the suppression with real saccades across a uniform background. This effect is demonstrated in Figure 7A, which shows the average psychometric curve across all subjects when a negative polarity flash appeared over a dark background at 47 ms after image translation onset (magenta curve). For reference, the black curve in the same figure shows the average psychometric curve associated with "real" saccadic suppression over a uniform (dark) background at our shortest flash time (i.e., associated with maximal saccadic suppression in our data set). As can be seen, perceptual thresholds were strongly elevated even with the simulated saccades, just like in condition 3. Across flash times, Figure 7B shows that immediately after image shift onset, the absolute value of threshold contrast over a dark background was 0.54 Weber contrast for negative polarity flashes. This value was much higher than that for real saccades across uniform backgrounds (0.13 Weber contrast for the shortest flash time with the real saccade; 40 ms). Statistically, we confirmed this by doing a paired comparison of thresholds between condition 4 (0.54 ± 0.11 *SEM*

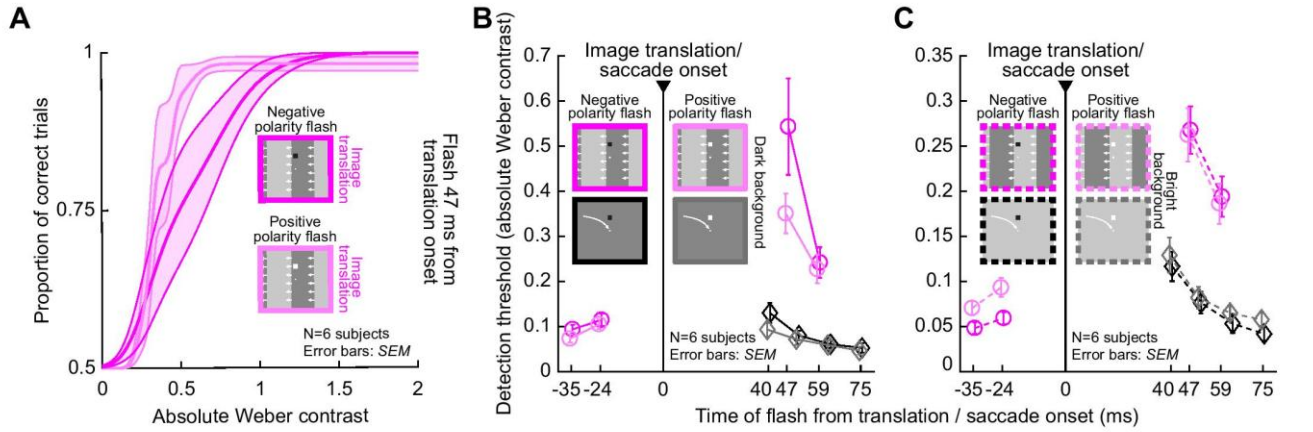

Figure 8. Stronger suppression for negative polarity flashes over dark backgrounds when compared to positive polarity flashes, even in the absence of saccades. (A) Average psychometric curves for negative and positive polarity flashes occurring at 47 ms after image translation onset and appearing over a dark background. Saturated colors show results with negative polarity flashes, and unsaturated colors show results with positive polarity flashes. Error bands denote *SEM* across subjects. Negative polarity flashes were associated with stronger perceptual suppression than positive polarity flashes. (B) Perceptual thresholds across subjects as a function of flash time after image translation onset in condition 4, comparing negative and positive polarity flashes over a dark background (error bars denote *SEM* across subjects). For reference, the time course of suppression from condition 1 is also shown in black. Consistent with Figure 7, perceptual suppression with an image translation (condition 4) was much stronger (higher perceptual thresholds) than in condition 1 with real saccades (compare colored to black curves). Moreover, perceptual saccadic suppression was stronger with negative polarity flashes than positive polarity flashes, especially near the time of peak suppression (47 ms). This is identical to the effect that we saw with real saccades in Figure 6. (C) With bright backgrounds, the effects of flash polarity were absent, again consistent with what we observed with real saccades (Figure 6).

Weber contrast) and condition 1 (0.13 ± 0.02 *SEM* Weber contrast) at the shortest positive flash time after either image translation onset or saccade onset ($t(5) = 4.7$, $p = 0.005$).

Second, we confirmed that there was stronger perceptual suppression over a dark background versus over a bright background with our simulated saccades of condition 4. This effect can be seen in Figure 7C, in which we plotted the average psychometric curves across all subjects at the same flash time, but with flashes occurring over either a bright or dark background. As we did above for simplicity in several other figures, we only plotted the curves for negative polarity flashes (but see below for explicit analysis of flash polarity in this condition as well). The psychometric curve for dark backgrounds (replicated from Figure 7A) was shifted farther to the right compared to the curve for bright backgrounds, consistent with stronger perceptual suppression. In Figure 7D, the full-time courses can be seen for both background luminances. For reference, the curves for saccadic suppression with real saccades over a uniform background are also shown in black (condition 1). At the first time point after visual transient onset in the simulated saccade condition, threshold contrast was 0.54 ± 0.11 *SEM* and 0.27 ± 0.03 *SEM* Weber contrast for dark and bright backgrounds, respectively (paired *t*-test: $t(5) = 4.5$, $p = 0.006$).

Finally, we also confirmed that the same interactions between flash polarity and background luminance also persisted with simulated saccade-like image shifts. Specifically, we used condition 4 to explore psychometric curves of perceptual detectability when flashes appeared at different times relative to image displacement onset and on different background luminances. Figure 8A shows such curves for the case of negative or positive polarity flashes appearing over a dark background 47 ms after the onset of rapid image displacement. The curve for the negative polarity flashes was shifted more to the right than the curve for positive polarity flashes, suggesting stronger perceptual suppression. This is similar to what we also saw with real saccades (Figure 6). Indeed, the time courses (Figures 8B, C) exhibited very similar dependencies on flash polarity to the real saccade conditions. For example, over a dark background (Figure 8B), perceptual thresholds were at 0.54 ± 0.11 *SEM* Weber contrast for negative polarity flashes, and 0.35 ± 0.04 *SEM* for positive polarity flashes, at the time closest to peak suppression in our data (47 ms). This was statistically significant (paired *t*-test: $t(5) = 2.7$, $p = 0.04$). For reference, Figure 8B also shows the thresholds from condition 1 with real saccades over a uniform background. As can be seen, the suppression was significantly stronger with translation of a luminance

edge across the retina than with real saccades over a uniform background. In fact, the threshold values in condition 4 (Figures 7, 8) immediately after simulated saccade onset were generally similar in strength to those obtained immediately after real saccades in condition 3 (e.g., Figures 4, 5); however, we caution against direct quantitative comparison, especially given the very different time courses of real versus simulated saccadic suppression profiles that can exist (Idrees, Baumann, Franke, et al., 2020).

The interaction between flash polarity and background luminance also extended to bright backgrounds. Specifically, with real saccades in conditions 2 and 3, we saw above (Figure 6) that flash polarity did not alter saccadic suppression strength when flashes appeared over a bright background, unlike the case with flashes occurring over a dark background. This happened in a similar way in condition 4 with simulated saccades (Figure 8C). Therefore, all of the visual dependencies that we observed with real saccades (Figures 3–6) also occurred in the absence of any saccades, when saccade-like image translations were introduced (Figures 7, 8).

It should be noted here that our simulated saccade condition was also important because it allowed us to additionally test probe flashes occurring before simulated saccade onset. In Figures 7, 8, flashes with negative time were presented before the image translation. Nonetheless, they were still associated with threshold elevations, as we also recently reported in similar experiments (Idrees, Baumann, Franke, et al., 2020). For example, in Figure 7B, perceptual threshold for a flash time of –24 ms was 0.11 Weber contrast, whereas it was only 0.09 at –35 ms. Therefore, there was elevation of threshold as time approached the onset of the image translation. These results, combined with earlier published work in the literature, make it likely that we would also observe pre-saccadic suppression in conditions 1, 2, and 3 above if we were to present flashes before the real saccades. Interestingly, even pre-translation flashes were clearly associated with stronger suppression when they occurred over a dark background as opposed to a bright background (Figure 7D), consistent with the post-translation flash times demonstrating an influence of background luminance, which are in turn consistent with real saccade background effects.

Luminance steps without saccade-like image sweeps cause modest perceptual suppression

Finally, for completeness, we also tested simple luminance steps during fixation, with no image translations (condition 5; Methods). In this case, we previously found that perceptual suppression does occur (Idrees, Baumann, Franke, et al., 2020), although in that previous study, we did not explore certain factors, like flash polarity, in much detail.

With luminance steps, perceptual suppression was significantly weaker than with image translations. For example, Figure 9A shows thresholds when a flash occurred over a dark background, and Figure 9B shows thresholds when a flash occurred over a bright background. For reference, saccadic suppression thresholds from condition 1 (i.e., with saccades across a uniform background) are also shown in black. Both conditions had the weakest overall suppression strengths in the whole study, and peak suppression in them was very similar. For example, at the first flash time after contrast change or saccade onset, the overall thresholds in both conditions were less than 0.18 Weber contrast (Figure 9), which is much less than threshold contrasts in all other experiments with luminance edges or stripes (whether with or without saccades). This suggests an interesting role of luminance transients over perifoveal image regions in perceptual saccadic suppression. Specifically, perifoveally, the uniformity of the display was similar during the real saccades (condition 1) and the contrast change experiment (condition 5); both conditions were lacking local image translation across the retinal regions that were also probed with brief flash stimuli. Even though the entire retinal image (including display outer edges) was translated across the retina during real saccades, it seems that such a local image translation is necessary to maximize perceptual suppression of temporally close probe flashes.

Figure 9 also reveals interesting differential effects of flash polarity on perceptual thresholds, but only at longer times after contrast change. Specifically, at both 71 ms and 106 ms after background luminance change (from bright to dark or vice versa), there was an interaction between flash polarity and background luminance: negative polarity flashes were harder to detect compared to positive polarity flashes over dark backgrounds, whereas positive polarity flashes over bright backgrounds were harder to detect than negative polarity flashes. To statistically validate this, we pooled the two latest flash times together and compared, with a paired t-test for each background, whether the detection thresholds differed for the two flash polarities. With a dark background, the positive polarity (mean threshold: 0.07 ± 0.01 SEM Weber contrast) significantly differed from the negative polarity (mean threshold: 0.09 ± 0.01 SEM) ($t(5) = 5.8$, $p = 0.0022$). Over a bright background, the positive polarity (threshold: 0.09 ± 0.01 SEM Weber contrast) significantly differed from the negative polarity (0.06 ± 0.01 SEM) ($t(5) = -16$, $p < 10^{-4}$). This effect was not present in any of our real or simulated saccade conditions (conditions 1–4), and it also might be a

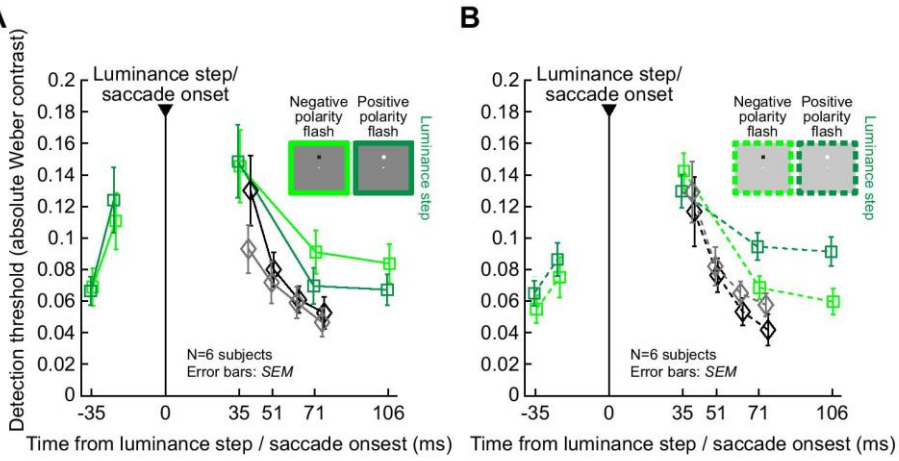

Figure 9. Weak perceptual suppression with simple luminance steps during fixation. (A) Perceptual contrast thresholds from condition 5 with just luminance steps (colored curves). Each curve shows results for either a positive (dark green) or negative (light green) polarity flash over a dark background, and error bars denote *SEM* across subjects. For reference, thresholds from condition 1 are shown in black. Peak suppression with a luminance step was as weak as the suppression with real saccades over a uniform background (this was our weakest suppression condition in all experiments; Figures 1–8). Moreover, during recovery, negative polarity flashes were harder to detect than positive polarity flashes. (B) Similar results for flashes occurring over a bright background. Now, it was positive polarity flashes that were harder to detect than negative polarity flashes during the recovery phase (at times 71 and 106 ms after luminance step occurrence). All other conventions are similar to Figures 4, 5.

simple instantiation of Weber's law, irrespective of perceptual suppression. Interestingly, in our recent investigation of a similar perceptual paradigm (Idrees, Baumann, Korympidou, et al., 2020), there was no clear impact of flash polarity. However, in that study, we did not use the more sensitive psychometric approach that we used here, so we could have been affected by floor and ceiling effects in that earlier study. Nonetheless, it is interesting that visual-visual interactions in saccadic suppression are best matched under fixation when saccade-like image displacements take place; other transients, such as just simple background luminance steps (Figure 9), also cause mild suppression, but with different visual dependencies.

Discussion

We investigated the visual components of perceptual saccadic suppression. We collected psychometric curves of perceptual detectability for brief peri-saccadic flashes and used these curves to estimate thresholds. We found that perceptual thresholds were only elevated mildly when saccades were made across a uniform background, but they were dramatically increased when gaze crossed a luminance edge (e.g., Figures 3, 4). Moreover, the luminance at which gaze landed after saccade end did not have to be different to the luminance at saccade onset for the strength of saccadic suppression to increase; crossing a luminance stripe was also associated with very strong saccadic suppression when compared to the uniform background (condition 2, e.g., Figure 4). Interestingly, saccadic suppression was the strongest when the luminance of the background was dark, and there was an impact of flash polarity relative to the background luminance (particularly with negative polarity flashes over dark backgrounds; e.g., Figures 5, 6). Critically, all of these visual dependencies of saccadic suppression still occurred when we replaced saccades with image displacements in the absence of any saccadic eye movements (e.g., Figures 7, 8).

Our results from condition 3 confirm and extend those of (Maij et al., 2012). In that study, the authors used a condition similar to ours (Figure 1A, bottom), and they asked subjects to indicate whether they missed seeing a peri-saccadic flash or not (the overall context of the task was to study mislocalization of observed flash location, so the flashes were supra-threshold in general compared to ours). When the saccades were made over a uniform background, the subjects almost never missed the flashes. However, when the saccades involved gaze crossing a vertical luminance edge, there was an increased likelihood of misses. This is also what we saw with our more sensitive threshold measurements in the current study (e.g., Figures 3, 4). As stated above, we also saw almost equally strong suppression when the edge was replaced with just a luminance stripe (condition 2, i.e., the starting and landing gaze positions

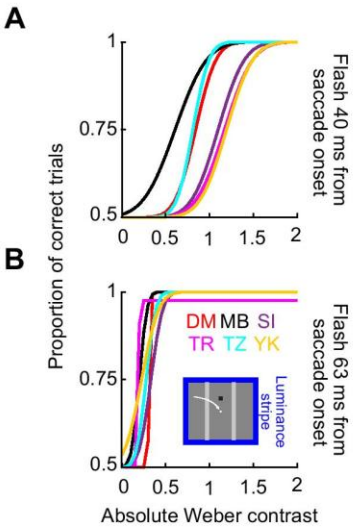

Figure 10. Raw psychometric curves at two flash times from each individual subject in condition 2. (A) Psychometric curves of all subjects with a negative polarity flash at 40 ms and dark backgrounds. (B) The same for the flash at 63 ms. There was strong coherence across subjects in the modulations of perceptual detectability in our experiments.

were on the same background luminance; Figures 3, 4). Combined, these results suggest that visual-visual interactions, in the form of gaze crossing a luminance pattern (one vertical edge in condition 3 or two vertical edges in condition 3), matter a great deal for saccadic suppression.

Moreover, the effects are highly repeatable across individuals. In all analyses, average measurements across subjects were very consistent and repeatable, as evidenced by the small error bars in all our figures. Indeed, when we plotted the individual psychometric curves of each subject for one of the conditions, as in the example of Figure 10, we saw remarkable repeatability across subjects. This was true in our earlier study as well (Idrees, Baumann, Franke, et al., 2020). Therefore, the effects that we report here are clearly robust across individuals.

It is also interesting that the background luminance has a strong influence on the strength of saccadic suppression, as was also suggested previously (Brooks & Fuchs, 1975; Brooks et al., 1980). In all analyses, we assessed perceptual thresholds based on calculating the absolute luminance difference between the probe flash and the background, normalized against the background luminance (i.e., Weber contrast). We observed that subjects needed more luminance contrast relative to the background (even with positive polarity flashes) to detect stimuli peri-saccadically (or peri-translation in condition 4) when the overall background was dark than when it was light. The fact that this effect was stronger with the dark background compared to the bright one rules out the possibility that this was a simple instantiation of basic Weber's law (i.e., that more luminance needs to be added to a bright background than to a dark background for equal detectability). Rather, there was an apparent interaction between image translation and gaze finally encountering an image patch with a dark region. Similarly, there was also an interaction associated with the probe polarity itself: after saccades (or image translations), dark backgrounds required larger negative polarity contrasts for perceptual detection than positive polarity contrasts, but no polarity effects existed with a bright background (e.g., Figure 6). It could be the case that crossing an image patch to a darker background induces a stronger visual transient (e.g., in the retina) than crossing an image patch to a brighter background, which then modifies the subsequent visual response to the probe flash itself.

It would be interesting to explore this mechanism by relating how our observed interaction effects (that is, perceptually) relate to the activity of ON and OFF channels in ex-vivo mouse and pig retinae, similar to our recent investigations (Idrees, Baumann, Korympidou, et al., 2020). Intriguingly, preliminary data from that study indicate that ex-vivo non-human primate retinae may exhibit ON and OFF dependencies that might be similar to human effects (Idrees, Baumann, Korympidou, et al., 2020), at least in our condition 5. On the other hand, our probe flash polarity effects (e.g., Figures 6, 8) demonstrate that strong perceptual suppression can occur irrespective of the combination of visual transient polarity and probe flash polarity; this suggests the presence of other suppressive mechanisms beyond the dynamic reversal suppression mechanism (which depends on a difference in polarity between visual transient and probe flash) that we uncovered in the mouse and pig retinae in the same study.

Of course, it would also be interesting to investigate the visual-visual interactions of saccadic suppression in neural circuits downstream of the retina in non-human primates (as well as other relevant species used in systems neuroscience). Indeed, neurons preferring "black" stimuli are prevalent in the primary visual cortex (Yeh, Xing, & Shapley, 2009), and sensory processing times are also different for dark versus bright stimuli (Jin, Wang, Lashgari, Swadlow, & Alonso, 2011; Komban et al., 2014). Moreover, there are asymmetric interactions between background luminance and the effectiveness of ON and OFF early visual processing channels (Rahimi-Nasrabadi et al., 2021). Finally, dark versus bright stimuli can have differential effects on visuo-motor processing in monkeys (Malevich, Buonocore, & Hafed, 2020). All of these results, combined with our current study, motivate future experiments on sensory-motor processing with dark stimuli in brain areas downstream of the retina.

The importance of visual-visual interactions in perceptual saccadic suppression also makes us consider the possibility that with our uniform background condition (condition 1), the edges of the monitor may have had a non-negligible modulatory effect on the phenomenon. Specifically, for both the bright and dark background luminances used in the uniform background condition, the display monitor was still brighter than the rest of the laboratory. Therefore, there was a rectangular frame that was moved on the retina by the saccades. This likely affected perception since our other conditions (with luminance edges crossing the fovea) had a very strong effect on the strength of saccadic suppression. Nonetheless, it is still intriguing that, by far, the largest effects on peri-saccadic perceptual thresholds that we observed required that the luminance edges or patterns cross the fovea during the saccades. Such foveal crossing (or, more generally, crossing of the retinal patch experiencing the probe flashes) also happened in our simulated saccade condition (condition 4), which again showed strong perceptual suppression effects. This could be a function of the spatial resolution of the retinal regions (and associated downstream visual areas) that experience temporal luminance modulations during the saccades and the flashes.

In addition to the above effects in real saccades, we also saw essentially the same visual dependencies in experiments with visual-visual interactions no longer involving real saccades. Specifically, in our condition 4, we translated the luminance edge across the fovea and presented probe flashes near the time of the translation. We observed the same dependencies on background luminance, and the same interactions with flash luminance polarity, as with real saccades. This confirms our hypothesis (Idrees, Baumann, Franke, et al., 2020; Idrees, Baumann, Korympidou, et al., 2020) that visual-visual interactions play an important role in saccadic suppression, and it also extends the image conditions under which we could observe remarkable similarities between real and simulated saccades in terms of perceptual suppression (Idrees, Baumann, Franke, et al., 2020). All of this is in agreement with other phenomena, like the fact that intra-saccadic motion can still be perceived if its speed is within the detectability range of our motion sensors in the brain (Castet et al., 2001; Castet & Masson, 2000), and also the fact that intra-saccadic motion streaks provide important reference frames for keeping track of object locations (Schweitzer & Rolfs, 2020). This evidence highlights the role of vision even during rapid eye movements. In that sense, suppression occurring before saccades or image translations (e.g., Figures 7–9) may be viewed as reflecting visual-visual interactions such as backward masking (Breitmeyer, 2007; Brooks & Fuchs, 1975; Judge, Wurtz, & Richmond, 1980; Mackay, 1970; Mitrani et al., 1975).

Naturally, a role for prior knowledge of movement commands at the time of saccade generation (e.g., corollary discharge) must additionally matter for saccadic suppression, and the real question becomes how visual and non-visual mechanisms interact in this phenomenon. In other words, it need not be the case that saccadic suppression is only purely motor or only purely visual. For example, experiments under conditions of whiteout (i.e., absolutely uniform illumination across the entire retina) might suggest a role for a movement-related impact on perceptual saccadic suppression (Riggs & Manning, 1982). Interestingly, at the neural level, enhancement, rather than suppression, seems to take place in human LGN and V1 across saccades without visual stimulation (Sylvester, Haynes, & Rees, 2005; Sylvester & Rees, 2006). This suggests a very different role for knowledge of saccade commands than simply to actively reduce visual sensitivity. Similarly, we recently found that while the visual properties of perceptual suppression were highly similar with or without real saccades, there was a massive difference in the time course of suppression when real saccades were generated: perceptual suppression was much more short-lived when it was associated with real saccades than when it was triggered by visual-visual interactions in the absence of saccades (Idrees, Baumann, Franke, et al., 2020). This is very reassuring, in retrospect, because of the strong need to minimize saccade-induced disruptions in vision as much as possible. However, it also raises highly interesting and unanswered questions on what exactly the role of saccade-related movement commands is in modulating the properties of perceptual saccadic suppression. Could it be that corollary discharge is there to shorten saccadic suppression, rather than to cause it? This is a topic that we think will lead to very interesting new neurophysiological insights on the field of trans-saccadic perception.

Conclusions

The phenomenon of perceptual saccadic suppression possesses a strong visual component, reflecting interactions between visual activation caused by saccade-induced image translations and visual activation caused by the brief probe flashes used to measure the sensitivity of the visual system around the time of saccades. This visual component of saccadic suppression motivates future neurophysiological, perceptual, and theoretical investigations on how this component interacts with internal knowledge of saccadic movement generation commands (i.e., efference copies or corollary discharge) for minimizing the disruptions to vision that can be caused by saccades.

Keywords: saccadic suppression, stimulus polarity, luminance contrast, trans-saccadic perception, ON channels, OFF channels, retina

Acknowledgments

MPB and ZMH were funded by the Deutsche Forschungsgemeinschaft (DFG) Collaborative Research Center SFB 1233 on "Robust Vision" (project number: 276693517). SI and TAM were funded by DFG grant number MU3792/3-1.

Commercial relationships: none.
Corresponding author: Matthias P. Baumann.
Email: matthias-philipp.baumann@student.uni-tuebingen.de.
Address: Werner Reichardt Centre for Integrative Neuroscience, Tübingen University, Tübingen, Germany.

References

Adey, W. R., & Noda, H. (1973). Influence of eye movements on geniculo-striate excitability in the cat. *Journal of Physiology, 235*(3), 805–821, https://doi.org/10.1113/jphysiol.1973.sp010418.

Beeler, G. W., Jr. (1967). Visual threshold changes resulting from spontaneous saccadic eye movements. *Vision Research, 7*(9), 769–775.

Bellet, J., Chen, C. Y., & Hafed, Z. M. (2017). Sequential hemifield gating of alpha- and beta-behavioral performance oscillations after microsaccades. *Journal of Neurophysiology, 118*(5), 2789–2805, https://doi.org/10.1152/jn.00253.2017.

Bellet, M. E., Bellet, J., Nienborg, H., Hafed, Z. M., & Berens, P. (2019). Human-level saccade detection performance using deep neural networks. *Journal of Neurophysiology, 121*(2), 646–661, https://doi.org/10.1152/jn.00601.2018.

Benedetto, A., & Morrone, M. C. (2017). Saccadic Suppression Is Embedded Within Extended Oscillatory Modulation of Sensitivity. *Journal of Neuroscience, 37*(13), 3661–3670, https://doi.org/10.1523/JNEUROSCI.2390-16.2016.

Berman, R. A., Cavanaugh, J., McAlonan, K., & Wurtz, R. H. (2017). A circuit for saccadic suppression in the primate brain. *Journal of Neurophysiology, 117*(4), 1720–1735, https://doi.org/10.1152/jn.00679.2016.

Binda, P., & Morrone, M. C. (2018). Vision During Saccadic Eye Movements. *Annu Rev Vis Sci, 4*, 193–213, https://doi.org/10.1146/annurev-vision-091517-034317.

Bogadhi, A. R., Buonocore, A., & Hafed, Z. M. (2020). Task-irrelevant visual forms facilitate covert and overt spatial selection. *Journal of Neuroscience, 40*(49), 9496–9506, https://doi.org/10.1523/JNEUROSCI.1593-20.2020.

Brainard, D. H. (1997). The Psychophysics Toolbox. *Spatial Vision, 10*(4), 433–436.

Breitmeyer, B. G. (2007). Visual masking: past accomplishments, present status, future developments. *Advances in Cognitive Psychology, 3*(1), 9–20.

Bremmer, F., Kubischik, M., Hoffmann, K. P., & Krekelberg, B. (2009). Neural dynamics of saccadic suppression. *Journal of Neuroscience, 29*(40), 12374–12383, https://doi.org/29/40/12374 [pii] 10.1523/JNEUROSCI.2908-09.2009.

Brooks, B. A., & Fuchs, A. F. (1975). Influence of stimulus parameters on visual sensitivity during saccadic eye movement. *Vision Research, 15*(12), 1389–1398, https://doi.org/10.1016/0042-6989(75)90196-0.

Brooks, B. A., Impelman, D. M., & Lum, J. T. (1980). Influence of background luminance on visual sensitivity during saccadic eye movements. *Experimental Brain Research Experimentelle Hirnforschung Experimentation Cerebrale, 40*(3), 322–329, https://doi.org/10.1007/BF00237797.

Brooks, B. A., Impelman, D. M., & Lum, J. T. (1981). Backward and forward masking associated with saccadic eye movement. *Perception and Psychophysics, 30*(1), 62–70.

Burr, D. C., Morrone, M. C., & Ross, J. (1994). Selective suppression of the magnocellular visual pathway during saccadic eye movements. *Nature, 371*(6497), 511–513, https://doi.org/10.1038/371511a0.

Castet, E., Jeanjean, S., & Masson, G. S. (2001). 'Saccadic suppression' — no need for an active extra-retinal mechanism. *Trends in Neuroscience (Tins), 24*(6), 316–318.

Castet, E., & Masson, G. S. (2000). Motion perception during saccadic eye movements. *Nature Neuroscience, 3*(2), 177–183, https://doi.org/10.1038/72124.

Chen, C. Y., & Hafed, Z. M. (2013). Postmicrosaccadic enhancement of slow eye movements. *Journal of Neuroscience, 33*(12), 5375–5386, https://doi.org/10.1523/JNEUROSCI.3703-12.2013.

Chen, C. Y., & Hafed, Z. M. (2017). A neural locus for spatial-frequency specific saccadic suppression in visual-motor neurons of the primate superior

colliculus. *Journal of Neurophysiology, 117*(4), 1657–1673, https://doi.org/10.1152/jn.00911.2016.

Chen, C. Y., Ignashchenkova, A., Thier, P., & Hafed, Z. M. (2015). Neuronal Response Gain Enhancement prior to Microsaccades. *Current Biology, 25*(16), 2065–2074, https://doi.org/10.1016/j.cub.2015.06.022.

Cornelissen, F. W., Peters, E. M., & Palmer, J. (2002). The Eyelink Toolbox: eye tracking with MATLAB and the Psychophysics Toolbox. *Behavior Research Methods, Instruments, & Computers: A Journal of the Psychonomic Society, Inc, 34*(4), 613–617, https://doi.org/10.3758/bf03195489.

DeYoe, E. A., & Van Essen, D. C. (1988). Concurrent processing streams in monkey visual cortex. *Trends in Neuroscience (Tins), 11*(5), 219–226, https://doi.org/10.1016/0166-2236(88)90130-0.

Diamond, M. R., Ross, J., & Morrone, M. C. (2000). Extraretinal control of saccadic suppression. *Journal of Neuroscience, 20*(9), 3449–3455.

Duffy, F. H., & Lombroso, C. T. (1968). Electrophysiological evidence for visual suppression prior to the onset of a voluntary saccadic eye movement. *Nature, 218*(5146), 1074–1075, https://doi.org/10.1038/2181074a0.

Gremmler, S., & Lappe, M. (2017). Saccadic suppression during voluntary versus reactive saccades. *Journal of Vision, 17*(8), 8, https://doi.org/10.1167/17.8.8.

Hafed, Z. M. (2013). Alteration of visual perception prior to microsaccades. *Neuron, 77*(4), 775–786, https://doi.org/10.1016/j.neuron.2012.12.014.

Hafed, Z. M., Chen, C.-Y., & Tian, X. (2015). Vision, perception, and attention through the lens of microsaccades: mechanisms and implications. *Front Syst Neurosci, 9*, 167, https://doi.org/10.3389/fnsys.2015.00167.

Hafed, Z. M., & Krauzlis, R. J. (2010). Microsaccadic suppression of visual bursts in the primate superior colliculus. *Journal of Neuroscience, 30*(28), 9542–9547, https://doi.org/30/28/9542 [pii] 10.1523/JNEUROSCI.1137-10.2010.

Hass, C. A., & Horwitz, G. D. (2011). Effects of microsaccades on contrast detection and V1 responses in macaques. *Journal of Vision (Charlottesville, Va.), 11*(3), 1–17, https://doi.org/10.1167/11.3.3.

Idrees, S., Baumann, M. P., Franke, F., Munch, T. A., & Hafed, Z. M. (2020). Perceptual saccadic suppression starts in the retina. *Nature communications, 11*(1), 1977, https://doi.org/10.1038/s41467-020-15890-w.

Idrees, S., Baumann, M. P., Korympidou, M. M., Schubert, T., Kling, A., & Franke, K., . . .Munch, T. A. (2020). Suppression without inhibition: A novel mechanism in the retina accounts for saccadic suppression. *bioRxiv*, https://doi.org/10.1101/2020.08.21.261198.

Jin, J., Wang, Y., Lashgari, R., Swadlow, H. A., & Alonso, J. M. (2011). Faster thalamocortical processing for dark than light visual targets. *Journal of Neuroscience, 31*(48), 17471–17479, https://doi.org/10.1523/JNEUROSCI.2456-11.2011.

Judge, S. J., Wurtz, R. H., & Richmond, B. J. (1980). Vision during saccadic eye movements. I. Visual interactions in striate cortex. *Journal of Neurophysiology, 43*(4), 1133–1155.

Kagan, I., Gur, M., & Snodderly, D. M. (2008). Saccades and drifts differentially modulate neuronal activity in V1: effects of retinal image motion, position, and extraretinal influences. *Journal of Vision (Charlottesville, Va.), 8*(14), 19 11–25, https://doi.org/10.1167/8.14.19.

Kleiner, M., Brainard, D., & Pelli, D. G. (2007). What's new in Psychtoolbox-3? (Abstract). *Perception, 36*(14), 1–16.

Komban, S. J., Kremkow, J., Jin, J., Wang, Y., Lashgari, R., Li, X., . . . Alonso, J. M. (2014). Neuronal and perceptual differences in the temporal processing of darks and lights. *Neuron, 82*(1), 224–234, https://doi.org/10.1016/j.neuron.2014.02.020.

Latour, P. L. (1962). Visual threshold during eye movements. *Vision Research, 2*(3), 261–262.

Mackay, D. M. (1970). Elevation of visual threshold by displacement of retinal image. *Nature, 225*(5227), 90–92, https://doi.org/10.1038/225090a0.

Macknik, S. L., & Livingstone, M. S. (1998). Neuronal correlates of visibility and invisibility in the primate visual system. *Nature Neuroscience, 1*(2), 144–149, https://doi.org/10.1038/393.

Maij, F., Matziridi, M., Smeets, J. B., & Brenner, E. (2012). Luminance contrast in the background makes flashes harder to detect during saccades. *Vision Research, 60*, 22–27, https://doi.org/10.1016/j.visres.2012.03.003.

Malevich, T., Buonocore, A., & Hafed, Z. M. (2020). Rapid stimulus-driven modulation of slow ocular position drifts. *Elife, 9*:e57595, https://doi.org/10.7554/eLife.57595.

Matin, E. (1974). Saccadic suppression: a review and an analysis. *Psychological Bulletin, 81*(12), 899–917.

Melcher, D. (2011). Visual stability. *Philosophical Transactions of the Royal Society of London. Series B: Biological Sciences, 366*(1564), 468–475, https://doi.org/10.1098/rstb.2010.0277.

Merigan, W. H., & Maunsell, J. H. (1993). How parallel are the primate visual pathways? *Annual*

Review of Neuroscience, 16, 369–402, https://doi.org/10.1146/annurev.ne.16.030193.002101.

Mitrani, L., Mateeff, S., & Yakimoff, N. (1971). Is Saccadic Suppression Really Saccadic. *Vision Research, 11*(10), 1157–1161, https://doi.org/10.1016/0042-6989(71)90119-2.

Mitrani, L., Radil-Weiss, T., Yakimoff, N., Mateeff, S., & Bozkov, V. (1975). Various background pattern-effect on saccadic suppression. *Activitas Nervosa Superior, 17*(3), 161–164.

Mitrani, L., Yakimoff, N., & Mateeff, S. (1973). Saccadic suppression in the presence of structured background. *Vision Research, 13*(2), 517–521.

Noda, H., & Adey, W. R. (1974). Retinal ganglion cells of the cat transfer information on saccadic eye movement and quick target motion. *Brain Research, 70*(2), 340–345, https://doi.org/10.1016/0006-8993(74)90323-0.

Pelli, D. G. (1997). The VideoToolbox software for visual psychophysics: transforming numbers into movies. *Spatial vision, 10*(4), 437–442.

Rahimi-Nasrabadi, H., Jin, J., Mazade, R., Pons, C., Najafian, S., & Alonso, J. M. (2021). Image luminance changes contrast sensitivity in visual cortex. *Cell reports, 34*(5), 108692, https://doi.org/10.1016/j.celrep.2021.108692.

Reppas, J. B., Usrey, W. M., & Reid, R. C. (2002). Saccadic eye movements modulate visual responses in the lateral geniculate nucleus. *Neuron, 35*(5), 961–974, https://doi.org/S0896627302008231 [pii].

Riggs, L. A., & Manning, K. A. (1982). Saccadic suppression under conditions of whiteout. *Investigative Ophthalmology & Visual Science, 23*(1), 138–143.

Robinson, D. L., & Wurtz, R. H. (1976). Use of an extraretinal signal by monkey superior colliculus neurons to distinguish real from self-induced stimulus movement. *Journal of Neurophysiology, 39*(4), 852–870.

Ross, J., Morrone, M. C., Goldberg, M. E., & Burr, D. C. (2001). Changes in visual perception at the time of saccades. *Trends in Neuroscience (Tins), 24*(2), 113–121, https://doi.org/S0166-2236(00)01685-4 [pii].

Scholes, C., McGraw, P. V., & Roach, N. W. (2018). Selective modulation of visual sensitivity during fixation. *Journal of Neurophysiology, 119*(6), 2059–2067, https://doi.org/10.1152/jn.00819.2017.

Schutt, H. H., Harmeling, S., Macke, J. H., & Wichmann, F. A. (2016). Painfree and accurate Bayesian estimation of psychometric functions for (potentially) overdispersed data. *Vision Research, 122*, 105–123, https://doi.org/10.1016/j.visres.2016.02.002.

Schweitzer, R., & Rolfs, M. (2020). Intra-saccadic motion streaks as cues to linking object locations across saccades. *Journal of Vision (Charlottesville, Va.), 20*(4), 17, https://doi.org/10.1167/jov.20.4.17.

Sylvester, R., Haynes, J. D., & Rees, G. (2005). Saccades differentially modulate human LGN and V1 responses in the presence and absence of visual stimulation. *Current Biology, 15*(1), 37–41, https://doi.org/10.1016/j.cub.2004.12.061.

Sylvester, R., & Rees, G. (2006). Extraretinal saccadic signals in human LGN and early retinotopic cortex. *Neuroimage, 30*(1), 214–219, https://doi.org/10.1016/j.neuroimage.2005.09.014.

Watson, A. B., & Pelli, D. G. (1983). QUEST: a Bayesian adaptive psychometric method. *Perception and Psychophysics, 33*(2), 113–120.

Wurtz, R. H. (2008). Neuronal mechanisms of visual stability. *Vision Research, 48*(20), 2070–2089, https://doi.org/S0042-6989(08)00172-7 [pii] 10.1016/j.visres.2008.03.021.

Wurtz, R. H., Joiner, W. M., & Berman, R. A. (2011). Neuronal mechanisms for visual stability: progress and problems. *Philosophical transactions of the Royal Society of London. Series B, Biological sciences, 366*(1564), 492–503, https://doi.org/10.1098/rstb.2010.0186.

Yakimoff, N., Mitrani, L., & Mateeff, S. (1974). Saccadic suppression as visual masking effect. *Agressologie, 15*(6), 387–394.

Yeh, C. I., Xing, D., & Shapley, R. M. (2009). "Black" responses dominate macaque primary visual cortex v1. *Journal of Neuroscience, 29*(38), 11753–11760, https://doi.org/10.1523/JNEUROSCI.1991-09.2009.

Zimmermann, E., & Bremmer, F. (2016). Visual Neuroscience: The Puzzle of Perceptual Stability. *Current Biology, 26*(5), R199–201, https://doi.org/10.1016/j.cub.2016.01.050.

Zuber, B. L., & Stark, L. (1966). Saccadic suppression: elevation of visual threshold associated with saccadic eye movements. *Experimental Neurology, 16*(1), 65–79, https://doi.org/0014-4886(66)90087-2 [pii].

Appendix C: Publication 3

Sensory tuning in neuronal movement commands

Baumann, M. P., Bogadhi, A. R., Denninger, A. F., & Hafed, Z. M.

Proceedings of the National Academy of Sciences, (2023) Vol. 120, No. 38, e2305759120.

doi: 10.1073/pnas.2305759120.

PNAS RESEARCH ARTICLE | NEUROSCIENCE

Sensory tuning in neuronal movement commands

Matthias P. Baumann[a,b,1], Amarender R. Bogadhi[a,b,c,1], Anna F. Denninger[a,b], and Ziad M. Hafed[a,b,2]

Edited by Stephen Lisberger, Duke University School of Medicine, Durham, NC; received April 10, 2023; accepted August 2, 2023

Movement control is critical for successful interaction with our environment. However, movement does not occur in complete isolation of sensation, and this is particularly true of eye movements. Here, we show that the neuronal eye movement commands emitted by the superior colliculus (SC), a structure classically associated with oculomotor control, encompass a robust visual sensory representation of eye movement targets. Thus, similar saccades toward different images are associated with different saccade-related "motor" bursts. Such sensory tuning in SC saccade motor commands appeared for all image manipulations that we tested, from simple visual features to real-life object images, and it was also strongest in the most motor neurons in the deeper collicular layers. Visual-feature discrimination performance in the motor commands was also stronger than in visual responses. Comparing SC motor command feature discrimination performance to that in the primary visual cortex during steady-state gaze fixation revealed that collicular motor bursts possess a reliable perisaccadic sensory representation of the peripheral saccade target's visual appearance, exactly when retinal input is expected to be most uncertain. Our results demonstrate that SC neuronal movement commands likely serve a fundamentally sensory function.

active vision | superior colliculus | saccades | perisaccadic perception | perceptual stability

Besides supporting a broad range of cognitive functions (1), the superior colliculus (SC) plays a fundamental role in oculomotor control (2, 3). It issues saccade motor commands in the form of perimovement "motor" bursts time-locked to movement onset (4–6). Such bursts specify saccade metrics (direction and amplitude) via a distributed place code of bursting neurons (7), and they are also widely believed to determine saccade kinematics, such as speed (8), via a rate code within the bursts themselves. However, practically all models of saccade control by the SC rely on observations with small light spots as the saccade targets (Fig. 1 *A* and *B*). Instead, in natural behavior, we generate eye movements toward image features, such as faces, cars, or trees.

If SC movement-related motor bursts were purely a neuronal control signal (8–11), then similar saccades to different visual images should yield similar motor bursts. We tested this by training monkeys to generate saccades toward different image patches. The patches were always placed within the movement-related response field (mRF) of a recorded neuron, thus being associated with strong motor bursts. When we modified the visual features of the image patches, we also strongly modified the SC motor bursts and for a wide range of visual image features. This modification, which also differentiated between coherent and scrambled images of real-life objects, was the outcome of a transformed representation of the peripheral saccade target visual appearance at the time of eye movement triggering. Our results document a potential neuronal mechanism for bridging the transsaccadic period of maximal sensory uncertainty caused by rapid saccade-induced retinal image shifts, and they help account for a wide range of well-known perisaccadic alterations in visual perception.

Results

Saccade Motor Bursts Are Sensory Tuned. Consider the example neuron of Fig. 1*C*. When tested classically with a spot as the saccade target, it exhibited practically no visual sensitivity at stimulus onset (Fig. 1 *C*, *Top*), but it was clearly motor related (Fig. 1 *C*, *Bottom*): It emitted a strong burst of action potentials time-locked to eye movement triggering. In Fig. 1*D*, we presented a grating inside the same neuron's mRF, and we measured saccade-related motor bursts. In one example manipulation, we randomly varied the spatial frequency of the target across trials, and in another, we altered its contrast; in a third manipulation, we varied orientation. We always ensured that within each image manipulation, the generated saccades were behaviorally matched across the different images serving as the saccade targets (Fig. 1*E*; an example from the spatial frequency manipulation is shown; *Materials and Methods*). In every case, the neuron's

Significance

The superior colliculus (SC) triggers rapid orienting gaze shifts, called saccades, via strong movement-locked "motor" bursts. We show that these bursts are strongly detached from direct motor control and are instead visual-feature tuned, changing in their properties for different eye-movement target images (despite similar movements). Such visual feature tuning of SC motor commands is not haphazard, being most prominent for coherent real-life object images as the eye movement targets, as opposed to featureless pictures, and also being strongest in the SC's most motor neurons. Our results suggest that the SC can relay, via re-entrant projections to the visual system, an internal estimate of peripheral saccade target appearance exactly when retinal image signals are most unreliable due to rapid eyeball rotations.

Author affiliations: [a]Physiology of Active Vision Laboratory, Werner Reichardt Centre for Integrative Neuroscience, Tübingen University, Tübingen 72076, Germany; [b]Hertie Institute for Clinical Brain Research, Tübingen University, Tübingen 72076, Germany; and [c]Central Nervous Systems Diseases Research, Boehringer Ingelheim Pharma GmbH & Co. KG, Biberach 88400, Germany

Author contributions: M.P.B., A.R.B., A.F.D., and Z.M.H. designed research; performed research; analyzed data; and wrote the paper.

The authors declare no competing interest.

This article is a PNAS Direct Submission.

[1]M.P.B. and A.R.B. contributed equally to this work.

[2]To whom correspondence may be addressed. Email: ziad.m.hafed@cin.uni-tuebingen.de.

This article contains supporting information online at https://www.pnas.org/lookup/suppl/doi:10.1073/pnas.2305759120/-/DCSupplemental.

Published September 11, 2023.

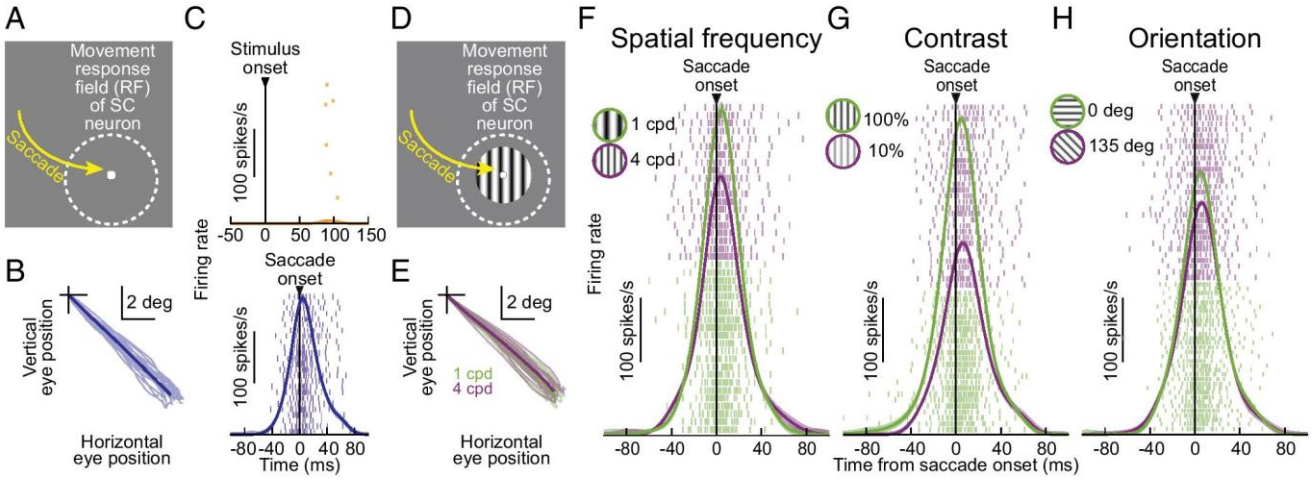

Fig. 1. Sensory tuning in SC neuronal movement commands. (*A*) A light spot was placed within the movement-related response field of a neuron. (*B*) Individual saccade vectors and their average (saturated line). (*C*) Stimulus-aligned (*Top*) and saccade-aligned (*Bottom*) firing rates from the neuron. Rasters show spike times across individual trial repetitions. The neuron exhibited practically no visual response but a strong movement-related burst. (*D*) The saccade target was now a grating. (*E*) Individual saccade vectors to a 1 cpd (green) or 4 cpd grating (purple) and their averages. The saccades were matched across different images. (*F*) Nonetheless, the motor bursts of the same neuron were different for different images. (*G* and *H*) Similar results when we manipulated target image contrast (*G*) or orientation (*H*). Error bars indicate 95% CIs, and numbers of trials are conveyed by the rows in the spike rasters.

movement-related motor bursts were different for different images (Fig. 1 *F*–*H*). This occurred even though the neuron itself was not particularly visually sensitive (Fig. 1*C*) and also despite the vector-matched saccades (Fig. 1*E*). Thus, this example neuron's motor bursts contained information about the visual appearance of the saccade target.

Similar observations held across our entire neuronal population and for all image manipulations that we tested (including contrasts, spatial frequencies, orientations, and bright-versus-dark luminance contrast polarities; also see Fig. 4 below for real-life visual object images). To summarize such sensory tuning in SC neuronal movement commands, we identified, for each neuron, the image associated with the strongest (most preferred visual feature) or weakest (least preferred visual feature) motor burst. In every image manipulation, the difference in motor bursts between the most and least preferred image features (expectedly always present by the definition of this analysis) was large, despite the matched saccades (Fig. 2*A*). In Fig. 2*B*, we also plotted raw perisaccadic neuronal firing rates in each shown image manipulation. Even though we know that SC motor bursts can be dissociated from movement kinematics (12, 13), we also confirmed that this difference in SC motor bursts was not trivially explained by equally large differences in eye movement kinematics. We did so by plotting saccade peak velocity (Fig. 2*C*) from the very same trials as in Fig. 2 *A* and *B*: The impact of the most and least preferred trial classification on the firing rates was much larger than that on movement kinematics. We also calculated a neuronal and a kinematic modulation index for each neuron and its recorded saccades; the index was zero if there were no differences between the most and least preferred trials (*Materials and Methods*). Neuronally, the modulation index was strongly skewed away from zero (Fig. 2*D*), but it straddled zero kinematically (Fig. 2*E*). Fig. 2*F* also plots the modulation indices against each other, showing that they were not correlated [P = 0.511, 0.059, 0.341, 0.064 in the spatial frequency, contrast, orientation, and luminance polarity manipulations, respectively; Pearson correlations: r(322) = −0.037, r(318) = 0.106, r(305) = 0.055, r(239) = −0.12]. Thus, sensory tuning in SC motor bursts (Figs. 1 and 2) was not explained by eye movement kinematics.

Naturally, the SC's population code (7) can also alter SC motor bursts. For example, a slightly deviated saccade vector for one image could be associated with an altered neuronal response, simply by activating a different portion of a given neuron's mRF. We minimized this by a clear marker at the center of every image (e.g., Fig. 1*D*; *Materials and Methods*), to better guide saccades. More importantly, we also performed post hoc vector matching of the saccades before analyzing the motor bursts, removing any outlier eye movement vectors (*Materials and Methods*; see Fig. 1*E*). To confirm the effectiveness of such vector matching, we tested saccade metrics in the accepted trials. For each neuron, and for the very same trials as in Fig. 2, we plotted saccade amplitude and direction errors, as well as their differences, for the most and least preferred images. The results, shown in *SI Appendix*, Fig. S1, confirm that saccade metric differences do not trivially explain the large SC motor burst differences of Figs. 1 and 2.

We also entertained the possibility that subsequent corrective saccades, sometimes called catch-up saccades, might have been different for different images. That is, we checked whether the different motor bursts that we observed for different images were associated with altered motor drives for the subsequent corrective movements. While this is unlikely, since corrective saccades are typically smaller than the primary saccades and therefore recruit different groups of SC neurons, we measured the onset time, amplitude, peak velocity, and direction of the first catch-up saccade to occur after the primary movement. We then plotted these distributions for the different feature exemplars within each of our image manipulations. Once again, there were no clear differences in catch-up saccade properties (*SI Appendix*, Fig. S2) despite the clear neuronal differences in the motor burst strengths.

It might additionally be argued that the intrinsic salience of individual image features might have introduced an internal reward signal (14, 15) associated with some saccade targets versus others. However, reward expectation affects both SC activity (16) (globally, including visual bursts, delay-period activity, and motor bursts) and the eye movement properties themselves (14), whereas we saw minimal kinematic alterations with large neuronal effects (Fig. 2 and *SI Appendix*, Fig. S1; also see refs. 12 and 13 for further evidence of dissociation between motor bursts and kinematics in other contexts). We also equalized the image conditions as much as possible, by associating all trials with the same rewards for the animal, and also by enforcing a time delay between stimulus onset

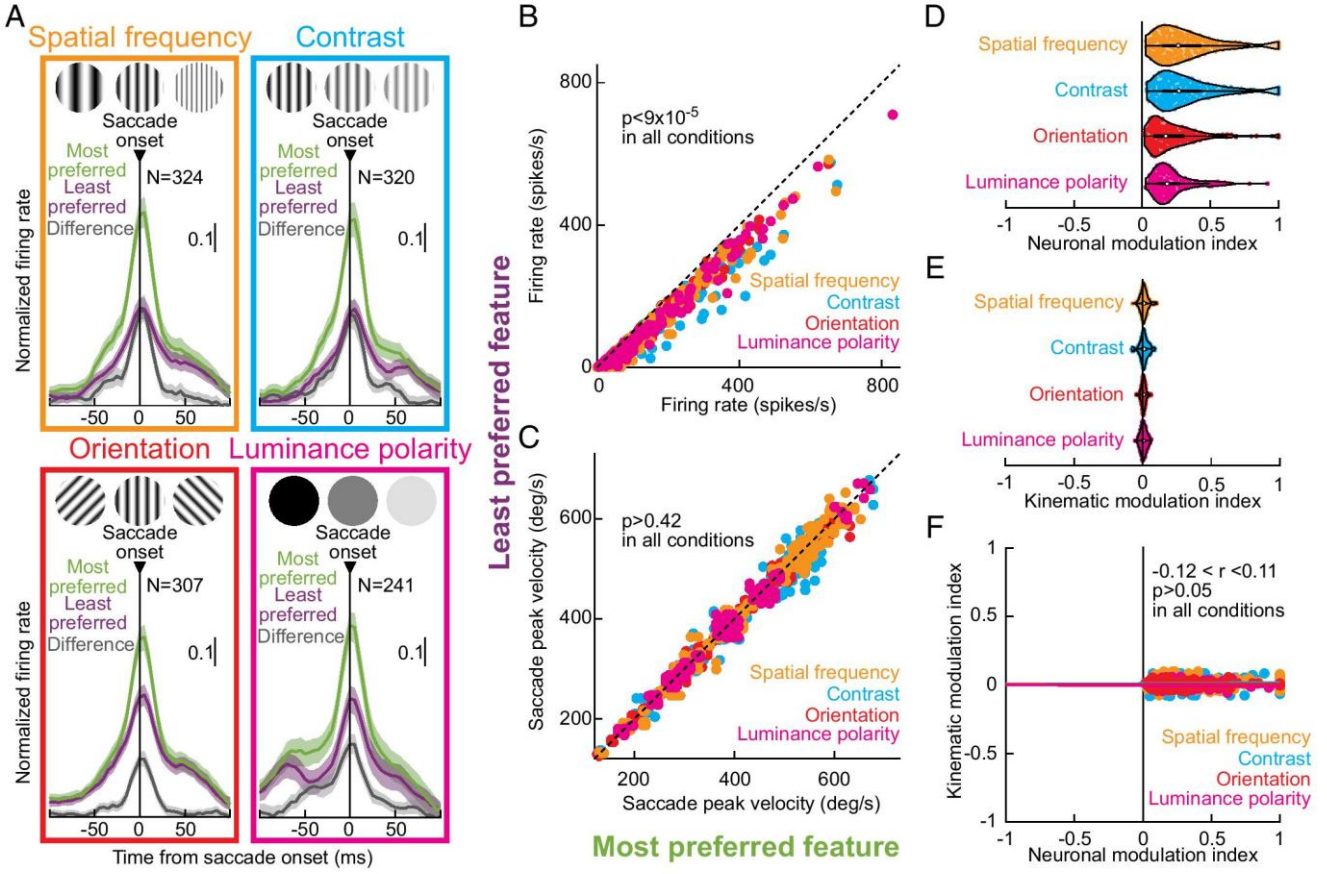

Fig. 2. Robustness of sensory tuning in SC neuronal movement commands across image manipulations. (*A*) Average normalized population firing rates for the most (green) and least (purple) preferred stimuli within each image manipulation and their differences (gray). In all cases, we observed a robust difference in SC motor bursts for different images. Note that for luminance polarity, the task was a reflexive visually guided saccade task. Thus, visual and motor bursts occurred in close temporal proximity, explaining secondary firing rate elevation at approximately −75 ms. Error bars indicate 95% CIs, and neuron numbers are indicated in each panel. (*B*) Individual neuron raw perisaccadic firing rates (−50 to 25 ms from movement onset; *Materials and Methods*) for most and least preferred targets, color-coded by each image manipulation as in *A*. (*C*) From the same trials as in *A* and *B*, saccade peak velocities were very similar for most and least preferred images, despite the large SC motor burst differences (*A* and *B*) (*P*-values indicate rank-sum test results in each image manipulation). (*D*) Violin plots of neuronal modulation indices between the most and least preferred features (*Materials and Methods*). Contrast and spatial frequency had the strongest neuronal effects. In each violin plot, the white circle indicates the median, and the thick bar indicates the interquartile range. (*E*) Kinematic modulation indices from the very same trials of each neuron. Despite the large neuronal modulations (*D*), the kinematic modulations straddled zero, consistent with *C*. (*F*) Neuronal and kinematic modulation indices were not correlated, suggesting that our results were not explained by differences in saccades for different images. *SI Appendix*, Fig. S1 also shows that other behavioral properties of saccades did not explain our neuronal results. Neuron numbers in *B*–*F* are the same as in *A*. Also see Fig. 4 showing sensory tuning in SC neuronal movement commands with real-life object images.

and the instruction to make a saccade (*Materials and Methods*). Besides ensuring a stable scene image at the time of saccade triggering, which is more similar to natural-looking behavior, this enforced delay reduced the impacts of potential differences in intrinsic image salience. For example, saccadic reaction time distributions were strongly overlapping for different spatial frequencies (*SI Appendix*, Fig. S3*A*), unlike what would happen with no enforced fixation (17, 18); similar results were also obtained in our other image manipulations (*SI Appendix*, Fig. S3 *B* and *C*), suggesting that potential intrinsic image salience did not explain the results of Figs. 1 and 2. Indeed, in one image manipulation (luminance polarity), we also explicitly skipped enforced fixation (*Materials and Methods*). Both example neurons (*SI Appendix*, Fig. S4 *A* and *B*) and the population (Fig. 2, luminance polarity data) revealed the same sensory tuning in SC neuronal movement commands even though saccadic reaction times were different across different conditions in this dataset (ref. 19 and *SI Appendix*, Fig. S4*C*). Therefore, whether stimuli were intrinsically salient (e.g., having low spatial frequency or high contrast) or not, sensory tuning in SC neuronal movement commands was still present. Our subsequent feature discrimination and population dynamic analyses, described in more detail below, will further demonstrate that different image orientations, which were of roughly equal visual salience across exemplars (when compared to our other tested feature sets), were still well differentiated in their associated SC motor bursts (e.g., see Fig. 3 *C* and *F* below and *SI Appendix*, Fig. S8 for more details).

Stronger Effect than in SC Visual Bursts. To quantitatively test discrimination performance of the most and least preferred image features from the visual or motor bursts of individual SC neurons, we used area under the ROC (receiver-operating-characteristic) curve (AUC) analyses (*Materials and Methods*), like in visual cortical presaccadic analyses (21). In Fig. 3 *A*–*C*, *Left*, we calculated the AUC at every time bin relative to stimulus onset, comparing a neuron's distribution of firing rates for most and least preferred images during steady-state gaze fixation. We defined the most and least preferred images in the visual bursts similarly to how we defined them for motor bursts: The most or least preferred image was that evoking the strongest or weakest visual response by a neuron, respectively (*Materials and Methods*; raw population firing rates are shown in *SI Appendix*, Fig. S5,

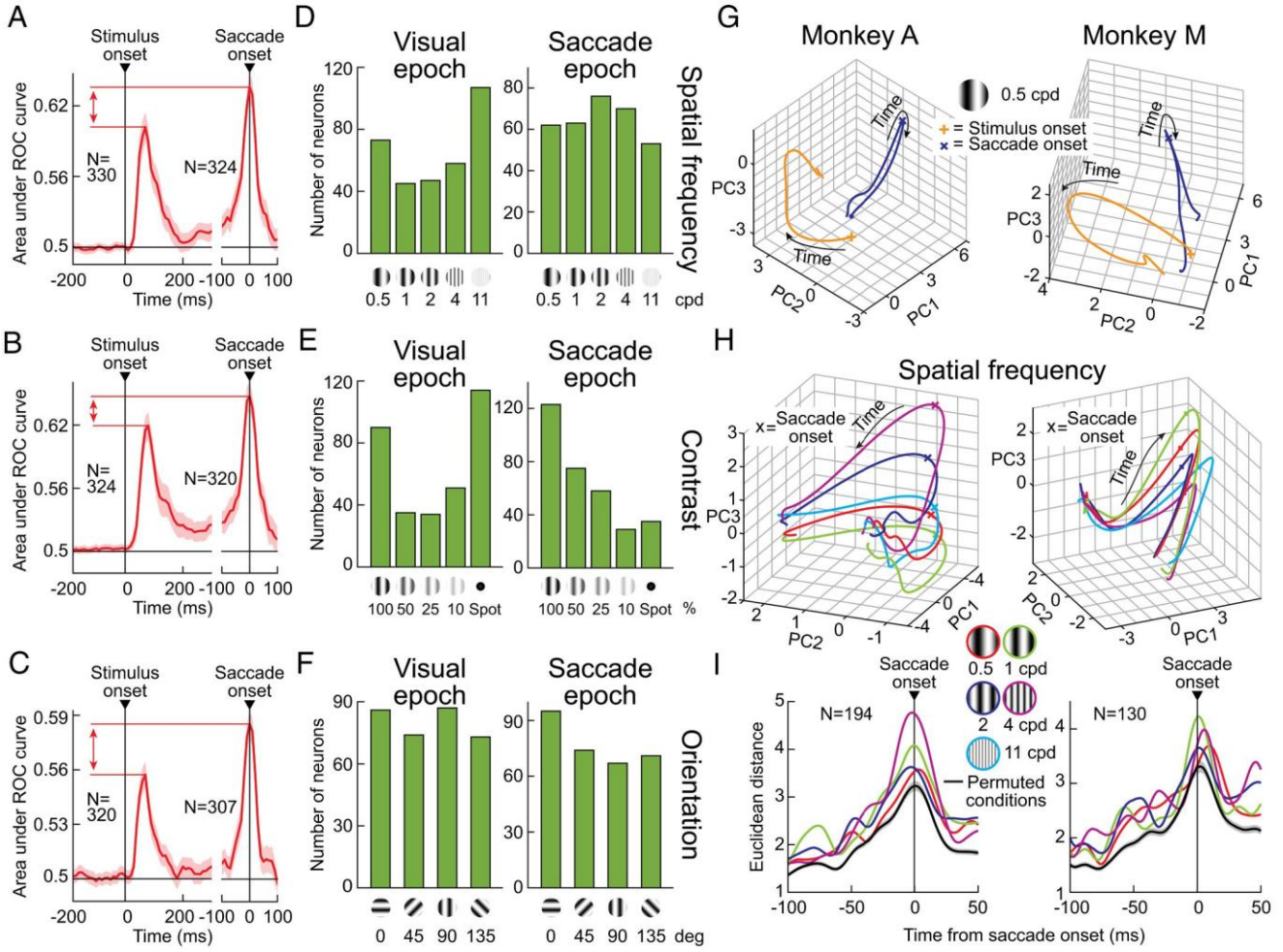

Fig. 3. Transformation of the visual sensory representation of saccade targets in the SC at the time of eye movement generation. (*A–C*) AUC discrimination performance between the most and least preferred images as a function of time from stimulus or saccade onset: (*A*) spatial frequency; (*B*) contrast; (*C*) orientation. In each case, it was possible to better discriminate between the most and least preferred images from the motor than visual bursts of individual SC neurons (vertical red arrows). Error bars indicate 95% CIs across neurons; neuron numbers are indicated in each panel. Note that for saccade burst analyses, we sometimes excluded a small number of neurons if there were not enough vector-matched movements across all image conditions of a given manipulation (*Materials and Methods*). This explains the small difference in neuron numbers between visual and motor burst epochs. (*D–F*) In each image manipulation, distribution of preferred features in the initial visual response (left column; visual epoch) or in saccade motor bursts (right column; saccade epoch). Sensory tuning in SC neuronal movement commands increased representation of visual features that were not normally preferred in visual epochs. (*G*) For an example image (0.5 cpd grating), trajectory of each monkey's entire population of neurons' firing rates after stimulus onset (orange; 0 to 200 ms) or perisaccadically (dark blue; −100 to 50 ms), after PCA dimensionality reduction (*Materials and Methods*). Perisaccadic population activity was more spatially constrained, consistent with recent evidence (20). Additionally, population activity occupied almost orthogonal manifolds in the visual and motor burst epochs, suggesting a transformed representation (*A–F*). (*H*) When we plotted the motor burst epochs (with higher zoom and a different view), but now for all the different spatial frequency images, the population trajectories were differentiated for each feature. Thus, it is possible for recipient neurons to read out information about saccade target visual appearance from SC motor bursts. (*I*) We picked a reference perisaccadic trajectory (11 cpd) in the high-dimensional population activity space of each monkey's neurons, and we then plotted Euclidean distances of population activity in each other image feature from this trajectory. For each image, Euclidean distances peaked at saccade onset (consistent with Figs. 1 and 2), and they were higher than distances obtained with randomly shuffled reference and nonreference trajectories (black ± 95% CIs). Thus, individual features were discriminable within SC motor bursts. *SI Appendix*, Figs. S8 and S9 show similar population analyses from all other image manipulations.

formatted similarly to Fig. 2). We only focused on the conditions enforcing a delay between stimulus onset and saccade generation, to avoid a temporal mixing between visual and motor bursts in reflexive saccade paradigms. In Fig. 3 *A–C*, *Right*, we performed the same analysis around saccade onset. In the visual epoch, there was an expected peak in the AUC value soon after stimulus onset; SC visual responses represent visual-scene image information (17, 22, 23). Critically, across the population, and in all image manipulations, there was also a strong perisaccadic peak in AUC discrimination performance, consistent with Figs. 1 and 2. This peak was at least as high as that in presaccadic elevations of visual cortical activity in area V4 (21). Thus, SC saccade motor bursts possess robust information about the visual appearance of the peripheral saccade target.

Intriguingly, we could better discriminate the most and least preferred images from SC motor rather than visual bursts (compare visual and motor epoch peaks in Fig. 3 *A–C*; error bars denote 95% CIs). These results likely represent a yet-to-be-appreciated underlying neuronal mechanism for well-known presaccadic enhancements of visual perception relative to steady-state gaze fixation (24–27).

It is also worth noting that a peak in perisaccadic AUC discrimination performance also clearly emerged in the reflexive saccade version of our tasks. Specifically, in this task, individual neurons preferred stimuli of different luminance polarity and contrast in their motor bursts (Fig. 2, luminance polarity data), with similar AUC discrimination performance levels as those seen in the other image manipulations (*SI Appendix*, Fig. S6*A*). We additionally

note here that this task did not have a small fixation marker in the middle of the presented images, as in the other tasks of Figs. 1–3. Yet, it still showed robust sensory tuning in the SC motor bursts (Fig. 2, luminance polarity data; *SI Appendix*, Figs. S4 and S6). Therefore, sensory tuning in SC neuronal movement commands still persisted for reflexive orienting responses.

Transformed Perisaccadic Scene Coding. Across all image manipulations shown so far, and irrespective of delayed or reflexive saccades, our results document a robust sensory signal embedded within SC motor bursts, which is not fully accounted for by saccade metric and kinematic properties, and which is at least as good as that present in initial visual sensory responses (and also in presaccadic visual cortical activity; ref. 21). We next investigated which image features individual neurons preferred.

In the visual burst epochs, we observed expected SC sensory tuning properties. For example, SC neuron visual bursts expectedly (17, 23, 28–30) preferred low spatial frequencies (Fig. 3*D*) and high contrasts (Fig. 3*E*), with the caveat being that the spot at each patch center (used to improve saccade vector matching; *Materials and Methods*) interacted with the underlying image patch, especially when the patch was least visible (e.g., having low contrast or high spatial frequency). The spot (introducing a broadband spatial frequency signal), therefore, changed the spectral and luminance content of the overall image, and this increased the numbers of neurons preferring high spatial frequencies or low contrasts in Fig. 3 *D* and *E* when compared to the literature (17, 23, 28–30). This, in itself further confirms that our neurons behaved as expected in their stimulus-evoked visual sensory responses (23).

Perisaccadically, all image features were well represented by the motor bursts (Fig. 3 *D–F*, saccade epoch). Critically, neurons often changed their preferred image features relative to the initial visual burst epoch (see example neurons in *SI Appendix*, Fig. S7). The result, across the population, was a transformed visual representation in the motor bursts, evidenced by different distributions of preferred image features across neurons (compare visual and saccade epochs in Fig. 3 *D–F*). For example, unlike in visual responses, mid-spatial frequencies became more prevalently represented in the motor bursts (Fig. 3*D*). This difference in feature preference from the visual burst epoch was statistically significant ($P = 4.8 \times 10^{-6}$; $\chi^2 = 30.0312$; χ^2 test comparing the two histograms). Similarly, for the contrast manipulation, lower contrasts (e.g., 25%) became preferred more often (Fig. 3*E*); again, the histograms of preferences across the visual and motor burst epochs were statistically significantly different from each other ($P = 3.5 \times 10^{-15}$; $\chi^2 = 73.8329$). Interestingly, in both of these cases, these results suggest that intrinsic salience on its own (e.g., low spatial frequency or high contrast) was not the sole factor determining SC motor burst strength in our experiments. This is because relatively more neurons actually preferred the "weaker" stimuli in their motor bursts than in their visual responses. For the orientation tuning task, the differences in histograms (Fig. 3*F*) were not statistically significant ($P = 0.2544$; $\chi^2 = 4.0663$), consistent with the fact that all orientations were already well represented to begin with in the visual burst epoch. Thus, overall, there was effectively a relative equalization of preferred features in the motor bursts: Images that were less likely to be preferred in visual bursts were more preferred during the motor commands.

The above transformation of visual information in the SC motor bursts is very interesting given that spatial frequency perception in humans increases its bandwidth (shifting toward higher spatial frequencies; like in Fig. 3*D*) presaccadically (27). Presaccadic contrast sensitivity is also enhanced (26, 29), consistent with the enhanced preferences for low contrasts in our SC motor bursts. In fact, in our reflexive saccade paradigm, we used a relatively smaller saccade target (as opposed to large gratings; *Materials and Methods*). Even in that case, a clear preference for high contrasts in the visual response epochs was transformed into one in which lower contrasts became better represented by the SC population at saccade triggering (*SI Appendix*, Fig. S6 *B* and *C*; also see the example neuron of *SI Appendix*, Fig. S4*B*). Therefore, the visual appearance of the saccade target is represented by SC motor bursts using a transformed code amplifying weak visual signals.

To further understand the transformation of visual target representations in SC motor bursts, we estimated the high-dimensional state-space trajectory (20) of our recorded neurons' activities either after stimulus onset or perisaccadically (*Materials and Methods*). We first created, for each time, a point in an N-dimensional space of N recorded neurons. For visualization purposes, we then performed principal components analysis (PCA) and plotted the three-dimensional trajectory of population activity using the first three principal components, which accounted for a great majority of the variance in the neuronal data (*Materials and Methods*). Prior work suggested that the population trajectory in the motor burst epoch should be relatively straight, compared to that in the visual burst epoch, suggesting a temporal alignment of the population at saccade triggering (20). We confirmed this (Fig. 3*G*). Critically, however, we uncovered two additional key properties of the SC population activity that are particularly relevant here.

First, there was an almost orthogonal relationship between population trajectory during the visual and motor burst epochs (Fig. 3*G*). Thus, areas reading out SC population activity encounter largely different state-space loci during fixation and saccades, consistent with the altered feature preferences of Fig. 3 *D–F*.

Second, when we repeated the same analyses around saccade onset, but now differentiating trials based on the different presented images, we confirmed the results of Figs. 1, 2, and 3 *A–F*: Perisaccadic population trajectory was different for different saccade target images, despite the matched vectors and kinematics across all spatial frequency conditions (Fig. 3*H*). To demonstrate that feature information was indeed present in the population during motor bursts, we then used one image feature [11 cpd (cycles per deg) in the example of Fig. 3*I*] as a reference high-dimensional population trajectory. Then, we calculated the Euclidean distance, at every time point, between each other feature condition (e.g., 4 cpd) and this reference condition. The Euclidean distance always peaked at motor burst time, and it was different for different image features (Fig. 3*I*). Moreover, all of the peak Euclidean distances were larger than those expected by random permutation of reference and condition trajectories (black line in Fig. 3*I*; *Materials and Methods*). *SI Appendix*, Fig. S8 shows how perisaccadic distances were consistently different for different images in our other image manipulations as well. Therefore, at the time of saccades, there was a graded, differentiated representation of visual image features by SC populations.

Visual Objects Are Also Well Represented. Since natural-looking behavior typically involves foveating specific objects, a strong test of the ecological relevance of sensory tuning in SC neuronal movement commands would be to check high-level visual object representations. We, therefore, studied motor bursts for luminance-equalized natural images of animate and inanimate objects, as well as feature- and spectral-scrambled versions of them (Fig. 4*A*; *Materials and Methods*). We recently found that SC visual responses are indeed sensitive to coherent visual object images (31), so we wondered whether this also held in the motor bursts.

The largest differences in SC motor burst strengths between the most and least preferred images occurred with such naturalistic

images. For example, Fig. 4*B* shows that the motor burst of an example neuron was almost completely abolished when making saccades toward a nonpreferred scrambled image. Across the population, there was a larger difference between preferred and least preferred images in this experiment than with simple feature dimensions (compare Fig. 4*B*, right to Fig. 2*A*), and AUC discrimination performance was also still higher during the motor bursts than during earlier visual bursts (Fig. 4*C*). These effects were, again, not explained by eye movement effects (Fig. 4 *D* and *E* and *SI Appendix*, Fig. S9 *A–C*).

Most interestingly, a majority of neurons had the most preferred image during saccade motor bursts as a real object image (first two columns in the histogram of Fig. 4 *F*, *Top*) and the least preferred image as a scramble (last two columns in the histogram of Fig. 4 *F*, *Bottom*). Individual SC neurons' motor bursts also contained significant information about whether a saccade target was a coherent or scrambled object image, as revealed by a significant peak in perisaccadic AUC discrimination performance in Fig. 4*G*. And, high-dimensional population trajectories in the motor burst epoch systematically differentiated between coherent and both types of scrambled object images (*SI Appendix*, Fig. S9 *D–G*).

Thus, sensory tuning in SC neuronal movement commands extended to high-level visual object representations. This suggests an ecological relevance of sensory tuning in SC neuronal movement commands in more naturalistic active vision scenarios.

Strongest Effect in Least Visual Neurons. Sensory tuning in SC neuronal movement commands was not restricted to a single functional cell type, but it was a robust property of all movement-related neurons. In fact, AUC discrimination performance was highest for the most motor neurons, occupying the deeper SC layers (5, 6) and typically having weak to nonexistent visual responses. We visualized this in each task (with dissociated visual and motor burst times) by repeating our AUC analyses of Fig. 3 *A–C*, but now after classifying how each neuron responded in either the visual or motor epoch of the task (*Materials and Methods*).

Fig. 5*A* shows example normalized population firing rates clarifying the different functional cell types in our database (*Materials and Methods*). In Fig. 5 *B–E*, we plotted AUC discrimination performance in either the visual or motor burst epochs across the different cell types. AUC discrimination performance in the motor bursts was always the highest for the most motor neurons. We first confirmed this by plotting, for each task (each row in Fig. 5 *B–E*), a horizontal dashed line marking the peak perisaccadic AUC discrimination performance in the most motor neurons (rightmost column) and extending this horizontal line leftward toward the

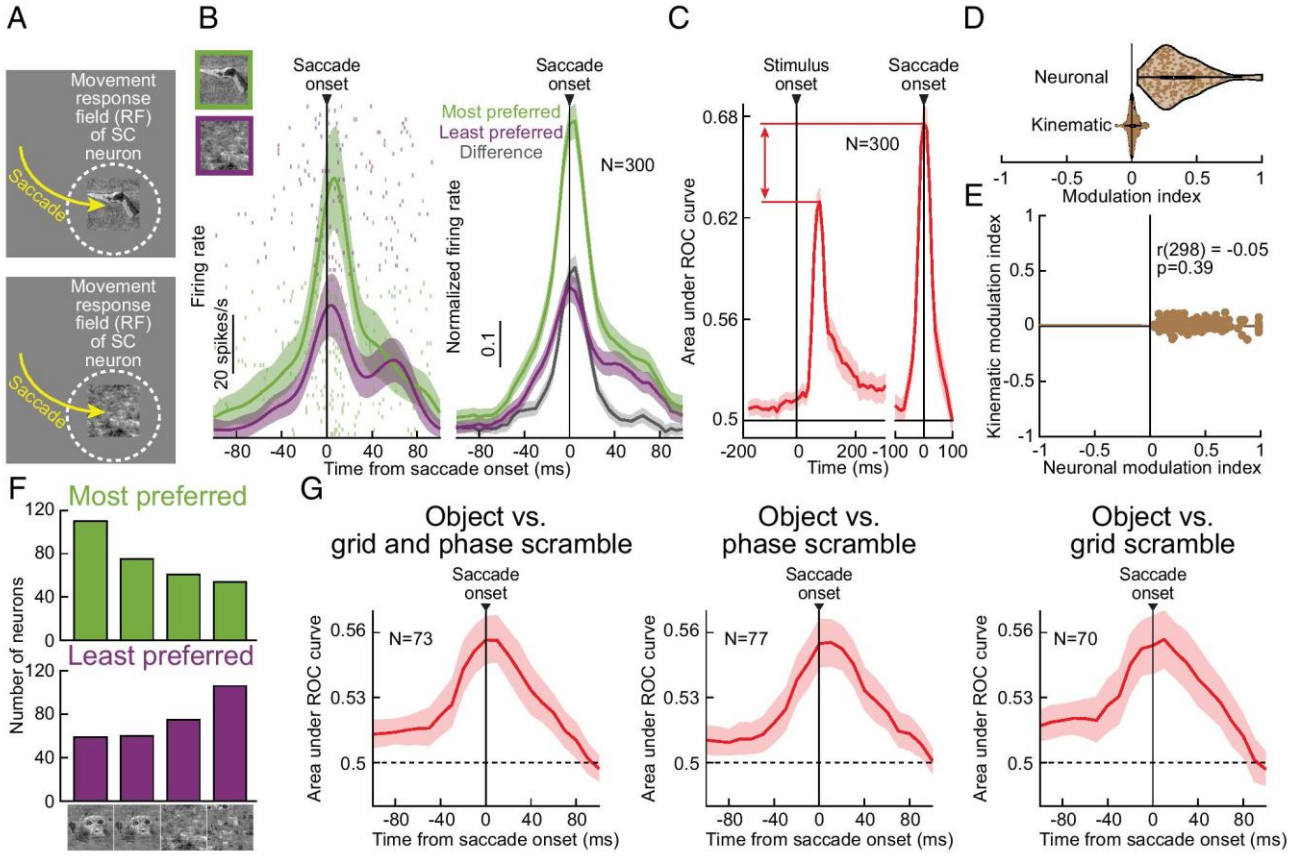

Fig. 4. Sensitivity of SC neuronal movement commands to coherent visual object images. (*A*) We tested saccades to real-life objects or their scrambles (31). (*B*) *Left*: Example neuron's saccade motor bursts for an image of a hand (green) or a phase-scrambled (31) version of it (purple); the neuron preferred the coherent image. *Right*: Across the population, most preferred images (green) had a much higher perisaccadic firing rate than least preferred images (purple), and the difference (gray) was larger than in our other image manipulations (compare to Fig. 2*A*). (*C*) Like in Fig. 3 *A–C*, AUC discrimination performance was higher in motor than visual bursts. (*D* and *E*) Moreover, there was no correlation between neuronal and kinematic modulation indices (as in Fig. 2 *D–F*). *SI Appendix*, Fig. S9 *A–C* shows additional controls for other saccade behavioral metrics. (*F*) In the SC motor bursts, the most preferred images were most likely to be coherent object images (first two columns; top histogram); the least preferred images were most likely to be scrambles (last two columns; bottom histogram). Also see *SI Appendix*, Fig. S9 *D–G* for further evidence from high-dimensional population state-space analyses. (*G*) Consistent with this, we found a substantial number of neurons with significant (*Materials and Methods*) AUC discrimination performance between real and scrambled images of different kinds in the saccade motor bursts. Thus, SC motor bursts are sensitive to real-life object images as saccade targets. Error bars: 95% CIs.

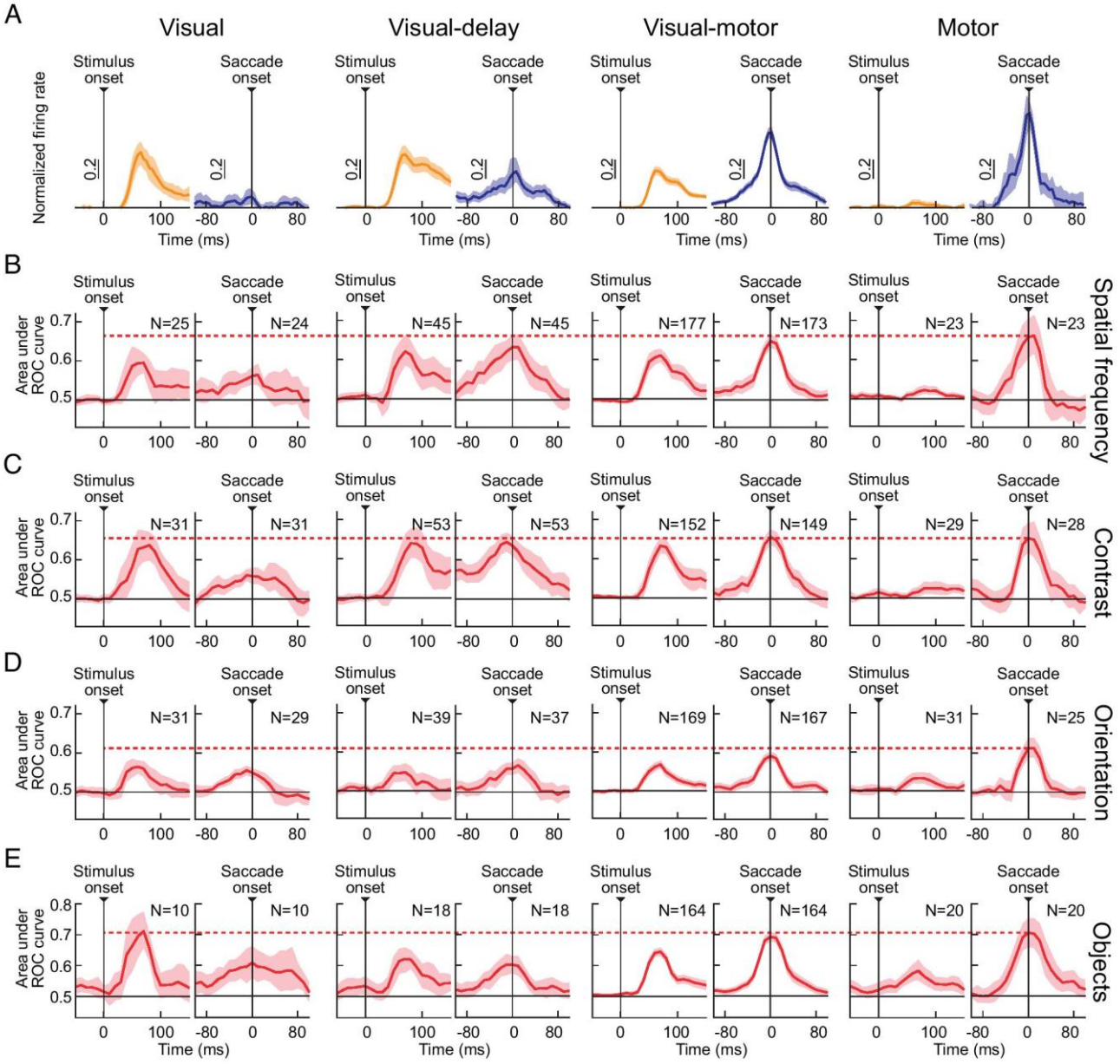

Fig. 5. Pervasiveness of sensory tuning in SC neuronal movement commands across movement-related cell types. (*A*) In each image manipulation, we classified neurons as visual (leftmost column), visual-delay (second column), visual-motor (third column), or motor (fourth column) based on their peristimulus, perisaccadic, or delay-period activity (*Materials and Methods*). The example shown is for the preferred conditions of the spatial frequency manipulation. (*B–E*) For each image manipulation, we plotted peristimulus or perisaccadic AUC discrimination performance (like in Figs. 3 and 4) but for each functionally identified cell type separately. Visual neurons had the weakest perisaccadic discrimination performance because they had weak or nonexistent motor bursts. However, for all other cell types, discrimination performance in the motor bursts was at least as good as, if not better, than discrimination performance in the visual bursts. Moreover, motor burst discrimination performance was the highest in each image manipulation for the most motor neurons (see the horizontal dashed line comparing motor neuron perisaccadic performance to the other cell types). Error bars: 95% CIs.

panels of the other functional cell types. As can be seen, no other SC functional cell type reached a higher level of motor burst AUC discrimination performance than the most motor neurons, and some functional cell types had clearly lower motor burst AUC discrimination performance.

We then measured AUC discrimination performance in the motor burst epochs by averaging across the interval ±20 ms from saccade onset (*Materials and Methods*), and we performed a Kruskal–Wallis nonparametric ANOVA across cell types. In each task, there was a significant effect of functional cell type on motor burst AUC discrimination performance ($P = 4.55 \times 10^{-5}$, 9.94×10^{-6}, 0.0025, 0.0004 for spatial frequency, contrast, orientation, and real-life objects, respectively); post hoc tests suggested that visual–motor and motor neurons consistently had higher perimovement AUC discrimination performance than visual and visual-delay neurons. We additionally note that motor neurons also showed sensory tuning in our reflexive saccade paradigm with smaller targets (see the example neuron of *SI Appendix*, Fig. S4*A*).

Local field potential (LFP) analyses further confirmed that perisaccadic LFP modulations in the deeper (more motor) SC layers were different for different images as the saccade targets, again for metrically and kinematically matched saccades (*SI Appendix*, Fig. S10 *A–D*). LFP modulations also distinguished between real objects and scrambled versions of them (*SI Appendix*, Fig. S10 *E–G*). Thus, as part of the transformation in population representation of images alluded to above (Fig. 3), an increasingly

strong sensory tuning emerged in the most motor SC layers. While we saw this at the time of the motor burst itself, it is interesting to note that other work has revealed a hidden visual sensory response (to target onset) in the most motor SC layers when normal gaze fixation was experimentally disrupted (32).

Saccades toward a Blank Also Alter SC Motor Bursts. Given all of the above, a relevant question to ask is what happens in the extreme case of no visible saccade targets at all? The classic memory-guided saccade paradigm (33, 34) involves just that: A brief cue first indicates the target location; then, after the instruction to trigger an eye movement is issued (by the removal of a fixation spot), a saccade is generated toward a blank. In 2001, Edelman and Goldberg found that some SC neurons stopped emitting motor bursts completely in this case (13). This observation was similar to the ones made earlier by Mohler and Wurtz in 1976, in which they found that some SC neurons did not emit any motor bursts for spontaneous eye movements (5). These neurons, with so-called visually dependent saccade-related (VDSR) motor bursts, were subsequently generally assumed to be a rarity in the SC. However, when investigating memory-guided microsaccades (35), we recently found that up to approximately a fifth or a quarter of microsaccade-related neurons in the rostral SC did not emit motor bursts for microsaccades toward a blank (35). So, we next asked how SC neurons behaved for memory-guided saccades in general and whether it was easy to find neurons with VDSR motor burst properties.

We analyzed a dataset of 114 SC neurons in which monkeys generated vector-matched saccades toward the RF hotspot location under two conditions: with or without a visible white spot. The dataset was the same as that reported in our recent publication on the dissociation between SC motor bursts and saccade kinematics (12), but its presentation in that article was not easy to appreciate from the perspective of the current study. Here, we plotted the neuronal modulation indices of the population as a histogram. The modulation indices were negative when the motor bursts for a blank were weaker than those for a visible spot at the same location (12) (also see the *Inset* equation in Fig. 6*A*). As can be seen from Fig. 6*A*, 76.3% of the neurons (87/114) had a weaker motor burst for saccades toward a blank. Even though the peak velocities of the saccades were also slower in this case (12), thus violating the condition of matched kinematics that we enforced in all of our other experiments above, past work in the literature has shown that the weaker motor bursts for saccades toward a blank were not fully explained by slower peak velocities (12, 13). Therefore, saccades toward a blank are associated with generally weaker SC motor bursts than vector-matched saccades toward a visible spot.

Of course, and as also described in ref. 12, some neurons (about a quarter) actually increased their discharge for saccades toward a blank. This could reflect one aspect of the transformed visual representation at the time of saccade generation that we alluded to above (e.g., Fig. 3), and it warrants further investigation in future studies.

Next, and motivated by the VDSR phenomenon, we inspected the neurons in the lowest quintile of modulation indices from Fig. 6*A*. We found that their motor bursts for saccades toward a blank were drastically reduced or even completely eliminated. Four examples of such neurons are shown in Fig. 6*B*, and an additional four example neurons from the rest of the distribution of Fig. 6*A* are shown in *SI Appendix*, Fig. S11. Thus, SC neurons can exhibit a much larger impact of the absence of a visible saccade target on their discharge than might be accounted for by the slightly slower generated movements.

Finally, we inspected yet another dataset, now from Hafed and Chen (36) and containing more than 400 neurons (again with saccades toward either a spot or a blank). We again found it easy

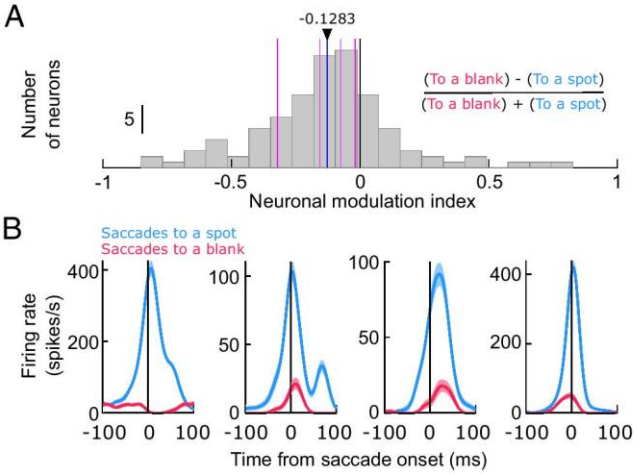

Fig. 6. Dependence of SC neuronal movement commands on the presence of a visual saccade target. (*A*) Distribution of neuronal modulation indices from the database of (12) comparing motor bursts for vector-matched saccades toward either a white spot or blank. The modulation indices were negative if motor bursts were weaker for the blank (see *Inset* equation). More than three quarters of the neurons had negative modulation indices; the thick blue line indicates the population mean (with numerical value indicated above the line). The thin magenta lines indicate the interquintile boundaries. (*B*) Perisaccadic firing rates from four example neurons from the lowest quintile of the distribution in *A* (left of the leftmost thin magenta line). In each panel, the light blue curve shows the average firing rate of a neuron when the monkey made saccades toward a single location, marked by a visible white spot. The light red curve shows the average firing rate of the very same neuron and for the very same saccade vector, but now when there was no visible target. There was a large reduction in motor bursts. See also four additional example neurons from this database in *SI Appendix*, Fig. S11, and six additional example neurons from yet another database in *SI Appendix*, Fig. S12. Error bars: SEM.

to identify neurons with VDSR characteristics, as can be seen from the six example neurons presented in *SI Appendix*, Fig. S12. Thus, an almost complete elimination of SC motor bursts with saccades toward a blank is a robust and relatively prevalent phenomenon in multiple datasets; sensory tuning in SC neuronal movement commands (Figs. 1–5) extends to the case of removing the visual stimulus altogether (Fig. 6 and *SI Appendix*, Figs. S11 and S12).

Relation to V1 Effect in Steady Fixation. Finally, why might there be sensory tuning in SC neuronal movement commands? In seminal work, Sommer and Wurtz (37) reported that SC motor bursts are relayed faithfully to the cortex. Our results imply that, besides the intended saccade vector, SC-sourced corollary discharge can provide a visual preview of the soon-to-be-foveated target, allowing the visual system to bridge a gap of sensory uncertainty caused by rapid eyeball rotation. Indeed, when we simultaneously recorded V1 activity in the same tasks of Fig. 1 (*Materials and Methods*), we found that AUC discrimination performance in SC motor bursts peaked perisaccadically to a level that was at least as good as how V1 neurons discriminated between their most and least preferred peripheral images during steady-state gaze fixation (Fig. 7; the orange SC curves show results from the SC neurons that were recorded simultaneously with the V1 neurons, with consistent results). Thus, during saccades, the SC possesses a reliable sensory representation, which may provide a transsaccadic sensory bridge for perception, exactly when coherent retinal image input is lacking due to rapid eyeball rotations.

Discussion

We observed a robust visual sensory representation embedded within SC neuronal eye movement commands (e.g., Figs. 1 and 2). This representation amplifies weak visual signals (e.g., Fig. 3 *D*–*F*),

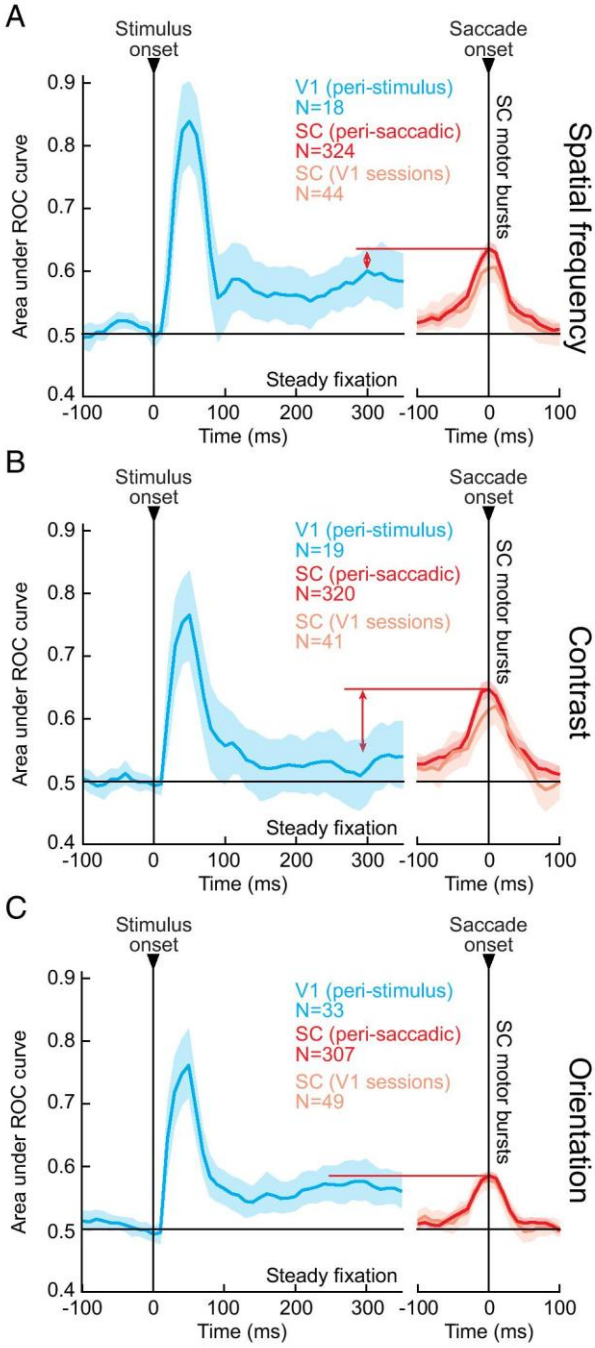

Fig. 7. SC motor bursts as a potential means for providing a transsaccadic sensory bridge of visual information across rapid eye movements. (*A*) We simultaneously recorded primary visual cortex (V1) activity with some of our SC neurons (with overlapping RF locations; *Materials and Methods*). For each V1 neuron, we calculated peristimulus AUC discrimination performance between its most and least preferred images in the visual burst epoch (light blue). After an initial peak in the stimulus-evoked visual bursts, the visual representation in peripheral V1 returned to a lower, but still feature-tuned, baseline during fixation, like in V4 (21, 38). The sensory-tuned perisaccadic SC motor burst signal that we observed (red: all neurons; orange: simultaneously recorded neurons with V1) had AUC discrimination performance (between the most and least preferred images) that peaked to a level similar to how V1 discriminated peripheral images in steady-state fixation. Thus, when the eyes rapidly move and the cortex expects uncertain retinal input, the SC still possesses a sensory representation of the peripheral saccade-target appearance (also see Fig. 3 *G–I*). (*B* and *C*) Similar results for the contrast and orientation image manipulations. In all cases, peak SC perisaccadic AUC discrimination performance was higher than or similar to steady-state AUC discrimination performance of peripheral image information in the visual cortex during fixation. Error bars: 95% CIs.

and it is strong for images of real-life objects (e.g., Fig. 4). It also occurs at a time in which a retinal transfer of visual information about the saccade target ballistically takes place from the periphery to the fovea, causing large afferent sensory uncertainty.

Given that the SC integrates a large amount of visual information from the retina and cortex (23, 39, 40), sensory tuning in its saccade movement commands is an ideal means for internally maintaining evidence about the visual appearance of saccade targets, at a time when such evidence from external afference might be unreliable. Indeed, amplification of weak visual signals during motor bursts fits with a large range of evidence that perception is enhanced at the saccade target around the time of eye movements (24–27). A presaccadic strengthening of feature-tuned neuronal representations in the visual cortex also takes place (38). Interestingly, even though SC visual responses to small spots of light are weak in the retinotopic lower visual field, SC motor bursts for downward saccades to such spots are stronger (12). Thus, amplification of weak SC visual signals might be a general property of this structure's motor bursts.

The results of Fig. 7 also suggest that sensory tuning in SC neuronal movement commands may be more relevant for the SC's ascending pathways to the cortex (41, 42) than for its descending projections to the oculomotor control network. While such ascending pathways have historically been suggested to provide only the vector information of the saccade, to spatially remap retinotopic visual representations (37, 41, 43), sensory tuning in SC motor bursts could allow the same pathways to additionally relay a sensory prediction signal of the peripheral saccade target appearance; such a peripheral preview (even though it is coarser than foveal visual analysis) could be perceptually useful, for example, in predicting the foveal visual sensory consequences of saccades (44), or in bridging transsaccadic perception (45–47). It could also presaccadically enhance perception of the saccade target (24–27) and aid in visual search (48).

If so, then classic perisaccadic perceptual phenomena, such as saccadic suppression (49) and mislocalization (50), which are thought to depend on SC-sourced corollary discharge signals (42, 43, 51, 52), should also be expected to vary with different saccade targets. In other words, if similar saccades toward different images are associated with different SC motor bursts, and if these bursts relay more than just the vector of the saccades via corollary discharge, then perisaccadic phenomena dependent on SC-sourced corollary discharge should also depend on saccade target appearance.

We recently investigated perceptual saccadic suppression with saccades made across backgrounds of low or high spatial frequency (53). Saccadic suppression was significantly stronger for the low spatial frequency condition (53). The saccade targets for the different background images were indeed different images, exactly like in our neurophysiological manipulations here. Therefore, it is indeed plausible that sensory tuning in the SC motor bursts might be linked to modulating the properties of perisaccadic suppression. Similarly, perisaccadic remapping of visual RF locations in the SC, a neurophysiological phenomenon that may be linked to perisaccadic perceptual mislocalization, was also found to strongly depend on the visual context (54).

It would be interesting in the future to further investigate the detailed dependence of perisaccadic perceptual suppression and mislocalization on the visual appearance of the saccade target. This would demonstrate that sensory tuning in SC neuronal movement commands may provide other brain areas with more than just the vector information of executed movements via SC-sourced corollary discharge signals.

We find this idea to also be particularly intriguing from the perspective of postsaccadic foveal visual processing. After every

saccade, foveal neurons, in the SC or in any other visually responsive brain area, suddenly experience a novel image that they did not experience before the eye movement. If SC motor bursts now contain information about the visual appearance of the peripheral saccade target, then this information could be transferred to foveal representations well before visual reafference has materialized. If so, then foveal neurons, in the SC or elsewhere, could receive a trans-saccadic prediction of the target appearance, which could aid in establishing perceptual stability. This idea is testable by recording foveal neuronal activity (say, in the SC) and altering peripheral images intrasaccadically in the middle of an eye movement. In this case, the foveal neurons would experience, via visual reafference, a different image than the peripheral presaccadic image that was present in the environment (but that was outside of the foveal neurons' response fields (RFs)). If these foveal neurons, in turn, had prior predictions about the presaccadic image's features (perhaps via sensory-tuned SC motor bursts), then such neurons might signal a sensory prediction error and mediate a sensation of perceptual change.

It is also intriguing to consider what the most motor neurons of the SC (in the deeper layers) represent. We found that these neurons were still influenced (in their motor bursts) by the visual appearance of the saccade target (e.g., Fig. 5 and *SI Appendix*, Fig. S10). This happened even though the neurons did not really exhibit much visual responses at stimulus onset. Interestingly, when they perturbed gaze fixation via a trigeminal blink reflex induced by airpuffs to the eye, Jagadisan and Gandhi also unmasked a strong visual response in motor neurons (32). This time, the response that they observed occurred to a visual target that appeared right after the blink perturbation, so it was a classic visual response. Thus, there really does seem to be a hidden, latent visual sensory signal even in the deeper, motor SC layers. It would be interesting in future studies to characterize further properties of this signal.

Indeed, there are a multitude of additional future tests to consider as a direct consequence of our results. For example, would there be center-surround interactions when generating a saccade toward the middle of, say, a donut-shaped stimulus with different features inside the middle of the donut hole than around it? Similarly, are there figure-ground interactions, which would give even more functional significance to our real-life object results of Fig. 4? And, what happens when memory-guided saccades are generated based on a memory of an image rather than a small spot of light? Answering all of these questions will help clarify the nature of the sensory representation that is present in the SC at the time of saccade triggering, and it can also help clarify to what extent image salience versus image features per se contribute to modifying SC motor bursts. Finally, it is important to also learn how timing matters in all of this: In other words, what happens if we suddenly remove or change an image right before saccade onset? When before the saccade would the stimulus need to change for the motor burst to be affected?

This question of timing can clarify how the SC representation gets transformed between the visual and motor burst epochs (Fig. 3 *D*–*I*), and how individual neurons alter their preferred features between these two time points. Hints regarding timing already exist in the work of Edelman and Goldberg (13). When studying saccades toward a blank, these authors changed the time at which a stimulus flash could disappear relative to saccade onset. With sufficient time between the disappearance event and the saccade (e.g., >100 to 200 ms), the visually dependent neurons stopped emitting a motor burst. However, with shorter time intervals, the same neurons emitted motor bursts as if the stimulus was still present. This leads us to hypothesize that a stimulus feature can influence SC motor bursts after enough afferent processing delay has passed for the visual signal to be present at the level of the SC (from the retina) by the time of saccade triggering.

Having said all of the above, the SC still contributes to saccade generation. The question now becomes how it does so. Even though it is often suggested that SC motor bursts are critical for saccade control (8, 10, 11), increasing evidence suggests a significantly smaller role, consistent with our observations. For example, SC motor bursts are affected by audio-visual combinations without altered saccades (55). Moreover, saccades toward a blank are often associated with opposite changes in SC bursts and movement kinematics, relative to what happens with saccades toward a visible spot (12, 13). And, on top of that, a substantial fraction of neurons outright stops bursting for saccades toward a blank (Fig. 6 and *SI Appendix*, Figs. S11 and S12) (5, 13, 35). Finally, reward expectation alters all aspects of SC responses in saccade paradigms, including both visual and motor bursts (16). Therefore, SC movement commands can be useful for other aspects of active behavior. Indeed, given that the SC is causally necessary for maintaining visual object representations in a patch of the temporal cortex (56), and given the sensitivity of SC neuronal movement commands to images of coherent visual objects (Fig. 4), it is intriguing to consider the possibility that the SC can influence the temporal cortex also at the time of saccades. This would provide an ideal active vision pathway to the processing of natural visual scenes in normal behavior.

We close with the thought that our results can potentially help resolve some long-standing mysteries about SC neuronal movement commands. For example, population activity spreads across the SC during saccades (57), but no convincing explanation for this exists. Since small spot targets are spectrally broadband stimuli, it could be that perisaccadic spreading activity for such targets is just a manifestation of different spatio-temporal response field properties for images of different spatial frequencies. This, along with investigating whether the SC can causally influence cortical visual feature updating across saccades, will undoubtedly significantly clarify long-lasting mysteries on perception, action, and the self-monitoring internal processes that necessarily link the two.

Materials and Methods

All experiments were approved by ethics committees at the regional governmental offices of Tübingen (under animal experimentation license CIN 4/19G).

We recorded SC activity from two adult, male rhesus macaque monkeys (M and A), aged 8 to 9 y and weighing 9.5 to 10 kg. We also simultaneously recorded V1 activity from monkey A.

Behavioral Tasks. Our primary task was the "Saccades-to-X" paradigm. This was a modified version of the delayed saccade paradigm, but now using an image as the saccade target. A spot was still placed at the image center to ensure similar saccade metrics and kinematics across trials.

In different blocks, we used different series of images. For Saccades-to-Spatial-Frequency, the saccade target consisted of a disc (3° radius), the inside of which was a vertical sine wave grating (100% contrast). In Saccades-to-Contrast, the grating was still vertical, but it now had a fixed spatial frequency (1 cpd). For Saccades-to-Orientation, both the spatial frequency (1 cpd) and contrast (100%) were fixed. Finally, for Saccades-to-Objects, we had images of objects as the eccentric images.

To test the generalizability of our results to immediate, visually guided saccade situations, we designed a second Saccades-to-X paradigm, but now without a forced delay. When the fixation spot was removed, an eccentric gray target appeared simultaneously. The visual feature was now luminance contrast polarity: Targets darker/brighter than the background were defined as negative/positive polarity stimuli (19, 58). Also note that in this task, we did not provide a central

marker spot on the discs, and this was because the discs were already smaller than the other images.

For V1, we ran the Saccades-to-Spatial-Frequency, Saccades-to-Contrast, and Saccades-to-Orientation tasks; the gratings were placed such that overlapping SC/V1 visual RFs were visually stimulated.

Gratings approximately filled SC visual RFs. For simultaneous SC/V1 recordings, this meant larger images than V1 RFs, since we observed that V1 visual RFs were smaller than in the SC. However, the gratings still robustly activated V1 neurons (e.g., Fig. 7).

Eye Movement Data Analysis. We detected saccades using our established methods (59, 60).

To ensure similar saccadic execution across all different image types within a given paradigm, we first ensured that saccade vectors were matched by removing outliers. To further rule out subtle systematic differences between saccades, we then analyzed the movements' metrics and kinematics across image conditions.

To analyze catch-up saccades (*SI Appendix*, Fig. S2), we collected the very first saccade to occur after the primary movement.

Neuronal Data Analysis. Our primary goal was to analyze saccade-related motor bursts. To do so, we defined a motor burst epoch as the time interval between −50 ms and 25 ms from saccade onset. For comparison, we also analyzed stimulus-evoked visual bursts. For classifying SC neurons into different functional cell types, we additionally measured baseline and delay-period activity.

For analyzing SC saccade-related motor bursts, in each task variant (e.g., Saccades-to-Contrast), we defined (for each neuron) the image associated with the strongest saccade-related motor burst as the "most preferred" image. We also defined the image associated with the weakest saccade-related motor burst as the "least preferred" image. Because different neurons had different preferred and nonpreferred images (see *Results*), this classification allowed us to obtain population-level effect sizes across neurons. To do so, we normalized each neuron's firing rate and then averaged across neurons.

We also calculated neuronal modulation indices. The neuronal modulation index was defined as the motor burst strength of the neuron for the most preferred feature minus the motor burst strength for the least preferred feature divided by the sum of the two.

We additionally performed comparisons on raw firing rates, either by plotting the raw measurements directly (e.g., Fig. 2*B*) or by using ROC analyses in a manner similar to other studies (21). Our AUC calculations were similar to those we used recently (31). For Saccades-to-Objects, we were struck by the preference of saccade-related motor bursts to real object images as opposed to scrambles (e.g., Fig. 4*F*). Therefore, we checked whether neurons had significant perimovement AUC elevations when comparing object images to scrambled images.

For LFP analyses, we obtained raw wide-band signals from each electrode contact. We then applied zero-lag filtering as described previously (36). To classify whether an LFP channel was in the more visual (superficial) or more motor (deep) SC layers, we classified each electrode channel's multiunit activity using a visual–motor index (61, 62).

For state-space analyses, we performed a pseudopopulation analysis (20, 63). For each task, the instantaneous firing rate of all neurons that we recorded from was a point in an N-dimensional space of the activity of the population of N neurons. As all neurons' firing rates changed across time (e.g., after stimulus onset or perisaccadically), the population activity representation moved in this N-dimensional space. We, thus, assumed stability across sessions of SC activity since not all neurons in our population were recorded simultaneously (20).

V1 visual response analyses were similar to SC analyses, except that our measurement interval was 30 to 150 ms after stimulus onset.

Additional methodological details are provided in *SI Appendix, SI Extended Methods*.

Data, Materials, and Software Availability. The raw SC visual and motor burst data collected for the purposes of this study are publicly available at: https://osf.io/qpj7m/ (64).

ACKNOWLEDGMENTS. We thank Tong Zhang for help in plotting some data from their study. This study was funded by the Deutsche Forschungsgemeinschaft: 1) BO5681/1-1; and 2) SFB 1233, Robust Vision: Inference Principles and Neural Mechanisms, TP 11, project number: 276693517.

1. M. A. Basso, P. J. May, Circuits for action and cognition: A view from the superior colliculus. *Annu. Rev. Vis. Sci.* **3**, 197–226 (2017), 10.1146/annurev-vision-102016-061234.
2. N. J. Gandhi, H. A. Katnani, Motor functions of the superior colliculus. *Annu. Rev. Neurosci.* **34**, 205–231 (2011).
3. D. A. Robinson, Eye movements evoked by collicular stimulation in the alert monkey. *Vision Res.* **12**, 1795–1808 (1972).
4. R. H. Wurtz, M. E. Goldberg, Activity of superior colliculus in behaving monkey. 3. Cells discharging before eye movements. *J. Neurophysiol.* **35**, 575–586 (1972).
5. C. W. Mohler, R. H. Wurtz, Organization of monkey superior colliculus: Intermediate layer cells discharging before eye movements. *J. Neurophysiol.* **39**, 722–744 (1976).
6. D. P. Munoz, R. H. Wurtz, Saccade-related activity in monkey superior colliculus. I. Characteristics of burst and buildup cells. *J. Neurophysiol.* **73**, 2313–2333 (1995).
7. C. Lee, W. H. Rohrer, D. L. Sparks, Population coding of saccadic eye movements by neurons in the superior colliculus. *Nature* **332**, 357–360 (1988).
8. I. Smalianchuk, U. K. Jagadisan, N. J. Gandhi, Instantaneous midbrain control of saccade velocity. *J. Neurosci.* **38**, 10156–10167 (2018).
9. H. H. Goossens, A. J. Van Opstal, Blink-perturbed saccades in monkey. II. Superior colliculus activity. *J. Neurophysiol.* **83**, 3430–3452 (2000).
10. H. H. Goossens, A. J. van Opstal, Optimal control of saccades by spatial-temporal activity patterns in the monkey superior colliculus. *PLoS Comput. Biol.* **8**, e1002508 (2012).
11. D. M. Waitzman, T. P. Ma, L. M. Optican, R. H. Wurtz, Superior colliculus neurons mediate the dynamic characteristics of saccades. *J. Neurophysiol.* **66**, 1716–1737 (1991).
12. T. Zhang, T. Malevich, M. P. Baumann, Z. M. Hafed, Superior colliculus saccade motor bursts do not dictate movement kinematics. *Commun. Biol.* **5**, 1222 (2022).
13. J. A. Edelman, M. E. Goldberg, Dependence of saccade-related activity in the primate superior colliculus on visual target presence. *J. Neurophysiol.* **86**, 676–691 (2001).
14. M. Xu-Wilson, D. S. Zee, R. Shadmehr, The intrinsic value of visual information affects saccade velocities. *Exp. Brain Res.* **196**, 475–481 (2009).
15. R. O. Deaner, A. V. Khera, M. L. Platt, Monkeys pay per view: Adaptive valuation of social images by rhesus macaques. *Curr. Biol.* **15**, 543–548 (2005).
16. T. Ikeda, O. Hikosaka, Positive and negative modulation of motor response in primate superior colliculus by reward expectation. *J. Neurophysiol.* **98**, 3163–3170 (2007).
17. C. Y. Chen, L. Sonnenberg, S. Weller, T. Witschel, Z. M. Hafed, Spatial frequency sensitivity in macaque midbrain. *Nat. Commun.* **9**, 2852 (2018).
18. C. J. Ludwig, I. D. Gilchrist, E. McSorley, The influence of spatial frequency and contrast on saccade latencies. *Vision Res.* **44**, 2597–2604 (2004).
19. T. Malevich, T. Zhang, M. P. Baumann, A. R. Bogadhi, Z. M. Hafed, Faster detection of "darks" than "brights" by monkey superior colliculus neurons. *J. Neurosci.* **42**, 9356–9371 (2022).
20. U. K. Jagadisan, N. J. Gandhi, Population temporal structure supplements the rate code during sensorimotor transformations. *Curr. Biol.* **32**, 1010–1025 (2022).
21. T. Moore, M. H. Chang, Presaccadic discrimination of receptive field stimuli by area V4 neurons. *Vision Res.* **49**, 1227–1232 (2009).
22. C. Y. Chen, Z. M. Hafed, Orientation and contrast tuning properties and temporal flicker fusion characteristics of primate superior colliculus neurons. *Front. Neural Circuits* **12**, 58 (2018).
23. Z. M. Hafed, K. P. Hoffmann, C. Y. Chen, A. R. Bogadhi, Visual functions of the primate superior colliculus. *Annu. Rev. Vis. Sci.*, 10.1146/annurev-vision-111022-123817 (2023).
24. H. Deubel, W. X. Schneider, Saccade target selection and object recognition: Evidence for a common attentional mechanism. *Vision Res.* **36**, 1827–1837 (1996).
25. E. Kowler, E. Anderson, B. Dosher, E. Blaser, The role of attention in the programming of saccades. *Vision Res.* **35**, 1897–1916 (1995).
26. M. Rolfs, M. Carrasco, Rapid simultaneous enhancement of visual sensitivity and perceived contrast during saccade preparation. *J. Neurosci.* **32**, 13744–13752a (2012).
27. L. M. Kroell, M. Rolfs, The peripheral sensitivity profile at the saccade target reshapes during saccade preparation. *Cortex* **139**, 12–26 (2021).
28. C. Y. Chen, A. Ignashchenkova, P. Thier, Z. M. Hafed, Neuronal response gain enhancement prior to microsaccades. *Curr. Biol.* **25**, 2065–2074 (2015).
29. X. Li, M. A. Basso, Preparing to move increases the sensitivity of superior colliculus neurons. *J. Neurosci.* **28**, 4561–4577 (2008).
30. C. Tailby, S. K. Cheong, A. N. Pietersen, S. G. Solomon, P. R. Martin, Colour and pattern selectivity of receptive fields in superior colliculus of marmoset monkeys. *J. Physiol.* **590**, 4061–4077 (2012).
31. A. R. Bogadhi, Z. M. Hafed, Express detection and discrimination of visual objects by primate superior colliculus neurons. bioRxiv [Preprint] (2022), https://doi.org/10.1101/2022.02.08.479583 (Accessed 10 February 2022).
32. U. K. Jagadisan, N. J. Gandhi, Disruption of fixation reveals latent sensorimotor processes in the superior colliculus. *J. Neurosci.* **36**, 6129–6140 (2016).
33. O. Hikosaka, R. H. Wurtz, Visual and oculomotor functions of monkey substantia nigra pars reticulata. III. Memory-contingent visual and saccade responses. *J. Neurophysiol.* **49**, 1268–1284 (1983).
34. S. Funahashi, C. J. Bruce, P. S. Goldman-Rakic, Mnemonic coding of visual space in the monkey's dorsolateral prefrontal cortex. *J. Neurophysiol.* **61**, 331–349 (1989).
35. K. F. Willeke *et al.*, Memory-guided microsaccades. *Nat. Commun.* **10**, 3710 (2019).
36. Z. M. Hafed, C. Y. Chen, Sharper, stronger, faster upper visual field representation in primate superior colliculus. *Curr. Biol.* **26**, 1647–1658 (2016).
37. M. A. Sommer, R. H. Wurtz, What the brain stem tells the frontal cortex. I. Oculomotor signals sent from superior colliculus to frontal eye field via mediodorsal thalamus. *J. Neurophysiol.* **91**, 1381–1402 (2004).
38. T. Moore, A. S. Tolias, P. H. Schiller, Visual representations during saccadic eye movements. *Proc. Natl. Acad. Sci. U.S.A.* **95**, 8981–8984 (1998).
39. V. H. Perry, A. Cowey, Retinal ganglion cells that project to the superior colliculus and pretectum in the macaque monkey. *Neuroscience* **12**, 1125–1137 (1984).

40. C. M. Cerkevich, D. C. Lyon, P. Balaram, J. H. Kaas, Distribution of cortical neurons projecting to the superior colliculus in macaque monkeys. *Eye Brain* **2014**, 121–137 (2014).
41. M. A. Sommer, R. H. Wurtz, What the brain stem tells the frontal cortex. II. Role of the SC-MD-FEF pathway in corollary discharge. *J. Neurophysiol.* **91**, 1403–1423 (2004).
42. R. A. Berman, J. Cavanaugh, K. McAlonan, R. H. Wurtz, A circuit for saccadic suppression in the primate brain. *J. Neurophysiol.* **117**, 1720–1735 (2017).
43. M. A. Sommer, R. H. Wurtz, Influence of the thalamus on spatial visual processing in frontal cortex. *Nature* **444**, 374–377 (2006).
44. L. M. Kroell, M. Rolfs, Foveal vision anticipates defining features of eye movement targets. *Elife* **11**, e78106 (2022).
45. G. W. McConkie, C. B. Currie, Visual stability across saccades while viewing complex pictures. *J. Exp. Psychol. Hum. Percept. Perform.* **22**, 563–581 (1996).
46. B. Bridgeman, A. H. van der Heijden, B. M. Velichkovsky, A theory of visual stability across saccadic eye movements. *Behav. Brain Sci.* **17**, 247–292 (1994).
47. A. Buonocore, O. Dimigen, D. Melcher, Post-saccadic face processing is modulated by pre-saccadic preview: Evidence from fixation-related potentials. *J. Neurosci.* **40**, 2305–2313 (2020).
48. A. Nuthmann, A. C. Clayden, R. B. Fisher, The effect of target salience and size in visual search within naturalistic scenes under degraded vision. *J. Vis.* **21**, 2 (2021).
49. B. L. Zuber, L. Stark, Saccadic suppression: Elevation of visual threshold associated with saccadic eye movements. *Exp. Neurol.* **16**, 65–79 (1966).
50. J. Ross, M. C. Morrone, D. C. Burr, Compression of visual space before saccades. *Nature* **386**, 598–601 (1997).
51. S. Shin, M. A. Sommer, Division of labor in frontal eye field neurons during presaccadic remapping of visual receptive fields. *J. Neurophysiol.* **108**, 2144–2159 (2012).
52. R. A. Berman, W. M. Joiner, J. Cavanaugh, R. H. Wurtz, Modulation of presaccadic activity in the frontal eye field by the superior colliculus. *J. Neurophysiol.* **101**, 2934–2942 (2009).
53. S. Idrees, M. P. Baumann, F. Franke, T. A. Munch, Z. M. Hafed, Perceptual saccadic suppression starts in the retina. *Nat. Commun.* **11**, 1977 (2020).
54. J. Churan, D. Guitton, C. C. Pack, Context dependence of receptive field remapping in superior colliculus. *J. Neurophysiol.* **106**, 1862–1874 (2011).
55. M. A. Frens, A. J. Van Opstal, Visual-auditory interactions modulate saccade-related activity in monkey superior colliculus. *Brain Res. Bull.* **46**, 211–224 (1998).
56. A. R. Bogadhi, L. N. Katz, A. Bollimunta, D. A. Leopold, R. J. Krauzlis, Midbrain activity shapes high-level visual properties in the primate temporal cortex. *Neuron* **109**, 690–699.e5 (2021).
57. D. P. Munoz, R. H. Wurtz, Saccade-related activity in monkey superior colliculus. II. Spread of activity during saccades. *J. Neurophysiol.* **73**, 2334–2348 (1995).
58. T. Malevich, A. Buonocore, Z. M. Hafed, Dependence of the stimulus-driven microsaccade rate signature in rhesus macaque monkeys on visual stimulus size and polarity. *J. Neurophysiol.* **125**, 282–295 (2021).
59. C. Y. Chen, Z. M. Hafed, Postmicrosaccadic enhancement of slow eye movements. *J. Neurosci.* **33**, 5375–5386 (2013).
60. M. E. Bellet, J. Bellet, H. Nienborg, Z. M. Hafed, P. Berens, Human-level saccade detection performance using deep neural networks. *J. Neurophysiol.* **121**, 646–661 (2019).
61. C. Massot, U. K. Jagadisan, N. J. Gandhi, Sensorimotor transformation elicits systematic patterns of activity along the dorsoventral extent of the superior colliculus in the macaque monkey. *Commun. Biol.* **2**, 287 (2019).
62. C. Bourrelly, C. Massot, N. J. Gandhi, Rapid input-output transformation between local field potential and spiking activity during sensation but not action in the superior colliculus. *J. Neurosci.* **43**, 4047–4061 (2023).
63. E. F. Kutter, J. Bostroem, C. E. Elger, F. Mormann, A. Nieder, Single neurons in the human brain encode numbers. *Neuron* **100**, 753–761.e4 (2018).
64. M. P. Baumann, A. R. Bogadhi, A. F. Denninger, Z. M. Hafed, Sensory tuning in neuronal movement commands. OSF. https://osf.io/qpj7m. Deposited 1 September 2023.

PNAS

Supporting Information for
Sensory tuning in neuronal movement commands

Matthias P. Baumann, Amarender R. Bogadhi, Anna F. Denninger, & Ziad M. Hafed

* Ziad M. Hafed
Email: ziad.m.hafed@cin.uni-tuebingen.de

This PDF file includes:

SI Extended Methods
Figures S1 to S12
SI References

SI Extended Methods

Here, we provide exhaustive details on our experimental and data analysis methods.

Laboratory setup and animal preparation

The animal laboratory setup was the same as that described in our recent work (1). Briefly, each animal was placed in a darkened room ~72 cm from a calibrated and linearized cathode-ray-tube (CRT) display (spanning approximately 30 deg horizontally and 23 deg vertically). We controlled the stimulus presentations and data acquisition procedures using a custom-built modification of PLDAPS (2), interfacing with the Psychophysics Toolbox (3-5) and an OmniPlex data acquisition system (Plexon, inc.).

We prepared the animals for behavioral training and neurophysiological experiments described earlier (1, 6, 7). Briefly, in each animal, we implanted a head holder, to stabilize head position, and a scleral search coil in one eye (8), to allow tracking eye movements with high quality using the electromagnetic induction technique (9). We also implanted a recording chamber centered on the midline and tilted 38 deg posterior of vertical. In monkey A, we positioned the chamber to allow access to the SC in the upper half of the chamber and dorsal portions of V1 in the lower half. SC and V1 recordings were performed in the left hemisphere of monkey A. Monkey M's SC recordings were performed in both hemispheres.

We recorded neuronal activity using 16- or 24-channel linear electrode arrays with 50 μm inter-electrode spacing (V-Probes from Plexon, inc.).

Behavioral tasks

Our primary behavioral task was the "Saccades-to-X" paradigm. This was a modified version of the classic delayed, visually-guided saccade task, with the main difference being that we used an image as the eccentric saccade target rather than just a small spot of light.

Each trial started with the presentation of a white fixation spot (10.8 by 10.8 min arc dimensions) presented at display center. The spot had a luminance of 79.9 cd/m^2, and it was presented over a gray background of luminance 26.11 cd/m^2. After the monkey fixated the spot stably for 300-700 ms, an image was presented at an eccentric location. The monkey was instructed to maintain fixation on the spot even after the onset of the eccentric image. After 500-1000 ms of successful gaze fixation, the central fixation spot was removed, instructing the monkey to generate a saccade towards the center of the eccentric image. To minimize saccade vector variability across trials, which was critical for ruling out metric and kinematic changes in the saccades as the main sources of our results, we always provided a clear visual marker at the center of the eccentric image, which served as an anchor for directing the saccades towards. This marker was superimposed on the eccentric image, and it consisted of a white spot, just like the fixation spot, surrounded by a gray disc (0.54 deg diameter) of the same luminance as the background. The surrounding gray disc ensured that the marker spot was visible irrespective of the background image, allowing us to experimentally control, as much as possible, trial-to-trial variability of the saccades made to the extended images. This was important because saccades can span a range of locations on an extended foveated image (10), complicating the interpretation of whether motor burst changes were due to the image or due to different saccade vectors activating different parts of movement-related response fields (mRF's). In subsequent post-hoc analyses (see below), we further controlled trial-to-trial variability of the saccades, again to rule out a trivial motor variance explanation of our results. The monkey was rewarded for successfully generating a saccade towards the image center within 500 ms from fixation spot offset, as well as for maintaining gaze

on the eccentric image center for an additional 500 ms. The reward amount was always the same regardless of what image was presented on a given trial.

In different blocks of trials, we used different series of images as the eccentric saccade targets. For example, in Saccades-to-Spatial-Frequency, the saccade target image consisted of a disc of 3 deg radius, the inside of which was a vertical, stationary sine wave grating of 100% contrast and a specific spatial frequency. The spatial frequency was randomly picked for each trial from among the following values: 0.5, 1, 2, 4, and 11 cycles/deg (cpd).

In the Saccades-to-Contrast variant of the task, the grating image was still vertical like in Saccades-to-Spatial-Frequency, but it now had a fixed spatial frequency (1 cpd). Across trials, we varied the contrast of the grating from among the following values: 100%, 50%, 25%, 10%, and 0%. Note that the 0% contrast grating had no luminance variation in it at all, but the marker spot (described above) was still visible at its center. Therefore, the 0% contrast condition looked identical to a classic delayed, visually-guided saccade task with a small spot as the saccade target. In fact, we used this condition as our “spot” condition in Results. Also note that because high spatial frequencies are also associated with reduced visibility (due to the contrast sensitivity function) as well as weakened SC visual responses (11), the 11 cpd condition from the Saccades-to-Spatial-Frequency paradigm above was also visually quite similar to a classic spot paradigm; it was thus more like a broad-band stimulus rather than a narrow-band one. This explains some of the neuron preference histograms of early stimulus-evoked visual bursts that are shown in Results (e.g. Fig. 3D, E, visual epoch).

We also ran a Saccades-to-Orientation version of the same task. In this case, both the spatial frequency (1 cpd) and contrast (100%) were fixed across trials. However, the grating could have different orientations. We tested 4 orientations across trials, with the following convention of defining orientation: horizontal was defined as 0 deg, and 45, 90, and 135 deg, respectively, were counterclockwise rotations from horizontal.

For Saccades-to-Objects, we were interested in whether our recent observation of visual object detection in the SC (1) extended to the saccade motor burst epoch. We had images of objects as the eccentric images. Each image was now in a square shape rather than a circular aperture as in the task variants above, and we actually analyzed the motor burst data from the same experiments conducted for our recent work (1). In that work, we only analyzed the visual burst data at image onset; here, we analyzed the saccade motor bursts. In each session, we had a total of seven natural images, one from each of seven object categories: human face, human hand, monkey neutral face, monkey aggressive face, snake, fruit, and artificial object. We also had another seven images with a grid of horizontal and vertical lines in front of them (as if the object was behind a wire mesh); another seven images with the phase information scrambled but the spatial frequency and luminance content unaltered; and another seven images with grid scrambling, or a random reshuffling of the grid locations from the image with the objects behind a grid of horizontal and vertical lines (1). The procedures for obtaining all 28 images were described recently (1), and we used existing toolboxes (12) to equalize the images in terms of luminance and spatial frequency content (1). Thus, in total, the monkey made saccades to one of 28 different images in this version of the paradigm. Across sessions, we generated new images that were not used in the previous sessions.

In all of the above task variants, there was a forced delay between target onset and saccade onset. However, in natural behavior, image onsets might “reflexively capture” saccades immediately, meaning that the visual and motor SC bursts occur much closer to each other in time. Therefore, to test the generalizability of our results to immediate, visually-guided saccade situations, we designed a second Saccades-to-X paradigm, but now without a forced delay. The monkey fixated a central fixation spot. After 600-1500 ms, the fixation spot was removed, and an eccentric gray target appeared simultaneously. We used a new feature dimension in this variant of the task, in order to demonstrate the robustness of the phenomenon of sensory tuning in SC neuronal movement bursts. The feature that we used this time was luminance contrast polarity:

targets darker than the background were defined as negative polarity stimuli, and targets brighter than the background were defined as positive polarity stimuli (13, 14). The targets consisted of discs of 0.51 deg radius, and they had one of three absolute Weber contrasts (10%, 50%, and 100%). Thus, in this Saccades-to-Luminance-Polarity task, we had six conditions: two luminance polarities (dark versus bright), and three Weber contrasts per polarity. Also note that in this task, we did not provide a central marker spot on the discs as in the above tasks, and this was because the discs were smaller than the other images already; we chose such smaller discs to demonstrate that the results from the above experiments were not specific to only larger images. Visual bursts from this task were analyzed in our recent study (14), but saccade-related motor bursts were not inspected.

We collected 50 repetitions per condition per session from the Saccades-to-Spatial-Frequency, Saccades-to-Contrast, Saccades-to-Orientation, and Saccades-to-Luminance-Polarity tasks, and we collected 30 repetitions per condition per session from the Saccades-to-Objects task (because of the increased number of conditions in this task). We typically collected Saccades-to-Spatial-Frequency, Saccades-to-Contrast, and Saccades-to-Orientation within the same session. However, Saccades-to-Objects required dedicated sessions due to the larger numbers of trials that were needed. The Saccades-to-Luminance-Polarity tasks were run, largely, in separate sessions as parts of other experiments, like those described in our recent work (14). Finally, for the V1 recordings, we ran the Saccades-to-Spatial-Frequency, Saccades-to-Contrast, and Saccades-to-Orientation tasks, and in simultaneous recording sessions of both the SC and V1; the gratings were placed such that overlapping visual response fields (RF's) of the recorded neurons were visually-stimulated.

In all cases, we placed the saccade target at our estimated best RF and/or mRF hotspot location of the recorded neurons, and we maintained its position throughout a block. This meant that we ran RF mapping tasks before the main paradigms. These tasks were often the classic delayed, visually-guided saccade task or a fixation variant of it, in which no saccade at the end of the trial was required (1). We sometimes also ran memory-guided saccades (with target location defined by a small spot of light). The primary reason for running these saccades was to check for a dissociation of SC motor burst properties from movement kinematics (15), which was a relevant point to make for the current study. However, we also used results from this dataset here as well for some of our analyses (e.g. Fig. 6 and Fig. S11). Our choice of grating size in the main experiments was to approximately fill classic SC visual RF's at the eccentricities that we tested. For simultaneous SC and V1 recordings, this meant that the grating was larger than V1 RF's, since we observed that V1 visual RF's were smaller than in the SC. However, the gratings still very robustly activated V1 neurons, as seen in Fig. 7 in Results.

Eye movement data analysis

We detected saccades in all trials using our established methods (16, 17).

To ensure that we were comparing neuronal activity with similar saccadic execution across all different image types within a given paradigm (e.g. Saccades-to-Contrast), we first ensured that saccade vectors were matched across the image types of the block before proceeding with any neuronal comparisons. This is because SC movement-related RF's are organized topographically (18, 19); therefore, if one image systematically elicited slightly different saccade vectors from another image, then two different parts of a given neuron's movement-related RF would be activated by the two images, rendering any differences in motor burst strengths trivially explained by a difference in the saccade vectors. As a result, we always first ensured that we were comparing motor bursts for vector-matched saccades across all image manipulations within a given task block. For example, for Saccades-to-Contrast, we collected all saccades for each image contrast. We then binned all vector endpoints of the saccades into a binning grid with 0.5 deg resolution (in each of the horizontal and vertical directions). We only included trials into any subsequent analyses if a given vector bin had saccades from all image types in the blocks (i.e. all

contrasts in the example of Saccades-to-Contrast). In our example of the Saccades-to-Contrast task, if a binning grid location had only saccade vectors from low contrast images but not high contrast images, then this would mean that the saccade vectors for low and high contrasts were slightly different from each other. These saccades were, therefore, excluded from any further analyses. Because we provided a central marker on most images to guide the saccades during the experiments, we still ended up with sufficient trial repetitions for the analyses after the vector matching procedures, as evidenced by the individual example trial rasters shown in Figs. 1, 4 and Figs. S4, S7.

To further rule out subtle systematic differences between saccades to one image type versus another as the trivial explanation of our results, after matching the vectors of the saccades per the above procedure, we proceeded to analyze the movements' metrics and kinematics across image conditions. For metrics, we calculated the direction error and the amplitude error of each saccade. Direction error was defined as the angular difference between the vector of the executed saccade and the vector of the image center relative to fixation; amplitude error was defined as the difference in radial amplitude between the vector of the executed saccade and the radial eccentricity of the image center (the saccade target). For kinematics, we calculated saccadic peak velocity. For a given saccade amplitude (as in our task design), the peak velocity should be relatively constant because of the well-known saccadic main sequence relationship (20) (the monkeys were equally rewarded across trials, so other variables that influence saccade speed, like reward, were equalized). Thus, if the peak velocity is similar for saccades to different image types and the SC motor bursts are very different, then this represents a clear dissociation between SC neuronal activity at the time of saccades from the control of saccade execution, as we and others also observed earlier (15, 21).

To analyze catch-up saccades (Fig. S2), we collected the very first saccade to occur after the primary movement had ended. Some trials did not have any catch-up saccades until the monkey was rewarded. These trials were discarded. For the rest, we calculated the onset time of the first catch-up saccade relative to the end of the primary movement. We also calculated the saccade's amplitude, peak velocity, and direction relative to the direction of the primary saccade. Within each task (e.g. Saccades-to-Contrast), we plotted the distributions of catch-up saccade properties in different colors for the different image features that were tested.

For Saccades-to-Objects, analyses of saccade metrics and kinematics (e.g. Fig. 4D, E and Fig. S9) convinced us that the eye movement properties were already well matched across conditions. Therefore, we analyzed all trials in this task, skipping post-hoc vector matching filters. This was useful because there was a larger number of conditions to run in this task, and because vector matching might have caused severe biases in which images were included or removed as opposed to others in a given analysis.

As we describe in more detail below, we typically grouped trials according to the SC motor burst strength. For example, if a neuron had the strongest motor burst for a high contrast image as the saccade target, we defined this image as the "most preferred image" for the "motor burst". Similarly, if the same neuron had the weakest motor burst for a low contrast image, then this image was the "least preferred image" for the "motor burst". With such classification, we could compare saccade metric and kinematic properties for the most and least preferred trials. Therefore, we also analyzed the saccades of such trials. We always showed full distributions of our data points, and we also included descriptive statistics (e.g. mean or median values). For kinematic comparisons between most and least preferred images, we additionally calculated a kinematic modulation index. This index was defined as the peak speed of the eye for saccades to the most preferred image minus peak speed for saccades to the least preferred image, divided by the sum of peak speeds. Thus, if the kinematic modulation index was zero, it meant that saccade peak speed was the same for trials with the most and least preferred images. For each neuron, we had a kinematic modulation index from its sessions' saccades, which we compared to a neuronal modulation index described below. Note that we often recorded multiple neurons simultaneously. However, since different neurons could have different most and least preferred

images, the saccades used for computing kinematic modulation indices (or for other plots of saccadic behavior) were not necessarily the very same saccades for multiple simultaneously recorded neurons.

Neuronal data analysis

We sorted individual neurons offline using the Kilosort Toolbox (22), followed by manual curation using the phy software. We then proceeded to analyze spike times and firing rates in the different conditions. To obtain firing rates, we convolved spike times with Gaussian kernels of s 10 ms.

Our primary goal was to analyze saccade-related "motor" bursts in the SC. To do so, we defined a motor burst epoch as the time interval between -50 ms and 25 ms from saccade onset, in which we measured average firing rates. For comparison, we also analyzed stimulus-evoked visual bursts occurring immediately after image onset. For those, we defined a visual burst epoch as the time interval between 50 ms and 150 ms after image onset during gaze fixation, and we measured average firing rate in this interval.

For classifying SC neurons into different functional cell types (e.g. visual, visual-delay, visual-motor, or motor), we also had additional measurement intervals. The baseline interval was defined as -100 to 0 ms relative to image onset at trial beginning, and the delay-period interval was 400-500 ms after image onset. Within each task variant that we analyzed (e.g. Saccades-to-Contrast), we classified each neuron as being predominantly visual (exhibiting only stimulus-evoked visual bursts), predominantly motor (exhibiting only saccade-related bursts), visual-motor, or visual-delay (exhibiting visual and saccade-prelude activity but no significant motor activity); see Fig. 5A for examples. To do so, we used the measured firing rates in the four measurement epochs described above (baseline, visual epoch, delay epoch, and motor burst epoch) and computed a non-parametric ANOVA (Kruskal-Wallis). We then determined neuronal class by post-hoc tests at the $p<0.05$ level. Very few well-isolated neurons were not classified into any of the above categories, whether due to low activity levels or other reasons causing the statistical tests to fail. In our population analyses pooling all neuron types, we also included these minority unclassified neurons because inspecting them revealed the same patterns as those of the well-categorized neurons. Also note that we classified neurons separately in each task variant because our primary goal was to ask whether sensory-tuning in SC neuronal movement commands was robust even in neurons with relatively stronger movement-related rather than visual-related activity (e.g. Fig. 5) within any given task. The question of whether SC mRF's themselves are different for different image types is orthogonal to this investigation and requires dedicated mRF mapping sessions with multiple image types (a technically-challenging endeavor due to the numbers of trials required). Moreover, there could be task-related variability in firing rates (e.g. differences in delay-period activity) across different stimulus types. Finally, our neuron classification was highly robust across the different tasks, as evidenced by the similarity of our visual-motor indices (described below) across tasks (e.g. Fig. S10A).

For analyzing SC saccade-related "motor" bursts, in each task variant (e.g. Saccades-to-Contrast), we defined (for each neuron) the image associated with the strongest saccade-related motor burst as the "most preferred" image. We also defined the image associated with the weakest saccade-related motor burst as the "least preferred" image. This was done after the vector-matching procedures described above. Because different neurons had different preferred and non-preferred images (see Results), this classification allowed us to obtain population-level effect sizes across neurons. To do so, we normalized each neuron's firing rate and then averaged across neurons. Normalization was done as follows. In each neuron, we found the peak firing rate occurring either after stimulus onset or around saccade triggering. We then used the larger of the two peaks and subtracted the neuron's baseline activity from it. This constituted our normalization constant. For any firing rate that we wanted to normalize in the neuron's data, we subtracted the neuron's baseline activity from it and then divided by the baseline-subtracted maximal response of the neuron (i.e. by our normalization constant). After obtaining the population saccade-related

motor burst strengths for the most and least preferred images, we plotted the differences between them as well (e.g. Fig. 2A, gray).

We also calculated neuronal modulation indices, similar to what we did with the kinematic modulation indices described above. For each neuron, we plotted the average firing rate curve of the neuron around saccade onset. We then measured the maximum of this curve in the interval from -50 to 25 ms relative to saccade onset, and we did this for either the most or least preferred feature. The neuronal modulation index was defined as the burst strength of the neuron for the most preferred feature minus the burst strength for the least preferred feature divided by the sum of the two. We then plotted the distributions of neuronal modulation indices across neurons in our different tasks. To compare neuronal modulation indices to kinematic modulation indices, we plotted the two indices against each other for each task, and we calculated correlation coefficients. This allowed us to assess whether a large change in burst firing rate in a given neuron (e.g. Fig. 2A) was associated with an equally large change in saccade kinematics or not.

Because we found that the most and least preferred images could be different within a single neuron between the early stimulus-evoked visual burst epoch and the saccade-related motor burst epoch (e.g. Fig. S7A, B), we also repeated the above procedure for the early “visual” epoch of the trials (immediately after image onset during fixation), but after first identifying the most and least preferred images of each neuron in this visual epoch. The normalization of firing rates was not re-done since the above normalization was applied to entire trials and not just the motor burst epochs.

To compare the distributions of preferred features in the early stimulus-evoked visual burst epoch and the saccade-related motor burst epoch (e.g. Fig. 3D-F), we performed χ^2 tests for each image manipulation. We also did this for the reflexive version of the saccade task (Saccades-to-Luminance-Polarity; Fig. S6).

We also performed comparisons on raw firing rates, either by plotting the raw measurements directly (e.g. Fig. 2B), or by using receiver-operating-characteristic (ROC) analyses in a manner similar to other studies (23). We calculated the area under the ROC curve (AUC) as a function of time in either saccade or stimulus-evoked visual epochs. For each trial of the “most preferred” image, we measured instantaneous firing rate at a given point (e.g. near saccade onset), and we did the same for the “least preferred” image. We then calculated the AUC across the distribution of trials at that time point. We repeated this procedure as a function of time, and this gave us time courses of AUC changes relative to either saccade onset or stimulus onset. This procedure allowed us to demonstrate differences in saccade-related bursts despite matched saccade vectors, and it is similar to analyses performed for pre-saccadic elevations in visual cortical neurons of area V4 (23). In some analyses, we also performed AUC analyses as a function of identified cell type. Here, we used the classification of neurons described above and performed the analysis only on neurons within a given functional cell class. We then performed a statistical test to evaluate whether the AUC value at saccade onset depended on cell type (e.g. Fig. 5). Specifically, for each peri-saccadic AUC curve in one task (e.g. Saccades-to-Contrast), we measured the average AUC value in the interval from -20 to +20 ms from saccade onset, and we did this for each classified cell type. Then, we ran a non-parametric ANOVA (Kruskal-Wallis) to assess whether cell type influenced the value of the peak peri-saccadic AUC or not. We then performed post-hoc comparisons between pairs of cell types. Our AUC calculations were similar to those we used recently (1).

For Saccades-to-Objects, we were particularly struck by the preference of saccade-related motor bursts to real object images as opposed to scrambles (e.g. Fig. 4F). Therefore, we checked whether neurons had significant peri-movement AUC elevations when comparing object images to scrambled images. Thus, we grouped all seven image categories into one. This resulted in four groups: real objects, grid-covered real objects, phase-scrambled objects, and grid-scrambled objects. We then checked for significant peri-movement AUC values when comparing real objects to either phase or grid-scrambled categories (or both). We assessed significance, similarly to how

we did it recently for SC visual responses to objects (1). Specifically, we calculated bootstrapped confidence intervals for AUC measures; neurons that had AUC values significantly different from 0.5 at the $p<0.05$ anywhere from times -100 to 100 ms relative to saccade onset were deemed to be significant.

For local field potential (LFP) analyses, we obtained raw wide-band signals from each electrode contact. We then applied zero-lag filtering procedures as described previously (24). Briefly, we used notch filtering to remove the line noise frequency (50 Hz) and its next two harmonics (100 and 150 Hz), and we also kept signals <300 Hz as the LFP band. To classify whether the channel from which we collected LFP's was from the more visual (superficial) or more motor (deep) SC layers, we classified each electrode channel's multi-unit activity (MUA) as being predominantly visual or predominantly motor using a visual-motor index (VMI) (25, 26). Specifically, for each channel, we filtered the wide-band signal using a fourth-order Butterworth band-pass filter (750 to 5000 Hz), and we then rectified the signal before passing it through a second low-pass filter (fourth-order Butterworth) with 500 Hz frequency cutoff. For each condition, we plotted stimulus- and saccade-aligned MUA responses after subtracting the baseline MUA level (defined as the average MUA in the final 200 ms before image onset); superficial channels had stronger visual than motor responses, whereas deeper channels had stronger motor than visual response (25, 26). To quantify this, we measured a motor MUA value and a visual MUA value. These were defined as the average baseline-subtracted MUA in the interval -25 to 25 ms from saccade onset (for the motor MUA measurement) or 30 to 200 ms after image onset (for the visual MUA measurement). The VMI was defined as the motor MUA measurement minus the visual MUA measurement divided by the sum of the two. VMI's larger than zero were more motor than visual (e.g. Fig. S10A).

For state-space analyses, we performed a pseudo-population analysis (27, 28). For each task, the instantaneous firing rate of all neurons that we recorded from was a point in an N-dimensional space of the activity of the population of N neurons. As all neurons' firing rates changed across time (e.g. after stimulus onset or peri-saccadically), the population activity representation moved in this N-dimensional space. We, thus, assumed stability across sessions of SC activity since not all neurons in our population were recorded simultaneously (27). Since population activity likely occupied a much lower dimension than the number of neurons, we performed principal components analysis (PCA) and plotted the population trajectory within the first 3 PCA dimensions. These typically accounted for the majority of the variance of population firing rates (e.g. 70-89%). We used such state-space analysis to first compare visual and motor burst population trajectories and then to check for tuning in the motor bursts. In both cases, we normalized each neuron's firing rate before performing PCA, using the same normalization procedure described above.

To compare visual and motor burst population trajectories in PCA space, we concatenated each neuron's activity in a visual interval (from 0 to 200 ms relative to stimulus onset) with activity in a saccade epoch (from -100 to 50 ms relative to saccade onset). Then, we projected the population activity on 3-dimensional PCA space. This allowed us to assess whether visual and motor SC activity occupied similar or different subspaces (e.g. Fig. 3G).

To check for sensory tuning in the motor bursts themselves, we focused on the peri-saccadic interval only, and we projected SC population activity in this interval, using PCA, for different images as the saccade targets. If there was sensory tuning in the SC population motor bursts, then the population peri-saccadic state-space trajectories should differ as a function of which image was the saccade target (despite the vector- and kinematically-matched saccades) (e.g. Fig. 3H). To quantitatively confirm such difference, we then picked a reference peri-saccadic trajectory from one of the image features of the experiment (e.g. spot in the Saccades-to-Contrast experiment), and we calculated the Euclidean distance of each other image feature's population activity trajectory from this reference trajectory. We did this for times around saccade onset. Moreover, we calculated Euclidean distances from the entire high-dimensional population space, and not just from the 3-dimensional PCA sub-projection of only 3 principal components. For

checking Euclidean distances against a null distance distribution, we performed 1000 permutations in which we randomly picked a reference and a condition trajectory, and we then calculated the Euclidean distance between the two.

Analyses of V1 visual responses were similar to those of SC visual responses, except that our measurement interval was 30 to 150 ms after stimulus onset, since we observed that V1 neurons had slightly earlier visual response latencies than SC neurons.

Finally, in our analysis of memory-guided saccades from past experiments (15), we replotted the same neuronal modulation indices calculated earlier (15) but now as a histogram distribution (Fig. 6A). The modulation indices involved measuring the motor burst for vector-matched saccades towards either a spot or a blank. They were calculated as indicated in the equation in Fig. 6A (15).

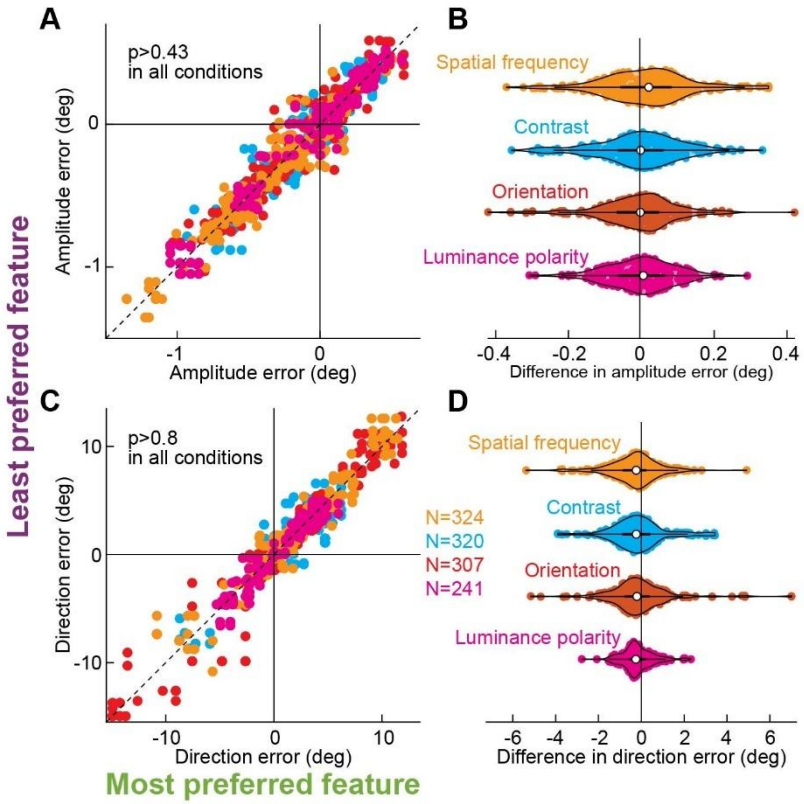

Fig. S1. Independence of sensory tuning in SC neuronal movement commands from eye movement metric properties. (A) For each image manipulation of Fig. 2 (different colors), and for each neuron (individual symbols), we plotted the amplitude error of the saccades to the most and least preferred images of the neuron (based on its motor burst strengths). Despite the large differences in saccade motor bursts (Fig. 2), the amplitude errors were similar across images. This confirms our vector matching procedures (Materials and Methods). P-values indicate rank-sum test results from each image manipulation. **(B)** Distributions of amplitude error differences between most and least preferred image trials from **A**. The violin plots always straddled zero. **(C, D)** Similar observations with saccade direction errors. The numbers of neurons indicated apply to **A**, **B** as well.

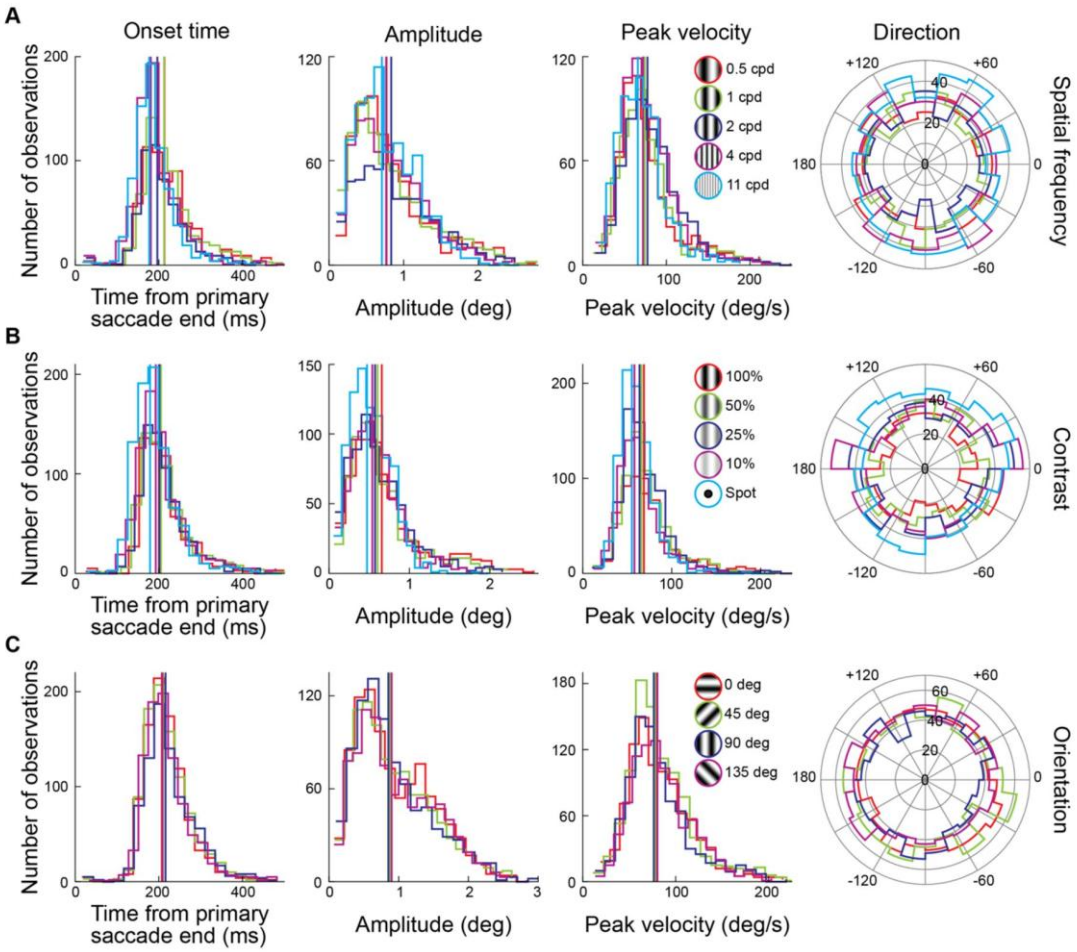

Fig. S2. Independence of sensory tuning in SC neuronal movement commands from the properties of catch-up saccades after the primary movements. (A) For the spatial frequency image manipulation, the leftmost panel shows the distribution of catch-up saccade onset times after the end of the primary saccade. Each color shows a specific image feature towards which the primary saccade was directed. The vertical lines indicate the means of the individual distributions. The second plot shows similar distributions but for catch-up saccade amplitude, and the third plot does it for catch-up saccade peak velocity. The final polar plot shows the distribution of catch-up saccade directions relative to the direction of the primary saccade (that is, a direction of zero in the plot would indicate that the catch-up saccade was in the same direction as the primary saccade). In all panels, the distributions of catch-up saccades were very similar to each other for the different image features, despite the differences in SC motor burst strengths that we observed (Figs. 1, 2). **(B)** Similar observations for the contrast image manipulation. **(C)** Similar observations for the orientation image manipulation. Note that our other tasks (Materials and Methods) also had similar properties of catch-up saccades.

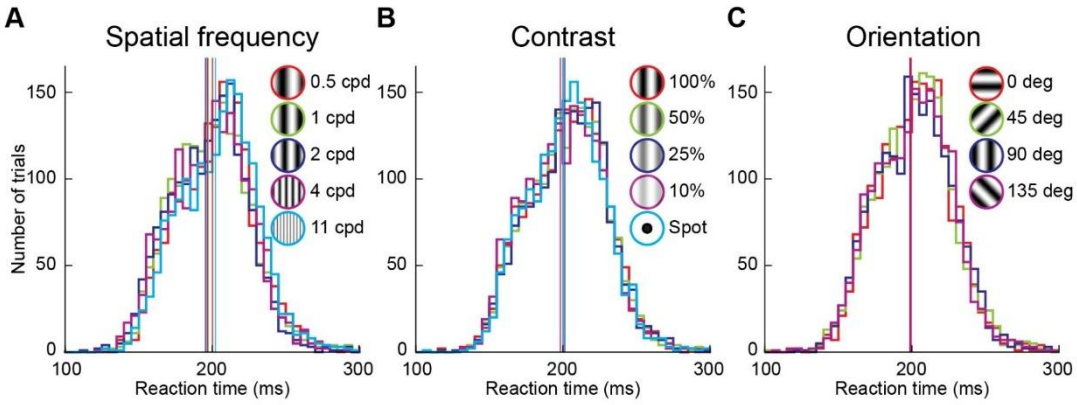

Fig. S3. Independence of sensory tuning in SC neuronal movement commands from intrinsic image salience, as inferred from saccadic reaction times. (A-C) In each of the spatial frequency, contrast, and orientation image manipulations, we used a delayed-saccade paradigm to enforce a period of steady-state gaze fixation between image onset and saccade triggering. This allowed us, as much as possible, to equalize saccadic reaction times across image features within each image manipulation, as can be confirmed from the strongly overlapping saccadic reaction time histograms in each panel. Thus, even though some image features, like low spatial frequencies (11), might be more intrinsically salient than others we equalized this as much as possible by our delayed-saccade paradigm. Note also that in our luminance polarity image manipulation, we used reflexive saccades instead, and the results were unchanged despite strong differences in saccadic reaction times with different image features (see Fig. S4). Vertical lines indicate mean reaction times for each image feature.

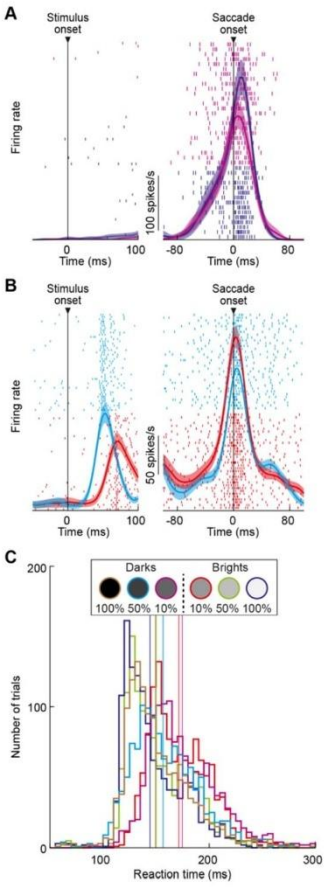

Fig. S4. Independence of sensory tuning in SC neuronal movement commands from reflexive versus delayed saccades. (A) An example neuron's firing rates from our luminance polarity image manipulation. In this image manipulation, we avoided delayed saccades, and the monkeys reflexively looked at the peripheral stimulus as soon as it appeared. This example neuron had almost non-existent visual responses to stimulus onset, but it had strong motor bursts. For two different image features, the motor bursts were very different, similar to the example neuron of Fig. 1. Error bars: 95% confidence intervals, and the numbers of trials are indicated by the number of spike raster rows shown. Other conventions are similar to Fig. 1, and the colors indicate the individual image features, as per the legend in **C**. **(B)** A second example neuron possessing both visual and motor bursts. Note how the visual burst had strongly different latencies from stimulus onset in the two shown conditions, which was also reflected in different saccadic reaction times (**C**). Nonetheless, the motor bursts were still sensory-tuned like in the delayed-saccade paradigm of Fig. 1. Also note how the neuron flipped its image feature preference between visual and motor burst epochs, showing weaker visual bursts but stronger motor bursts for the same image. This is consistent with a transformed SC representation of images at the time of saccade triggering (also see Fig. 3 and Figs. S6-S8). Error bars: 95% confidence intervals, and trial numbers can be inferred from the shown spike rasters. **(C)** With the reflexive saccade paradigm used in this image manipulation, saccadic reaction times strongly depended on image contrast, and there were modulatory effects of luminance polarity (14). Thus, whether saccadic reaction times were equalized (Fig. S3) or not (this figure), sensory tuning in SC neuronal movement commands was still robustly observed. Vertical lines indicate mean saccadic reaction times for each image feature.

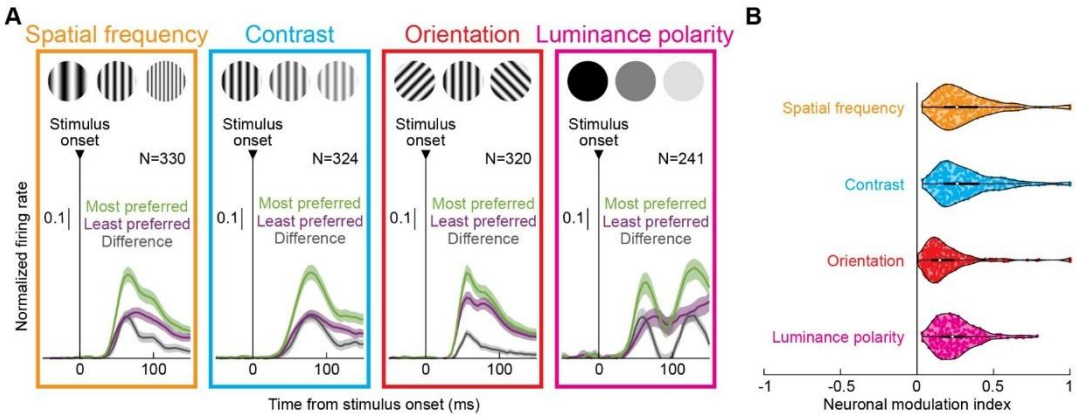

Fig. S5. Sensory tuning in SC visual responses. (A) Analyses like those in Fig. 2A, but for the visual responses of the neurons rather than their activity at the time of saccade triggering. The differences in firing rates between most and least preferred images in the visual bursts were smaller than in the saccade bursts of Fig. 2A, consistent with the AUC discrimination performance results documented in Fig. 3A-C. **(B)** Neuronal modulation indices from the visual burst epoch; these were calculated similarly to the modulation indices in the motor bursts, but based on visual burst measurements and feature preferences (Materials and Methods). All conventions are similar to Fig. 2. Also note that the luminance polarity image manipulation was from the reflexive saccade paradigm. Therefore, there were secondary elevations in firing rates after the initial visual responses in **A**, reflecting the saccade motor bursts. Error bars: 95% confidence intervals, and neuron numbers are indicated in **A**.

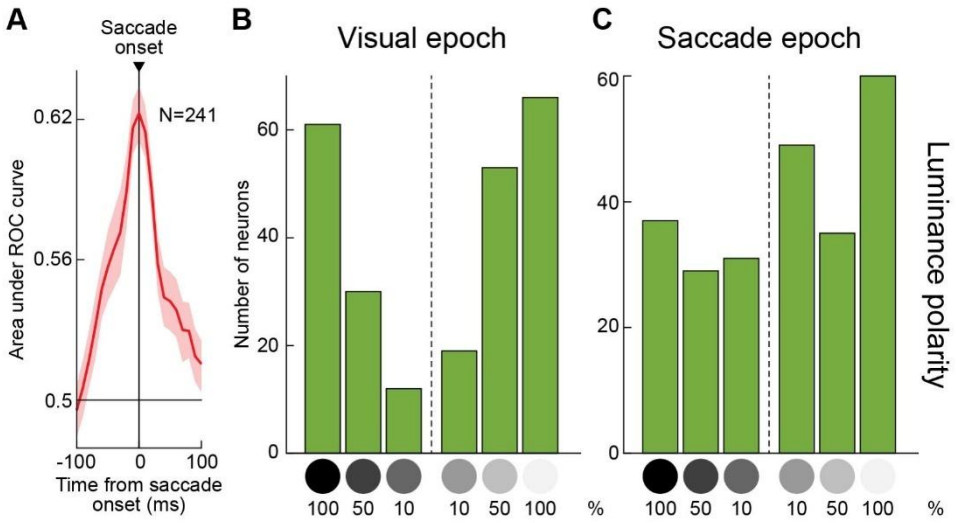

Fig. S6. Similar observations to Fig. 3A-F during the reflexive saccade paradigm. (A) From the luminance polarity image manipulation, we plotted peri-saccadic AUC discrimination performance across neurons. Consistent with Fig. 3 and the example neurons of Fig. S4, there was a peak in AUC discrimination performance at the time of SC motor bursts. **(B, C)** Also consistent with Fig. 3, the distribution of preferred image features at saccade onset (**C**) was broader than that at stimulus onset (**B**), suggesting amplification of weak visual signals at the time of saccade generation even with reflexive, visually-guided saccades. This difference in distributions was statistically significant ($p=7.4 \times 10^{-6}$; $\chi^2=31.4927$; χ^2 test). Figure S4B shows an example neuron with such amplification at the time of saccades. Also see Fig. S8 for high-dimensional population activity trajectories in the reflexive saccade paradigm.

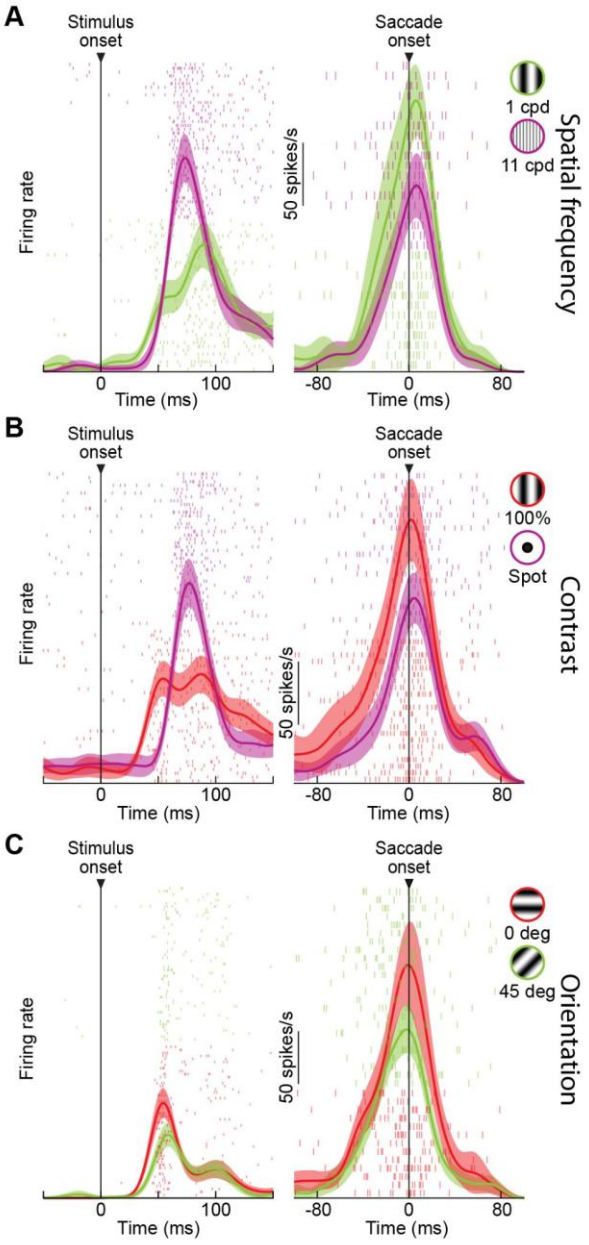

Fig. S7. Potential transformation of image preferences between stimulus and saccade onsets in individual SC neurons. (A-C) Three example neurons from our three image feature manipulations with the delayed saccade paradigm, demonstrating how a changed feature preference can occur between visual and motor epochs with simple grating stimuli. Note how the weak signals in the visual epochs in **A**, **B** were transformed into stronger motor bursts at the time of saccade triggering. Also note that this is similar to the example neuron of Fig. S4B in the immediate, reflexive saccade paradigm. The neuron in **C**, on the other hand, did not exhibit an altered preference between its visual and motor epochs. Error bars: 95% confidence intervals, and trial numbers can be inferred from the shown spike rasters.

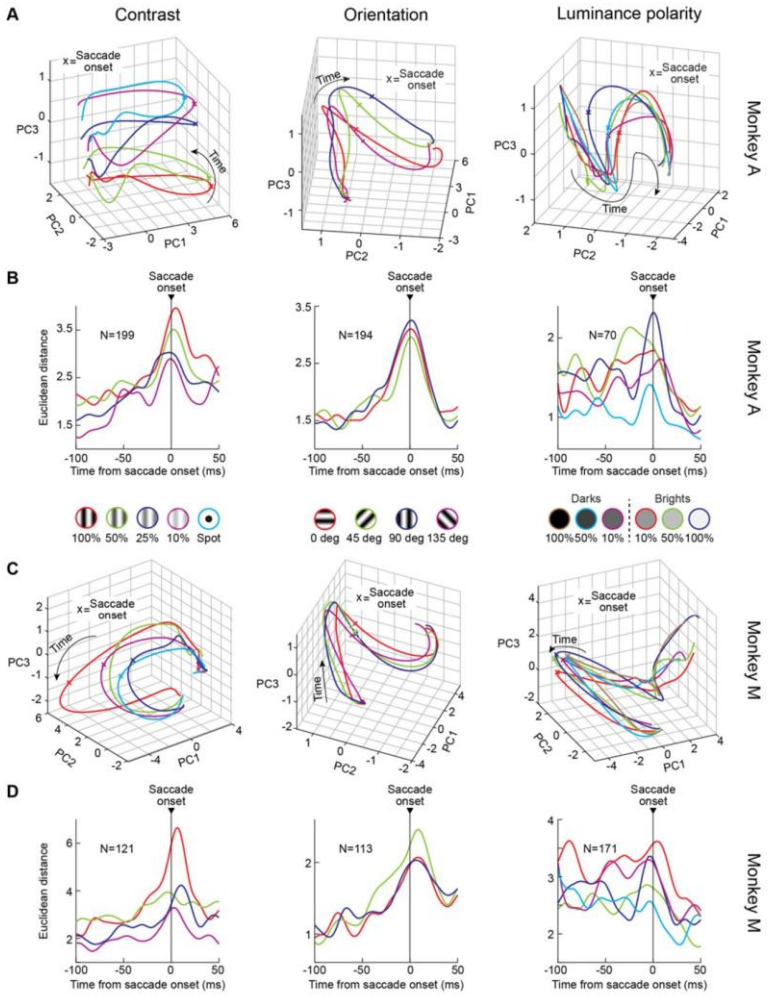

Fig. S8. Embedding of image feature information in SC population activity at the time of saccades. (A) Monkey A population activity trajectories in the first 3 principal components after PCA decomposition in the contrast, orientation, and luminance polarity image manipulations (spatial frequency was shown in Fig. 3H). Consistent with Fig. 3H, SC neurons occupied different manifolds in population activity space at the time of saccade triggering for different image features. Note that in luminance polarity, the saccades were reflexive. Thus, visual and motor bursts occurred in close temporal proximity to each other. Nonetheless, their transformation into quasi-orthogonal manifolds between the visual and motor epochs was still visible, consistent with Fig. 3G. **(B)** For each image manipulation, we picked a reference condition (spot for contrast, 135 deg for orientation, and 100% dark for luminance polarity), and we then plotted the peri-saccadic Euclidean distance of high-dimensional SC population activity from this condition at the time of saccade generation. In each case, the Euclidean distances were different for different image features, suggesting the embedding of sensory information at the time of SC motor bursts (despite vector and kinematic saccade matching). Note that for luminance polarity, the sustained elevation of Euclidean distances before saccade onset reflects the visual epochs of this reflexive saccade task, which were also sensory-tuned. **(C, D)** Similar results from monkey M. Also see Fig. S9D-G for consistent results of sensory tuning in SC neuronal movement commands with real-life object images.

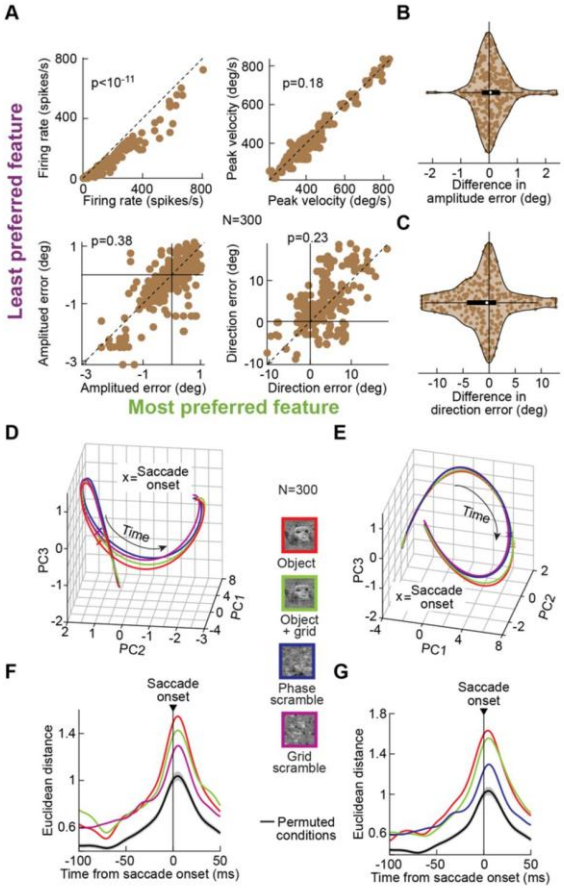

Fig. S9. Real-life object representations in SC neuronal movement commands. (A) Plots similar to Fig. 2B, C and Fig. S1A, C showing a dissociation between motor burst effects between most/least preferred images (top left) and saccade kinematics (top right) or saccade metrics (bottom left and right) in the experiment testing real-life object images (Fig. 4). **(B, C)** Distributions of saccade amplitude and direction error differences between most and least preferred images like in Fig. S1B, D, consistent with the interpretation that SC motor burst differences in this experiment were not explained by systematic differences in eye movement parameters (also see Fig. 4D, E). **(D, E)** Two different views of the peri-saccadic PCA-space population trajectories from both monkeys in the experiments with object images. Note how object and object+grid images (having coherent visual form images within them) were more differentiated from phase-scrambled and grid-scrambled images. **(F)** High-dimensional space Euclidean distances as a function of time from saccade onset when phase-scrambled images were the reference trajectory. This is a similar analysis to that in Fig. 3I, but for the real-life object experiments. Euclidean distances peaked near saccade onset, and they were consistently higher than distances obtained with randomly shuffled reference and non-reference trajectories (black +/- 95% confidence intervals). Object and object+grid images were also more differentiated (higher Euclidean distances) from phase-scrambled images than grid-scrambled images at the time of saccade triggering, consistent with Fig. 4F. **(G)** Similar analysis to **F** but with grid-scrambled images now providing the reference trajectory. Once again, the object and object+grid images were the most differentiated at the time of saccades from grid-scrambled images. All other conventions are similar to **F**. Therefore, whether referencing to phase- or grid-scrambled images, SC motor bursts for real-life objects were most differentiated from those for scrambled images.

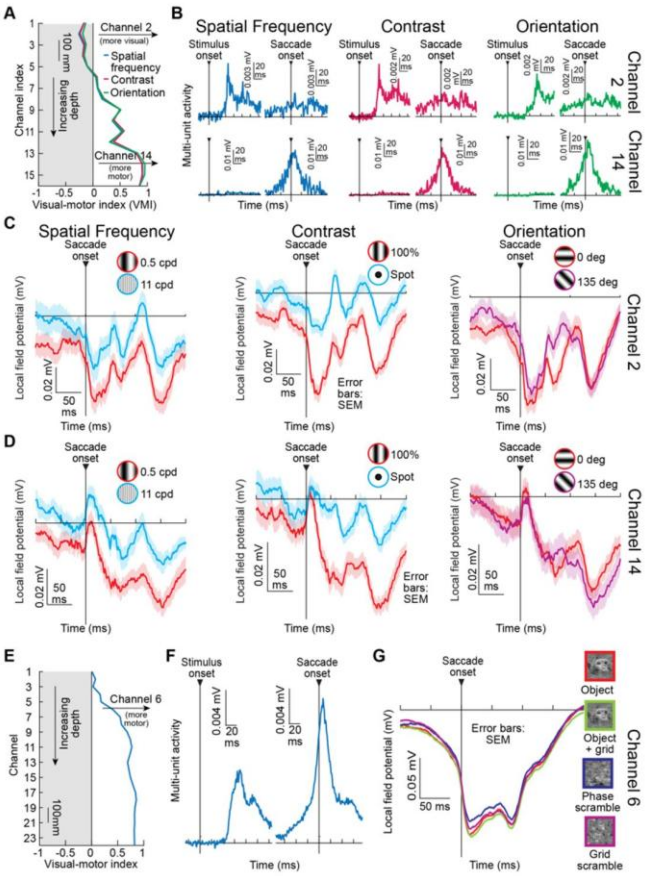

Fig. S10. Embedding of sensory information at saccade onset within the deeper SC layers. **(A)** We calculated a visual-motor index (VMI) (Materials and Methods and refs. 25, 26) across electrode depths from the example session shown in Fig. 1. The VMI, which is inferred from multi-unit activity (MUA) near a given electrode contact, is positive for more motor layers and negative for more visual layers, and the example neuron of Fig. 1 was recorded from channel 14 (that is, from a strongly motor layer). The VMI was calculated for each image manipulation separately (3 colors), and it was robust across them. **(B)** Example MUA activity profiles near stimulus or saccade onset from the same example session. Responses are shown from channel 2 and channel 14, demonstrating how channel 2 was predominantly visual (no motor bursts) and channel 14 was predominantly motor (no visual bursts). **(C)** Local field potential (LFP) profiles around saccade onset for two example features (e.g. 0.5 and 11 cpd) from each image manipulation tested in this session (spatial frequency, contrast, and orientation). The LFP responses from channel 2 are shown. There were differences in peri-saccadic LFP responses for different image features of the saccade targets, despite matched saccade kinematics and metrics. This is consistent with the presence of sensory information in the local SC network at the time of saccade motor burst generation. Note how the effect was weakest for the orientation image manipulation. **(D)** Similar analyses from the deeper motor layer of channel 14 (where the example neuron of Fig. 1 was recorded). There was still a clear sensory signal in the peri-saccadic LFP responses despite the depth of the recording, consistent with the results of Figs. 1-3, 5. Again, the effect was weakest in the orientation image manipulation. **(E-G)** VMI, MUA, and LFP responses from another session from the real-life object experiment. Peri-saccadic LFP responses from an example motor layer (same as that of the example neuron of Fig. 4B) also differentiated between coherent and scrambled object images (**G**). Error bars in all cases: SEM.

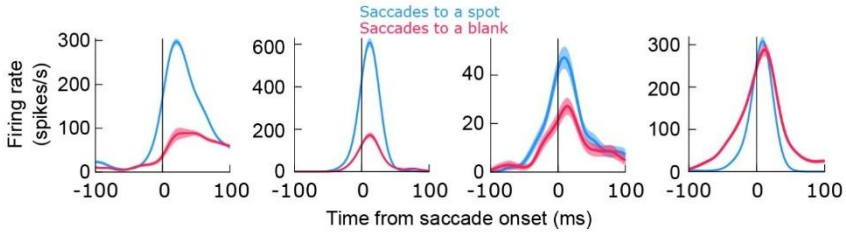

Fig. S11. Comparison of SC motor bursts for saccades made towards either a white spot or a blank. Four additional example neurons from different parts of the distribution of neuronal modulation indices of Fig. 6A. The leftmost two neurons had much weaker peak saccade-related discharge for the blank condition than for the visible target condition. This was the case despite the fact that the neurons emitted strong motor bursts of up to almost 300 or 600 spikes/s peak discharge when the saccade target was visible. The third neuron was less strongly affected by the absence of a visual target for the saccade, and the fourth neuron was even less affected (this example represented a minority in the population, as can be seen from the distribution of Fig. 6A). Error bars denote SEM, and the saccade vectors were always matched between the visible target and blank conditions (15).

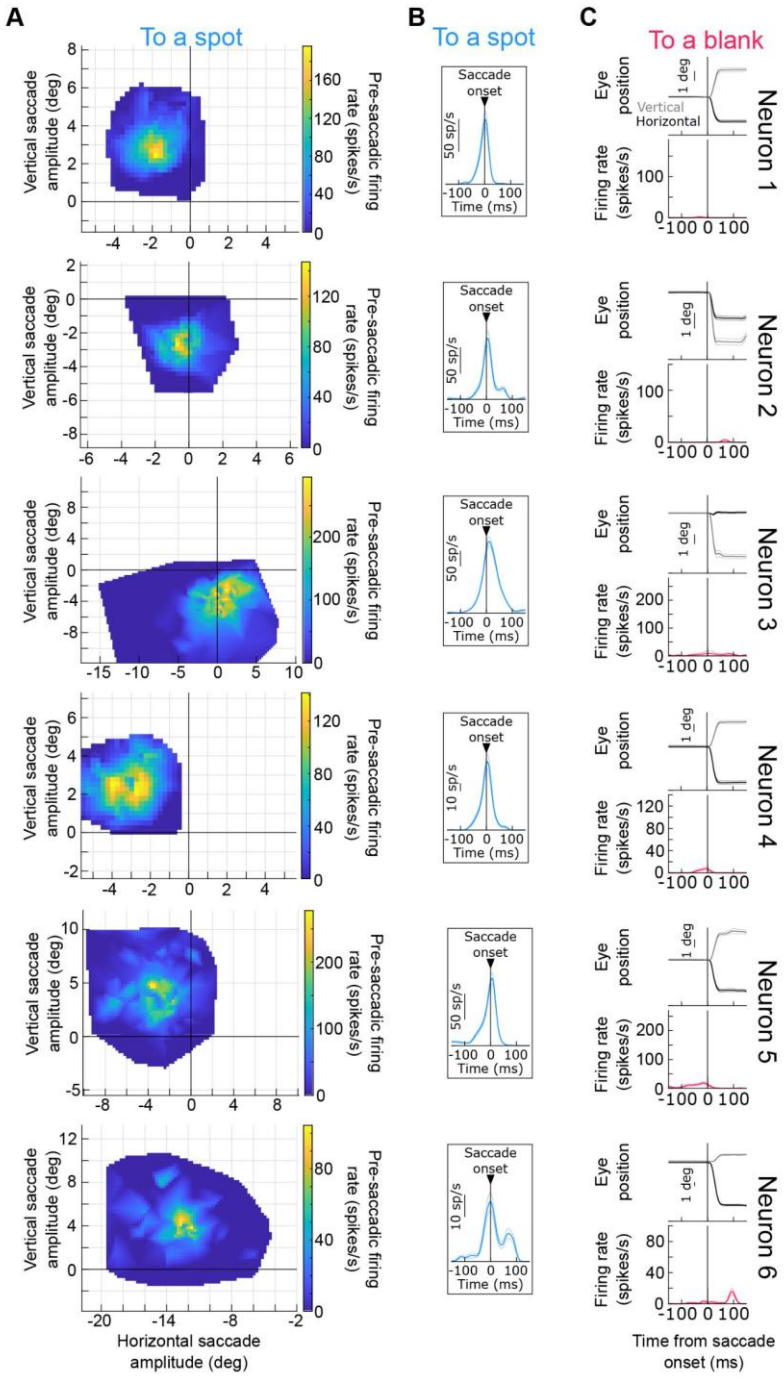

Fig. S12. Example SC neurons with visually-dependent saccade-related discharge from the database of a previous study (24). (A) Each row represents an example neuron in which we plotted the saccade-related motor RF map, from a task in which the saccade target was a white spot. The horizontal and vertical axes indicate horizontal and vertical saccade amplitudes, respectively. The z-axis denotes the average pre-saccadic firing rate (in the final 50 ms before saccade onset) emitted by the neuron. Note that peak motor burst strength typically occurs after saccade onset, suggesting that all six shown neurons had strong motor burst peaks of >100

spikes/s. **(B)** For each neuron, we plotted the average peri-movement firing rate curve from all RF sample locations displayed in **A**. There was a clear saccade-related motor burst. Note that the shown plots under-represent the peak motor burst strength of each neuron because they included all sampled saccade vectors from **A** (including those outside of the RF and with minimal saccade-related discharge). Nonetheless, clear saccade-related motor bursts could still be seen. **(C)** We then plotted each neuron's discharge for a single saccade vector to a location near the RF hotspot location from **A**. This time, the saccade was made towards a blank (memory-guided saccade). Each panel plots the eye position time course (top) and the associated average firing rate (bottom), both aligned to saccade onset. In all six cases, the neurons did not emit motor bursts with saccades towards a blank, despite being clearly saccade-related in **A**, **B**. Error bars: SEM.

SI References

1. A. R. Bogadhi, Z. M. Hafed, Express detection and discrimination of visual objects by primate superior colliculus neurons. *BioRxiv* 10.1101/2022.02.08.479583 (2022).
2. K. M. Eastman, A. C. Huk, PLDAPS: A Hardware Architecture and Software Toolbox for Neurophysiology Requiring Complex Visual Stimuli and Online Behavioral Control. *Front Neuroinform* **6**, 1 (2012).
3. D. H. Brainard, The Psychophysics Toolbox. *Spatial vision* **10**, 433-436 (1997).
4. D. G. Pelli, The VideoToolbox software for visual psychophysics: transforming numbers into movies. *Spatial vision* **10**, 437-442 (1997).
5. M. Kleiner, D. Brainard, D. G. Pelli, What's new in Psychtoolbox-3? (Abstract). *Perception* **36** (2007).
6. J. Skinner, A. Buonocore, Z. M. Hafed, Transfer function of the rhesus macaque oculomotor system for small-amplitude slow motion trajectories. *J Neurophysiol* **121**, 513-529 (2019).
7. K. F. Willeke *et al.*, Memory-guided microsaccades. *Nat Commun* **10**, 3710 (2019).
8. S. J. Judge, B. J. Richmond, F. C. Chu, Implantation of magnetic search coils for measurement of eye position: an improved method. *Vision Res* **20**, 535-538 (1980).
9. A. F. Fuchs, D. A. Robinson, A method for measuring horizontal and vertical eye movement chronically in the monkey. *J Appl Physiol* **21**, 1068-1070 (1966).
10. T. Moore, Shape representations and visual guidance of saccadic eye movements. *Science* **285**, 1914-1917 (1999).
11. C. Y. Chen, L. Sonnenberg, S. Weller, T. Witschel, Z. M. Hafed, Spatial frequency sensitivity in macaque midbrain. *Nat Commun* **9**, 2852 (2018).
12. V. Willenbockel *et al.*, Controlling low-level image properties: the SHINE toolbox. *Behav Res Methods* **42**, 671-684 (2010).
13. T. Malevich, A. Buonocore, Z. M. Hafed, Dependence of the stimulus-driven microsaccade rate signature in rhesus macaque monkeys on visual stimulus size and polarity. *J Neurophysiol* **125**, 282-295 (2021).
14. T. Malevich, T. Zhang, M. P. Baumann, A. R. Bogadhi, Z. M. Hafed, Faster Detection of "Darks" than "Brights" by Monkey Superior Colliculus Neurons. *J Neurosci* **42**, 9356-9371 (2022).
15. T. Zhang, T. Malevich, M. P. Baumann, Z. M. Hafed, Superior colliculus saccade motor bursts do not dictate movement kinematics. *Commun Biol* **5**, 1222 (2022).
16. C. Y. Chen, Z. M. Hafed, Postmicrosaccadic enhancement of slow eye movements. *The Journal of neuroscience : the official journal of the Society for Neuroscience* **33**, 5375-5386 (2013).
17. M. E. Bellet, J. Bellet, H. Nienborg, Z. M. Hafed, P. Berens, Human-level saccade detection performance using deep neural networks. *J Neurophysiol* **121**, 646-661 (2019).
18. D. A. Robinson, Eye movements evoked by collicular stimulation in the alert monkey. *Vision Res* **12**, 1795-1808 (1972).
19. D. L. Sparks, C. Lee, W. H. Rohrer, Population coding of the direction, amplitude, and velocity of saccadic eye movements by neurons in the superior colliculus. *Cold Spring Harb Symp Quant Biol* **55**, 805-811 (1990).
20. B. L. Zuber, L. Stark, G. Cook, Microsaccades and the velocity-amplitude relationship for saccadic eye movements. *Science* **150**, 1459-1460 (1965).
21. J. A. Edelman, M. E. Goldberg, Dependence of saccade-related activity in the primate superior colliculus on visual target presence. *J Neurophysiol* **86**, 676-691 (2001).
22. M. Pachitariu, N. A. Steinmetz, S. N. Kadir, M. Carandini, K. D. Harris, Fast and accurate spike sorting of high-channel count probes with KiloSort. *Advances in Neural Information Processing Systems (NIPS 2016)* **29** (2016).
23. T. Moore, M. H. Chang, Presaccadic discrimination of receptive field stimuli by area V4 neurons. *Vision Res* **49**, 1227-1232 (2009).

24. Z. M. Hafed, C. Y. Chen, Sharper, Stronger, Faster Upper Visual Field Representation in Primate Superior Colliculus. *Curr Biol* **26**, 1647-1658 (2016).
25. C. Massot, U. K. Jagadisan, N. J. Gandhi, Sensorimotor transformation elicits systematic patterns of activity along the dorsoventral extent of the superior colliculus in the macaque monkey. *Commun Biol* **2**, 287 (2019).
26. C. Bourrelly, C. Massot, N. J. Gandhi, Rapid Input-Output Transformation between Local Field Potential and Spiking Activity during Sensation but not Action in the Superior Colliculus. *J Neurosci* **43**, 4047-4061 (2023).
27. U. K. Jagadisan, N. J. Gandhi, Population temporal structure supplements the rate code during sensorimotor transformations. *Current Biology* **32**, 1010-1025 (2022).
28. E. F. Kutter, J. Bostroem, C. E. Elger, F. Mormann, A. Nieder, Single Neurons in the Human Brain Encode Numbers. *Neuron* **100**, 753-761 e754 (2018).

Appendix D: Publication 4

Perisaccadic perceptual mislocalization strength depends on the visual appearance of saccade targets

Baumann, M. P., Denninger, A. F., & Hafed, Z. M.

Journal of Neurophysiology, (2025) Vol. 133, pp. 85-100.

doi: 10.1152/jn.00368.2024.

american physiological society | JNP JOURNAL OF NEUROPHYSIOLOGY.

J Neurophysiol 133: 85–100, 2025.
First published November 19, 2024; doi:10.1152/jn.00368.2024

RESEARCH ARTICLE

Sensory Processing

Perisaccadic perceptual mislocalization strength depends on the visual appearance of saccade targets

Matthias P. Baumann,[1,2]* Anna F. Denninger,[1,2,3,4]* and Ziad M. Hafed[1,2]

[1]*Werner Reichardt Centre for Integrative Neuroscience, University of Tübingen, Tübingen, Germany;* [2]*Hertie Institute for Clinical Brain Research, University of Tübingen, Tübingen, Germany;* [3]*Department for Psychiatry and Psychotherapy, University of Tübingen, Tübingen, Germany; and* [4]*Center for Mental Health (TüCMH), University of Tübingen, Tübingen, Germany*

Abstract

We normally perceive a stable visual environment despite eye movements. To achieve such stability, visual processing integrates information across a given saccade, and laboratory hallmarks of such integration are robustly observed by presenting brief perisaccadic visual probes. In one classic phenomenon, probe locations are grossly mislocalized. This mislocalization is believed to depend, at least in part, on corollary discharge associated with saccade-related neuronal movement commands. However, we recently found that superior colliculus motor bursts, a known source of corollary discharge, can be different for different image appearances of the saccade target. Therefore, here we investigated whether perisaccadic mislocalization also depends on saccade target appearance. We asked human participants to generate saccades to either low (0.5 cycles/°) or high (5 cycles/°) spatial frequency gratings. We always placed a high-contrast target spot at grating center, to ensure matched saccades across image types. We presented a single, brief perisaccadic probe, which was high in contrast to avoid saccadic suppression, and the subjects pointed (via mouse cursor) at the seen probe location. We observed stronger perisaccadic mislocalization for low-spatial frequency saccade targets and for upper visual field probe locations. This was despite matched saccade metrics and kinematics across conditions, and it was also despite matched probe visibility for the different saccade target images (low vs. high spatial frequency). Assuming that perisaccadic visual mislocalization depends on corollary discharge, our results suggest that such discharge might relay more than just spatial saccade vectors to the visual system; saccade target visual features can also be transmitted.

NEW & NOTEWORTHY Brief visual probes are grossly mislocalized when presented in the temporal vicinity of saccades. Although the mechanisms of such mislocalization are still under investigation, one component of them could derive from corollary discharge signals associated with saccade movement commands. Here, we were motivated by the observation that superior colliculus movement bursts, one source of corollary discharge, vary with saccade target image appearance. If so, then perisaccadic mislocalization should also do so, which we confirmed.

corollary discharge; perisaccadic mislocalization; saccadic compression; spatial frequency; superior colliculus

INTRODUCTION

Vision is a highly active process, continuously utilizing eye movements to both sample and modulate incoming retinal image streams. Because eye movements, such as saccades, necessarily shift retinal images even with a completely stable environment, perceptual processes bridging inter- and intrasaccadic image sequences are supposed to take place (1–4). One classic approach to the study of perisaccadic vision has been to present very brief visual probes before, during, and after saccades (5–11). Such presentation has led to two classic observations. First, there is a strong reduction in visual sensitivity to brief perisaccadic probes (7–9, 12–14), called perceptual saccadic suppression. Second,

*M. P. Baumann and A. F. Denninger contributed equally to this work.
Correspondence: Z. M. Hafed (ziad.m.hafed@cin.uni-tuebingen.de).
Submitted 20 August 2024 / Revised 6 November 2024 / Accepted 11 November 2024

with high-contrast probes, these probes are successfully detected but grossly mislocalized relative to their true displayed positions (5, 6, 10, 11, 15–18), in a phenomenon called perisaccadic mislocalization.

Perisaccadic mislocalization has different properties depending on the visual and motor conditions under which it is observed. For example, the presence of visual reference frames makes the mislocalization appear like a convergence toward the saccade target (15). That is, brief probes presented ahead of the saccade target are mislocalized backward in position, and probes presented nearer to the initial fixation position than the saccade target are reported as being forward in position (11). On the other hand, mislocalization is uniform in direction in complete darkness (5, 6, 15), meaning that both probes ahead of and nearer to the initial fixation point than the saccade target are mislocalized in a forward direction parallel to the saccade vector. In addition, with the convergent mislocalization (which we focus on here), the two-dimensional landscape of perisaccadic mislocalization strongly depends on saccade direction, with upward saccades causing particularly large backward errors for probes presented ahead of the saccade target (17).

Because the properties of perisaccadic mislocalization depend on the visual conditions, one neuronal mechanism underlying this phenomenon could be sensory in nature (19). For example, in some models, classic perisaccadic convergent mislocalization (11) can be easily explained using saccade-induced retinotopic shifts of probe representations from the periphery to the perifovea; when these shifts occur on anatomically distorted topographic visual maps having foveal magnification, then a so-called "compression" is a simple consequence of readout from such anatomically distorted maps (20). Indeed, a simple modification of such models to include both foveal as well as upper visual field magnification can also conceptually account for the greater mislocalization strength observed for upward saccades (17). Specifically, in a sensory-motor area such as the superior colliculus (SC), there exist both foveal (21) as well as upper visual field (22) magnification. Thus, if mislocalization depends on how retinotopic representations of probes are translated from the periphery to the fovea on anatomically distorted maps, then larger perisaccadic mislocalization for upward saccades would be expected if such maps additionally differentially represent the upper visual field (17).

Having said that, it is also generally assumed that perisaccadic mislocalization does have a motor component associated with it. Besides the different representations for upward saccades in the SC (22, 23), and the resultant implications for mislocalization strength (17), the SC is a known source of saccade-related corollary discharge signals (24–31). Such corollary discharge signals are sufficient to cause perisaccadic retinotopic remapping of visual response fields in the cortex (32). Thus, if such cortical remapping is indeed one neuronal basis for perceptual mislocalization (33, 34), despite some controversy (35–38), then studying the roles of SC saccade-related discharge in perceptual mislocalization is very worthwhile.

One interesting recently reported property of SC motor discharge is related to the saccade target's visual appearance. Specifically, we recently observed that SC motor bursts can be different for different saccade target images, even under matched saccade metrics and kinematics (39). Since SC motor bursts are relayed to the cortex virtually unchanged (25), this implies that perisaccadic corollary discharge from the SC (24, 26, 32) may potentially relay not only the movement vector information to the cortex but also integrated information about the visual appearance of the saccade target. If so, then perceptual phenomena that are believed to depend, at least partially, on perisaccadic corollary discharge, such as perisaccadic mislocalization, may be additionally modulated by the visual appearance of the saccade target. This is what we investigated here.

METHODS

Experimental Subjects and Ethical Approvals

We ran a visual mislocalization paradigm on eight human subjects (4 female), aged 23–29 yr. We also ran a control experiment testing the detectability of perisaccadic visual probes on eight human subjects (5 female), aged 23–27 yr. Four subjects were shared between the two paradigms, performing both variants of the experiments in different sessions.

The experiments were approved by ethical committees at the Medical Faculty of the University of Tübingen, and the subjects provided written informed consent. They were also financially compensated for their time, and the experiments were in line with the Declaration of Helsinki.

Laboratory Setup

The laboratory setup was the same as that used in our recent studies (14, 40), and we largely used similar procedures. Briefly, the subjects sat in a dark room 57 cm from a calibrated and linearized CRT display with 41 pixels/° resolution. We tracked their eye movements at 1 kHz with a desk-mounted video-based eye tracker (EyeLink 1000; SR Research), and we stabilized their head position with a custom-built apparatus described previously (41). Stimuli were presented on a gray background of 20.01 cd/m^2 luminance, and fixation spots (7 × 7 min arc) were white (with 49.25 cd/m^2 luminance). The experiments were controlled with the Psychophysics Toolbox (42–44) with EyeLink Toolbox extensions (45).

Experimental Procedures

Perisaccadic mislocalization experiment.

In the perisaccadic mislocalization experiment, the subjects fixated a white spot placed ~8.5° either to the right or left of display center. After 500 ms, a low [0.5 cycles/° (cpd)] or high (5 cpd) spatial frequency Gabor grating was presented at screen center. The grating had a Gaussian smoothing window with $\sigma = 0.49°$ (and thus spanned a diameter of ~2.4°), and it had high contrast (100%); its phase was also randomized. The subjects were still required to maintain fixation for another 1,000–1,500 ms (because we wanted to avoid any sensory transients associated with grating onset). When the fixation spot was removed, the subjects made a saccade toward the center of the grating, which had a central marker in its middle as in our neurophysiology experiments (39) (to minimize intertrial saccade variance and to also control for postsaccadic fixation position). This instructed, visually

guided saccade was the one of primary experimental interest for us in this study, because it was only this saccade that we paired with a strategically timed visual probe for localization. Specifically, once we detected a saccade onset after fixation spot removal, we presented a brief (1 frame; 85 Hz refresh rate in the display) flash of a white square (that is, of high contrast) of size 45 × 45 min arc (Fig. 1*A*). The times of the flash were either immediately upon online saccade detection or at +40 or +80 ms from such detection. In post hoc analyses, we recomputed the flash times to always report them relative to actual saccade onset (see *Data Analysis* and RESULTS).

Our online saccade detection algorithm was the same as the one that we used previously (14, 40, 46, 47). Briefly, we obtained a real-time estimate of radial eye speed by having a running history of recent eye position samples and how these samples differed (locally in time) from each other. Specifically, at every time sample, we obtained a best-fitting line to the latest five measurements of eye position data that were collected. We then took the slope of the fitted line as an indication of the rate of change in eye position. To reduce noise, we took the median of the three latest slope measurements as our final estimate. That is, at the current time t ms, we took the slope of the line best fitting the eye positions collected between times $t - 4$ ms and t ms. We then combined it with the slope calculated from the previous time sample (measuring eye positions from $t - 5$ ms to $t - 1$ ms) and the sample before that (measuring eye positions from $t - 6$ ms to $t - 2$ ms). The median of these three latest slope calculations was considered our rate of change of eye position, and we applied a user-adjustable threshold to decide whether this rate of change was large enough to qualify as a saccade onset. The key was to pick a threshold above the current noise levels of the eye tracker, and our use of the median helped stabilize our estimates against noise (with the small expense of needing to buffer up to time sample $t - 6$ ms for the calculations).

The behavioral task of the subjects was to indicate (with a computer mouse cursor) the perceived location of the recently presented flash. Specifically, after the subjects fixated the central grating for 500 ms (that is, after the end of the primary saccade), we removed all stimuli from the display and displayed a mouse cursor at display center. The subjects clicked on the seen flash location, and they were free to move their eyes until they responded (they typically made secondary saccades toward where they reported the flash position with the mouse cursor; see RESULTS). The mouse cursor itself was the standard cursor of the Mac OS operating system through which we controlled the experimental display: it was a black, oblique arrow spanning a total of ~14.4 min arc horizontally and 19.2 min arc vertically. It was thus significantly smaller than the perisaccadic flash, especially since the registered click location of the cursor was actually the single-pixel tip of the entire mouse cursor's arrow shape.

The mouse was moved by the subjects on a flat table-top surface orthogonal to the orientation of the vertical visual display in front of the subjects. However, our subjects were all highly experienced in using computers, so there was no learning involved in moving the mouse cursor to its intended position on the display before clicking to register their report. In addition, the mouse cursor was always visible on the display during the entire reporting period, allowing the subjects to accurately click the mouse cursor where they actually intended to do so.

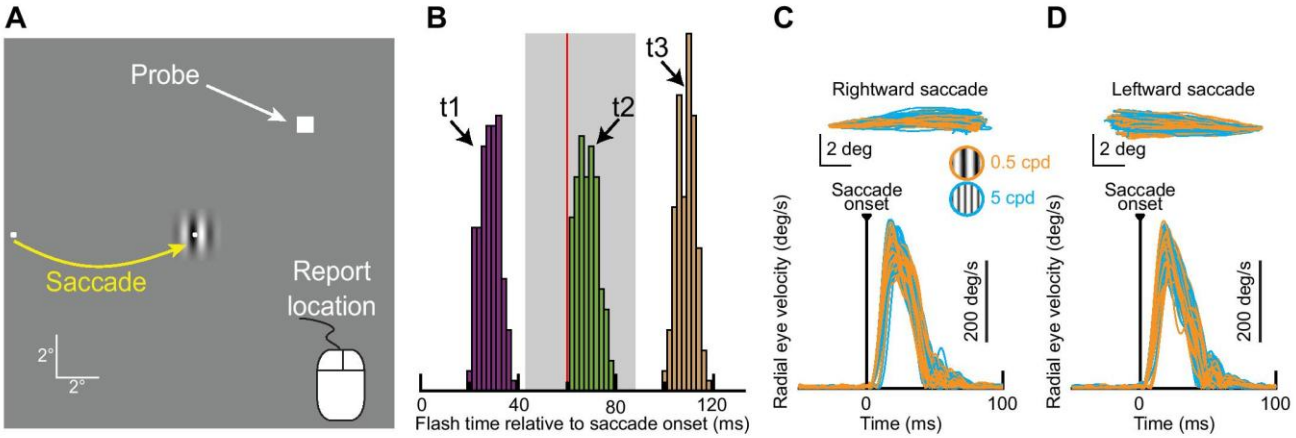

Figure 1. Probing perisaccadic perceptual mislocalization with different saccade target image appearances. *A*: subjects generated a rightward (shown) or leftward saccade toward the center of a low- or high-spatial frequency grating. The center of the grating always had a small spot, to improve saccade accuracy/precision and vector matching across different trials and different saccade target appearances (METHODS). At different times relative to online saccade detection, we presented a very brief probe flash at 1 of 4 positions. Later, all stimuli were removed, and subjects had to point to the perceived flash position with a mouse cursor. Stimuli are drawn to scale (see scale bars). *B*: distribution of probe flash times relative to saccade onset in 1 example subject. We classified flash times according to the 3 seen peaks, and we labeled the categories *t1*, *t2*, and *t3*, respectively. We expected perceptual mislocalization to progressively get smaller and smaller from *t1* to *t3* (11). $N = 460$ trials. The gray region indicates the range of saccade end times observed in this subject, and the red line shows the mean value. *C*, *top*: horizontal and vertical eye position traces for rightward saccades from an example subject. Starting eye positions from all trials were aligned for better visualization of the saccade vectors, and the different colors show saccades toward either the low- or high-spatial frequency grating. *Bottom*: radial eye speed traces from the same trials. Note how saccade metrics (*top*) and kinematics (*bottom*) were matched across image types. Also note how the flash times in *B* spanned intrasaccadic flashes (*t1*) as well as flashes immediately after (*t2*) or later well beyond saccade end (*t3*). $N = 113$ and 117 for low- and high-spatial frequency saccade targets, respectively. cpd, cycles/°. *D*: same as *C* but for leftward saccades from the same subject. $N = 117$ and 113 for low- and high-spatial frequency saccade targets, respectively.

We also did not impose a requirement of speeded responses on the subjects, and this was a deliberate choice to allow them to be as accurate as possible in their reporting of perisaccadic flash location. Thus, we employed a very relaxed maximum duration value of 10 s for every single trial; if there was no subject response when the overall trial length (stimuli plus reaction time) reached 10 s, the computer registered that there was no behavioral response, and the trial was discarded. In reality, the manual reaction times of the subjects were much shorter than 10 s. Across subjects, the mean reaction time (measured 500 ms after the primary saccade, since the removal of the saccade target was the cue to respond in our task) was 996 ± 43 ms (SE), and the median reaction time was 972 ± 41 ms (SE). Moreover, across subjects, the minimum reaction time on any given trial was 466 ± 54 ms (SE), and the maximum reaction time was 2,173 ± 321 ms (SE).

We also note here that our prior work on visual localization (in the absence of perisaccadic visual probe flashes) revealed very minimal reporting errors with memory-based mouse cursor clicks, and this was the case even with several seconds of experimental working memory delay and subsequent reaction times by the subjects (17, 48, 49). Thus, our mislocalization errors reported in RESULTS cannot be explained by memory distortions.

We picked four possible perisaccadic flash locations on the display, each at a radius of ~7.3° from the saccade target center location. One flash was directly opposite the saccade target direction (i.e., on the horizontal axis), and the other three flashes were along the saccade direction and ahead of the saccade target location: one on the horizontal axis directly ahead of the saccade target (along the same vector) and the other two at the ±45° diagonals. Even though the flash opposite the saccade vector was expected to have the least mislocalization (17) (which we confirmed), we included it so that subjects could not expect to always see flashes ahead of the saccade target. Nonetheless, in the analyses (see below), we only analyzed the three flash locations ahead of the saccade target. This is because the mislocalization for the backward flash position was small in amplitude; past work that looked at mislocalization of the flash opposite the saccade vector typically used significantly larger saccades than we used, which made the smaller mislocalization of such a flash easier to detect than in our experiments (11, 16). In addition, and again because of our smaller saccade sizes than in previous studies, this backward probe location was actually close to the initial fixation spot (only ~1° away from it when the eye was still fixated before saccade onset), which made us worry that there could be interactions with the initial fixation spot location in the subjects' reported locations. Thus, it was more appropriate to analyze only the three forward probe flash locations.

Consistent with the above sentiment, we generally wanted to avoid having spatial reference frames (e.g., the edges of the display monitor) strongly influence performance in the visual mislocalization task. Therefore, across trials, we randomly shifted all stimulus positions in a given trial by a random (but constant) number from the range of ±1.2° in either horizontal or vertical direction (at pixel resolution; 1/41°). That is, on every trial, the overall displayed stimulus geometry was randomly shifted on the display monitor from previous trials, so that the monitor edges could not act (across trials) as reliable reference frames for probe flash localization. For example, if the initial fixation position was shifted by 1° to the right of its standard position on a given trial, then the grating position at the center of the display was also shifted by 1° to the right, and so was the perisaccadic probe flash (in other words, the stimulus relationships were all unchanged, but the overall absolute position was shifted by 1° to the right). This approach minimized the possibility of subjects remembering the absolute positions of flashes relative to the display monitor edges across trials. We are thus confident that the results that we report here were less affected by global biases of expected, world-centered, probe flash locations.

Finally, note that the low and high spatial frequencies chosen as the saccade targets were differentially represented by the SC motor bursts in our recent neurophysiological results (39). That is why we chose these particular spatial frequencies.

We collected 324 trials per spatial frequency in each subject.

Perisaccadic detection experiment.

In a second control experiment, we tested the visibility of the perisaccadic probes used in the above experiment. Subjectively, the subjects did report to us that they consciously perceived the perisaccadic probes in the above experiment, despite the large magnitudes of mislocalization errors seen in RESULTS. Nonetheless, we still wanted to objectively confirm that the contrast used for the probe flashes was indeed high enough to avoid effects of saccadic suppression. We also wanted to confirm that, even if suppression was avoided by the high probe contrasts, perceptual visibility for such high-contrast probe flashes was still independent of the saccade target appearance. To do so, we collected full psychometric curves of probe detection (14). Thus, the experiment was the same as that described above, except that the probe flash now had variable contrast from trial to trial. Additionally, the probe flash time was either immediate upon online saccade detection, or at +11 or +35 ms. As we show in RESULTS, this timing allowed us to investigate probe visibility in the two mislocalization intervals in which we observed significant perisaccadic perceptual mislocalization in the main experiment above. Finally, in this task variant, the probe flash could appear at one of four cardinal locations relative to the saccade target center (and at an eccentricity halfway from the initial fixation position). The subjects' task was to report which of the four locations had a brief flash at it, and they did so via a response button box (indicating that the flash was to the right of, left of, above, or below the saccade target location). Note that the eccentricity of the probe flashes used here was roughly similar to the perceived eccentricities that we report in RESULTS for the mislocalization experiment, making the comparisons of the results in the two task variants meaningful.

Across trials, we varied the flash luminance to obtain full psychometric functions of flash detection sensitivity. The procedure was similar to that we described recently (14). Briefly, we performed a staircase procedure in the first session to obtain an initial estimate of perceptual threshold in a subject; in subsequent sessions, we also added additional

samples of flash contrast to sample more locations on the *x*-axis of the psychometric curves. As in the mislocalization experiment above, we also randomized the starting position of the whole stimulus display items across trials. That is, a constant random shift was applied to all stimulus positions in any given trial.

We collected 450–500 trials per spatial frequency in each subject.

Data Analysis

We detected saccades and microsaccades with our previously described methods (47, 50). Before analyzing any behavioral reports, we filtered the eye movement data to ensure matched saccade execution across low- and high-spatial frequency saccade targets. In the perisaccadic mislocalization task, we did so by binning the saccade landing points into bins of 0.5 × 0.5°. We also binned the saccade main sequence (51, 52) data points into bins of 0.5° × 40°/s. We then only accepted trials into the analyses that fulfilled the following criterion: they came from landing position and main sequence bins that had at least one trial repetition within them from each of the two saccade target image appearances (low and high spatial frequencies). This way, the saccades across image appearances were matched for both metrics and kinematics (see RESULTS). The typical numbers of trials per condition that remained after such filtering are like those described in the legend of Fig. 2.

In the perisaccadic detection task, we used a slightly different, but equally effective (see RESULTS), way of vector and kinematic matching. First, we defined a maximal radius (2°) for initial eye position at saccade triggering, and made sure that trials with both high- and low-spatial frequency saccade targets had the same initial starting position ranges. Similarly, we defined a maximal radius for final eye position at the end of the saccade, to make sure we had matched saccade vector ranges. Then, for each saccade direction (rightward or leftward), we ensured that the amplitudes and peak velocities of the saccades were matched regardless of whether the saccade target had a high or low spatial frequency (see RESULTS). We also excluded trials with saccadic reaction times < 80 ms or > 500 ms.

To analyze perisaccadic mislocalization, we first confirmed that we had matched saccade vectors as described above. We also confirmed that saccade peak velocities (that is, kinematics) were similar for low- and high-spatial frequency saccade targets (see RESULTS). We then recomputed all flash times relative to the actual saccade onset times after we properly detected the eye movements. After that, we collected each subject's click locations at different flash times. We classified the flash times into three categories (*t1*, *t2*, and *t3*) according to the histograms of flash times that we observed after recomputing the saccade onsets from the recorded eye movement data (see Fig. 1*B*). To summarize the subjects' click locations, we first remapped all data from leftward saccades to reflect their results across the vertical axis. That is, we flipped the horizontal axis for leftward saccades, in order to pool all results with the rightward saccades. Thus, in RESULTS we always show observations on a schematic vector representation having rightward saccades. After such remapping, we picked the median click location for each subject, each flash probe time, each flash probe location, and each saccade target appearance condition (low- or high-spatial frequency saccade target). Note that we always measured click locations relative to the stimulus locations; thus, the across-trial random shifts in global stimulus positions that we applied experimentally were removed in the analyses. To summarize the mislocalization effects, we measured for each trial the Euclidean distance from the actual flash location to the click location. In such summary analyses, we took (within a subject) the median Euclidean distances from all trials with forward flash positions; that is, for each subject we obtained a single (across trial) Euclidean distance measure across the three probe flash locations that were ahead of the saccade target. Larger mislocalization for a given condition (e.g., 1 saccade image appearance) was associated with a larger Euclidean distance. We then plotted the mean and SE of the distance across subjects, and we showed descriptive statistics and underlying individual subject results. We report all the statistical tests in RESULTS.

We also looked at the direction of the mislocalization vector for oblique probe flash positions. That is, mislocalization is known to have a two-dimensional landscape (along saccade direction and orthogonal to it) even if the saccades themselves are cardinal (16, 17). This two-dimensional landscape can be investigated by measuring the component of mislocalization independently either parallel to the saccade direction vector or orthogonal to it. Thus, we picked the two oblique flash positions that were ahead of the saccade target (at the ±45° diagonals) and that were expected to have the strongest oblique mislocalization (16, 17). Then, we compared how either their parallel or orthogonal mislocalization was different between the two image appearances of the saccade targets. For the parallel component we measured the horizontal component of their Euclidean distance measure described above, and for the orthogonal component we measured the vertical component.

We additionally compared mislocalization for flashes presented in the upper versus lower visual fields. That is, it is well established that the SC has an asymmetric representation of the upper and lower visual fields, which has been shown to play a potential role in the influence of saccade direction and visual field location on the strength of both perceptual mislocalization (17) and perceptual saccadic suppression (53). We therefore asked whether such an asymmetry could also differentially affect mislocalization strengths for upper and lower visual field flashes even with the same saccade direction. We did this by pooling data from both image conditions together (0.5 and 5 cycles/°) and analyzing mislocalization strength for either the oblique flash that was presented in the upper visual field or the one that was presented in the lower visual field. Very similar results were obtained when only inspecting the data individually for either the low- or high-spatial frequency saccade target conditions, so we decided to pool across spatial frequencies and maximize the numbers of trials that went into this analysis.

Finally, we correlated the end points of uninstructed saccades during cursor movement to the final reported locations with the mouse clicks. For each trial, we plotted the entire scanpath after the primary saccade of interest. This

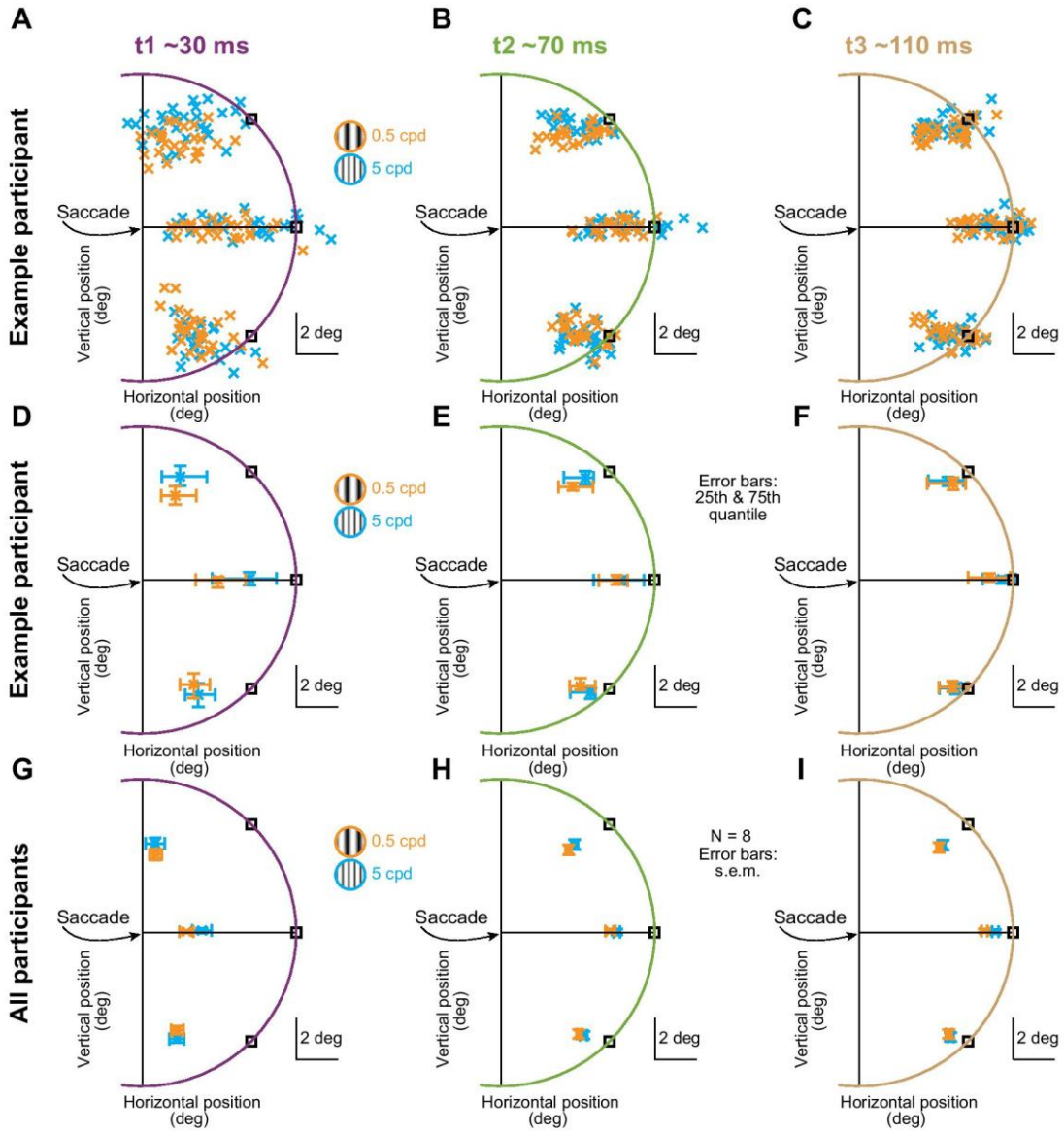

Figure 2. Stronger perisaccadic perceptual mislocalization with low-spatial frequency saccade targets. *A–C*: all click positions from 1 example subject (the same as in Fig. 1) after remapping all data to a rightward saccade direction (METHODS). The different panels show results from when the probe flashes were presented at *times t1* (*A*), *t2* (*B*), and *t3* (*C*), respectively, relative to saccade onset. Mislocalization got progressively weaker with time (compare the panels). Importantly, the mislocalization within a given time bin was different for the 2 different saccade target image appearances (compare the different colors in each panel). $N = 80, 73, 77$ trials for the clicks with the low-spatial frequency saccade target in *A*, *B*, and *C*, respectively. $N = 75, 77, 78$ trials for the clicks with the high-spatial frequency saccade target in *A*, *B*, and *C*, respectively. cpd, cycles/°. *D–F*: each symbol shows the median click location of the same subject for a given probe flash location, time, and saccade target image appearance. The range bars around each median click location indicate the interquartile extents of the data. *G–I*: for all analyses as in *D–F*, we averaged across 8 subjects. Error bars denote SE across the subjects. Also see Fig. 3 and Fig. 4 for more detailed quantitative analyses.

typically included a few saccades toward the final reported flash location (RESULTS). Then, we measured the final eye position at the time of the mouse cursor click, and we correlated this final eye position with the clicked location, both within individual subjects and across the population (and also across the different flash times).

All statistics on the perisaccadic mislocalization data were performed with MATLAB (version R2020b) and IBM SPSS Statistics (version 29.0).

In the perisaccadic detection experiment, we obtained psychometric curves of detection performance as a function of probe contrast level. To do that, we used the Psignifit 4

toolbox (54) for each subject individually, using a cumulative Gaussian function (and 0 lapse rate). We then averaged across the subjects' individual psychometric curves to obtain a population measure; thus, the population psychometric curve was the average of eight individual psychometric curves. We did this for each time bin of flash times relative to saccade onset (with the time bins defined as *t1a*, *t1b*, and *t2*, respectively; see RESULTS). Statistically, we performed bootstrapping to check whether perceptual detection depended on the saccade target image type. To do so, we created random permutations (10,000) in which we randomly picked trials for the two conditions (low- or high-spatial frequency saccade target) within each subject. When doing so, we kept the same numbers of observations per subject per condition, to maintain the sampling numbers consistent with our actual experimental data (especially after eye movement filtering). We then performed psychometric curve fits from such permuted data and measured the threshold at the 62.5% correct rate. Across the 10,000 permutations, we plotted the distributions of thresholds between the two sets of permuted conditions. If our actual measured threshold difference between low- and high-spatial frequency saccade targets was deviated by >95% of the threshold differences of the random permutations, then we deemed our measured threshold difference in the real experiment to be significant.

RESULTS

Our aim was to explore whether the strength of perisaccadic mislocalization could be modulated by the visual appearance of saccade targets, as might be predicted from observations of visual feature tuning in SC saccade-related motor bursts (39). To do so, we designed a psychophysical experiment in which humans reported the location of a brief perisaccadic probe flash that was presented at different times relative to saccade onset. Specifically, each trial consisted of an instruction to generate a primary saccade toward the center of a Gabor grating located near the center of the display screen (Fig. 1*A*). The initial fixation position was 8.5° to either the right or left of the grating center, thus requiring horizontal saccades. In addition, the Gabor grating could have one of two different spatial frequencies (METHODS). At different times relative to the online detection of a saccade (METHODS), we presented a brief, single-frame probe flash at one of four locations relative to the saccade target location. Three of these possible flashes were ahead of the saccade target, and one was behind it (Fig. 1*A*; METHODS). Note that, save for the saccade target image appearance manipulation, this task design was very similar to classic instantiations of the perisaccadic mislocalization paradigm (10, 11, 15, 16, 18), and also similar to our previous versions of it (17).

Figure 1*B* shows the distribution of probe flash times that we sampled for one example subject. During actual data collection, the computer triggered the probe flash at one of three possible delays after online saccade detection. However, the real delay was necessarily different, since online saccade detection required some data buffering for eye speed estimations (METHODS) and since there was some variance in the online speed estimates. Therefore, in post hoc analyses, we redetected all saccades (METHODS), and we then plotted the distributions of flash times in Fig. 1*B*. As can be seen, relative to the generated saccades (the gray region in Fig. 1*B* indicates the range of saccade end times observed for this subject, and Fig. 1, *C* and *D*, *bottom*, show radial eye speed from the same saccades), one set of times was intrasaccadic (labeled *t1*), another was around or shortly after saccade end (labeled *t2*), and the third was even longer after the saccades, when localization reports were expected to be nearer to the true probe flash locations on the display (labeled *t3*). Thus, our paradigm allowed us to analyze periods of significant perisaccadic mislocalization (*times t1* and *t2*) as well as periods closer to full recovery (*t3*). For simplicity, in what follows, we sometimes refer to *t1*, *t2*, and *t3* as 30 ms, 70 ms, and 110 ms, respectively.

Importantly, we ensured that the saccade vectors and kinematics were matched for the two different saccade target appearances. This was aided by having a small target spot in the middle of the gratings (39) (Fig. 1*A*), as well as by our filtering criteria described in METHODS. The net result was that the saccade distributions for the two different image types were virtually indistinguishable from each other between the low- and high-spatial frequency saccade targets (Fig. 1, *C* and *D*; 1 example subject's results are shown). Thus, we were now in a position to explore whether perisaccadic mislocalization was different for the two different saccade target images, despite the matched saccades.

Stronger Perisaccadic Mislocalization for Low-Spatial Frequency Saccade Targets

We analyzed each subject's click positions in each condition and time bin from Fig. 1. As stated in METHODS, we focused on the three probe flash locations ahead of the saccade target (1 directly along the saccade vector and 2 at ±45° oblique directions). This was the case especially because these three locations cause the strongest mislocalization (16, 17). Moreover, given that our saccades were significantly smaller than in previous studies of mislocalization (11, 16) [and were thus associated with smaller mislocalization strengths in general (17, 41)] and given the proximity of the probe opposite the saccade vector to the initial fixation position (METHODS), we felt that focusing only on the probe flash locations ahead of the saccade target was justified.

In Fig. 2, *A*–*C*, we show all click positions from one example subject's data. Each panel shows results from a given time bin, and this subject is the same subject whose eye movement data are shown in Fig. 1. As can be seen, the subject exhibited clear perisaccadic mislocalization, which diminished with increasing time from saccade onset. That is, regardless of which saccade target was visible (the 2 different colors in Fig. 2), the subject's click positions were closer to the saccade target in Fig. 2*A* than they were in Fig. 2, *B* and *C*. And, by *time t3* (110 ms), the click positions were closer to the true physical probe flash positions (Fig. 2*C*) (with the existence of some expected residual systematic undershoot biases; Refs. 48, 49). This fact, that the reported positions were more accurate for later flash times, confirms our intuition that the click errors seen in Fig. 2, *A* and *B*, were not due to distortions in the subject's memory of the flash position; if they were, then there was no reason for these errors to decrease for the later flash times, since the trial lengths after flash onsets were generally all very similar across conditions.

Indeed, in our previous work, we found very minimal impacts of long memory delays on (saccade free) memory-based reporting of stimulus locations with a mouse cursor (48, 49).

Importantly, Fig. 2, *A–C*, show that the subject's behavioral reports clearly depended on the appearance of the saccade target. This is seen through the different conditions in Fig. 2, *A–C*. In orange we show the clicks with the low-spatial frequency saccade target, and in blue we show clicks with the high-spatial frequency saccade target. There was stronger mislocalization, especially for the oblique probe flash positions, with the low-spatial frequency saccade target. This was also evident in the median click positions for the different probe flash locations and times (Fig. 2, *D–F*; error bars denote interquartile ranges). Thus, in this example subject, perisaccadic mislocalization depended on the visual appearance of the saccade target, even with metrically and kinematically matched saccades.

These results were consistent across our eight subjects. We repeated the analyses of Fig. 2, *D–F*, for each subject, and we then plotted the mean and SE values across the subjects in Fig. 2, *G–I*. There were systematic differences between the two different saccade target image appearances, which we investigated further in Fig. 3. Specifically, we computed, for each trial, the Euclidean distance between the physical location of the probe and the individual click position. Then, within each subject, we took the median distance across all three flash locations ahead of the saccade target location, and we did this separately for the different probe flash times. The saturated data points in Fig. 3 show the mean and SE across eight subjects, and the gray data points show individual subject results. Note that the *y*-axis ranges in Fig. 3, *A–C*, are not the same across the three panels, and this is because mislocalization got progressively smaller with increasing delay between the saccade and probe onsets (Fig. 2); we wanted to zoom into the data ranges of each panel individually. As can be seen, for each of *times t1* and *t2*, all but one subject showed a stronger perisaccadic mislocalization for the low-spatial frequency saccade target than for the high-spatial frequency saccade target (Fig. 3, *A* and *B*). At *time t3*, all but two subjects still showed this effect, although the overall mislocalization strength was much weaker given the longer time after the saccade (Fig. 2). Again, the weaker mislocalization with later flash times after the saccade rules out an interpretation of our results as being solely due to distortions in working memory.

We further quantified these effects by plotting in Fig. 3*D* the difference in the mislocalization strength between the low- and high-spatial frequency saccade target images as a function of probe flash time. This difference was similar for *times t1* and *t2*, and it was clearly positive at each of these two time points (with only 1 outlier subject in each case). Statistically, we performed a repeated-measures two-way ANOVA with the factors time and spatial frequency of the saccade target. Both main effects were significant [time: $F(2,14) = 67.78$, $P < 10^{-7}$, $\eta^2 = 0.906$; spatial frequency of the saccade target: $F(1,7) = 69.04$, $P < 10^{-4}$, $\eta^2 = 0.908$]. There was no significant interaction between these two factors. This is consistent with the observation that the difference in mislocalization strength for the two different saccade target image appearances was very similar for *times t1* and *t2* in Fig. 3*D*. We also performed post hoc tests (with Bonferroni correction), which revealed a significant difference in mislocalization strength between the saccade target image types for both *time t1* ($P = 0.015$) and *time t2* ($P = 0.025$). These results suggest that a perisaccadic phenomenon, which can potentially depend on

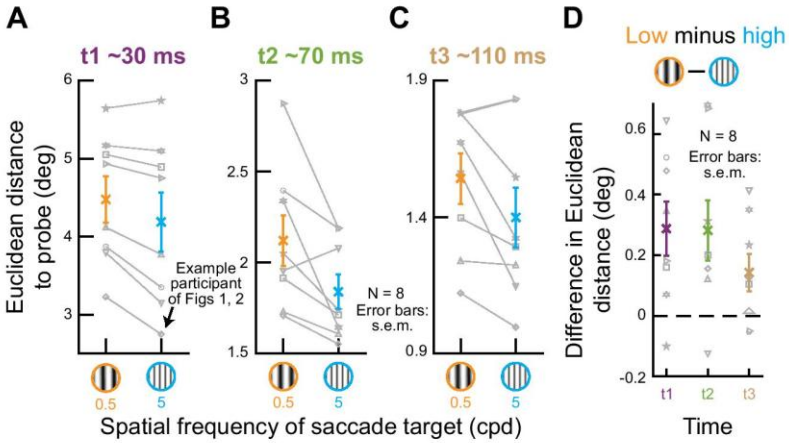

Figure 3. Population summaries of the results in Fig. 2. *A*: the saturated data points show the mean and SE across subjects ($N = 8$) of the Euclidean distances between the median click location at *time t1* and the true probe flash location (for the 3 probes ahead of the saccade target; Fig. 2). The gray data points show individual subject results. All but 1 subject had stronger perisaccadic perceptual mislocalization for the low-spatial frequency saccade target. The data with the diamond symbol in this and subsequent figures correspond to the same example subject of Fig. 1 and Fig. 2. *B*: similar results for *time t2*. Again, all but 1 subject had stronger perisaccadic perceptual mislocalization for the low-spatial frequency saccade target. *C*: similar results for *time t3*. Here, all but 2 subjects showed stronger mislocalization for the low-spatial frequency saccade target. Note that the *y*-axes are different in the different panels because of the time-varying amplitude of the mislocalization effect (Fig. 2). cpd, cycles/°. *D*: at each flash time (*x*-axis values), we plotted the difference in mislocalization strength between the low- and high-spatial frequency saccade target image trials. A positive difference indicates stronger mislocalization for the low-spatial frequency saccade target. The saturated data points show the mean and SE across subjects, and the gray data points show the individual subject results. Especially at *times t1* and *t2* (with strong perceptual mislocalization), there was stronger mislocalization for the low-spatial frequency saccade target appearance. Also see Fig. 4.

ascending SC projections (28–30, 32), depends on the visual appearance of the saccade target (especially at *times t1* and *t2*). This implies that visual feature tuning in SC neuronal movement commands (39) may, in turn, potentially provide more than just the vector information of executed movements via SC-sourced corollary discharge signals.

Stronger Orthogonal Mislocalization for Low-Spatial Frequency Saccade Targets

In the analyses of Fig. 2, we additionally noticed that oblique probe flash positions exhibited a stronger dependence of mislocalization strength on saccade target image appearance in the direction orthogonal to the saccade vector than in the direction parallel to it. Specifically, at *time t1*, with maximal mislocalization strengths in our experiments, both the example subject (Fig. 2, *A* and *D*) and the population (Fig. 2*G*) showed a bigger deviation in the vector direction between the true probe flash position and the behavioral reports of the subjects, suggesting a difference in the orthogonal component of mislocalization. Such a difference was masked by the analyses of Fig. 3, which pooled different probe flash positions and which were somewhat agnostic of the two-dimensional nature of perisaccadic mislocalization. Therefore, to explore this further, we expressed the mislocalization effect according to its two spatial components: one along the direction of the saccade (parallel to it) and one orthogonal to the saccade vector (Fig. 4*A*). We then compared the mislocalization effect in each direction separately for the two different saccade target image appearances.

We first compared the mislocalization effects along the saccade direction (Fig. 4, *B–E*), which is generally the direction in which mislocalization is strongest even for oblique flash positions (16, 17). Although the trends were all the same as those seen in Fig. 3, the clearest statistical effect now emerged only at *time t2*. Specifically, we performed a repeated-measures two-way ANOVA with the factors time and spatial frequency of the saccade target. Both main effects were significant [time: $F(2,14) = 47.27$, $P < 10^{-6}$, $\eta^2 = 0.871$; spatial frequency of the saccade target: $F(1,7) = 6.6$, $P = 0.037$, $\eta^2 = 0.486$], and there was no interaction. However, in post hoc tests (with Bonferroni correction), there was only a significant difference for the two types of saccade target at *time t2* (Fig. 4, *C* and *E*). Thus, this might indicate that the saccade target image appearance effects seen in Fig. 3, especially at maximal mislocalization periods (*time t1*), might have been dominated by the orthogonal component of mislocalization. We confirmed this to be the case. We performed the same tests but now on mislocalization orthogonal to the saccade direction (Fig. 4, *F–I*). Again both main effects were significant [time: $F(2,14) = 4.34$, $P = 0.034$, $\eta^2 = 0.383$; spatial frequency of the saccade target: $F(1,7) = 11.12$, $P = 0.013$, $\eta^2 = 0.614$]. On top of that, there was also an interaction between the factors time and spatial frequency of the saccade target [$F(2,14) = 9.47$, $P = 0.003$, $\eta^2 = 0.575$], indicating that the difference in mislocalization for the different

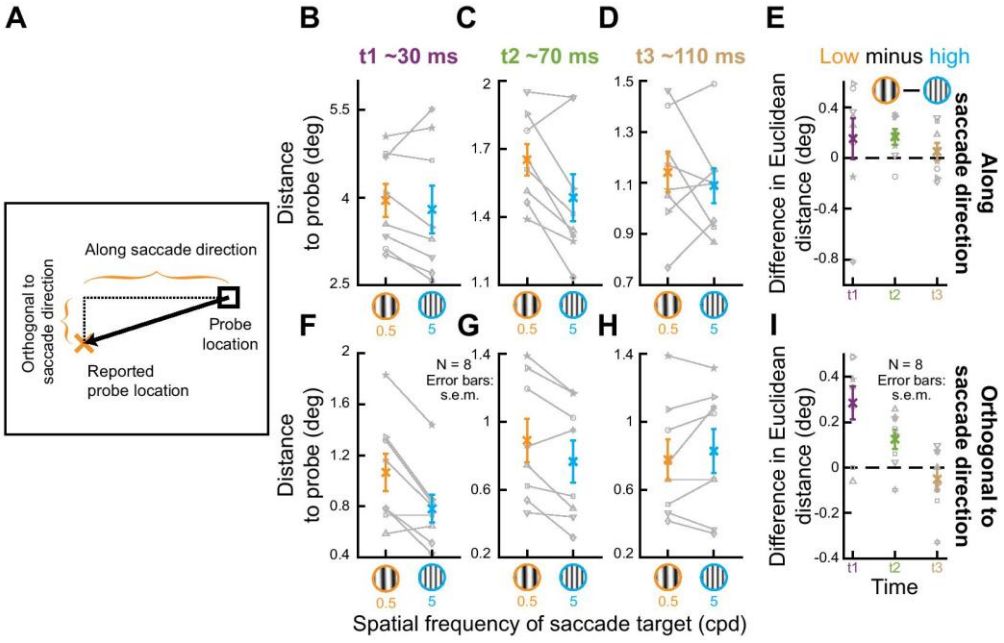

Figure 4. Stronger orthogonal mislocalization with low-spatial frequency saccade targets. *A*: our analysis approach for assessing the strength of orthogonal mislocalization. For the oblique probe flash positions ahead of the saccade target, we measured the 2 components of mislocalization separately. One component was along the saccade direction (measuring the horizontal distance between the reported and true probe locations), and one component was orthogonal to the saccade direction (measuring the distance between true and reported probe locations along the orthogonal axis). *B–E*: same as Fig. 3, *A–D*, but for the parallel component of mislocalization. The trends were all the same as in Fig. 3. but the significant effect of saccade target image appearance only emerged at *time t2* (see text). This might suggest that orthogonal mislocalization might have dominated the effects of Fig. 3. especially at *time t1*. *F–I*: we confirmed this by repeating the same analyses, but this time for the orthogonal component of mislocalization. Note how there was clearly stronger orthogonal mislocalization for low- than high-spatial frequency saccade targets, especially at *time t1*. All other conventions in this figure are the same as those in Fig. 3. cpd, cycles/°.

saccade targets differed as a function of time. Consistent with this, a post hoc test (with Bonferroni correction) revealed that the significant difference as a function of saccade target image appearance was present at both *times t1* ($P = 0.006$) and *t2* ($P = 0.022$) (Fig. 4*I*). Thus, even the two-dimensional landscape of perisaccadic mislocalization (16, 17) depends on the saccade target image appearance, and this effect was clearest at *time t1* (Fig. 4*I*).

Stronger Mislocalization for Probes in the Upper Rather than Lower Visual Field

The SC is known for its asymmetric representation of the upper and lower visual fields (22, 23). Therefore, we also wondered whether, even for purely horizontal saccades, mislocalization strength could additionally depend on the visual field locations of the probe flashes. For example, it could be the case that upper visual field magnification in the SC (22) is an additional topographic map distortion that can potentially modify mislocalization patterns. Testing this possibility would provide even further motivation for the idea of a putative involvement of the SC in remapping mechanisms that can cause perisaccadic mislocalization. Moreover, if validated, showing different perisaccadic mislocalization for the upper and lower visual fields would add to increasing evidence that perisaccadic vision in general might follow SC visual field asymmetries rather than asymmetries in performance that occur in the absence of saccades (likely cortically mediated), which are of exactly opposite sign to the SC asymmetries (55–58). Indeed, this is already known to be the case for perisaccadic suppression of visual sensitivity (53). Other human evidence includes perisaccadic visual meridian effects (59), visual field asymmetries in crowding and saccadic precision (60), and visual motion processing in the brain (for example, while walking) (61).

Combining all trials from both the low- and high-spatial frequency saccade targets, we compared mislocalization strength when the probe was presented in either the upper or lower visual field. That is, we explored the two oblique probe locations ahead of the saccade target location, which were perfectly symmetric with respect to the saccade vector, except for the visual field difference (METHODS). The results are shown in Fig. 5, which is formatted similarly to Fig. 3 and Fig. 4. However, here, instead of comparing the effects of the saccade target image appearance on mislocalization, we now compared probe flash locations. As can be seen, there was clearly stronger mislocalization in the upper, rather than lower, visual field. We tested this statistically with a repeated-measures two-way ANOVA (factors: time and probe location). The test results were significant for both the factors of time [$F(2,14) = 62.58$, $P < 10^{-6}$, $\eta^2 = 0.899$] and probe location [$F(1,7) = 23.22$, $P = 0.002$, $\eta^2 = 0.768$]. There was also a significant interaction between these two factors [$F(2,14) = 6.46$, $P = 0.01$, $\eta^2 = 0.48$) (Fig. 5*D*). Moreover, post hoc tests revealed that the difference between upper and lower visual field probe locations was significant at all three tested times (*t1*: $P = 0.001$; *t2*: $P = 0.005$; *t3*: $P = 0.014$) (Fig. 5*D*). Therefore, there was a clear dependence of perisaccadic mislocalization strength on visual field location, even with purely horizontal saccades. Note that we reached similar conclusions when we performed these analyses individually for either the low- or high-spatial frequency saccade targets as well (this can also be easily inferred from Fig. 2).

Thus, our results so far indicate that perisaccadic mislocalization depends on both saccade target image appearance (Figs. 2–4) and retinotopic probe flash location (Fig. 5). We next related these effects to unin-structed eye movements during the response phase of our experimental trials, and we then confirmed that our mislocalization observations were not explained by an altered visibility of the probe flashes by the visual conditions of our experiments.

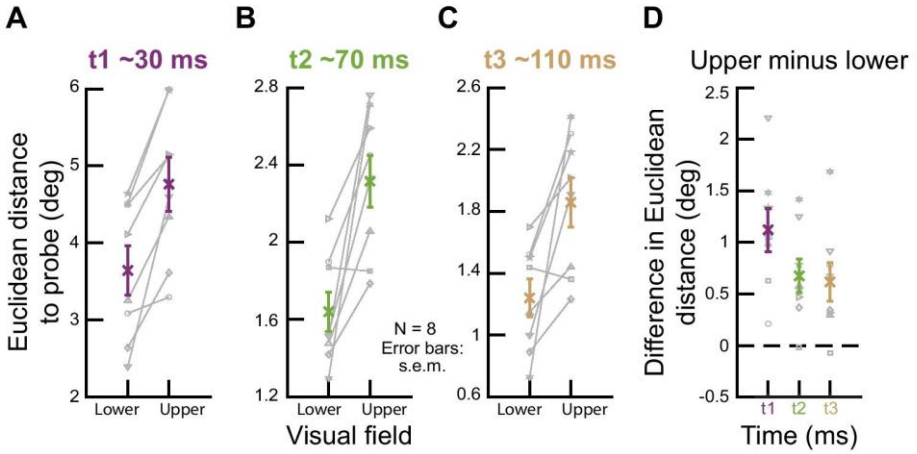

Figure 5. Stronger perisaccadic perceptual mislocalization for probe flashes in the upper, rather than lower, visual field. This figure is formatted identically to Fig. 3 except that the comparison is now between visual field locations rather than saccade target image appearances. Specifically, we now combined all trials, whether the spatial frequency of the saccade target grating was 0.5 or 5 cycles/°. Then, we considered the mislocalization strength of the 2 probe locations that were in oblique directions relative to the saccade target. Because of the configuration of our display, these 2 probe locations were at identical positions relative to the saccade target (METHODS). However, one of them was in the upper visual field, and the other was in the lower visual field. As can be seen, there was stronger mislocalization for upper visual field probes. All other conventions are identical to those in Fig. 3. *A*, *B*, and *C*: results for *times t1*, *t2*, and *t3*, respectively. *D*: difference between upper and lower visual fields.

J Neurophysiol • doi:10.1152/jn.00368.2024 • www.jn.org

Similar Mislocalization Effects by Analyzing Uninstructed Saccades While Subjects Responded

In our mislocalization paradigm, we did not provide any instructions to our subjects on what to do with their eyes while reporting their perceived flash locations via mouse cursor clicks (METHODS). Nonetheless, we consistently observed that the subjects automatically generated secondary saccades pointing almost exactly to where they clicked (Fig. 6*A* shows such example trials from one of our subjects). This prompted us to ask whether the eye movement end point locations at the time of mouse cursor clicks correlated with the mouse cursor click positions that we had asked for. This was most definitely the case. For example, for the same subject as in Fig. 6*A*, Fig. 6*B* plots the Euclidean distance between the mouse cursor click location and the true flash location on the *x*-axis, and the figure simultaneously plots, on the *y*-axis, the Euclidean distance between the same subject's eye position (measured −50 to 0 ms relative to mouse cursor click time) and the true flash location. The two measures were highly correlated (Pearson's $r = 0.92$; $P < 10^{-12}$; including all trials from the subject with all possible probe flash times and also pooling across spatial frequencies of the saccade target). This was also true across all of our subjects, as shown in Fig. 6*C*. In this figure, each subject is represented by three symbols covering the three possible flash times. As can be seen, there was clear correlation between mouse cursor reports and uninstructed eye position reports (Pearson's $r = 0.98$; $P < 10^{-17}$ across all shown data points). Therefore, in perisaccadic mislocalization paradigms (for example, in monkeys), it is possible to use secondary eye movements after the primary saccade of interest to objectively measure mislocalization effects (see DISCUSSION).

Similar Flash Visibility for Low- and High-Spatial Frequency Saccade Targets

In the above experiment and analyses, we were confident that the probe flashes were suprathreshold (and thus highly visible to the subjects) because of their high contrast (METHODS). Therefore, we interpreted the results as suggesting that mislocalization can indeed depend on the visual appearance of the saccade target (Figs. 1–4). However, it could still be the case that the appearance of the saccade target (especially given that it was a relatively big image patch) could, in one way or another, cause different detectability levels of the brief perisaccadic probe flashes. Therefore, in a second experiment, we explicitly characterized the detectability of the flashes at different contrast levels. This allowed us to confirm that the detectability of the high-contrast probe flashes in the results above was the same for either the low- or high-spatial frequency saccade targets.

We perisaccadically flashed brief, low-contrast probes (METHODS), and we measured contrast sensitivity curves. The paradigm itself was very similar to that used above. However, instead of localizing probe flashes, the subjects knew in advance that the probe could appear at one of the four cardinal directions around the saccade target (Fig. 7*A*; METHODS). They simply had to report which of the four locations displayed the flash.

As in the mislocalization experiment, we also had variable probe flash times relative to saccade onset. Specifically, Fig. 7*B* shows the timing of the probe flashes in this new experiment. As can be seen, the trigger points of the probe flashes after online saccade detection (METHODS) resulted in a bimodal distribution of flash times. The second mode (at

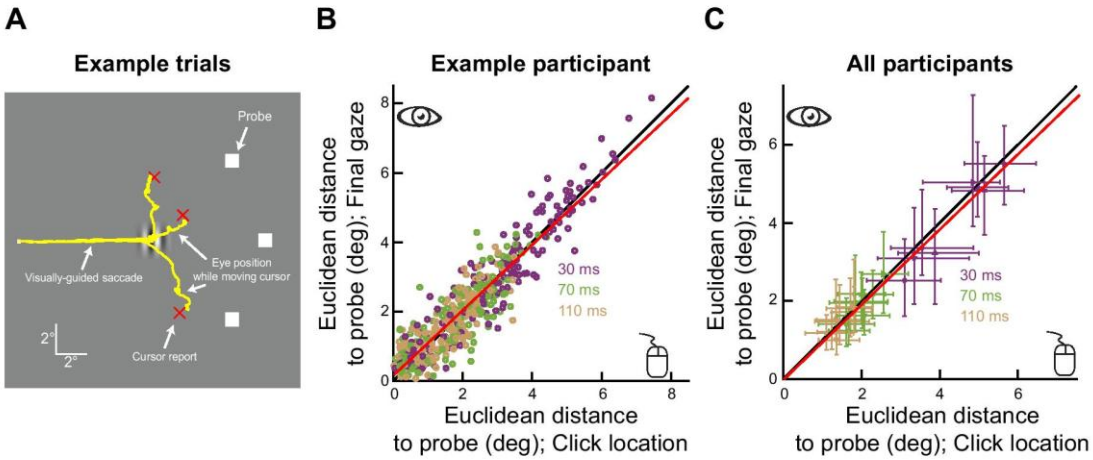

Figure 6. Uncovering of perisaccadic perceptual mislocalization via uninstructed eye movements during the reporting phase of our experimental trials. *A*: 3 example trials from 1 subject (different from that of Fig. 1 and Fig. 2), showing eye movement behavior and the corresponding cursor click locations for a probe flash presented at *time t1* in our perisaccadic mislocalization experiment. The primary, visually guided saccade was from the left to the right, and it is this saccade that was paired with a brief probe flash. When it was time to report the perceived flash location, there were uninstructed saccades by the subject while moving the cursor. The first of these saccades in each trial clearly reflected the mislocalization effect because it was very different from a veridical saccade to the true flash location (indicated by the white squares); the subject then typically made 1 or 2 more smaller saccades and fixations, to fine-tune the final report. In the end, eye position was very close to the final report (red cross) on each trial. Thus, uninstructed eye movements during the final reporting phase of our trials reflected the perisaccadic mislocalization effect. *B*: for the same subject, we measured the Euclidean distance of final eye position at the time of the cursor click to the true probe flash location. We then plotted this measure against the Euclidean distance of the cursor click location itself to the true probe flash location. There was a very high correlation across all trials (black is the unity slope line, and red is the regression line). *C*: median Euclidean distances of each subject for each flash probe time (each subject's data are represented by 3 distinct points for the 3 tested flash times). Error bars denote the 25th to 75th quantiles, and the red line is the regression fit to the data.

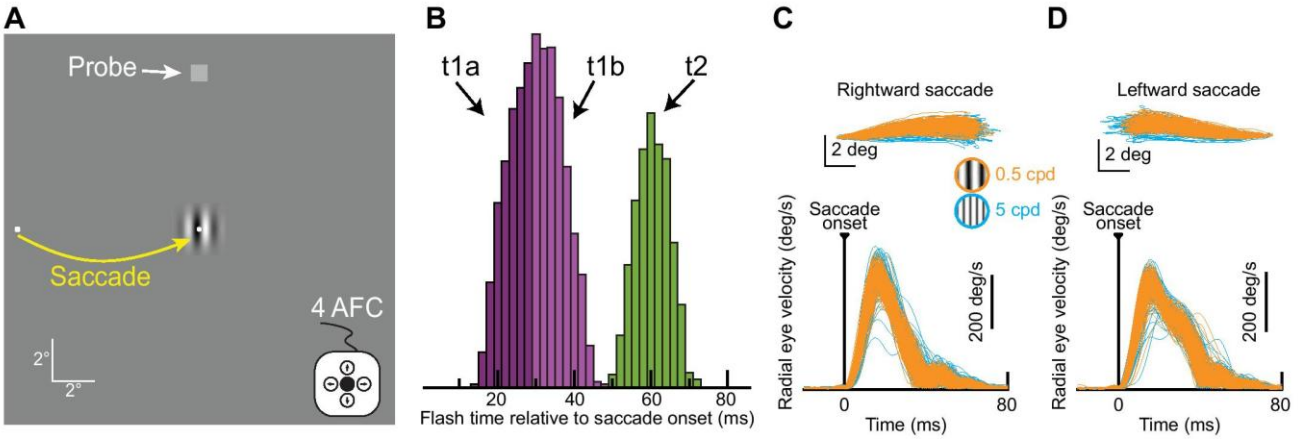

Figure 7. Probing perisaccadic perceptual detectability with different saccade target image appearances. *A*: subjects generated a rightward (shown) or leftward saccade toward the center of a low- or high-spatial frequency grating. At different times relative to online saccade detection, we presented a very brief probe flash at 1 of 4 cardinal positions (pure up shown). Subjects had to indicate at which 1 of the 4 locations they detected the stimulus [4-alternative forced choice (4 AFC) task]. *B*: distribution of flash times relative to saccade onset in our data from a sample subject (different from the ones of Figs. 1, 2, and 6). We classified flash times according to the 3 seen categorizations, and we labeled the categories *t1a*, *t1b*, and *t2*, respectively. *t2* was quantitatively similar to *t2* in the perceptual mislocalization experiment above. *C* and *D*: analyses similar to Fig. 1, *C* and *D*, demonstrating that we matched saccades in terms of both their metrics and kinematics across the 2 saccade target image appearances. cpd, cycles/°.

~70 ms; Fig. 7*B*) was very similar to that in *t2* of the original experiment. Since *time t2* in that experiment was still a time in which we had clear differential mislocalization performance for the two different saccade target image appearances (Figs. 2–5), this time bin in the current experiment was ideal to check whether the detectability of the probe flashes was any different for the two different saccade target image features. We thus labeled this second mode in Fig. 7*B* as *t2*, since it was quantitatively similar to *time t2* in the original experiment. As for the first mode in the histogram of Fig. 7*A*, we split it into two subcategories (*t1a* and *t1b*) because we wanted to check for a worst-case scenario about potential visibility differences with maximal saccadic suppression, which would be expected for *t1a* (the closest time to saccade onset).

In the current experiment, we also matched the saccade metrics and kinematics across the two different image appearances of the saccade target, just like we did in the perisaccadic mislocalization experiment above. For example, Fig. 7, *C* and *D*, show eye movement analyses very similar to those in Fig. 1, *C* and *D*, from a sample subject. As can be seen, the saccade properties were well matched across the two different image appearances of the saccade target. Therefore, we could now check the psychometric curves.

Even under the worst-case scenario of maximal saccadic suppression, perceptual detection reached ceiling performance at probe luminances well below those that we used in the perisaccadic mislocalization experiment described above. This can be seen from Fig. 8. In Fig. 8*A*, we show the psychometric curves of performance from one example subject (the same one as in Fig. 7, *C* and *D*). One pair of curves is for probe flashes occurring at *time t1a* from Fig. 7*B*, and another pair is for probe flashes occurring at *time t2*. In each pair, one curve is for the low-spatial frequency saccade target, and the other is for the high-spatial frequency saccade target. For reference, the probe contrast used in the perisaccadic mislocalization experiment above was at an *x*-axis value of 70 in these psychometric curves. Thus, in all cases, this subject's performance reached ceiling performance for much lower probe contrasts, even at the worst-case scenario of near-maximal saccadic suppression. Importantly, at *time t2*, when mislocalization still showed significant differential effects between saccade target appearances (Figs. 2–4), the full psychometric curves in this current experiment were completely overlapping (and with very low detection thresholds). Thus, the results of Figs. 2–4 cannot be explained by different probe detectability due to the different saccade target image appearances used in the experiments.

These results were consistent across all eight subjects (Fig. 8*B*). Interestingly, at the population level, we found a small, but significant ($P < 0.05$; bootstrapping; METHODS) difference in the semisaturation contrasts of the two saccade target image appearances only at *time t1a* (but not at *times t1b* and *t2*). This might suggest that even perisaccadic suppression itself, which can putatively also rely on corollary discharge information (28, 62), might also depend on the saccade target visual features. This is consistent with both the predictions of the neurophysiology (39) and the general motivations for the present study. Nonetheless, from the perspective of perisaccadic mislocalization, which is the main topic of the present study, the most important feature of the results of Fig. 8*B* is that, at the probe contrasts used in Figs. 1–5 (*x*-axis luminance of 70 in Fig. 8*B*), perceptual detectability of the probe flashes was clearly at ceiling and did not depend on the saccade target image appearance. Thus, the results of Figs. 2–4 cannot be explained by visual-visual interactions caused by the different image appearances of the low- and high-spatial frequency saccade target gratings.

Therefore, our observations, combined, suggest that perisaccadic mislocalization seems to depend on the visual appearance of the saccade target (Figs. 1–4) and that this dependence is not explained by a simple visual interaction

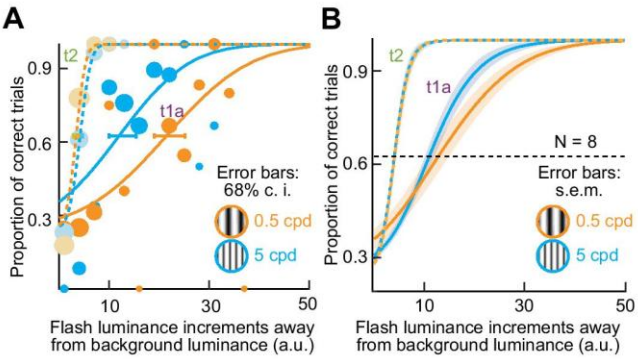

Figure 8. Dependence of probe detection on the saccade target image appearance, but only for very low-contrast probes and only during maximal saccadic suppression. *A*: psychometric curves of perceptual detection performance from 1 example subject (same as that of Fig. 7). Since this was a 4-alternative forced choice task, chance performance was at a 25% correctness rate, and threshold was defined as the contrast giving rise to a 62.5% correctness rate. When the probe appeared during *time t1a* in Fig. 7*B*. the subject showed a higher detection threshold for the low-spatial frequency saccade target than for the high-spatial frequency saccade target. However, note that ceiling performance was reached by luminance index 50 above background. For reference, the probe luminance in Figs. 1–5 was at 70 on the *x*-axis. Thus, even at *time t1a*, the probe in Figs. 1–5 was highly detectable. For *time t2*, the thresholds were much lower, and the psychometric curves were almost completely overlapping. Note that at this time perceptual mislocalization still significantly differentiated between the saccade target image appearances (Figs. 2–4), suggesting that such differentiation was not mediated by different probe visibility for the 2 different types of saccade targets that we used. Error bars denote 68% confidence interval (c.i.). The size of each shown data point is scaled by the numbers of observations. a.u., Arbitrary units. *B*: population results. Each curve shows the average of the 8 subjects' psychometric curves, and error bars denote SE. At *time t1a*, there was a small threshold difference between the different saccade target appearances ($P < 0.05$; bootstrapping; METHODS). However, at *t2* (and *t1b*; not shown), there were no differences. Importantly, performance was clearly at ceiling at the probe contrasts used in the mislocalization experiment. Thus, the results of Figs. 2–5 cannot be explained by altered detectability of the probe flashes by the different saccade target image appearances.

between such appearance and the ability to detect high-contrast perisaccadic probe flashes (Fig. 7 and Fig. 8).

DISCUSSION

In this study, we were motivated by our recent observations that SC motor bursts can be different for different visual appearances of the saccade target, even with matched saccade metrics and kinematics (39). Such difference suggests that the motor bursts in the SC might be dissociated from the exact moment-to-moment execution of the eye movements (23, 63). Assuming that such visual sensory tuning in SC motor bursts underlies a function, we hypothesize that it is used via the ascending projections from the SC to other brain areas. Such projections may be thought of as corollary discharge (24, 31, 32, 64): neurons on the SC map that are active at the time of saccade onset indicate the vector of the intended saccade (65), and such vector information (and the concomitant time-locked onset of the bursts) could help to either suppress visual sensitivity (29, 66) or remap retinotopic response fields (32) in the cortex. Given that the SC integrates a large amount of visual information from many brain areas, including from the retina (67), visual information in the SC motor bursts at the time of saccades could allow the predictive processes associated with corollary discharge (29, 32, 38, 68) to be more general than just informing cortex of the timing and vector of saccades. These processes could additionally enable transsaccadic feature prediction to anticipate the foveated image appearance after the saccade. In other words, visual information in the SC at the time of saccade onset could be relayed for postsaccadic visual processing in the fovea. Although this idea needs to be explicitly tested neurophysiologically (for example, by investigating the transfer of visual information to foveal neurons in the SC and elsewhere across saccades), our goal here was to check whether perceptual correlates of it could potentially be observed. Thus, the scope of our present contribution is solely the documentation of a new type of phenomenology that is associated with perisaccadic mislocalization.

We specifically found that the properties of perisaccadic mislocalization depended on the appearance of the saccade target. Moreover, this effect was not explained by different visibility of the perisaccadic high-contrast probe flashes as a function of the saccade target appearance. We believe that these results motivate revisiting earlier neurophysiological investigations of corollary discharge from the SC (25, 26, 29, 31, 64, 66), but now from the perspective of saccades to images. For example, one could start mapping neurons in the pulvinar or medio-dorsal thalamus, which are involved in corollary discharge signaling from the SC to the cortex, but specifically during active vision tasks involving saccades to images rather than to spots. This could clarify if and how these brain areas may relay information about the visual appearance of saccade targets to their recipient neurons. It could also help explain what other roles these relay areas might have. For example, if SC visual responses, and not just saccade-related motor bursts, are relayed (25), then what is the purpose of such relaying, and what are the feature tuning properties of visual responses in areas like the pulvinar and the medio-dorsal thalamus?

These and related questions can also help identify the potential ecological benefits of having stronger perisaccadic mislocalization for low-spatial frequency saccade targets, as we found here. Of course, in general, we believe that it would be quite rare to experience perisaccadic mislocalization in real life, since it is unlikely that brief visual stimuli will suddenly appear right around the time of a saccade. However, and as mentioned above, the key to perisaccadic mislocalization is that the mechanisms revealed by such a laboratory phenomenon will still be relevant in everyday life. We speculate that certain aspects of visual processing in the brain must (and do) emphasize the processing of low spatial frequencies in the incoming retinal images, particularly given the known spectral content of natural scenes (69, 70). For example, saccades in both humans and monkeys have consistently faster reaction times for low-spatial frequency targets (71–73), and SC visual responses are consistently stronger and earlier for low-spatial frequency images (73). Thus, it could be that an alteration of transsaccadic processing for low-spatial frequency saccade targets, as revealed by stronger perisaccadic mislocalization, enables a targeted highlighting, both pre- and postsaccadically, of such important images.

Although we did not focus on perisaccadic suppression too much in our present study, our second experiment already allowed us to additionally measure perceptual suppression at *time t1a* (Fig. 7 and Fig. 8). Interestingly, both the sample subject (Fig. 8*A*) and the population of subjects (Fig. 8*B*) showed that there was potentially stronger suppression (higher thresholds in the psychometric curves) when the saccade target had a low spatial frequency than when it had a high spatial frequency. This might suggest that even saccadic suppression strength, and not just perisaccadic mislocalization, can depend on the visual appearance of the saccade targets. In addition to being consistent with our hypotheses above about corollary discharge incorporating saccade target appearance in its signal, this is also consistent with our observations on perisaccadic mislocalization in our main experiment. Indeed, we previously measured perceptual saccadic suppression in humans, with saccades across different visual textures, and we again observed stronger perisaccadic suppression with low-spatial frequency textures (14). Although our interpretations in that earlier study focused on the visual components of perisaccadic suppression, results from the present study and the sensory-tuned SC motor bursts (39) hint that motor-related components could also potentially account for at least some of these differences. Nonetheless, what is clear from our present detection experiments is that they cannot fully explain the mislocalization ones. This is because the probe contrasts in the mislocalization experiments were very high compared to when there could be any potential image dependencies of detection performance. In fact, at *time t2*, the detection psychometric curves were completely overlapping for the two different saccade target image appearances (and almost fully recovered relative to *time t1a*), but the mislocalization strength was still different.

Having said that, the saccade target in our experiment (and not just the representations of the probe flashes) was swept on the retina across saccades. As a result, there was a retinal motion sweep, which could potentially contribute to our observed results. In other words, if the motion sweep had different properties for the two different saccade target images, then it could still be possible that visual-visual interactions could account for our observations of different mislocalization strengths across the image types. However, by deliberate experimental design choice, our gratings were orthogonal to the saccade vector direction. Thus, there was maximal retinal blurring of these gratings by the saccades. So, it seems less likely that this could have fully explained our mislocalization results. Moreover, we always placed a small fixation spot (over a gray background) right in the middle of each grating (39), which further allowed us to control for the postsaccadic fixation statistics across trials (and independently of the spatial frequency of the saccade target). Also, our detectability experiments suggested that the probe contrast was so much above threshold contrast, especially at *time t2*, as to be affected by potential subtle differences in the retinal motion sweeps associated with low- and high-spatial frequency grating saccade targets. Finally, perisaccadic mislocalization can still occur with saccades toward a blank (74).

More generally, we believe that our experiments motivate the study of visual perception from an active perspective. In addition, taking a more ecological approach to active vision than with simple dot stimuli would be useful. It can reveal visual-visual and visual-motor interactions that are most relevant for natural behavior. More importantly, such an ecological perspective should also consider the state of the body itself, and not just the environmental context (63). Indeed, maintaining proper bodily posture and orientation requires a sustained tonic activation of eye and neck muscles, and proprioception of the neck muscles can have a significant impact on aligning a pointing response with a visual target impinging on the retina (63). Taking such an approach can merge fields of vision, oculomotor control, body posture, and reference frames in a most interesting manner.

In our case, our segue into an ecological approach was driven by our interest in visual field asymmetries. For example, it is believed that overrepresentation of the upper visual field by the SC (22) could be ecologically relevant for active orienting across species (67, 75). Intriguingly, this motivated us to explore the effects of upper and lower visual field flashes in terms of mislocalization strength (Fig. 5), and we indeed found stronger perisaccadic mislocalization in the upper visual field. This is reminiscent of a differential effect also in saccadic suppression strength between the upper and lower visual fields (53), and it would be interesting in the future to further merge the topics of visual field asymmetries and perisaccadic vision but from a much more neurophysiological perspective.

In that regard, we have already utilized our observations in Fig. 6 to port our visual mislocalization paradigms to the monkey animal model (for further neurophysiology) (76). Specifically, the results of Fig. 6 provided us with very useful information because they suggest that one could train monkeys to report their perceived flash location with a secondary eye movement after the primary one. This opens the door for advanced neurophysiological experiments, including with causal perturbation manipulations, using identical behavioral paradigms to humans. This is an enticing opportunity.

DATA AVAILABILITY

Data will be made available upon reasonable request.

GRANTS

We were funded by the Deutsche Forschungsgemeinschaft (DFG; German Research Foundation) through the SFB 1233 Robust Vision (project number: 276693517). We were also funded by the DFG through the SPP 2205 Evolutionary Optimization of Neuronal Processing (project number: HA 6749/3-2) and the SPP 2411 Sensing LOOPS: Cortico-subcortical Interactions for Adaptive Sensing (project number: HA 6749/11-1).

DISCLOSURES

No conflicts of interest, financial or otherwise, are declared by the authors.

AUTHOR CONTRIBUTIONS

M.P.B., A.F.D., and Z.M.H. conceived and designed research; performed experiments; analyzed data; interpreted results of experiments; prepared figures; drafted manuscript; edited and revised manuscript; and approved final version of manuscript.

REFERENCES

1. **Bridgeman B**, **Hendry D**, **Stark L.** Failure to detect displacement of the visual world during saccadic eye movements. *Vision Res* 15: 719–722, 1975. doi:10.1016/0042-6989(75)90290-4.
2. **Bridgeman B**, **van der Heijden AH**, **Velichkovsky BM.** A theory of visual stability across saccadic eye movements. *Behav Brain Sci* 17: 247–258, 1994. doi:10.1017/S0140525X00034361.
3. **Schweitzer R**, **Rolfs M.** Intra-saccadic motion streaks as cues to linking object locations across saccades. *J Vis* 20: 17, 2020. doi:10.1167/jov.20.4.17.
4. **Rolfs M**, **Schweitzer R.** Coupling perception to action through incidental sensory consequences of motor behaviour. *Nat Rev Psychol* 1: 112–123, 2022. doi:10.1038/s44159-021-00015-x.
5. **Honda H.** Perceptual localization of visual stimuli flashed during saccades. *Percept Psychophys* 45: 162–174, 1989. doi:10.3758/bf03208051.
6. **Dassonville P**, **Schlag J**, **Schlag-Rey M.** Oculomotor localization relies on a damped representation of saccadic eye displacement in human and nonhuman primates. *Vis Neurosci* 9: 261–269, 1992. doi:10.1017/s0952523800010671.
7. **Latour PL.** Visual threshold during eye movements. *Vision Res* 2: 261–262, 1962. doi:10.1016/0042-6989(62)90031-7.
8. **Zuber BL**, **Stark L.** Saccadic suppression: elevation of visual threshold associated with saccadic eye movements. *Exp Neurol* 16: 65–79, 1966. doi:10.1016/0014-4886(66)90087-2.
9. **Beeler GW Jr.** Visual threshold changes resulting from spontaneous saccadic eye movements. *Vision Res* 7: 769–775, 1967. doi:10.1016/0042-6989(67)90039-9.
10. **Cai RH**, **Pouget A**, **Schlag-Rey M**, **Schlag J.** Perceived geometrical relationships affected by eye-movement signals. *Nature* 386: 601–604, 1997. doi:10.1038/386601a0.
11. **Ross J**, **Morrone MC**, **Burr DC.** Compression of visual space before saccades. *Nature* 386: 598–601, 1997. doi:10.1038/386598a0.
12. **Hafed ZM**, **Krauzlis RJ.** Microsaccadic suppression of visual bursts in the primate superior colliculus. *J Neurosci* 30: 9542–9547, 2010. doi:10.1523/JNEUROSCI.1137-10.2010.
13. **Chen CY**, **Hafed ZM.** A neural locus for spatial-frequency specific saccadic suppression in visual-motor neurons of the primate superior colliculus. *J Neurophysiol* 117: 1657–1673, 2017. doi:10.1152/jn.00911.2016.
14. **Idrees S**, **Baumann MP**, **Franke F**, **Münch TA**, **Hafed ZM.** Perceptual saccadic suppression starts in the retina. *Nat Commun* 11: 1977, 2020. doi:10.1038/s41467-020-15890-w.
15. **Lappe M**, **Awater H**, **Krekelberg B.** Postsaccadic visual references generate presaccadic compression of space. *Nature* 403: 892–895, 2000. doi:10.1038/35002588.
16. **Kaiser M**, **Lappe M.** Perisaccadic mislocalization orthogonal to saccade direction. *Neuron* 41: 293–300, 2004. doi:10.1016/s0896-6273(03)00849-3.
17. **Grujic N**, **Brehm N**, **Gloge C**, **Zhuo W**, **Hafed ZM.** Perisaccadic perceptual mislocalization is different for upward saccades. *J Neurophysiol* 120: 3198–3216, 2018. doi:10.1152/jn.00350.2018.
18. **Klingenhoefer S**, **Krekelberg B.** Perisaccadic visual perception. *J Vis* 17: 16, 2017. doi:10.1167/17.9.16.
19. **Ostendorf F**, **Fischer C**, **Gaymard B**, **Ploner CJ.** Perisaccadic mislocalization without saccadic eye movements. *Neuroscience* 137: 737–745, 2006. doi:10.1016/j.neuroscience.2005.09.032.
20. **VanRullen R.** A simple translation in cortical log-coordinates may account for the pattern of saccadic localization errors. *Biol Cybern* 91: 131–137, 2004. doi:10.1007/s00422-004-0514-2.
21. **Chen CY**, **Hoffmann KP**, **Distler C**, **Hafed ZM.** The foveal visual representation of the primate superior colliculus. *Curr Biol* 29: 2109–2119.e7, 2019. doi:10.1016/j.cub.2019.05.040.
22. **Hafed ZM**, **Chen CY.** Sharper, stronger, faster upper visual field representation in primate superior colliculus. *Curr Biol* 26: 1647–1658, 2016. doi:10.1016/j.cub.2016.04.059.
23. **Zhang T**, **Malevich T**, **Baumann MP**, **Hafed ZM.** Superior colliculus saccade motor bursts do not dictate movement kinematics. *Commun Biol* 5: 1222, 2022. doi:10.1038/s42003-022-04203-0.
24. **Sommer MA**, **Wurtz RH.** A pathway in primate brain for internal monitoring of movements. *Science* 296: 1480–1482, 2002. doi:10.1126/science.1069590.
25. **Sommer MA**, **Wurtz RH.** What the brain stem tells the frontal cortex. I. Oculomotor signals sent from superior colliculus to frontal eye field via mediodorsal thalamus. *J Neurophysiol* 91: 1381–1402, 2004. doi:10.1152/jn.00738.2003.
26. **Sommer MA**, **Wurtz RH.** What the brain stem tells the frontal cortex. II. Role of the SC-MD-FEF pathway in corollary discharge. *J Neurophysiol* 91: 1403–1423, 2004. doi:10.1152/jn.00740.2003.
27. **Sommer MA**, **Wurtz RH.** Brain circuits for the internal monitoring of movements. *Annu Rev Neurosci* 31: 317–338, 2008. doi:10.1146/annurev.neuro.31.060407.125627.
28. **Berman RA**, **Joiner WM**, **Cavanaugh J**, **Wurtz RH.** Modulation of presaccadic activity in the frontal eye field by the superior colliculus. *J Neurophysiol* 101: 2934–2942, 2009. doi:10.1152/jn.00053.2009.
29. **Berman RA**, **Cavanaugh J**, **McAlonan K**, **Wurtz RH.** A circuit for saccadic suppression in the primate brain. *J Neurophysiol* 117: 1720–1735, 2017. doi:10.1152/jn.00679.2016.
30. **Shin S**, **Sommer MA.** Division of labor in frontal eye field neurons during presaccadic remapping of visual receptive fields. *J Neurophysiol* 108: 2144–2159, 2012. doi:10.1152/jn.00204.2012.
31. **Guthrie BL**, **Porter JD**, **Sparks DL.** Corollary discharge provides accurate eye position information to the oculomotor system. *Science* 221: 1193–1195, 1983. doi:10.1126/science.6612334.
32. **Sommer MA**, **Wurtz RH.** Influence of the thalamus on spatial visual processing in frontal cortex. *Nature* 444: 374–377, 2006. doi:10.1038/nature05279.
33. **Zirnsak M**, **Steinmetz NA**, **Noudoost B**, **Xu KZ**, **Moore T.** Visual space is compressed in prefrontal cortex before eye movements. *Nature* 507: 504–507, 2014. doi:10.1038/nature13149.
34. **Zirnsak M**, **Moore T.** Saccades and shifting receptive fields: anticipating consequences or selecting targets? *Trends Cogn Sci* 18: 621–628, 2014. doi:10.1016/j.tics.2014.10.002.
35. **Hartmann TS**, **Zirnsak M**, **Marquis M**, **Hamker FH**, **Moore T.** Two types of receptive field dynamics in area V4 at the time of eye movements? *Front Syst Neurosci* 11: 13, 2017. doi:10.3389/fnsys.2017.00013.
36. **Neupane S**, **Guitton D**, **Pack CC.** Dissociation of forward and convergent remapping in primate visual cortex. *Curr Biol* 26: R491–R492, 2016. doi:10.1016/j.cub.2016.04.050.
37. **Neupane S**, **Guitton D**, **Pack CC.** Two distinct types of remapping in primate cortical area V4. *Nat Commun* 7: 10402, 2016. doi:10.1038/ncomms10402.
38. **Wang X**, **Fung CC**, **Guan S**, **Wu S**, **Goldberg ME**, **Zhang M.** Perisaccadic receptive field expansion in the lateral intraparietal area. *Neuron* 90: 400–409, 2016. doi:10.1016/j.neuron.2016.02.035.
39. **Baumann MP**, **Bogadhi AR**, **Denninger AF**, **Hafed ZM.** Sensory tuning in neuronal movement commands. *Proc Natl Acad Sci USA* 120: e2305759120, 2023. doi:10.1073/pnas.2305759120.
40. **Baumann MP**, **Idrees S**, **Münch TA**, **Hafed ZM.** Dependence of perceptual saccadic suppression on peri-saccadic image flow properties and luminance contrast polarity. *J Vis* 21: 15, 2021. doi:10.1167/jov.21.5.15.
41. **Hafed ZM.** Alteration of visual perception prior to microsaccades. *Neuron* 77: 775–786, 2013. doi:10.1016/j.neuron.2012.12.014.
42. **Brainard DH.** The Psychophysics Toolbox. *Spat Vis* 10: 433–436, 1997.
43. **Kleiner M**, **Brainard D**, **Pelli DG.** What's new in Psychtoolbox-3? (Abstract). *Perception* 36, 2007.
44. **Pelli DG.** The VideoToolbox software for visual psychophysics: transforming numbers into movies. *Spat Vis* 10: 437–442, 1997.
45. **Cornelissen FW**, **Peters EM**, **Palmer J.** The Eyelink Toolbox: eye tracking with MATLAB and the Psychophysics Toolbox. *Behav Res Methods Instrum Comput* 34: 613–617, 2002. doi:10.3758/bf03195489.
46. **Greilich J**, **Baumann MP**, **Hafed ZM.** Microsaccadic suppression of peripheral perceptual detection performance as a function of foveated visual image appearance. *J Vis* 24: 3, 2024. doi:10.1167/jov.24.11.3.
47. **Chen CY**, **Hafed ZM.** Postmicrosaccadic enhancement of slow eye movements. *J Neurosci* 33: 5375–5386, 2013. doi:10.1523/JNEUROSCI.3703-12.2013.
48. **Willeke KF**, **Tian X**, **Buonocore A**, **Bellet J**, **Ramirez-Cardenas A**, **Hafed ZM.** Memory-guided microsaccades. *Nat Commun* 10: 3710, 2019. doi:10.1038/s41467-019-11711-x.

49. **Willeke KF**, **Cardenas AR**, **Bellet J**, **Hafed ZM.** Severe distortion in the representation of foveal visual image locations in short-term memory. *Proc Natl Acad Sci USA* 119: e2121860119, 2022. doi:10.1073/pnas.2121860119.
50. **Bellet ME**, **Bellet J**, **Nienborg H**, **Hafed ZM**, **Berens P.** Human-level saccade detection performance using deep neural networks. *J Neurophysiol* 121: 646–661, 2019. doi:10.1152/jn.00601.2018.
51. **Bahill AT**, **Clark MR**, **Stark L.** The main sequence, a tool for studying human eye movements. *Math Biosci* 24: 191–204, 1975. doi:10.1016/0025-5564(75)90075-9.
52. **Zuber BL**, **Stark L**, **Cook G.** Microsaccades and the velocity-amplitude relationship for saccadic eye movements. *Science* 150: 1459–1460, 1965. doi:10.1126/science.150.3702.1459.
53. **Fracasso A**, **Buonocore A**, **Hafed ZM.** Peri-saccadic orientation identification performance and visual neural sensitivity are higher in the upper visual field. *J Neurosci* 43: 6884–6897, 2023. doi:10.1523/JNEUROSCI.1740-22.2023.
54. **Schütt HH**, **Harmeling S**, **Macke JH**, **Wichmann FA.** Painfree and accurate Bayesian estimation of psychometric functions for (potentially) overdispersed data. *Vision Res* 122: 105–123, 2016. doi:10.1016/j.visres.2016.02.002.
55. **Barbot A**, **Xue S**, **Carrasco M.** Asymmetries in visual acuity around the visual field. *J Vis* 21: 2, 2021. doi:10.1167/jov.21.1.2.
56. **Montaser-Kouhsari L**, **Carrasco M.** Perceptual asymmetries are preserved in short-term memory tasks. *Atten Percept Psychophys* 71: 1782–1792, 2009. doi:10.3758/APP.71.8.1782.
57. **He S**, **Cavanagh P**, **Intriligator J.** Attentional resolution and the locus of visual awareness. *Nature* 383: 334–337, 1996. doi:10.1038/383334a0.
58. **Rubin N**, **Nakayama K**, **Shapley R.** Enhanced perception of illusory contours in the lower versus upper visual hemifields. *Science* 271: 651–653, 1996. doi:10.1126/science.271.5249.651.
59. **Liu X**, **Melcher D**, **Carrasco M**, **Hanning NM.** Presaccadic preview shapes postsaccadic processing more where perception is poor. *Proc Natl Acad Sci USA* 121: e2411293121, 2024. doi:10.1073/pnas.2411293121.
60. **Greenwood JA**, **Szinte M**, **Sayim B**, **Cavanagh P.** Variations in crowding, saccadic precision, and spatial localization reveal the shared topology of spatial vision. *Proc Natl Acad Sci USA* 114: E3573–E3582, 2017. doi:10.1073/pnas.1615504114.
61. **Gilaie-Dotan S.** Visual motion serves but is not under the purview of the dorsal pathway. *Neuropsychologia* 89: 378–392, 2016. doi:10.1016/j.neuropsychologia.2016.07.018.
62. **Diamond MR**, **Ross J**, **Morrone MC.** Extraretinal control of saccadic suppression. *J Neurosci* 20: 3449–3455, 2000. doi:10.1523/JNEUROSCI.20-09-03449.2000.
63. **Goffart L.** Cerebralization of mathematical quantities and physical features in neural science: a critical evaluation. *Eur Phys J Web Conf* 300: 01007, 2024. doi:10.1051/epjconf/202430001007.
64. **Sparks DL**, **Porter JD.** Spatial localization of saccade targets. II. Activity of superior colliculus neurons preceding compensatory saccades. *J Neurophysiol* 49: 64–74, 1983. doi:10.1152/jn.1983.49.1.64.
65. **Lee C**, **Rohrer WH**, **Sparks DL.** Population coding of saccadic eye movements by neurons in the superior colliculus. *Nature* 332: 357–360, 1988. doi:10.1038/332357a0.
66. **Berman RA**, **Wurtz RH.** Signals conveyed in the pulvinar pathway from superior colliculus to cortical area MT. *J Neurosci* 31: 373–384, 2011. doi:10.1523/JNEUROSCI.4738-10.2011.
67. **Hafed ZM**, **Hoffmann KP**, **Chen CY**, **Bogadhi AR.** Visual functions of the primate superior colliculus. *Annu Rev Vis Sci* 9: 361–383, 2023. doi:10.1146/annurev-vision-111022-123817.
68. **Duhamel JR**, **Colby CL**, **Goldberg ME.** The updating of the representation of visual space in parietal cortex by intended eye movements. *Science* 255: 90–92, 1992. doi:10.1126/science.1553535.
69. **Ruderman DL**, **Bialek W.** Statistics of natural images: scaling in the woods. *Phys Rev Lett* 73: 814–817, 1994. doi:10.1103/PhysRevLett.73.814.
70. **Tolhurst DJ**, **Tadmor Y**, **Chao T.** Amplitude spectra of natural images. *Ophthalmic Physiol Opt* 12: 229–232, 1992. doi:10.1111/j.1475-1313.1992.tb00296.x.
71. **White BJ**, **Stritzke M**, **Gegenfurtner KR.** Saccadic facilitation in natural backgrounds. *Curr Biol* 18: 124–128, 2008. doi:10.1016/j.cub.2007.12.027.
72. **Ludwig CJ**, **Gilchrist ID**, **McSorley E.** The influence of spatial frequency and contrast on saccade latencies. *Vision Res* 44: 2597–2604, 2004. doi:10.1016/j.visres.2004.05.022.
73. **Chen CY**, **Sonnenberg L**, **Weller S**, **Witschel T**, **Hafed ZM.** Spatial frequency sensitivity in macaque midbrain. *Nat Commun* 9: 2852, 2018. doi:10.1038/s41467-018-05302-5.
74. **Zimmermann E**, **Morrone MC**, **Burr DC.** The visual component to saccadic compression. *J Vis* 14: 13, 2014. doi:10.1167/14.12.13.
75. **Previc FH.** Functional specialization in the lower and upper visual-fields in humans - its ecological origins and neurophysiological implications. *Behav Brain Sci* 13: 519–542, 1990. doi:10.1017/S0140525X00080018.
76. **Baumann MP, Hafed ZM.** Two-dimensional perisaccadic visual mislocalization in rhesus macaque monkeys (Preprint). *bioRxiv*, 2024. doi:10.1101/2024.11.20.624548.

Appendix E: Publication 5

Two-dimensional perisaccadic visual mislocalization in rhesus macaque monkeys

Baumann, M. P., & Hafed, Z. M.

BioRxiv, (2025)

doi: https://doi.org/10.1101/2024.11.20.624548

Title:

Two-dimensional perisaccadic visual mislocalization in rhesus macaque monkeys

Abbreviated title:

Perisaccadic mislocalization in macaque monkeys

Authors:

Matthias P. Baumann[1,2] and Ziad M. Hafed[1,2]

1. Werner Reichardt Centre for Integrative Neuroscience, University of Tübingen, Tübingen, Germany, 72076
2. Hertie Institute for Clinical Brain Research, University of Tübingen, Tübingen, Germany, 72076

Correspondence:

Z. Hafed: ziad.m.hafed@cin.uni-tuebingen.de

Acknowledgements:

We thank Tong Zhang, Tatiana Malevich, and Antimo Buonocore for help in data collection.

Conflict of interest:

Authors report no conflict of interest.

Funding sources:

We were funded by the Deutsche Forschungsgemeinschaft (DFG; German Research Foundation) through the SFB 1233 Robust Vision (project number: 276693517) as well as the SPP 2205 Evolutionary Optimization of Neuronal Processing (project number: HA 6749/3-2) and the SPP 2411 Sensing LOOPS: Cortico-subcortical Interactions for Adaptive Sensing (project numbers: 520617944 and 520283985, HA 6749/11-1).

Abstract

Perceptual localization of brief, high contrast perisaccadic visual probes is grossly erroneous. While this phenomenon has been extensively studied in humans, more needs to be learned about its underlying neural mechanisms. This ideally requires running similar behavioral paradigms in animals. However, during neurophysiology, neurons encountered in the relevant sensory and sensory-motor brain areas for visual mislocalization can have arbitrary, non-cardinal response field locations. This necessitates using mislocalization paradigms that can work with any saccade direction. Here, we first established such a paradigm in three male rhesus macaque monkeys. In every trial, the monkeys generated a visually-guided saccade towards an eccentric target. Once a saccade onset was detected, we presented a brief flash at one of three possible locations ahead of the saccade target location. After an experimentally-imposed delay period, we removed the saccade target, and the monkeys were then required to generate a memory-guided saccade towards the remembered flash location. All three monkeys readily learned the task, and, like humans, they all showed strong backward mislocalization towards the saccade target, which recovered for later flashes from the saccade time. Importantly, we then replicated a well-known property of human perisaccadic mislocalization, as revealed by two-dimensional mislocalization paradigms: that mislocalization is strongest for upward saccades. For horizontal saccades, we additionally found stronger mislocalization for upper visual field flashes, again consistent with humans. Our results establish a robust two-dimensional mislocalization paradigm in monkeys, and they pave the way for exploring the neural mechanisms underlying the dependence of perisaccadic mislocalization strength on saccade direction.

Significance statement

Visual perception is strongly altered around the time of saccades. Such alteration is often studied by characterizing how brief perisaccadic visual flashes are perceptually localized. While the properties of visual mislocalization have been exhaustively studied, the underlying neural mechanisms remain elusive, and this is due to a lack of suitable behavioral paradigms in animal models. We describe such a paradigm for macaques, which are ideal for exploring sensory-motor neural processes related to perisaccadic mislocalization.

Introduction

Studying visual perception requires investigating the interplays between visual sensory processing and eye movements. This is because eye movements, such as saccades, can drastically alter retinal images even if the external environment is completely stable.

Multiple alterations in visual information processing are known to accompany saccades. For example, perisaccadic visual sensitivity is reduced, sometimes rendering brief visual presentations completely invisible (Latour, 1962; Zuber and Stark, 1966; Beeler, 1967). Moreover, when stimulus contrasts are high enough to be detected, these stimuli are grossly mislocalized (Honda, 1989; Cai et al., 1997; Ross et al., 1997). Such mislocalization depends on various factors related to the visual environment (Lappe et al., 2000). For example, in complete darkness, brief presaccadic flashes are perceived to have appeared ahead of their true positions (Dassonville et al., 1992; Lappe et al., 2000); such mislocalization is often referred to as forward mislocalization, since the error in reported position has a vector of similar direction to the saccade vector direction (Klingenhoefer and Krekelberg, 2017). Interestingly, the mislocalization is biphasic (Honda, 1991, 1993), with postsaccadic flashes being perceived as having been shifted opposite, rather than along, the saccade vector. On the other hand, with visual references, perisaccadic mislocalization is no longer biphasic, and appears like a "compression" towards the saccade target: brief flashes presented ahead of the saccade target experience mislocalization in the opposite direction from the saccade, even presaccadically (Ross et al., 1997; Klingenhoefer and Krekelberg, 2017); flashes presented in between the initial gaze position and the saccade target undergo forward mislocalization. Such "compression" could reflect the importance of the saccade goal in updating visual-motor reference frames (Schoppik and Lisberger, 2006; Zirnsak et al., 2014), and it implies that in structured visual environments, observing forward or backward mislocalization is no longer a function of time (like in complete darkness), but a function of spatial location (Honda, 1999).

Even though much of the early work on perisaccadic mislocalization has focused on only one dimension (horizontal saccades and perceptual reports on only the horizontal position of flashes), subsequent pioneering work demonstrated that, even with horizontal saccades, mislocalization has a distinct two-dimensional landscape (Kaiser and Lappe, 2004). More importantly, saccade directions themselves alter the two-dimensional mislocalization landscape, with upward saccades causing particularly strong reverse mislocalization for flashes presented ahead of the saccade target (Grujic et al., 2018). This latter result, which was motivated by a difference between upper and lower visual field representations in the superior colliculus (Hafed and Chen, 2016; Zhang et al., 2022; Hafed, 2025), suggests a clear need to study perisaccadic mislocalization, whether perceptually or with neurophysiological experiments, using more than just horizontal saccades.

Here, we aimed to establish a robust and flexible perisaccadic visual mislocalization paradigm in macaque monkeys, setting the stage for subsequent neurophysiological experiments. Four previous studies demonstrated perisaccadic mislocalization in monkeys, but all used only horizontal saccades and with only one-dimensional mislocalization measures (analyzing the horizontal component of flash positions). In one study, forward

mislocalization was observed in complete darkness (Dassonville et al., 1992), consistent with human studies (Honda, 1989; Lappe et al., 2000). In another, backward mislocalization was observed in the absence of complete darkness (even for flashes behind the saccade target location), inconsistent with so-called "compression" (Jeffries et al., 2007). However, the flashes used in that study were not the very brief flashes typical of mislocalization experiments in humans. In the third study, perisaccadic "compression" was observed like in humans, and under identical experimental conditions between species (Klingenhoefer and Krekelberg, 2017). And, most recently, evidence of "compression" was again documented, enabling simultaneous recordings of visual cortical neurons during the behavior (Weng et al., 2024). Thus, it is indeed plausible to use monkeys for mislocalization experiments.

Having said that, the reality of neurophysiological experiments is that saccade direction could be completely arbitrary. For example, if one were to record superior colliculus saccade motor bursts, as a potential source of corollary discharge signals (Sommer and Wurtz, 2004, 2006; Berman et al., 2009; Berman and Wurtz, 2010, 2011; Berman et al., 2017) that may contribute to mislocalization, then it is more likely to record from oblique rather than horizontal saccade representations. This is also true when probing the representations of brief perisaccadic flashes themselves. Therefore, and given the dependence of perisaccadic mislocalization strength on saccade direction (Grujic et al., 2018), true translation of the classic human mislocalization studies to neurophysiological experiments would only be possible with a general, and robust, two-dimensional mislocalization paradigm in monkeys. This is what we document here.

Materials and Methods

Experimental animals and ethical approvals

We collected data from three adult, male rhesus macaque monkeys (*Macaca mulatta*). The monkeys (A, F, and M) were aged 11-15 years, and they weighed 10-13 kg.

All experiments were approved by the ethics committees at the regional governmental offices of the city of Tübingen.

Laboratory setup and animal procedures

The monkeys were seated in front of a brightly-lit computer-controlled display, spanning approximately 31 deg horizontally and 23 deg vertically. The display was at a distance of ~72 cm from the animals. We tracked eye movements with high precision using the scleral search coil technique (Robinson, 1963; Fuchs and Robinson, 1966; Judge et al., 1980), and the experiment was controlled in real-time using a modified version of PLDAPS (Eastman and Huk, 2012). Stimulus presentation and control were performed via the Psychophysics Toolbox (Brainard, 1997; Pelli, 1997; Kleiner et al., 2007), which provided exact time stamps at every frame update, ensuring accurate synchronization with the refresh cycle of the display. Prior tests with photodiodes (during the first few years of existence of the Hafed laboratory) confirmed the accurate timings of the Psychophysics Toolbox time, as expected given that the toolbox directly accesses the vertical blanking signal of the graphics card.

The animals were prepared for behavioral and neurophysiological experiments earlier (Tian et al., 2018; Buonocore et al., 2019; Skinner et al., 2019). This entailed a first surgery to implant a head fixation apparatus. During data collection, this apparatus was attached to a coupled device on the monkey chair in order to stabilize head position. Then, a later surgery was performed to implant a scleral search coil in one eye for eye movement tracking purposes.

Experimental procedures

The main task involved generating a primary visually-guided saccade, around which a very brief probe flash was presented; later on in the very same trial, the monkeys generated a "report" saccade aiming at where they remembered the perisaccadic flash to have appeared.

Each trial (Fig. 1) started with an initial white fixation spot (of 79.9 cd/m^2 luminance) presented over a uniform gray background (26.11 cd/m^2). This illumination created a clear border along the edges of the display, providing a consistent visual reference frame throughout the experiments; thus, we were measuring "compression"-style mislocalization (Ross et al., 1997; Lappe et al., 2000). The fixation spot was displaced from display center (by 7 deg, except for the cardinal saccade directions of monkey M, in which case it was by 5 deg), and it could appear in one of eight (equally spaced) directions from this center. After 600-1000 ms, the fixation spot disappeared, and a simultaneous saccade target appeared at

the display center. This target consisted of a vertical Gabor grating of either 0.5 cycles/deg (cpd) or 8 cycles/deg (cpd) spatial frequency, and it had a radius of 1.5 deg. The grating had high contrast (100%), and it featured a white central marker surrounded by a small gray disc, as in our previous experiments (Baumann et al., 2023). This central marker aided in maintaining saccade accuracy and precision across trials having different image appearances of the saccade target. The onset of the grating was the cue to generate a visually-guided saccade.

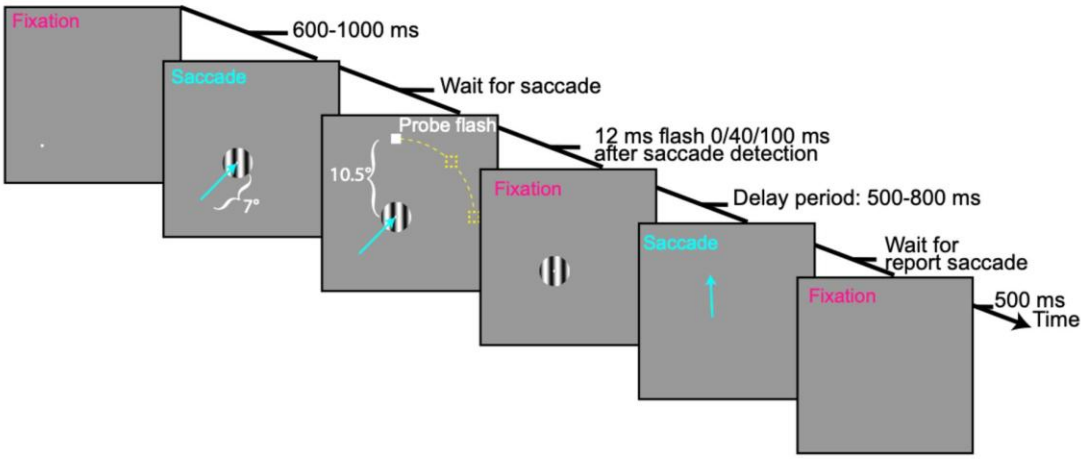

Figure 1 Perisaccadic visual mislocalization task for macaque monkeys. Each trial started with fixation of an eccentric spot (bottom-left corner of the display in the shown example). Upon removal of the spot, a saccade target appeared (Gabor grating), and the monkeys generated a visually-guided saccade towards it (oblique cyan arrow). We detected saccade onset online, and we presented a brief, single-frame probe flash at one of three possible delays from saccade detection. The probe flash could appear at one of three possible locations on a virtual circle (dashed yellow curve and placeholders) around the saccade target: one directly ahead of the saccade target along the saccade vector direction, and two at +/- 45 deg relative to the saccade vector (the shown example flash is at the 45 deg counterclockwise position). After an enforced delay, we removed the grating, and the monkeys reported their perceived flash location with a second, memory-guided, saccade. They had to maintain their gaze on the reported location for an additional delay time before being rewarded. In baseline trials, the probe flash appeared 100 ms after saccade detection and remained visible for 400 ms. Thus, it was clearly visible well after the end of the first saccade, resulting in an expected veridical percept.

We monitored the monkeys' eye position in real-time and detected the onset of a saccade when the eye position deviated by 1.5 degrees from the initial fixation spot. Following saccade detection, a probe flash was presented either immediately or with a delay of 40 or 100 ms (in subsequent post-hoc analyses, we recalculated exact probe times; see below). The probe flash was displayed for a brief duration of ~12 ms (1 frame at a display refresh rate of 85 Hz) and was positioned 10.5 degrees away from the center of the grating (7.5 deg for the slightly smaller cardinal saccades of monkey M). The probe flash could appear either directly along the saccade vector direction (and farther away from the saccade target) or at an angle of +/-45 deg relative to the saccade vector (again farther away than the saccade target location). Thus, there were three possible probe flash locations, all of which were expected to experience backward mislocalization for probe flash times very close to saccade

onset, especially given the bright display and clear visual reference frames in the environment (Honda, 1999; Lappe et al., 2000).

After the monkeys made the visually-guided saccade, with a maximum allowed reaction time of 500 ms, they maintained stable fixation on the saccade target for an additional 500-800 ms; this delay period started once the eye entered a predefined window around the saccade target. After the delay period, the grating disappeared, cueing the monkeys to make a memory-guided saccade "reporting" the remembered probe flash location. The monkeys were rewarded if they made the report saccade within <500 ms, and we allowed a radius of 8 deg tolerance window around the true flash location for the landing position of the eye. This large tolerance window was intentional because we wanted to avoid penalizing the monkeys for their mislocalized percepts; otherwise, the monkeys would have learned, over time, to constrain their report saccades to the regions gaining them rewards. On successful trials, the monkeys received juice rewards; on unsuccessful trials (e.g. late initial saccade or broken fixation), the trials were aborted and juice rewards were withheld.

We also interleaved trials containing what we called a "baseline" condition. In this condition, which occurred in a total of 6.25% of all trials in a given session, the probe flash was always presented 100 ms after online saccade detection, and the probe also remained visible for a full 400 ms. That is, the probe was still clearly visible while the monkeys' were in a stable fixation position on the grating center after the end of the primary saccade. This allowed assessing the monkeys' eye movement behavior in the report saccade when no perceptual mislocalization was to be expected (of course, other small errors, such as those associated with memory-guided saccades, could still occur, as we also clarify in Results).

To avoid that the monkeys were solving the task by remembering absolute flash locations across trials, for example, by guessing their position relative to the edges of the display, we applied a global constant shift in all stimulus positions, which we changed randomly from trial to trial, but which we kept constant for all stimulus events within a trial. Specifically, on every trial, the whole stimulus geometry (initial fixation position, final fixation position, and the virtual circle on which the probe flashes could occur) was shifted randomly by a constant known amount, within a range of ±0.5 deg both horizontally and vertically. In all analyses, all positions were re-referenced to the true saccade target location on any given trial. This is a similar approach to our recent human perisaccadic mislocalization experiments (Baumann et al., 2024).

Across data collection sessions, we varied the primary saccade direction, in order to demonstrate the two-dimensional flexibility of our paradigm. We selected eight distinct initial fixation positions on a virtual circle around display center, allowing us to test eight different saccade vectors. Although our paradigm was designed to support any starting and end position in theory, we focused on these eight equally spaced directions for simplicity and for the opportunity to collect many trial repetitions of any given condition. In practice, we blocked trials of a given saccade direction in a given data collection session. This was done purely for pragmatic reasons. Specifically, we typically collected multiple sessions of data from each animal, and we wanted to have large numbers of trials for each saccade direction. Therefore, it was simpler to specify a given saccade direction for any given block that we ran. This is also the expected situation during neurophysiological experiments, in

which a given saccade vector would be constant for a given recording site (for example, in the superior colliculus). However, once the monkeys are proficient in this task, we believe that randomizing saccade directions within a single session would still be very easily performed by them (see our note on training trajectory below).

For monkey M, as stated above, the cardinal saccades were only horizontal, and they had an amplitude of 5 deg (rather than 7 deg). Also, the probe flashes were 7.5 deg away from the saccade target in these cases (rather than 10.5). Thus, when summarizing this monkey's results, we separated the oblique conditions (with 7 deg saccades) from the cardinal ones (see Results). We did this in order to avoid potential confusion with respect to the quantitative amplitude of mislocalization for the two different saccade sizes that we tested in this animal. On the other hand, showing qualitatively similar results with different saccade sizes, both in the same monkey and also across animals (see Results), further confirms our interpretation of the robustness and flexibility of our visual mislocalization paradigm.

Finally, in the task above, the report by the animals was made through a memory-guided saccade to the "perceived" flash location. Memory-guided saccades have systematic (and variable) errors in their landing positions (White et al., 1994; Willeke et al., 2019), which can also depend on saccade direction (Hafed and Chen, 2016). However, as mentioned above, and as we also show in Results, we varied saccade directions across our experimental sessions, in order to convince ourselves that what we saw was true mislocalization (Grujic et al., 2018) and not only errors in memory-based reporting (e.g. Fig. 4 in Results). Moreover, the perisaccadic flash eccentricities were far enough from the saccade target to make the peak mislocalization errors significantly larger than any systematic or variable errors expected from memory-guided saccades (see Results).

We collected approximately 350-500 successful trials per session from each monkey. In total, we analyzed 7582, 16005, and 20902 successful and accepted trials for the saccade direction analysis, as well as 14953, 23830, and 23371 successful and accepted trials for the saccade target appearance analysis from monkeys A, F, and M, respectively (see below for our definitions of saccade direction data analysis and saccade target appearance data analysis).

Training trajectory

Success in our task was built on a very simple training trajectory that each monkey underwent, and that we describe here briefly. All three monkeys easily mastered the task.

All three monkeys were already experts in the individual task components before starting this project. Specifically, they knew how to perform both visually-guided and memory-guided saccades. To get the monkeys to report flash position in our current mislocalization task, we first started with the visually-guided saccade component of the paradigm; the monkeys simply made a saccade towards the grating image when they were instructed to do so (by removal of the initial fixation spot and the appearance of the grating). They were also rewarded classically, immediately after removal of the grating image.

We then introduced a second delayed, visually-guided saccade in every trial. Upon detection of the first saccade to the grating center, we presented the probe. However, instead of being

flashed briefly, the probe remained visible until trial end. After the first saccade to the grating center, the monkeys performed a delayed saccade to the probe after grating removal. The reward now only came after a sequence of two instructed saccades (both visually-guided). Since the monkeys were already proficient in delayed, visually-guided saccades, this stage of training was achieved already from the first trial, allowing us to proceed.

We next introduced trials in which we presented the flash like in the main task above, except for two differences. First, the flash occurred always 100 ms after detecting the visually-guided saccade. That is, we were sure that it should be minimally mislocalized since it appeared much later than the saccade time (Ross et al., 1997; Grujic et al., 2018). Second, the flash was presented for a long period of time (400 ms) on every trial (like in our baseline condition). This ensured that the flash was minimally mislocalized by the previous saccade, and that it was still visible during stable fixation of the grating center. Upon removal of the grating, the monkeys made a relatively accurate memory-guided saccade towards the flash position, and we immediately rewarded them for having their gaze enter a relaxed virtual window of 8 deg radius around the true flash position. This made them quickly realize that the reward was now contingent on reporting the remembered flash position after completing their initial visually-guided saccade.

We then gradually increased the period in which the monkeys had to maintain fixation on the remembered flash position before getting rewarded. This allowed them to maintain stable gaze position for a few hundred milliseconds before getting rewarded (Fig. 1). Thus, by now, the monkeys were proficient in performing an initial visually-guided saccade to an image, and then making a second memory-guided saccade towards the remembered flash location (with the flash itself being veridically perceived since it occurred long after saccade onset, and also since it was visible for a long time). For one monkey (A), the animal had some difficulty transitioning to the memory-guided component of the task so far. Therefore, we introduced a few extra sessions in which the probe reappeared when the grating disappeared. This prompted the monkey to realize that the task was to focus on the remembered probe flash location.

When we were confident that the monkeys were performing this task with high fidelity, we then reduced the duration of the flash (down to a single display frame). And, finally, we started introducing the other flash times, in which we expected a large mislocalization error. As mentioned above, we maintained a relaxed virtual tolerance window radius around flash position, so that we did not penalize the monkeys for their mislocalized reports. All animals readily learned the task without much difficulties.

Data analysis

Primary saccade processing

We detected all saccades (in post-hoc analyses) using the methods that we described previously (Chen and Hafed, 2013). For the primary saccades, such detection allowed us to recalculate probe flash times relative to the actual saccade onset in the data. We found that the probe flashes in the experiment occurred at three distinct times from saccade onset,

consistent with our experimental design. Based on the recalculations, we specifically classified the probe flash times into the following three categories: probes occurring ~30 ms after primary saccade onset, probes occurring ~70 ms after primary saccade onset, and probes occurring ~130 ms after primary saccade onset. That is, the online saccade detection process described above took approximately 30 ms to trigger the flashes during the data collection (expected given the dependence of our detection algorithm on eye position deviating sufficiently from initial fixation, and also given the frame refresh rate of the display). Figure 2A shows an example of the relationship between primary saccade times and probe flash onset times from one example session of monkey A. The figure plots radial eye velocity of the primary saccade (each curve is a saccade), with all trials aligned to probe flash onset time. There were three distinct time periods separating saccade and flash times across all trials.

Besides checking timing, we also checked primary saccade consistency across conditions. That is, we wanted to avoid the possibility that any differences in visual mislocalization that we uncovered (for example, as a function of saccade direction) could be due to systematic differences in the actual primary saccade metrics and kinematics. Therefore, before analyzing the behavioral reports of the animals, we first filtered trials according to the eye movement data of the primary saccades. In one set of comparisons (see Results), we were interested in investigating the influences of primary saccade direction on perisaccadic visual mislocalization strength. Therefore, we ensured matched saccade vector and kinematic properties across the different directions of the primary saccades of our main task (Fig. 1). In another set of comparisons, we studied the influences of saccade target appearance on mislocalization strength; here, we matched the primary saccades across the different saccade target image types (low versus high spatial frequency).

For the vector and kinematic matching in the investigations of primary saccade direction influences, we binned all saccade main sequence data (Zuber et al., 1965; Bahill et al., 1975) into intervals of 0.5 deg in amplitude by 40 deg/s in peak velocity. We included in the analyses only those trials from the main sequence bins that had at least one trial from each of the eight saccade directions (four in the case of monkey M's oblique saccade data; this monkey's cardinal saccades were analyzed separately due to their smaller size). This ensured that we could compare saccades across different directions having similar ranges of amplitudes and peak velocities.

We also noticed that monkey M had a substantial difference in saccade peak velocity between rightward and leftward saccades (~350 versus ~550 deg/s, respectively). Therefore, for this monkey, we decided to report all analyses separately according to the hemifield of the saccade vector (see Results), meaning that we also separated the vector and kinematic matching procedures in this monkey for each hemifield individually. This way, we did not mask any possible quantitative effects of saccade peak velocity on mislocalization amplitude, but the results were always qualitatively the same across hemifields (and across animals).

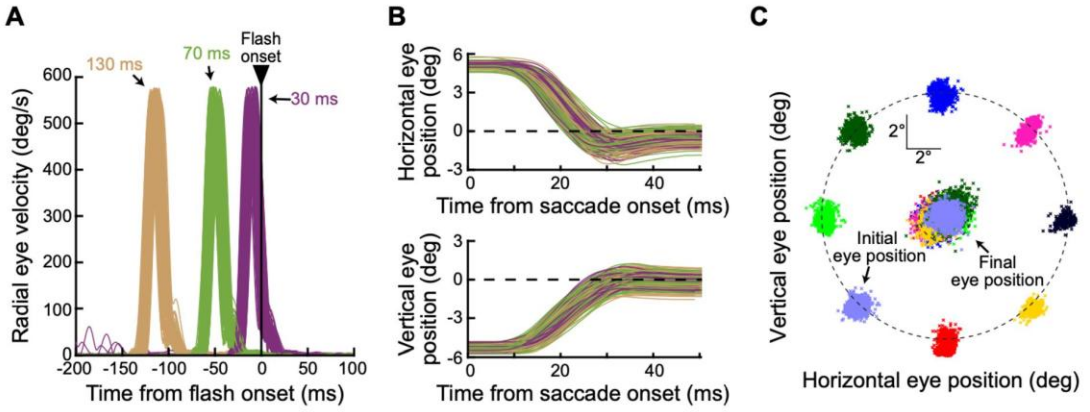

Figure 2 Controlling probe flash timing and saccade metrics and kinematics across conditions. (A) Radial eye velocity plots of all accepted primary saccades from an example session of monkey A. All traces are aligned to the onset of the probe flash, revealing three distinct perisaccadic flash times, which we categorized by the three different colors. We expected progressively less visual mislocalization for longer times between the saccades and the probe flashes. Baseline trials are not included in this panel. **(B)** Horizontal (top) and vertical (bottom) eye position traces from one example saccade vector direction (up and to the left) out of the same example session shown in **A**. Different colors show the different probe flash times, and the data suggest no systematic differences in the saccades across the flash times. **(C)** We also ensured that landing eye positions (central clouds of dots) overlapped for different saccade directions, again allowing us to investigate the influence of saccade direction on mislocalization strength with overlapping saccade properties (the kinematics were also matched as per the description in the text). The small black dashed circle indicates the extent of the grating towards which the primary instructed saccade was generated, and the big black dashed circle indicates the virtual circle along which the initial fixation positions were placed.

Figure 2B shows, for the same monkey and session as in Fig. 2A, example accepted saccades. Each panel shows either horizontal (top) or vertical (bottom) eye position aligned on saccade onset, and the different colors show the different probe flash time classifications of Fig. 2A. Figure 2C, in turn, shows all start and end eye positions from all trials of all sessions of the same monkey. These trials passed the vector and kinematic matching (for the investigation of saccade direction influences on visual mislocalization), and they, therefore, went into further analysis.

For investigating the influences of saccade target appearance on mislocalization strength, we applied the same binning strategy above in order to achieve vector and kinematic matching, but we now compared saccades to either low or high spatial frequency Gabor gratings. We, thus, pooled across all saccade directions. We included only those trials from the main sequence bins that contained at least one trial repetition from each of the two saccade-target image conditions (low and high spatial frequency) of each probe flash time. This ensured that saccades were matched for both metrics and kinematics across the different image conditions of the saccade target.

Establishing the existence of perisaccadic mislocalization

We next analyzed the report saccade endpoints, which constituted our experimental measure of perisaccadic visual mislocalization. We had three general classes of analyses in

the study. First, we established that we were indeed measuring genuine mislocalization and not artifacts of either memory-guided saccade errors or our particular analysis choices. Second, we focused on the effects of saccade direction on mislocalization properties. Finally, we investigated the effects of saccade target appearance. We now describe the first class of analyses.

To establish that we were measuring genuine mislocalization, we took the following measures, including control analyses to rule other potential explanations out. For each flash time and saccade direction, we measured the final eye position of the report saccade on every accepted trial, and we then plotted the raw two-dimensional data (e.g. Fig. 3D in Results) relative to the geometry of the saccade vector and probe flash location. We also collected summary statistics within each monkey. Specifically, for each probe flash location and time (for a given saccade direction), we calculated the mean and SEM of all reported probe flash locations. This allowed us to visualize the pattern of mislocalization (e.g. Fig. 3E, left in Results).

We quantified mislocalization strength as follows. For each flash location, we used the baseline condition to know the average reported location by the monkey when perception was expected to be veridical. Then, for each trial of the same flash location but for one of the experimental perisaccadic flash times, we measured the Euclidean distance between the reported location of this trial and the mean reported location of the baseline condition (e.g. Fig. 3E, right in Results). This allowed us to obtain average mislocalization across trials of a given flash time relative to any systematic error that might have existed in the report saccade in the absence of any perisaccadic mislocalization.

To explicitly confirm that we did indeed need to account for systematic errors in memory-guided saccades (White et al., 1994; Willeke et al., 2019), we also directly compared the error patterns between baseline and mislocalization trials relative to true flash location. For each trial (whether baseline or with a brief perisaccadic flash), we computed an error vector by connecting the veridical flash location to the reported location. We then calculated the angle of this vector relative to the primary saccade direction angle. If mislocalization errors were systematically related to the primary saccade direction, then their angular distributions were expected to be very tightly distributed around 180 deg (i.e. backward mislocalization). However, on the baseline trials, if the errors were just systematic errors devoid of any perisaccadic mislocalization, then they were not expected to depend on the primary saccade direction; thus, the angle distributions relative to the primary saccade direction were expected to span 360 deg.

We also confirmed that baseline reports were always more veridical than the reports for perisaccadic flashes, and we verified that differences in baseline errors (e.g. as a function of saccade direction) were not sufficient to explain the differences in peak mislocalization effects that we reported in Results.

Having established that the baseline trials were the proper reference measure for estimating veridical percepts, we next considered whether memory decay could account for the larger localization errors observed in perisaccadic trials than in baseline trials (which we report in Results). Specifically, the longer flash durations in our baseline trials (relative to perisaccadic

test trials) resulted in shorter delays between the probe flash offset time and the go-signal for the animal to report the probe flash location. To confirm that this was not sufficient to explain the differences in error magnitudes between perisaccadic and baseline trials, we explicitly related localization error amplitude in baseline trials to delay period duration. We binned delay period durations into 30 ms bins, and we plotted the baseline report error amplitudes as a function of these bins. This allowed us to assess whether error amplitudes on perisaccadic probe flash trials were simple extrapolations of memory decay effects.

We then examined the relationship between mislocalization strength and flash onset time relative to saccade offset, by implementing a more fine-grained temporal binning approach. Within each of the three original coarse flash time conditions, we introduced additional temporal bins to increase resolution. This finer binning was made possible by the natural variability in saccade durations across trials, and it allowed us to confirm that we were likely not observing a biphasic mislocalization pattern as might be expected from pure darkness conditions (Honda, 1989, 1991, 1993, 1999).

To ensure that the observed mislocalization effects were also not merely a consequence of differences in eye position during (intrasaccadic and postsaccadic) probe flash presentations, we assessed the relationship between eye position at the time of the probe flash onset and the mislocalization strength. For each monkey and each probe flash time condition, we binned the mislocalization strength according to the distance between the eye position and the saccade target at the moment of the probe flash presentation. Bins were set at intervals of 0.2 degrees. Eye positions were assigned negative values when the eye was located between the initial fixation point and the saccade target, and positive values indicated overshoots beyond the saccade target. This analysis allowed us to confirm that mislocalization magnitudes depended on flash times from primary saccade onset rather than on the exact eye position at probe flash occurrence (see Results).

On a related note, we next validated our expectation that differences in mislocalization strengths across probe flash presentation times were not driven by the presence of corrective saccades during the delay periods. We analyzed the temporal distribution of corrective saccades relative to the initial saccade onset. We aligned corrective saccade onset time to the initial saccade onset time, in order to assess these saccades' timing across different probe flash time conditions.

Exploring the effects of saccade direction on perisaccadic mislocalization

After being convinced that we were measuring genuine perisaccadic mislocalization, we proceeded to summarizing the effects of saccade direction on visual mislocalization strength. In one analysis, we averaged the Euclidean distance measure described above across all trials that involved either upward or downward saccades for each probe flash time, respectively. Upward saccades in this kind of analysis included oblique upward/rightward and oblique upward/leftward saccades, in addition to purely vertical upward saccades. Similarly, downward saccades also included the oblique saccades with a downward component. In this comparison, we averaged across all three probe flash locations of a given saccade direction. In related analyses, we also measured the mislocalization strength (Euclidean distance to the reports in the baseline condition) for each saccade direction

separately. Again, we pooled all flash locations per saccade direction together in this analysis, but we always treated flash times separately. Of course, we had previously inspected all the raw data of individual flash locations (e.g. Figs. 3D, 5A, B in Results) to justify pooling them in our summary analyses.

We also further summarized the difference in mislocalization strength between upward and downward saccades in a given analysis. To do so, we calculated the mathematical difference (at any given flash time) between the Euclidean distance measure (to the respective baseline condition of each flash location) obtained for upward saccades and the Euclidean distance measure obtained for downward saccades. We then plotted this difference measure across flash times. Again, this is a similar approach to how we reported changes in mislocalization strength across different experimental conditions in our recent human work (Baumann et al., 2024).

To once more validate that our observations were not dependent on our use of the baseline reports, we also repeated our saccade direction comparisons but by now relating the mislocalization errors to the reports on the trials with flashes presented ~130 ms after saccade onset (rather than the baseline trials). That is, we exploited the fact that perception recovered with long times after saccade onset, and used the latest flash time as the condition with closest-to-veridical percepts. As expected, similar results were observed.

Since perisaccadic mislocalization for a given saccade direction can also have a two-dimensional landscape (Kaiser and Lappe, 2004; Grujic et al., 2018), we additionally investigated the vector components of mislocalization, similar to what we had done recently with humans (Baumann et al., 2024). We examined the component of localization error that was parallel to the saccade direction and the component that was orthogonal. This analysis followed the same approach as that described above (measuring Euclidean distances to baseline reports for the different saccade directions), except that we separated the parallel and orthogonal components of the mislocalization errors.

In a separate comparison, we focused solely on the trials with horizontal primary saccades. In this case, we compared the Euclidean distance measure for probe flash locations in the upper versus lower visual fields. Thus, for such horizontal saccades, we compared the mislocalization strength between the two oblique probe flash locations associated with these saccades (by definition of the task, one oblique probe flash location would have been in the upper visual field, and ahead of the saccade target location, and the other would have been symmetrically in the lower visual field). We should also note here that even for vertical saccades, probe flashes ahead of the saccade target could be in either the upper or lower visual field (e.g. upper visual field for upward saccades and lower visual field for downward saccades). For oblique saccades, some flash locations were at the same vertical eccentricity as the saccade target, but they were still in the upper visual field presaccadically for upward oblique saccades, and still in the lower visual field presaccadically when the oblique saccade was downward. Thus, it is likely that some of our saccade direction effects interacted with visual field effects, as was also previously observed in humans (Grujic et al., 2018).

Exploring the effects of saccade target appearance on perisaccadic mislocalization
We also performed an investigation of the influences of the saccade target appearance on perisaccadic visual mislocalization. To do so, we averaged the Euclidean distance measures for all saccade directions and probe flash locations, but now separated trials based on the spatial frequency of the saccade target.

Statistical analyses
We statistically compared different conditions using a two-way ANOVA on the Euclidean distance measure, with the two factors of the ANOVA being probe flash time relative to saccade onset and either saccade direction, flash location, or saccade target appearance, depending on the particular comparison that we were making. We always performed these analyses within each monkey individually, to be able to compare the outcomes across the individual animals. Although we consistently presented monkey M's leftward and rightward saccades separately in all figures, we did not distinguish between them in the statistical analyses, as this separation did not affect the statistical results. We also statistically compared baseline reports under different comparison conditions. For example, we checked whether the errors in baseline reports (relative to the true flash location) were different whether saccades were upward or downward, and we did so by performing (for each monkey) a t-test. Details are provided in the relevant sections of Results, and the statistics were performed with IBM SPSS (Version 29.0).

Results

We aimed to establish a robust and flexible visual mislocalization paradigm in rhesus macaque monkeys. We tested this paradigm on three animals, and they all exhibited clear perisaccadic mislocalization, with expected recovery time courses. These animals also all replicated prior human findings of stronger mislocalization with upward saccades (Grujic et al., 2018), as well as stronger mislocalization for upper visual field flashes (with horizontal saccades) (Baumann et al., 2024). We also found subtle effects of saccade target image appearance on mislocalization strength (Baumann et al., 2024), but these effects were not as consistent as with humans, and they were also not as strong as the effects of saccade directions and flash locations in the same animals. We summarize all of these observations below.

Monkeys reported perisaccadic flashes as being closer to the saccade target
We trained our monkeys to report the location of a brief (~12 ms) probe flash presented at different perisaccadic time points (Figs. 1, 2). They did so by directing their gaze, via a memory-guided saccade, to the remembered flash location after an instruction to do so (Fig. 1). Note that such memory-guided reporting of percepts is present even in classic human invocations of this same task (Ross et al., 1997; Lappe et al., 2000). To confirm that there was indeed mislocalization, we interleaved baseline trials in which the flash was long-lasting, and thus clearly visible after primary saccade end (Materials and Methods). Therefore, any errors in reporting for this baseline flash condition should have been restricted to only those errors (whether systematic or variable) associated with memory-based behavioral reports (White

et al., 1994; Willeke et al., 2019; Willeke et al., 2022), and not directly related to perisaccadic mislocalization.

As a first step in our analyses, we first performed a detailed investigation of unsuccessful trials that were not analyzed for mislocalization reports. We did this in order to gain further insights into the monkeys' task performance and potential strategies. Unsuccessful trials were defined as those in which the monkey correctly initiated the trial by performing the instructed primary saccade (thereby triggering the probe flash presentation) but subsequently failed to obtain the reward due to performance-related errors. Trials in which the monkey did not initiate the task at all (e.g., due to a lack of motivation, blinks, or eye position instabilities at the initial fixation spot) were excluded from this analysis. Across all conditions, all three monkeys successfully completed 84.4%, 79.3% and 76.7% (Monkeys A, F, and M, respectively) of the initiated trials, confirming that the probe flash was clearly visible under all experimental conditions. The failure analysis revealed two primary categories of unsuccessful trials: (1) fixation breaks, and (2) incorrect saccade landings. Fixation breaks were errors in which the monkey broke fixation either before the go signal for the report saccade or during the final fixation period after the end of the report saccade. The proportion of fixation breaks was 9% for Monkey A, 12.5% for Monkey F, and 10.7% for Monkey M. Incorrect saccade landings were errors in which the monkey executed the report saccade but failed to land within the predefined spatial window required for successful reporting. The rates of this error type were 6.6% (shortest flash delay: 4.9%, medium delay: 1%, longest delay: 0.5%, and baseline: 0.2%) for Monkey A, 8.2% (shortest delay: 5.7%, medium delay: 1.3%, longest delay: 0.8%, and baseline: 0.4%) for Monkey F, and 12.5% (shortest delay: 9%, medium delay: 2%, longest delay: 0.5%, and baseline: 1%) for Monkey M. Thus, landing errors were always more frequent for the shortest probe flash times relative to the primary saccade onset.

The increased error rates for short probe flash delays are already the first hint that the monkeys really did experience perisaccadic visual mislocalization. Specifically, based on human research, shorter delays between saccade onset and probe flash presentation are associated with the largest mislocalization effects. Given the fixed spatial tolerance windows that we employed for accepting correct responses, larger mislocalization errors increased the likelihood that the monkeys' reported locations fell outside of these windows, leading to a higher task failure rate. In essence, when the perceived location of the probe was strongly shifted, the monkeys might have been aiming accurately based on their perception, but the degree of mislocalization caused their responses to be registered as failures. This observation encouraged us to further analyze the successful trials for hallmarks of perisaccadic mislocalization. All results that follow are now solely based on the successful and accepted trials.

Figure 3A shows example results from monkey F when generating an oblique upward/rightward primary saccade. The probe flash location in this case was rotated 45 deg counterclockwise from the saccade vector direction. In the figure, the probe flash is indicated by a white square, but it was not actually visible at the time of the report saccade. Each trace in the figure shows eye position from one example trial, and different traces show different trials. We plotted example trials from the baseline condition in green, and example trials from a perisaccadic condition (the one with the probe flash occurring 30 ms after

saccade onset) in yellow. As can be seen, the primary saccades (oblique upward/rightward movements and directed towards the grating center) were all the same whether the trials were baseline trials or perisaccadic flash trials; that is, the eye position traces nicely overlapped with each other. This is expected given our eye movement controls mentioned earlier (Materials and Methods). Importantly, the report saccades were very different depending on the properties of perisaccadic visual stimulation. In the baseline trials, the report saccades had a veridical direction (upward in this case); for brief perisaccadic flashes occurring 30 ms after saccade onset, the reported locations were strongly shifted backward along the reverse direction of the primary saccade vector (compare the black oblique arrows). Note that the baseline saccades were still memory-guided, just like the report saccades in the perisaccadic test trials. Therefore, the large difference between report saccades in the two conditions in Fig. 3A was attributed to brief, perisaccadic visual stimulation in one of the conditions, and not due to the memory-guided nature of the report saccades. Also note that there was larger variance in the report saccades in the perisaccadic test condition; this is also true in human perisaccadic mislocalization studies (Baumann et al., 2024). Thus, this monkey experienced strong backward perisaccadic mislocalization for brief flashes presented 30 ms after saccade onset, and this mislocalization happened with an oblique (rather than cardinal) saccade.

We also checked the other probe flash locations associated with this same saccade direction. Example traces from the same monkey and session are shown in Fig. 3B, C. Once again, there was always reverse mislocalization opposite in direction from the saccade vector. Specifically, in Fig. 3B, the probe flash was directly ahead of the saccade target, and the reported locations were generally in the same direction as the flash but closer to the saccade target location (mislocalized backward in direction). Similarly, with the probe flash location rotated clockwise relative to the saccade vector (Fig. 3C), the reported locations were now deviated both leftward and downward relative to the baseline reports (resulting in a mislocalization vector directly opposite the upward and rightward vector of the primary saccade). Thus, the mislocalization that this monkey experienced perisaccadically was always backward relative to the saccade vector direction, regardless of flash location.

Note also that there were systematic errors in the baseline report saccades themselves in Fig. 3A-C, which are expected (White et al., 1994; Willeke et al., 2019). For example, in Fig. 3C, a pure rightward report saccade was associated with a slight upward bias in eye position endpoints, along with saccade hypometry (White et al., 1994; Willeke et al., 2019; Willeke et al., 2022). However, the perisaccadic mislocalization errors were always larger than these baseline report errors. Moreover, the perisaccadic mislocalization errors had a clear systematic relationship in direction relative to the saccade vector direction, as we also describe in more detail below. Thus, the perisaccadic mislocalization effects of Fig. 3A-C were not fully explained by systematic errors associated with the reporting process itself (also see Fig. 4 below for a more detailed analysis of baseline reports).

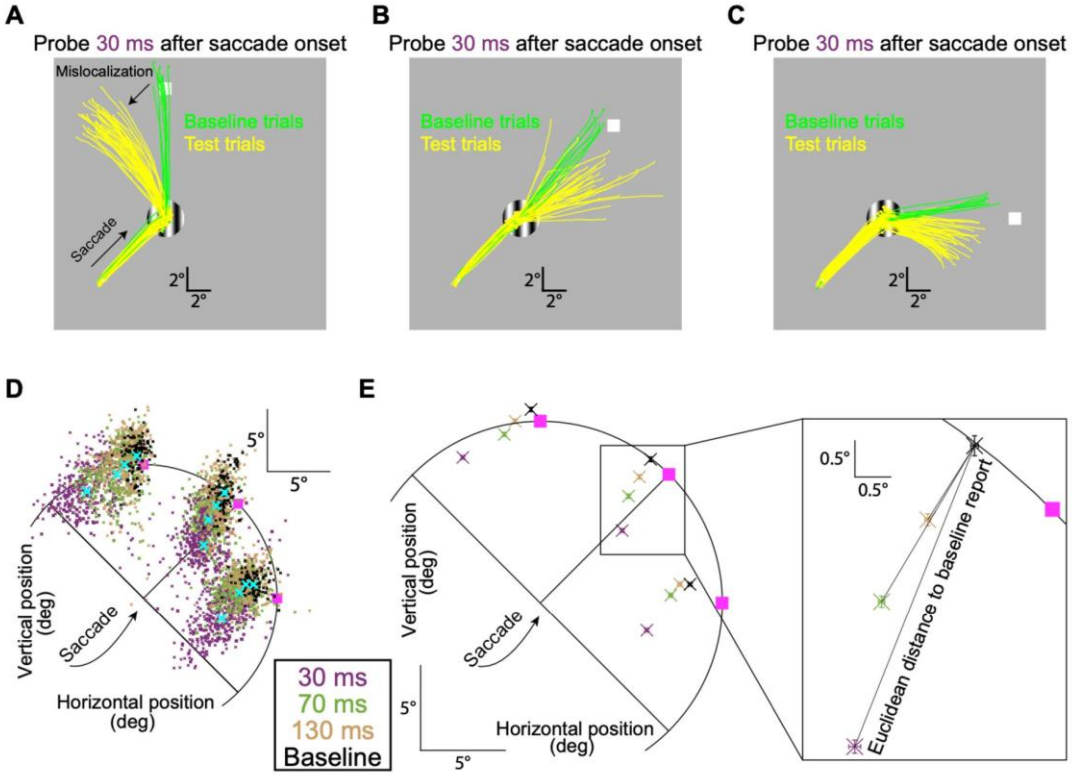

Figure 3 Two-dimensional perisaccadic "compression" in rhesus macaque monkeys. (A) Example eye position traces from monkey F when generating an oblique (upward/rightward) primary saccade, followed by a second report saccade. Individual traces show the entire eye movement sequence per trial (Materials and Methods), and we selected only trials with probe flashes directly above the saccade target location. The probe flash is schematized with a white square, but it was not actually visible at the time of the second saccade (the grating could also be different across trials; Materials and Methods). Green traces show baseline trials in which the probe flash remained visible for a prolonged period after the end of the primary saccade, but it was still invisible at the report saccade time (Materials and Methods). The monkey's report saccade was largely accurate, with a small systematic error expected from memory-guided eye movements. For perisaccadic flashes (yellow traces), there was a strong distortion in the opposite direction from the saccade vector (compare black oblique arrows). **(B, C)** Example trials from the same monkey for two other flash locations. There was always reverse mislocalization. **(D)** Across all sessions from the same monkey, and for all probe flash times and the same oblique saccade direction, we plotted the two-dimensional reported locations. On baseline trials (black), the percepts were mostly veridical (with expected small, but systematic, errors associated with memory-guided saccades). For perisaccadic flashes (colored small dots), there was maximal mislocalization at 30 ms, with a gradual temporal recovery. This is consistent with human mislocalization time courses. The pink squares indicate true flash locations, and the cyan crosses show the means of each colored cluster (also presented with proper color coding in **E**). **(E)** The main plot (left) shows mean and SEM summaries of the data of **D**. For longer and longer times, gradual recovery towards baseline performance occurred at each probe flash location. On the right, we magnified the data for one probe flash location, to demonstrate our summary measures in subsequent figures: we characterized mislocalization strength by calculating the Euclidean distance between reports on mislocalization trials to reports on baseline trials (Materials and Methods). In separate control analyses, we also checked the errors in baseline reports themselves (from true flash location).

Across all trials and all probe flash times and locations for the same oblique saccade direction, we found systematic mislocalization that gradually recovered with time from saccade onset. This is shown in Fig. 3D. Different colors indicate the different probe flash times, and individual small data points are individual trials (the cyan crosses show the means of each cluster). There was gradual recovery in mislocalization towards the baseline report locations when the probe flash time increased. This systematic trend can also be seen in Fig. 3E (left), in which we plotted the mean and SEM summary statistics of the same data. In the same figure (Fig. 3E, right), we also explained our measure of mislocalization strength that we used in subsequent figures. Specifically, mislocalization strength was defined as the Euclidean distance to the baseline report location for each probe flash position (Materials and Methods).

That the baseline reports were a proper reference point for canceling systematic errors of memory-guided saccades became even more clear to us when we related these baseline reports to individual saccade directions. Specifically, we compared error patterns in baseline trials to those observed during perisaccadic mislocalization (for the first flash time in which mislocalization was expected to be strongest from Fig. 3). The results of this analysis are presented in Fig. 4. Figure 4A shows (for monkey A) each primary saccade direction as a black arrow. For each such direction, we also represented the vector of the average baseline report error as a dark-colored arrow, and the vector of mislocalization (for the shortest flash time) as a ligher-colored arrow of the same general hue. As can be seen, mislocalization vectors were always opposite the saccade vector, but baseline error vectors were always of the same size and direction independent of primary saccade direction. Consistent with this, measuring the angle of the baseline error vector relative to primary saccade direction resulted in distributions spanning 360 deg (Fig. 4B-D, with each panel showing each monkey). On the other hand, measuring the angle of the mislocalization report vectors relative to primary saccade direction always revealed a 180 deg relationship (Fig. 4E-G). Thus, our mislocalization reports (Figs. 3, 4) were very distinct from baseline errors. Most importantly, closer inspection of Fig. 4A revealed that the baseline errors were (expectedly) always present, even in the mislocalization reports themselves. For example, for three sample primary saccade directions (those with a rightward component in the figure), when we corrected for the systematic baseline report vector error, mislocalization reports were better aligned with the 180 deg axis relative to the primary saccade direction than before. This makes perfect sense: if memory-guided saccades have systematic errors, then these systematic errors will still be present on brief probe flash trials. Thus, it was a valid choice for us to use baseline reports as the reference for veridical percepts in our analyses.

Our results so far suggest that we replicated human evidence of reverse perisaccadic visual mislocalization. Importantly, we did so for a non-horizontal saccade direction (Grujic et al., 2018), paving the way for generalized use of this paradigm in neurophysiological experiments. However, before diving deeper into additional properties of perisaccadic visual mislocalization in macaque monkeys, we first ruled out some additional caveats that might come up, especially with respect to our specific reporting mechanism (memory-guided saccades).

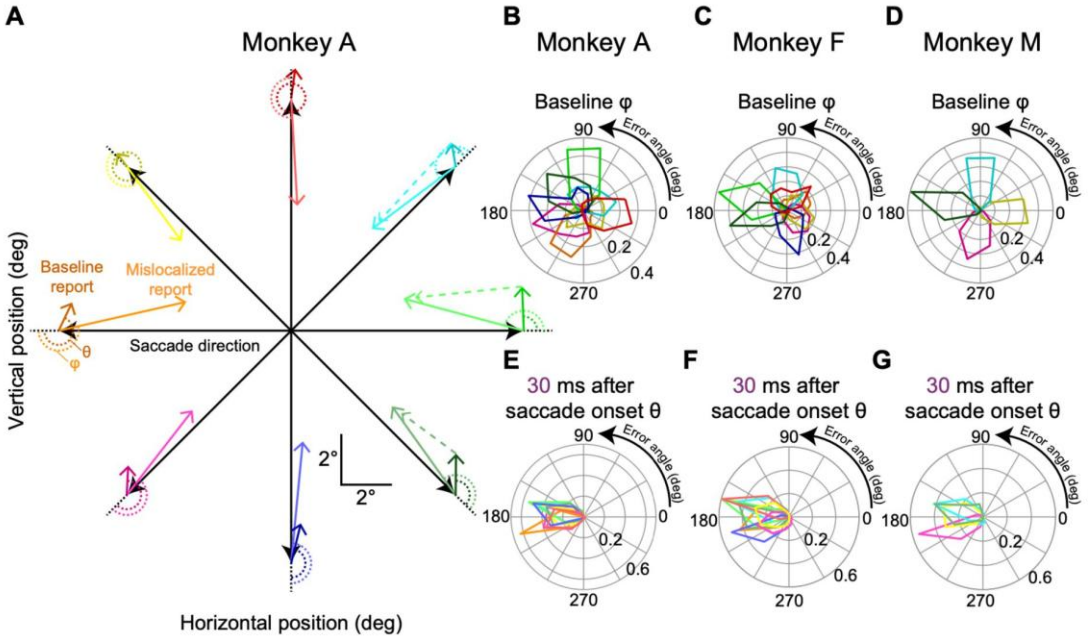

Figure 4 Comparison of error vector patterns between baseline and perisaccadic mislocalization trials. (A) Visualization of error vectors for Monkey A during the first flash time condition (30 ms after saccade onset), when mislocalization errors were most pronounced. Each colored vector connects the veridical flash location to the reported location, illustrating both baseline (darker-colored arrows) and mislocalization (brighter-colored, solid arrows) error vectors relative to the primary saccade direction (black arrows). Baseline errors consistently showed a small upward bias, independent of saccade direction. In contrast, mislocalization errors were systematically oriented in the direction opposite to the saccade vector. Dashed arrows indicate the direction of the mislocalization vector relative to the baseline report endpoint for selected saccade directions, demonstrating an even stronger 180-degree relationship with the primary saccade direction (other dashed vectors were not shown just to avoid clutter). **(B-D)** Polar histograms of angular errors (ϕ, as defined in **A**) for baseline error vectors across all primary saccade directions for Monkeys A, F, and M. Baseline errors showed a broad distribution spanning all 360 degrees, highlighting their independence from the saccade direction. Moreover, for each saccade direction, the baseline errors were clustered together, suggesting a single systematic baseline error direction independent of primary saccade direction (as in **A**). **(E-G)** Polar histograms of angular errors (θ, as defined in **A**) for mislocalization error vectors for Monkeys A, F, and M. Mislocalization errors were tightly clustered around 180 degrees relative to the saccade direction, indicating a robust and systematic divergence from baseline error patterns. **Extended Data Figure 4-1** shows the relationship between baseline localization errors and the delay period preceding report saccade execution. **Extended Data Figure 4-2** illustrates the relationship between mislocalization strengths and flash onset times relative to saccade offset, providing a more detailed time course depiction of perisaccadic mislocalization. **Extended Data Figure 4-3** demonstrates a lack of influence of eye position at the time of the probe flash presentation on mislocalization strength. **Extended Data Figure 4-4** shows the timing of corrective saccades relative to initial saccade onset across different probe flash presentation times.

First, our baseline trials had a particularly short time between probe flash onset time and the go signal for reporting (due to the long duration of the probe flash on these trials; Materials and Methods). Thus, it might be wondered whether our larger mislocalization effects in Figs. 3, 4 (for the non-baseline trials) were due to decays in working memory associated with longer wait times on perisaccadic probe flash trials. To assess this, we analyzed the relationship between delay period duration after probe flash offset and localization accuracy on the baseline trials (Extended Data Figure 4-1). Even though there

was a very subtle increase in localization error with longer delay durations, the effect was minimal and, even when extrapolated, it could not explain the mislocalization error amplitudes observed for the shortest flash onset times on the perisaccadic test trials. These findings align well with previous studies on memory-guided saccades, which demonstrated only minor (if any) memory decays over extended delays (White et al., 1994; Willeke et al., 2022). Thus, by including baseline trials in our analyses, we accounted for any general memory-related systematic errors, which were very temporally stable, ensuring that the reported mislocalization effects predominantly reflected genuine perisaccadic perceptual phenomena.

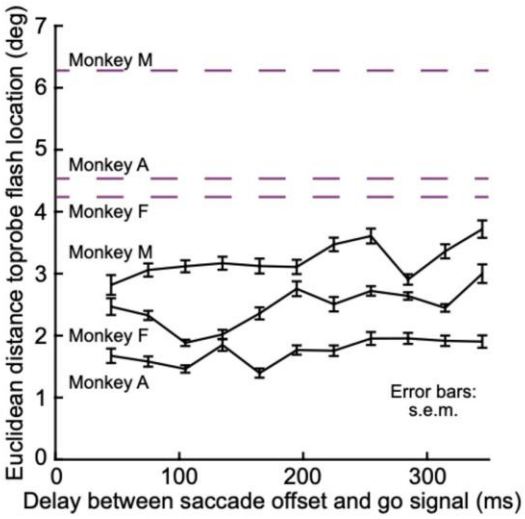

Extended Data Figure 4-1 Relationship between delay period duration and baseline localization error. Euclidean distance between the reported location and the actual probe flash position in baseline trials as a function of delay duration between primary saccade offset and the go signal for the report saccade. Each data point represents mean localization error per time bin, with error bars indicating SEM. The dashed purple lines indicate the peak mislocalization values for the individual monkeys, providing a reference for the maximal observed perceptual distortions in the perisaccadic period. Even with extrapolation for much longer delays, the baseline report errors were much smaller than actual perisaccadic mislocalization strengths.

To better contextualize the temporal dynamics of mislocalization, we also examined the relationship between mislocalization strength and the onset time of the probe flashes relative to saccade offsets. Aligning the data on saccade offsets enabled more fine-grained temporal analyses due to saccade duration variability. Extended Data Figure 4-2 shows the time courses for individual monkeys, revealing a continuous decrease in mislocalization strength over time, indicative of a gradual recovery.

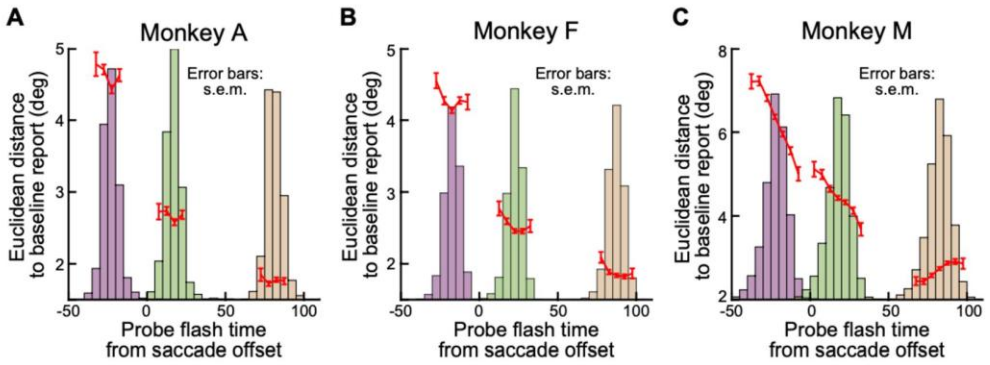

Extended Data Figure 4-2 Time course of perisaccadic mislocalization relative to saccade offset. (A-C) Euclidean distance to the baseline report as a function of probe flash onset time relative to saccade offset for each monkey (red). Mislocalization gradually decreased with increasing delay after saccade offset, indicating a recovery of veridical localization over time. Error bars represent SEM. The faint histograms in the background show the actual underlying probe flash times; note that we did not plot red data points if there were fewer than 100 observations in any histogram bin.

Because eye position could be variable at probe flash time, especially for intrasaccadic probes (shortest flash time), we also ruled out eye position effects as an explanation for the strong mislocalization results that we saw so far (e.g. Figs. 3, 4, Extended Data Figure 4-2). We plotted the distance of the eye position from the saccade target at the moment of the probe flash presentation against mislocalization strength for each monkey and probe flash time (Extended Data Figure 4-3). Across all three animals, no systematic relationship was observed between eye position at flash time and mislocalization strength. For instance, although the distributions of eye positions for probe flash times of 70 and 130 ms after saccade onset were very similar (as the saccade had already concluded for both flash times), a substantial difference in mislocalization strength persisted between these two conditions. This suggests that probe flash timing relative to the primary saccade exerted a much stronger influence on localization performance than the precise eye position at the time of flash presentation.

Finally, corrective saccades following the primary saccade also did not account for the observed differences in mislocalization strengths over time. In Extended Data Figure 4-4, we analyzed the temporal distribution of corrective saccades relative to the primary saccade onset. As expected from saccadic refractory periods, nearly all corrective saccades occurred after the probe flash presentations. Moreover, the timing of corrective saccades was highly similar for flash times of 30 and 70 ms after saccade onset. For trials with probe flashes presented 130 ms after saccade onset, corrective saccades were slightly delayed. This delay is due to saccadic inhibition, where the probe flash transiently suppresses the execution of corrective saccades when presented in close temporal proximity (Buonocore and Hafed, 2023). The presence of saccadic inhibition further supports the idea that the monkeys attended to the probe flash (White and Rolfs, 2016).

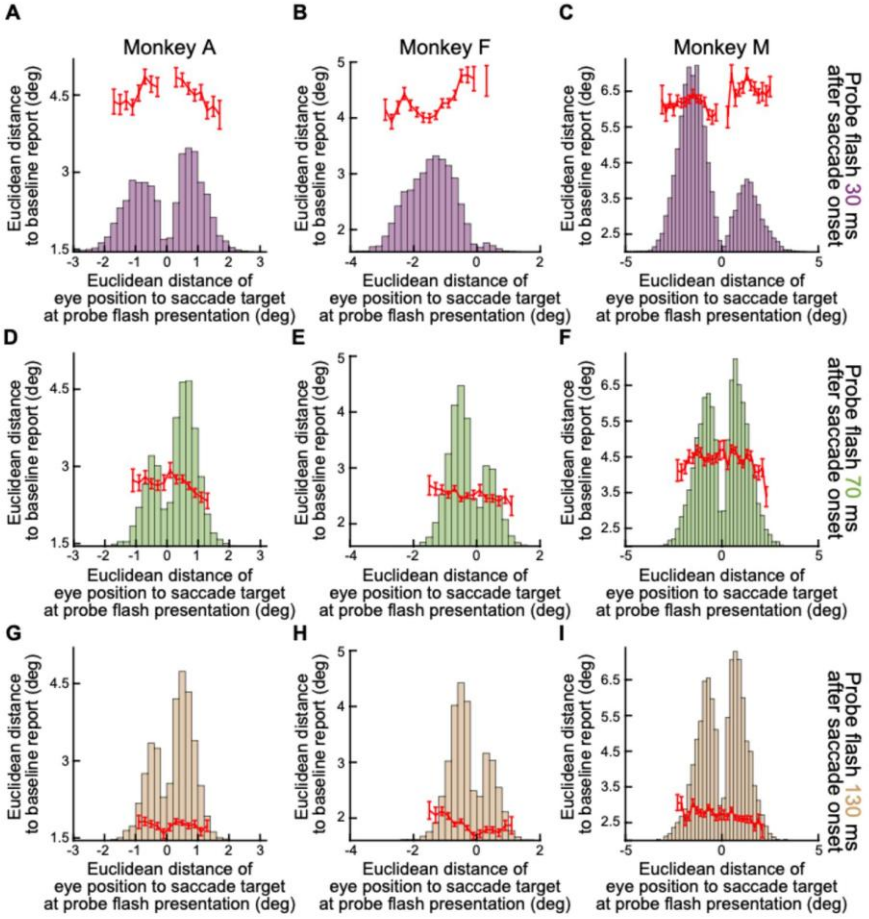

Extended Data Figure 4-3 Eye position at the time of probe flash presentation and its relationship to mislocalization strength. (A-C) Euclidean distance (red) to the baseline report as a function of eye position at the time of probe flash presentation for probe flashes occurring 30 ms after saccade onset for the individual monkeys. **(D-F)** The same relationship for probe flashes occurring 70 ms after saccade onset. **(G-I)** The same analysis for probe flashes occurring 130 ms after saccade onset. In each case, the faint histograms in the background show the bins in which we had eye position data to document. Across all three monkeys and all time points, no systematic relationship was found between eye position and mislocalization strength, confirming that localization errors were primarily driven by the timing of the flash rather than by momentary gaze position. Indeed, for each monkey, the mislocalization strength decreased much more strongly from the top to bottom row than within each row as a function of eye position.

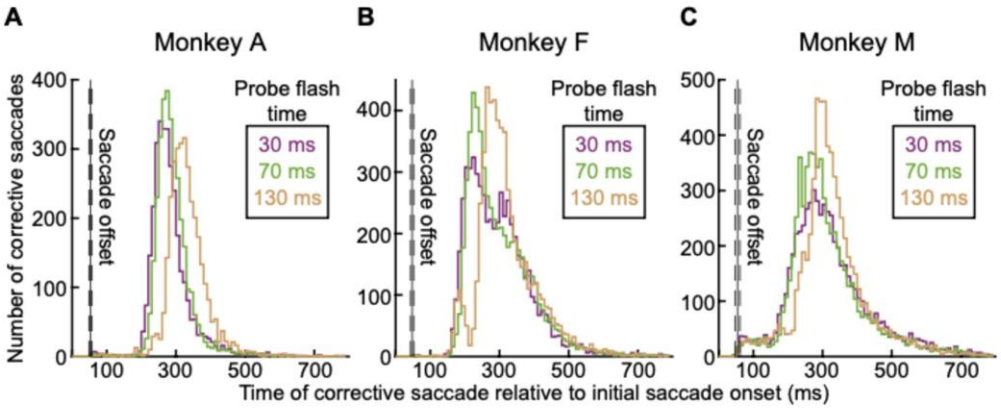

Extended Data Figure 4-4 Corrective saccades were too late to account for mislocalization effects. (A-C) The temporal distribution of corrective saccades relative to the initial saccade onset for each monkey. The number of corrective saccades is plotted over time, aligned to the initial saccade onset. The different probe flash timings (30 ms, 70 ms, and 130 ms after saccade onset) are color-coded. The majority of corrective saccades occurred after probe flash presentation, confirming that they did not influence perisaccadic mislocalization. A slight delay in corrective saccades for late probe flash presentations (130 ms) suggests transient saccadic inhibition, supporting the notion that the monkeys attended to the probe flash. The vertical black lines with surrounding dashed lines indicate the mean and SEM times of saccade offset.

Perisaccadic mislocalization was strongest for upward saccades

Having convinced ourselves that we were indeed measuring genuine perisaccadic mislocalization, we were now in a position to explore further properties.

We first focused on the influence of saccade direction. In previous work, we found that backward mislocalization in humans was particularly strong for upward saccades (Grujic et al., 2018). If our current paradigm is robust, and if macaques are indeed a suitable animal model for exploring this property of perisaccadic mislocalization with neurophysiology, then we should also obtain stronger perisaccadic visual mislocalization in our animals for upward saccades. This was indeed the case.

Consider the results of Fig. 5A, B, which are formatted similarly to Fig. 3D. In Fig. 5A, the animal (monkey A) generated purely upward saccades. The mislocalization was backward relative to the saccade direction (also see Fig. 4), and it was stronger for smaller perisaccadic probe flash times than for later times, as expected. Importantly, the mislocalization seen in Fig. 5A was substantially stronger than that observed for purely downward saccades in the same animal. Specifically, in Fig. 5B, we plotted the data for purely downward saccades in the same format as in Fig. 5A. There was still reverse mislocalization opposite the saccade direction, but the peak mislocalization strength (for 30 ms perisaccadic probe flash times) was significantly weaker than in Fig. 5A. This fact is rendered clearer by noting Fig. 5C. Here, we plotted the average (and SEM) reported locations for 30 ms perisaccadic probe flashes for the two saccade directions together in the same plot. To facilitate comparison of the effect sizes in the two cases, we rotated all data to a schematic representation in which the saccade vector was to the right, and the probe flashes were further ahead of it. We used exactly the same approach to visualize results from different saccade directions in our earlier

human studies (Grujic et al., 2018). As can be seen, relative to the baseline reports of each condition (black symbols and colored connecting arrows) there was clearly stronger perisaccadic mislocalization (in the backward, reverse direction) for upward saccades. Quantitatively, for purely upward saccades, the average Euclidean distance measure across all three flash locations in this figure was 5.8 deg, whereas it was only 3.5 deg for purely downward saccades. Therefore, there was stronger mislocalization for the upward saccades.

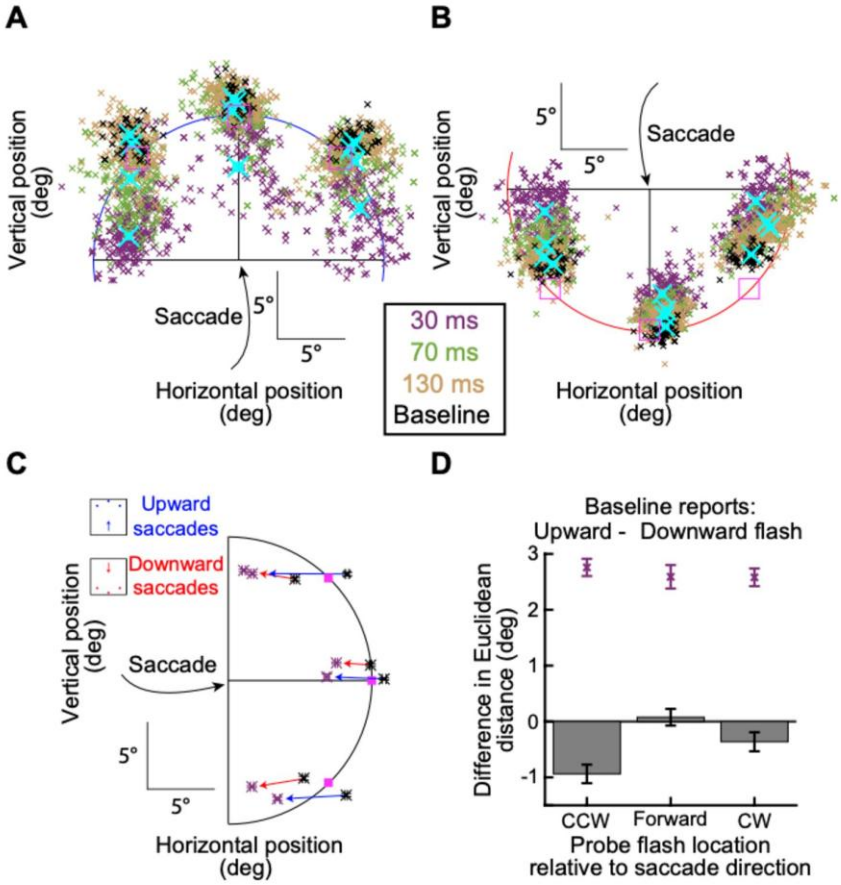

Figure 5 Stronger perisaccadic mislocalization for upward saccades. (A) Similar analysis to that in Fig. 3D but for purely upward saccades in monkey A. Reverse mislocalization can be seen, consistent with Fig. 3. **(B)** In the same animal, the strength of reverse mislocalization was weaker for purely downward saccades. This can be seen by the smaller (than in **A**) deviation in the reports for the 30 ms perisaccadic flashes from the baseline reports. Note that we showed the true flash location in **A**, **B** using outline pink squares in this case (unlike in Fig. 3), in order to avoid covering the data points. Otherwise, the figure is formatted like in Fig. 3. **(C)** Comparison of the strength of mislocalization for the two saccade directions in **A**, **B**. Here, we rotated the saccade vectors of **A**, **B** to a single schematic representation (shown here as a rightward saccade), like we did previously (Grujic et al., 2018). Purple symbols (along with SEM error bars) indicate reports with the 30 ms perisaccadic flashes, and black symbols (along with SEM error bars) indicate baseline reports. Pink squares indicate the true flash positions. Red and blue connecting arrows indicate whether the saccade was upward (blue) or downward (red). The blue arrows were always longer than the red arrows, indicating a stronger mislocalization (relative to baseline) for the upward than for the downward saccades. **(D)** Baseline reports exhibited minimal differences between upward and downward saccades for each flash location, highlighting that the stronger mislocalization for upward saccades relative to baseline reports (purple points) was not driven by differences in the baseline reports. For the individual probe flash locations, the difference in baseline reports between upward and downward saccades is shown as bars, and the difference in reports at peak mislocalization as purple data points. All error bars denote SEM.

Moreover, this difference in mislocalization strength between upward and downward saccades at peak mislocalization (30 ms flash times) was clearly larger than any systematic differences in the baseline report locations between upward and downward saccades: the Euclidean distance between the baseline report locations (black symbols) for purely upward and purely downward saccades in Fig. 5C was only 0.51 deg (again averaging the respective distances across all three flash locations); this was smaller than the difference in mislocalization strengths between the upward and downward saccades. This result can be seen in Fig. 5D, in which we plotted the difference in baseline reports for upward and downward saccades (for the individual flash locations) as bars; the difference at peak mislocalization between upward and downward saccades is shown as purple data points, confirming that the larger difference in mislocalization strengths between upward and downward saccades was not a consequence of equally large differences in baseline reports. Thus, there was indeed stronger perisaccadic visual mislocalization for upward saccades, replicating previous human observations (Grujic et al., 2018).

We next summarized the above observations across all three animals. In Fig. 6A, B, we measured the Euclidean distance of flash localizations (Fig. 3E, right and Materials and Methods) as a function of probe flash time from saccade onset. We did so separately for all upward saccades and for all downward saccades. In the two shown animals in these two panels, all upward saccades meant purely upward and two oblique upward saccade directions, and all downward saccades meant purely downward and two oblique downward saccade directions (see the inset schematics in Fig. 6A, B). We also included all flash locations per saccade direction. That is, for each saccade direction and saccade location, we collected the Euclidean distance, and we then averaged across all measurements. In both animals, at peak mislocalization (flashes occurring 30 ms after saccade onset in our experiments), there was stronger perisaccadic visual mislocalization for upward saccades, consistent with human observations (Grujic et al., 2018). We also reached the same conclusions when treating each saccade direction individually (Fig. 6C, D).

We also replicated these results in monkey M. In this monkey, we separated the visual hemifields towards which the primary saccades were directed because this monkey had significantly slower saccades with a rightward component, making it difficult to match kinematics across hemifields (Materials and Methods). The monkey again exhibited stronger perisaccadic visual mislocalization for upward saccades (Fig. 6E, F). This can also be seen in Fig. 6G, with the added observation being that perisaccadic visual mislocalization was stronger for the faster leftward saccades. This is also consistent with human observations (Ostendorf et al., 2007).

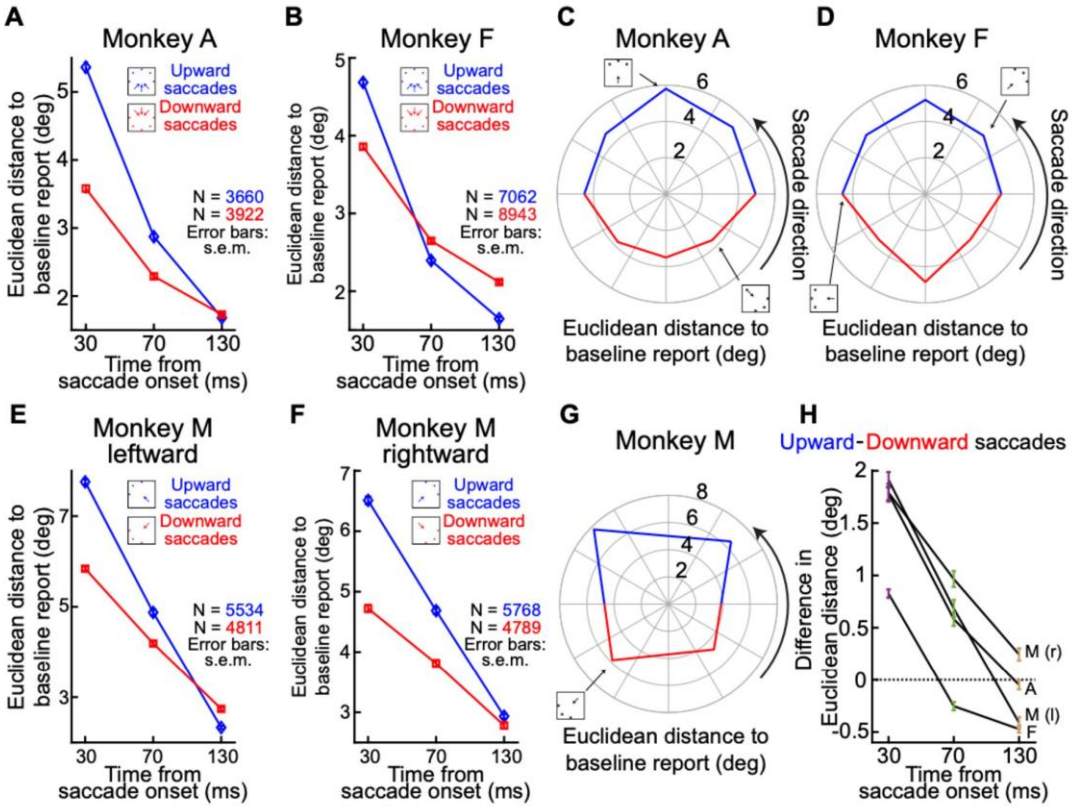

Figure 6 Consistently stronger perisaccadic mislocalization for upward saccades. (A) In monkey A, we measured the Euclidean distance of perisaccadic reports (relative to baseline reports) as a function of flash time from saccade onset. The two curves show mislocalization strengths when considering only trials with either upward (blue) or downward (red) saccades. The inset icons clarify the saccade vectors included for each curve (Materials and Methods), as well as their relevant flash locations (3 per saccade direction). There was stronger mislocalization for upward saccades. **(B)** Similar results for monkey F. This monkey also showed more rapid recovery dynamics, with time, for the upward saccades. **(C, D)** Same data as in **A**, **B**, but considering each saccade direction individually. In each plot, the angle indicates the direction of the saccade (see inset icon examples), and the radial value indicates the Euclidean distance measured for 30 ms flash times. There was stronger mislocalization for upward saccades. **(E, F)** Similar analyses to **A**, **B**, but for monkey M. In this monkey, we separated saccades with a leftward (**E**) or rightward (**F**) component. In both panels, the monkey still exhibited stronger mislocalization for upward saccades. **(G)** Same as **C**, **D**, but for monkey M. Again, there was stronger mislocalization for upward saccades. Note that there was also stronger mislocalization for leftward saccades. These were the faster eye movements (approximately 550 deg/s versus approximately 350 deg/s peak velocity), suggesting an interaction between saccade speed and mislocalization strength (Ostendorf et al., 2007). **(H)** We summarized the effects of saccade direction by calculating the difference in mislocalization strength between upward and downward saccades. For all monkeys, there was stronger mislocalization for upward saccades, especially at peak mislocalization times. Note that for monkey M, we show two curves for either leftward (l) or rightward (r) saccades. Error bars indicate SEM.

Statistically, all of the above results were robust at the individual monkey level. We conducted a two-way ANOVA to examine the effects of saccade direction and probe time relative to saccade onset on the Euclidean distance to the baseline report. There was a significant main effect of saccade direction for monkeys A ($F(1,7576)=421.07$, $p<0.001$) and M ($F(1,20896)=812.77$, $p<0.001$), indicating that the direction of the saccade had a significant impact on perisaccadic mislocalization. Monkey F did not show a significant main

effect for saccade direction ($F(1,15999)=1.92$, $p=0.16$), but this was only because this monkey exhibited faster recovery times than the other two monkeys (Fig. 6B). Indeed, this monkey, as well as the other two, showed a significant interaction between saccade direction and probe flash time relative to saccade onset (monkey A: $F(2,7576)=202.37$, $p<0.001$; monkey F: $F(2,15999)=265.66$, $p<0.001$; monkey M: $F(2,20896)=333.72$, $p<0.001$), indicating that the effect of saccade direction depended on the time point. There was also a significant main effect of probe time relative to saccade onset in all three monkeys (monkey A: $F(2,7576)=1870.19$, $p<0.001$; monkey F: $F(2,15999)=3371.03$, $p<0.001$; monkey M: $F(2,20896)=4434.12$, $p<0.001$), suggesting that saccadic mislocalization varied across different time points (as expected). Post-hoc comparisons using Bonferroni corrections for probe time relative to saccade onset revealed significant differences between all time points for all monkeys, with visual mislocalization decreasing progressively from 30 to 130 ms ($p<0.001$). All of these statistical results are summarized graphically in Fig. 6H.

We also quantified mislocalizations for probe flash presentations at 30 ms and 70 ms after saccade onset by measuring the Euclidean distance of these reports not to the baseline trials, but to the reported locations of trials with probe flash presentations at 130 ms after saccade onset. For Monkey A, the average mislocalization error for upward saccades was 4.9 deg ± 0.06 SEM at 30 ms and 2.4 deg ± 0.04 SEM at 70 ms, while for downward saccades, the error was only 3.1 deg ± 0.04 SEM (30 ms) and 1.7 deg ± 0.03 SEM (70 ms). Monkey F (upward saccade: 3.8 deg ± 0.03 deg (30ms), 1.8 deg ± 0.02 deg (70ms); downward saccade: 2.7 deg ± 0.03 deg (30 ms), 1.6 deg ± 0.02 deg (70ms)) and Monkey M (upward saccade(to the left): 6.6 deg ± 0.05 deg (30 ms), 3.8 deg ± 0.05 deg (70 ms); downward saccade (to the left): 4.5 deg ± 0.04 deg (30 ms), 3 deg ± 0.04 deg (70 ms); upward saccade (to the right): 5.6 deg ± 0.05 deg (30 ms), 3.4 deg ± 0.04 deg (70 ms); downward saccade (to the right): 4.3 deg ± 0.05 deg (30ms), 3.1 deg ± 0.04 deg (70 ms)) showed a similar pattern.

Returning to our more robust measures relative to baseline reports, and like we did in Fig. 5D, we also checked the differences in systematic errors in baseline reports themselves. Specifically, since memory-guided saccades of different directions can have different systematic error magnitudes (Hafed and Chen, 2016), we asked whether the differences in mislocalization strengths between upward and downward saccades that we saw in Fig. 6 were entirely due to differences in baseline report errors. For each monkey, we measured the error (from true flash location) in the baseline report saccade as a function of saccade direction (Fig. 7A). We did this only for the baseline trials in which perception was expected to be veridical (Materials and Methods). As anticipated (e.g. Figs. 3, 5), there were non-zero absolute errors in the baseline saccades. However, these errors were significantly smaller than the peak mislocalization effects (also seen in Figs. 3, 5). For example, monkey F had a peak mislocalization amplitude of around 4-5 deg (Fig. 6B), but only a baseline report error of around 1.5-1.6 deg. Most importantly, in all animals, the difference in baseline report errors between upward and downward saccades (Fig. 7B), although significant (monkey A: $t(647)=-6.04$, $p<0.001$; monkey F: $t(1323)=-5.03$,$p<0.001$; and monkey M: $t(689)=-4.11$,$p<0.001$ for leftward saccades and $t(704)=-5.78$,$p<0.001$ for rightward saccades; independent samples t-tests), was of the opposite sign from the mislocalization effects comparing upward and downward saccades (purple samples in Fig. 7B and Fig. 6). Thus, stronger perisaccadic mislocalization for upward saccades was not explained by systematic differences in baseline report errors.

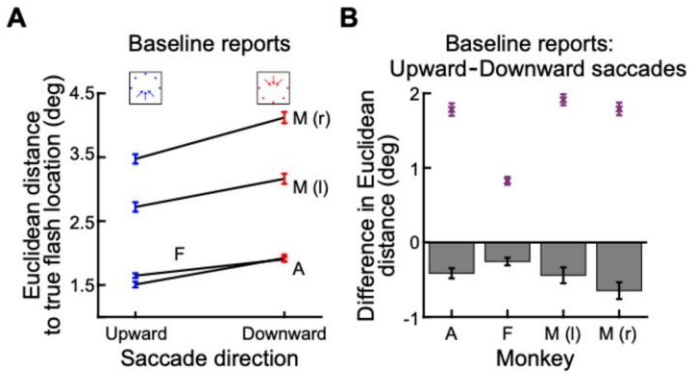

Figure 7 Different patterns of baseline report errors between upward and downward saccades than for mislocalization. (A) For each monkey, we measured the Euclidean distance between the baseline report saccade endpoints and the true flash locations in the data of Fig. 6. We did this separately for either upward or downward saccades. Error bars denote SEM. Note how there was still some error from the true flash location in the baseline reports in which no mislocalization was to be anticipated (also visible in Figs. 3, 5). This is expected from memory-guided saccades (White et al., 1994; Willeke et al., 2019; Willeke et al., 2022). However, such error was always smaller than peak mislocalization error (also visible in Figs. 3, 5). **(B)** For each monkey, we took the difference in the errors in **A** between upward and downward saccades (bar plots; similar to Fig. 5D). This difference revealed slightly larger errors for downward memory-guided saccades, consistent with earlier observations (Hafed and Chen, 2016). In contrast, the purple data points are the results from the time of peak mislocalization in Fig. 6. There was a clearly larger difference between upward and downward saccades during peak perisaccadic visual mislocalization than during baseline reports (and also with an opposite sign). Therefore, the results of Fig. 6 were not driven by differences in baseline report errors between upward and downward saccades.

Finally, mislocalization is known to exhibit a two-dimensional landscape, with a component parallel to the saccade direction and another orthogonal to it (see Fig. 8A). In Fig. 8, stronger mislocalization for upward saccades was evident in both directional components. Both the larger mislocalization effect along the saccade direction (Fig. 8B-E) and the smaller localization error orthogonal to the saccade direction (Fig. 8F-I) varied depending on the saccade direction in all three tested monkeys.

Therefore, our results so far indicate that all three monkeys experienced perisaccadic visual mislocalization, and that they all demonstrated an effect of saccade direction, consistent with human observations (Grujic et al., 2018). A quantitative comparison of effect magnitudes as a function of saccade speeds was also afforded to us by monkey M, and the results were again consistent with human observations (Ostendorf et al., 2007). This reinforces our interpretation of the flexibility and robustness of our paradigm.

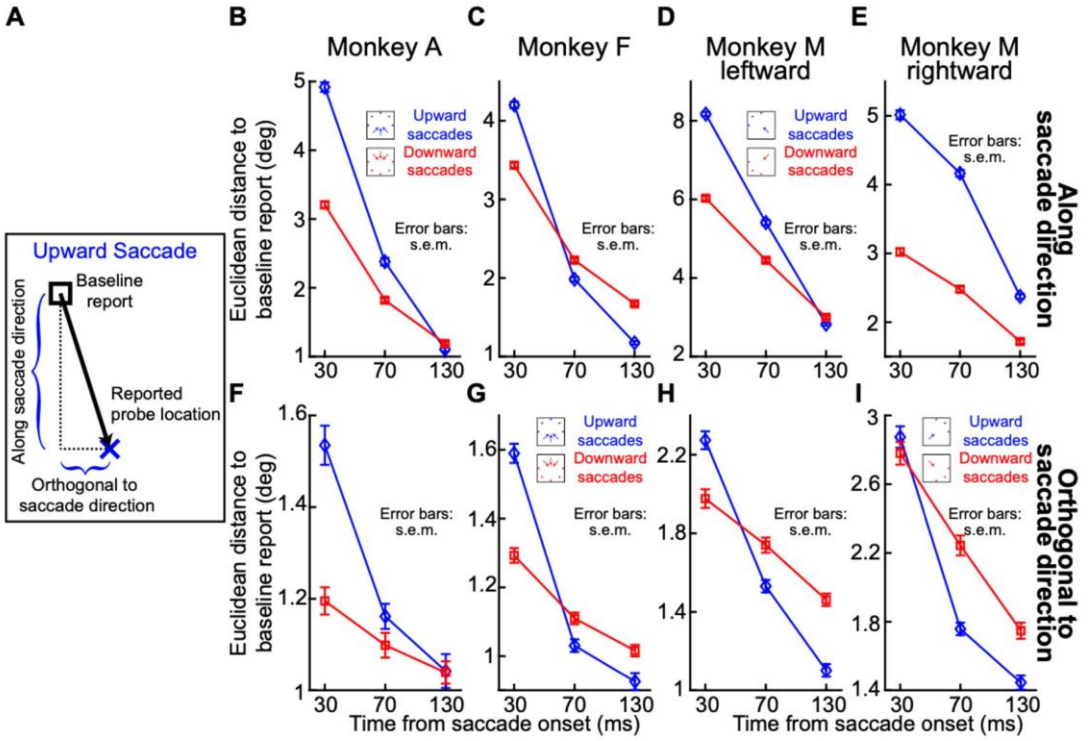

Figure 8 Two-dimensional perisaccadic mislocalization landscape in macaques. (A) our analysis approach for assessing the strength of orthogonal mislocalization (Baumann et al., 2024). We measured the two components of mislocalization separately. One component was along the saccade direction, and one component was orthogonal to the saccade direction (Baumann et al., 2024). **(B-E)** Mislocalization along the saccade direction for upward (blue) and downward (red) saccades in the three monkeys (A, F, M). Note that we show rightward and leftward saccade directions separately for Monkey M. Error bars represent SEM. There was consistently stronger mislocalization for upward saccades. **(F-I)** Localization error orthogonal to the saccade direction for the same conditions. Stronger mislocalization for upward saccades was still evident, with a pronounced effect along the saccade direction and a smaller but consistent error orthogonal to the saccade direction across all tested monkeys.

Perisaccadic mislocalization was stronger for upper visual field flashes

We next explored the effect of visual field location of the flashes relative to horizontal saccades. In humans, we recently found that, with such horizontal saccades, reverse mislocalization was stronger for upper visual field flashes (ahead of the saccade target location) than for symmetrically located lower visual field ones (Baumann et al., 2024). This was also the case in our monkeys. Specifically, in Fig. 9A-D, we analyzed mislocalization strength for only horizontal saccades in each monkey. This time, we separated the trials based on whether the perisaccadic flash location was above or below the horizon. That is, if the saccade was to the right, our paradigm included three potential flashes: one directly ahead of the saccade target (still on the horizontal axis), and two oblique ones (Fig. 1, Materials and Methods). The two oblique flashes were, by definition, either in the upper or lower visual field relative to the saccade direction, and we compared these two oblique flash positions in the current analysis. The results demonstrated that there was indeed generally stronger mislocalization associated with upper rather than lower visual field flashes.

Statistically, we performed a two-way ANOVA to evaluate the effects of probe location and probe time relative to horizontal saccade onset on the Euclidean distance to the baseline report. There was a significant main effect of probe location for all three monkeys (monkey A: $F(1,1632)=410.01$, $p<0.001$; monkey F: $F(1,1214)=65.2$, $p<0.001$; monkey M: $F(1,9687)=626.66$, $p<0.001$) indicating that the probe location had an impact on the strength of perisaccadic visual mislocalization. The main effect of probe time relative to saccade onset was also significant (monkey A: $F(2,1632)=552.54$, $p<0.001$; monkey F: $F(2,1214)=714.44$, $p<0.001$; monkey M: $F(2,9687)=1652.95$, $p<0.001$), suggesting that perisaccadic mislocalization varied across different time points. Finally, the interaction between probe location and probe time relative to saccade onset was also significant for all three monkeys (monkey A: $F(2,1632)=21.43$, $p<0.001$; monkey F: $F(2,1214)=21.93$, $p<0.001$; monkey M: $F(2,9687)=70.51$, $p<0.001$), indicating that the effect of probe location was dependent on flash time. These results are summarized in Fig. 9E showing difference measures similar to ones that we used earlier for summarizing saccade direction effects.

We also checked whether systematic differences (between upper and lower visual field flashes) in baseline report errors accounted for the above results. Specifically, just like in Fig. 7A, we plotted the Euclidean distance between baseline reports and true flash location for the upward and downward flash conditions of this analysis. The results are shown in Fig. 9F. Consistent with Fig. 7A, the absolute errors in baseline reports were smaller than the peak mislocalization effects; this is also consistent with the raw example data shown in Figs. 3, 5, demonstrating clear recovery with time from saccade onset (towards the baseline report locations). Importantly, the differences in baseline report errors between upward and downward flashes were not correlated with the differences in peak mislocalization strength (Fig. 9G). Thus, the effects of upper and lower visual field flashes in association with horizontal saccades were likely perisaccadic and not an artifact of report saccade errors.

Perisaccadic mislocalization strength was subtly modulated by the saccade target appearance

Finally, we explored whether mislocalization strength depended on the visual appearance of the saccade target (Materials and Methods). In two out of the three monkeys, there was a very subtle difference in mislocalization strength as a function of saccade target appearance; however, this dependence was not the same in both animals. Consider for example, Fig. 10A. The figure shows slightly stronger mislocalization for the low spatial frequency grating as the saccade target. However, Monkey F showed the opposite effect (Fig. 10B). Figure 10C, D shows the data of monkey M, showing no image dependency for the time bin with peak mislocalization, and neither for leftward nor for rightward saccades. These findings for the image dependence are smaller than the dependence for saccade direction.

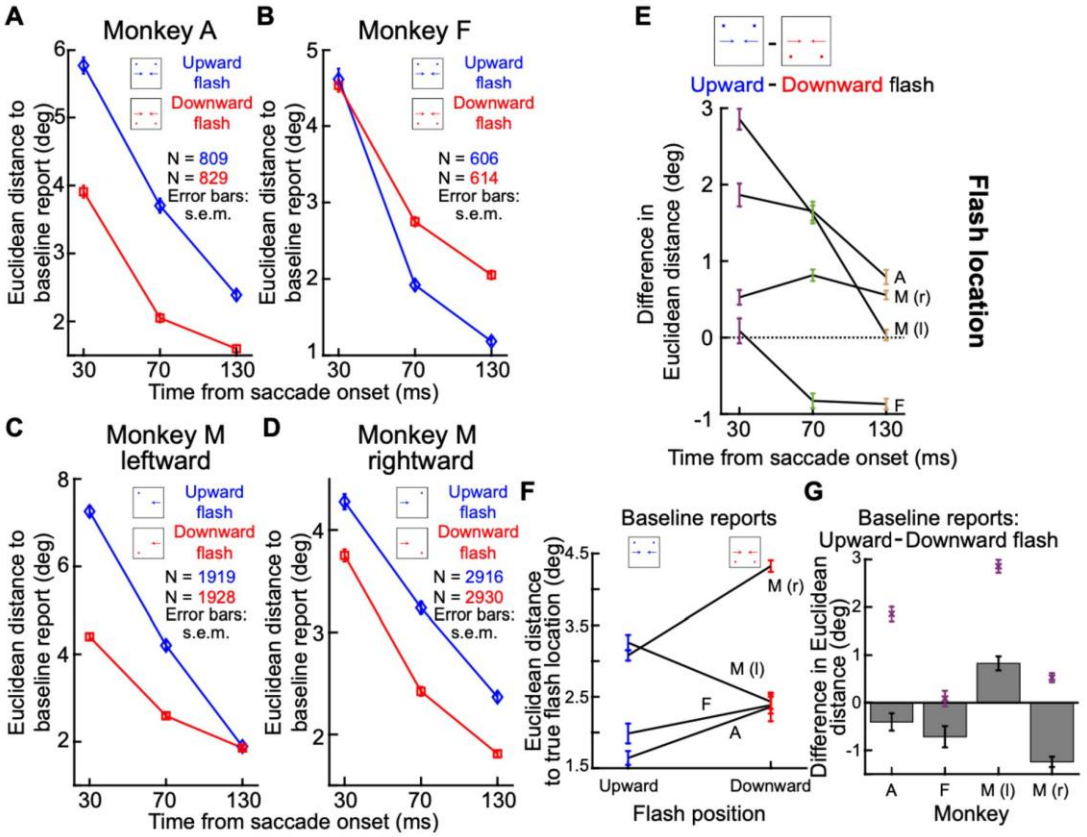

Figure 9 Stronger perisaccadic visual mislocalization for upper visual field probe flashes and horizontal saccades. (A) For monkey A, we only considered horizontal primary saccade directions. We then compared mislocalization strength (Euclidean distance to baseline reports) for probe flashes above or below the saccadic vector (see Materials and Methods and inset schematic). There was stronger mislocalization for upper visual field flashes, like in humans (Baumann et al., 2024). **(B)** In monkey F, the effect at peak mislocalization (flashes 30 ms from saccade onset) was much weaker than in monkey A, but with a similar trend. This monkey also had rapid time dynamics, like in Fig. 6, causing a reversal at longer times. **(C, D)** Monkey M replicated the results of monkey A regardless of the direction of the horizontal saccades. **(E)** Summary of the results in **A**-**D** shown here as the difference in mislocalization strength between upper and lower visual field flash locations, and as a function of flash time (like in Fig. 6H). **(F)** Errors in baseline reports from true flash location, like in Fig. 7A. Here, we plotted these errors for either the upward or downward flash conditions. The errors were always smaller in magnitude than the peak mislocalization effects in **A**-**E** (consistent with Figs. 3, 5). **(G)** More importantly, the difference in these errors between upward and downward flashes did not explain the differences in peak mislocalization. This panel is formatted similarly to Fig. 7B: the bars denote the differences in baseline report errors between upper and lower visual field flashes, and the purple symbols show the peak mislocalization differences from **A**-**E**. Differences in baseline reports did not explain differences in peak mislocalization strengths (except for monkey F where there were already no differences in mislocalization strength). Error bars denote SEM.

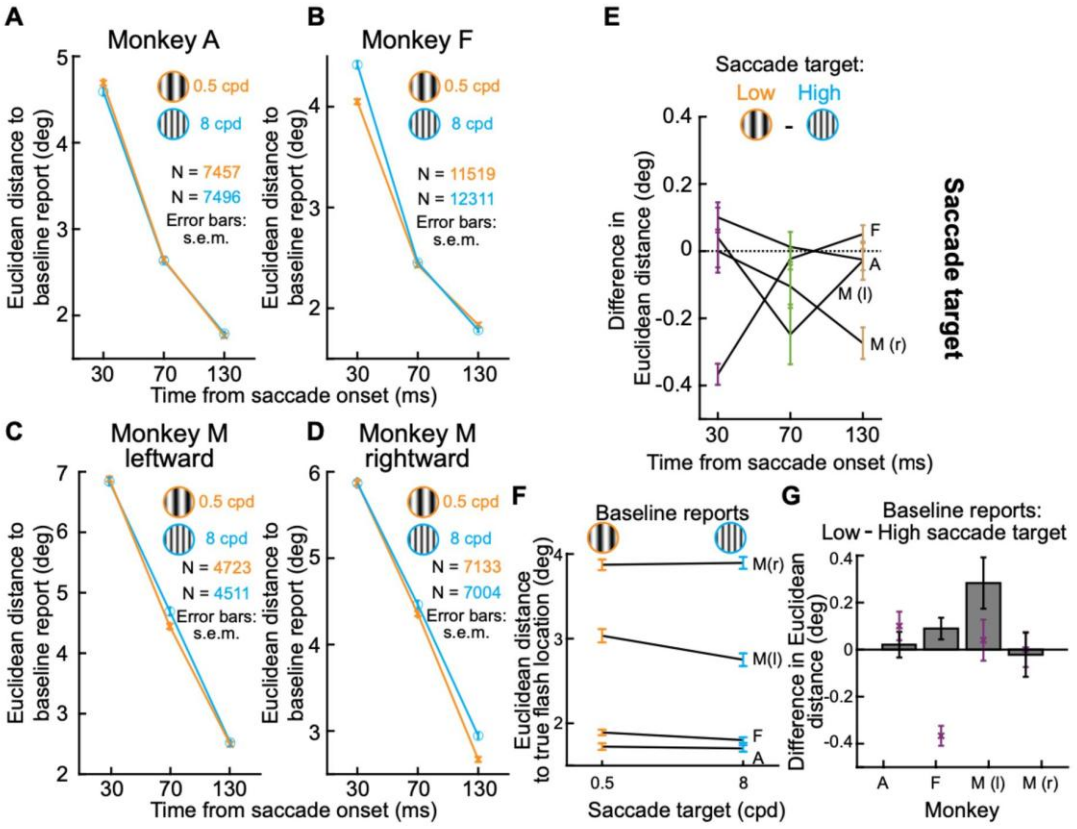

Figure 10 Inconsistent effects with respect to saccade target appearance. This figure is formatted identically to Fig. 9. Here, the comparison was between the different saccade target appearances. Therefore, we pooled across saccades of all directions (Materials and Methods) and only separated trials based on the appearance of the saccade target. There were subtle differences (**A**-**E**), but the differences were similar to the differences in baseline report saccades in the absence of perceptual mislocalization (**F, G**). Thus, the image dependence effect in perisaccadic mislocalization (Baumann et al., 2024) was likely masked by systematic errors in report saccades. All other conventions are similar to Fig. 9.

Statistically, we performed a two-way ANOVA to investigate the effects of saccade target appearance and probe time relative to saccade onset on the Euclidean distance to the baseline report. There was a significant main effect of saccade target appearance for two of the three monkeys (monkey A: $F(1,14947)=1.15$, $p=0.28$); monkey F: $F(1,23824)=33.05$, $p<0.001$; monkey M ($F(1,21454)=20.32$, $p<0.001$) indicating that the saccade target had an impact on the strength of perisaccadic mislocalization. However, monkeys' M and F results were not consistent with the previous human results: these monkeys exhibited stronger mislocalization for a high spatial frequency grating. As expected, there was also a significant main effect of probe time relative to saccade onset (monkey A: $F(2,14947)=3867.51$, $p<0.001$; monkey F: $F(2,23824)=5413.83$, $p<0.001$; monkey M: $F(2,21454)=4889.48$, $p<0.001$), suggesting that saccadic mislocalization varied across different time points. Additionally, the interaction between saccade target appearance and probe time relative to saccade onset was significant for all three monkeys (monkey A: $F(2,14947)=1.87$, $p<0.001$; monkey F: $F(2,23824)=42.36$, $p<0.001$; monkey M: $F(2,21454)=4.77$, $p<0.001$).

Thus, we cannot confidently conclude that there was an image dependence of mislocalization strength in our monkeys. This is likely caused, at least in part, by the differences in the ways monkeys and humans reported their percepts (see Discussion). Indeed, analyzing the baseline report errors was particularly revealing (Fig. 10F, G): the difference in magnitudes of baseline report errors between the different target image appearances (Fig. 10G) was of the same order of magnitude as the difference in the peak mislocalization strengths for the different saccade target images. This suggests that a possible image dependence of perisaccadic mislocalization in our monkeys might have been masked by errors in the memory-guided report saccades.

Discussion

We established a robust paradigm with which we could probe perisaccadic mislocalization (with clear visual references in the environment) in monkeys. Importantly, our paradigm allows mapping the two-dimensional landscape of mislocalization, and it can also be used with arbitrary saccade directions. This latter property enabled us to replicate the observation in humans (Grujic et al., 2018) that backward perisaccadic “compression” of flashes ahead of the saccade target is strongest for upward saccades. This dependency of mislocalization on saccade direction was also visible in both directional components, along and orthogonal to the saccade direction. Moreover, we replicated the human observation (Baumann et al., 2024) of stronger backward mislocalization for upper visual field stimuli during horizontal saccades.

Our results can be compared to human psychophysics conducted under similar visual reference conditions. Specifically, a biphasic perisaccadic mislocalization pattern, as reported by (Honda, 1991, 1993), is a well-established phenomenon observed primarily under complete darkness. In this case, when flashes are presented immediately before or at the onset of a saccade, mislocalization typically occurs in the same direction as the saccade. Conversely, when flashes are presented at the end or immediately after the saccade, the perceived location of the flash shifts in the direction opposite to the saccade direction, resulting in a characteristic forward and then backward pattern of mislocalization. However, the presence of visual references appears to significantly modulate this effect. For example, (Honda, 1999) demonstrated that introducing even minimal visual context, such as a faint frame pattern or a dimly illuminated structured background, substantially reduced mislocalization and disrupted the classic biphasic pattern. Under these conditions, mislocalization was more akin to a “compression” effect, where the perceptual error depended on the flash position relative to the saccade target rather than purely on the temporal relationship to the saccade onset. These findings align with the results of studies by (Ross et al., 1997) and (Lappe et al., 2000), which also showed that structured visual environments promoted “compression”-like mislocalization patterns. Since we included a stable visual reference (the saccade target) and bright display conditions, our results are consistent with this framework. Of course, in future work, we can confirm this explicitly by testing probe flash locations in between the initial and final saccade fixation points (Grujic et al., 2018).

Our work builds on previous demonstrations that perisaccadic visual mislocalization can be studied in macaques (Dassonville et al., 1992; Jeffries et al., 2007; Klingenhoefer and Krekelberg, 2017; Weng et al., 2024). Our work also relates to interesting monkey variants of the classic double-step saccade task (Hallett and Lightstone, 1976; Becker and Jurgens, 1979; Ottes et al., 1984; Vliegen et al., 2005), in which the target of the second saccade in the double-step sequence was presented during the progression of the first eye movement (and thus could be susceptible to some mislocalization) (Van Grootel et al., 2012). However, in the context of visual mislocalization studies, our approach adds paradigm flexibility that we believe is necessary for further success in porting these behavioral measures of perisaccadic mislocalization to neurophysiology. For example, it may not always be possible neurophysiologically to probe only horizontal flash position mislocalization or only horizontal saccades. This is because electrode positions in topographic maps may be in off-axis representations. More importantly, mislocalization has a two-dimensional landscape (Kaiser and Lappe, 2004). Thus, with our work, we provide an additional stepping stone towards direct neurophysiological experiments exploiting essentially identical behavioral tasks to those classically used in humans.

Indeed, we were motivated by the particularly strong backward mislocalization for upward saccades in humans (Grujic et al., 2018), and that we think deserves further investigation. We suspect that this phenomenon might be related to the asymmetry of representation in the superior colliculus between the upper and lower visual fields (Hafed and Chen, 2016; Zhang et al., 2022; Hafed, 2025), but this needs to be tested explicitly. In fact, besides recording activity related either to the saccade vector endpoint or to flash locations, we could make variants of our behavioral paradigm that can be more causal in nature. For example, we could replace the flash presentation with brief electrical microstimulation of the primary visual cortex, or higher-level cortical areas. Similarly, we could replace the visually-guided saccade with an electrically evoked saccade from the superior colliculus. This latter experiment would be particularly fascinating. For example, it is known that beyond a certain strength of electrical microstimulation in the superior colliculus, evoked saccades become more similar to each other under different stimulation parameters (Katnani and Gandhi, 2012). Thus, one could stimulate with two different “motor burst strengths” and ask how perisaccadic flashes are mislocalized under the two conditions (with the evoked saccades being the same). This would causally establish a functional role for sensory tuning in collicular motor bursts (Baumann et al., 2023) in perisaccadic perceptual phenomena that might, at least theoretically (Baumann et al., 2024), rely on saccade-related corollary discharge.

Similarly, we could perturb brain areas not implicated in corollary discharge and identify the limits of visual contributions to perisaccadic mislocalization. For example, if monkey M’s asymmetry in saccade peak speeds that we alluded to above was due to a region downstream of the superior colliculus, then it could be that the saccade motor commands (from the colliculus), and their associated (colliculus-related) corollary discharge, were the same for either rightward or leftward saccades in this monkey. If so, then the differences that we saw in the magnitude of perisaccadic mislocalization across hemifields in this animal would have been intrinsically visual in origin: the monkey would have had similar saccade commands (at the collicular level) but different speeds of retinal-image shifts.

The above example variants of our paradigm demonstrate why we think that this paradigm is useful for neurophysiology, and also why we think that it can meaningfully add to a wealth of previous work exploring perisaccadic modulations in visual processing in the brain (Duhamel et al., 1992; Nakamura and Colby, 2002; Krekelberg et al., 2003; Kusunoki and Goldberg, 2003; Sommer and Wurtz, 2006; Churan et al., 2011, 2012; Zirnsak et al., 2014; Neupane et al., 2016b, a, 2020; Qian et al., 2022). These prior experiments did not exploit a simultaneous behavioral report by the animals, which our paradigm allows.

Of course, and as mentioned above, we do acknowledge that we did not explicitly test flash positions between the initial and final fixation positions associated with the saccade (which should show forward mislocalization). However, our use of multiple different saccade directions, coupled with the consistent backward mislocalization seen in all cases, makes us confident that what we saw was indeed that the prior literature referred to as "compression". Indeed, the vectors of mislocalization that we observed (e.g. Figs. 3, 5) as a function of time (relative to the saccade vector direction) were similar to those that we observed earlier in humans using multiple different saccade directions (Grujic et al., 2018). Thus, we believe that our results are consistent with those of (Klingenhoefer and Krekelberg, 2017). Importantly, our paradigm can be easily modified to also include flashes nearer to the initial fixation position than the saccade target.

We also agree with (Klingenhoefer and Krekelberg, 2017) that there can (and should) be quantitative differences in the parameters of the observed perisaccadic mislocalization between monkeys and humans. This is totally expected because factors like foveal magnification and sensory transduction speeds, and others, can be quantitatively different between the two species, even when they are qualitatively similar. Such quantitative differences are inevitable given the different brain sizes. What is important is that the qualitative equivalence is present, and this motivates using these animals in particular for invasive neurophysiological investigations.

One caveat with our work is that we relied on memory-guided saccades to report flash location. Such saccades have systematic errors in their landing positions (White et al., 1994; Willeke et al., 2019), which could also depend on the visual field location of the flashes (Hafed and Chen, 2016). Such saccades also have larger dispersions across trials (variable errors) than visually-guided movements. Still, we chose to use memory-guided saccades because we did not want to impose any prior assumptions about where the monkeys were going to see the flashes. For example, if we had used "choice" targets, then we would have been imposing constraints on the spatial reports of the animals. This is problematic for a general two-dimensional paradigm like the one that we were trying to develop. Moreover, even manual pointing (via displayed cursors) by humans has systematic and variable errors (Willeke et al., 2019), and such pointing is generally used in mislocalization experiments (Grujic et al., 2018; Baumann et al., 2024). Thus, some amount of reporting errors is inevitable in any paradigm requiring a behavioral response from the subjects.

We also acknowledge that our choice to use memory-guided saccades could have come at the expense of having enough resolution to observe more subtle effects, like a potential dependence of perisaccadic mislocalization strength on the saccade target image appearance. Indeed, in parallel experiments with humans, we did find more systematic

effects across most subjects than with the monkeys in the current study (Baumann et al., 2024). Thus, the inconsistency of the image dependence effects that we saw with our monkeys (Fig. 10) could reflect either added contamination by errors in memory-guided saccades, species differences from humans, or the need to test more monkeys with our current paradigm before reaching a conclusion about an image dependence of perisaccadic mislocalization in the animals.

One possibility to avoid the noise associated with memory-guided saccades could be to modify our paradigm slightly: we could adopt the approach of (Klingenhoefer and Krekelberg, 2017; Weng et al., 2024). That is, at the end of every trial, we would display a very dense two-dimensional array of grid positions, and the monkeys would simply choose which grid position matched the perceived flash location. We do not expect this to cause an increased training burden to the task. In any case, for the effects of saccade directions on mislocalization strengths, our paradigm was sufficient.

We also chose to not test presaccadic flashes. This was motivated purely by the pragmatic decision to increase data yield. By presenting flashes contingent on detecting a saccade, we were essentially ensuring obtaining a usable data point for every saccade trial accepted into the analysis. On the other hand, if we had randomized flash times independent of the saccadic reaction time, we would have needed to collect more trials, and then recalculate flash times relative to saccade onset. This should work since it does not alter the paradigm dramatically, and it can also allow obtaining a full time course for perisaccadic mislocalization in monkeys. Moreover, we have previously used both approaches successfully in our experiments on perisaccadic visual suppression, in both humans and monkeys (Hafed and Krauzlis, 2010; Chen and Hafed, 2017; Idrees et al., 2020), and also in our perisaccadic perceptual mislocalization experiments in humans (Grujic et al., 2018; Baumann et al., 2024). Having said that, one has to carefully interpret trials in which the flash happened too long before saccade onset, especially because such a condition gives rise to a complete resetting of saccade plans (Buonocore and Hafed, 2023).

In all, we established a robust, two-dimensional perisaccadic mislocalization paradigm that is particularly useful for neurophysiological experiments with macaque monkeys.

References

Bahill AT, Clark MR, Stark L (1975) The main sequence, a tool for studying human eye movements. Mathematical Biosciences 24:191-204.

Baumann MP, Denninger AF, Hafed ZM (2024) Perisaccadic perceptual mislocalization strength depends on the visual appearance of saccade targets. Journal of Neurophysiology.

Baumann MP, Bogadhi AR, Denninger AF, Hafed ZM (2023) Sensory tuning in neuronal movement commands. Proc Natl Acad Sci U S A 120:e2305759120.

Becker W, Jurgens R (1979) An analysis of the saccadic system by means of double step stimuli. Vision Res 19:967-983.

Beeler GW, Jr. (1967) Visual threshold changes resulting from spontaneous saccadic eye movements. Vision Res 7:769-775.

Berman RA, Wurtz RH (2010) Functional identification of a pulvinar path from superior colliculus to cortical area MT. J Neurosci 30:6342-6354.

Berman RA, Wurtz RH (2011) Signals conveyed in the pulvinar pathway from superior colliculus to cortical area MT. The Journal of neuroscience : the official journal of the Society for Neuroscience 31:373-384.

Berman RA, Joiner WM, Cavanaugh J, Wurtz RH (2009) Modulation of presaccadic activity in the frontal eye field by the superior colliculus. J Neurophysiol 101:2934-2942.

Berman RA, Cavanaugh J, McAlonan K, Wurtz RH (2017) A circuit for saccadic suppression in the primate brain. J Neurophysiol 117:1720-1735.

Brainard DH (1997) The Psychophysics Toolbox. Spatial vision 10:433-436.

Buonocore A, Hafed ZM (2023) The inevitability of visual interruption. J Neurophysiol 130:225-237.

Buonocore A, Skinner J, Hafed ZM (2019) Eye Position Error Influence over "Open-Loop" Smooth Pursuit Initiation. J Neurosci 39:2709-2721.

Cai RH, Pouget A, Schlag-Rey M, Schlag J (1997) Perceived geometrical relationships affected by eye-movement signals. Nature 386:601-604.

Chen CY, Hafed ZM (2013) Postmicrosaccadic enhancement of slow eye movements. The Journal of neuroscience : the official journal of the Society for Neuroscience 33:5375-5386.

Chen CY, Hafed ZM (2017) A neural locus for spatial-frequency specific saccadic suppression in visual-motor neurons of the primate superior colliculus. J Neurophysiol 117:1657-1673.

Churan J, Guitton D, Pack CC (2011) Context dependence of receptive field remapping in superior colliculus. J Neurophysiol 106:1862-1874.

Churan J, Guitton D, Pack CC (2012) Perisaccadic remapping and rescaling of visual responses in macaque superior colliculus. PLoS One 7:e52195.

Dassonville P, Schlag J, Schlag-Rey M (1992) Oculomotor localization relies on a damped representation of saccadic eye displacement in human and nonhuman primates. Vis Neurosci 9:261-269.

Duhamel JR, Colby CL, Goldberg ME (1992) The updating of the representation of visual space in parietal cortex by intended eye movements. Science 255:90-92.

Eastman KM, Huk AC (2012) PLDAPS: A Hardware Architecture and Software Toolbox for Neurophysiology Requiring Complex Visual Stimuli and Online Behavioral Control. Front Neuroinform 6:1.

Fuchs AF, Robinson DA (1966) A method for measuring horizontal and vertical eye movement chronically in the monkey. J Appl Physiol 21:1068-1070.

Grujic N, Brehm N, Gloge C, Zhuo W, Hafed ZM (2018) Peri-saccadic perceptual mislocalization is different for upward saccades. J Neurophysiol 120:3198-3216.

Hafed ZM (2025) Superior colliculus peri-saccadic field potentials are dominated by a visual sensory preference for the upper visual field. iScience 28:112021.

Hafed ZM, Krauzlis RJ (2010) Microsaccadic suppression of visual bursts in the primate superior colliculus. J Neurosci 30:9542-9547.

Hafed ZM, Chen CY (2016) Sharper, Stronger, Faster Upper Visual Field Representation in Primate Superior Colliculus. Curr Biol 26:1647-1658.

Hallett PE, Lightstone AD (1976) Saccadic eye movements towards stimuli triggered by prior saccades. Vision Res 16:99-106.
Honda H (1989) Perceptual localization of visual stimuli flashed during saccades. Percept Psychophys 45:162-174.
Honda H (1991) The time courses of visual mislocalization and of extraretinal eye position signals at the time of vertical saccades. Vision Res 31:1915-1921.
Honda H (1993) Saccade-contingent displacement of the apparent position of visual stimuli flashed on a dimly illuminated structured background. Vision Res 33:709-716.
Honda H (1999) Modification of saccade-contingent visual mislocalization by the presence of a visual frame of reference. Vision Res 39:51-57.
Idrees S, Baumann MP, Franke F, Munch TA, Hafed ZM (2020) Perceptual saccadic suppression starts in the retina. Nat Commun 11:1977.
Jeffries SM, Kusunoki M, Bisley JW, Cohen IS, Goldberg ME (2007) Rhesus monkeys mislocalize saccade targets flashed for 100ms around the time of a saccade. Vision Res 47:1924-1934.
Judge SJ, Richmond BJ, Chu FC (1980) Implantation of magnetic search coils for measurement of eye position: an improved method. Vision Res 20:535-538.
Kaiser M, Lappe M (2004) Perisaccadic mislocalization orthogonal to saccade direction. Neuron 41:293-300.
Katnani HA, Gandhi NJ (2012) The relative impact of microstimulation parameters on movement generation. J Neurophysiol 108:528-538.
Kleiner M, Brainard D, Pelli DG (2007) What's new in Psychtoolbox-3? (Abstract). Perception 36.
Klingenhoefer S, Krekelberg B (2017) Perisaccadic visual perception. J Vis 17:16.
Krekelberg B, Kubischik M, Hoffmann KP, Bremmer F (2003) Neural correlates of visual localization and perisaccadic mislocalization. Neuron 37:537-545.
Kusunoki M, Goldberg ME (2003) The time course of perisaccadic receptive field shifts in the lateral intraparietal area of the monkey. J Neurophysiol 89:1519-1527.
Lappe M, Awater H, Krekelberg B (2000) Postsaccadic visual references generate presaccadic compression of space. Nature 403:892-895.
Latour PL (1962) Visual threshold during eye movements. Vision Res 2:261-262.
Nakamura K, Colby CL (2002) Updating of the visual representation in monkey striate and extrastriate cortex during saccades. Proc Natl Acad Sci U S A 99:4026-4031.
Neupane S, Guitton D, Pack CC (2016a) Two distinct types of remapping in primate cortical area V4. Nat Commun 7:10402.
Neupane S, Guitton D, Pack CC (2016b) Dissociation of forward and convergent remapping in primate visual cortex. Curr Biol 26:R491-492.
Neupane S, Guitton D, Pack CC (2020) Perisaccadic remapping: What? How? Why? Rev Neurosci 31:505-520.
Ostendorf F, Fischer C, Finke C, Ploner CJ (2007) Perisaccadic compression correlates with saccadic peak velocity: differential association of eye movement dynamics with perceptual mislocalization patterns. J Neurosci 27:7559-7563.
Ottes FP, Van Gisbergen JA, Eggermont JJ (1984) Metrics of saccade responses to visual double stimuli: two different modes. Vision Res 24:1169-1179.
Pelli DG (1997) The VideoToolbox software for visual psychophysics: transforming numbers into movies. Spatial vision 10:437-442.

Qian N, Goldberg ME, Zhang M (2022) Tuning curves vs. population responses, and perceptual consequences of receptive-field remapping. Frontiers in computational neuroscience 16:1060757.

Robinson DA (1963) A Method of Measuring Eye Movement Using a Scleral Search Coil in a Magnetic Field. IEEE Trans Biomed Eng 10:137-145.

Ross J, Morrone MC, Burr DC (1997) Compression of visual space before saccades. Nature 386:598-601.

Schoppik D, Lisberger SG (2006) Saccades exert spatial control of motion processing for smooth pursuit eye movements. J Neurosci 26:7607-7618.

Skinner J, Buonocore A, Hafed ZM (2019) Transfer function of the rhesus macaque oculomotor system for small-amplitude slow motion trajectories. J Neurophysiol 121:513-529.

Sommer MA, Wurtz RH (2004) What the brain stem tells the frontal cortex. II. Role of the SC-MD-FEF pathway in corollary discharge. J Neurophysiol 91:1403-1423.

Sommer MA, Wurtz RH (2006) Influence of the thalamus on spatial visual processing in frontal cortex. Nature 444:374-377.

Tian X, Yoshida M, Hafed ZM (2018) Dynamics of fixational eye position and microsaccades during spatial cueing: the case of express microsaccades. J Neurophysiol 119:1962-1980.

Van Grootel TJ, Van der Willigen RF, Van Opstal AJ (2012) Experimental test of spatial updating models for monkey eye-head gaze shifts. PLoS One 7:e47606.

Vliegen J, Van Grootel TJ, Van Opstal AJ (2005) Gaze orienting in dynamic visual double steps. J Neurophysiol 94:4300-4313.

Weng G, Akbarian A, Clark K, Noudoost B, Nategh N (2024) Neural correlates of perisaccadic visual mislocalization in extrastriate cortex. Nat Commun 15:6335.

White AL, Rolfs M (2016) Oculomotor inhibition covaries with conscious detection. J Neurophysiol 116:1507-1521.

White JM, Sparks DL, Stanford TR (1994) Saccades to remembered target locations: an analysis of systematic and variable errors. Vision Res 34:79-92.

Willeke KF, Cardenas AR, Bellet J, Hafed ZM (2022) Severe distortion in the representation of foveal visual image locations in short-term memory. Proc Natl Acad Sci U S A 119:e2121860119.

Willeke KF, Tian X, Buonocore A, Bellet J, Ramirez-Cardenas A, Hafed ZM (2019) Memory-guided microsaccades. Nat Commun 10:3710.

Zhang T, Malevich T, Baumann MP, Hafed ZM (2022) Superior colliculus saccade motor bursts do not dictate movement kinematics. Commun Biol 5:1222.

Zirnsak M, Steinmetz NA, Noudoost B, Xu KZ, Moore T (2014) Visual space is compressed in prefrontal cortex before eye movements. Nature 507:504-507.

Zuber BL, Stark L (1966) Saccadic suppression: elevation of visual threshold associated with saccadic eye movements. Exp Neurol 16:65-79.

Zuber BL, Stark L, Cook G (1965) Microsaccades and the velocity-amplitude relationship for saccadic eye movements. Science 150:1459-1460.